

University of Warwick institutional repository: <http://go.warwick.ac.uk/wrap>

A Thesis Submitted for the Degree of PhD at the University of Warwick

<http://go.warwick.ac.uk/wrap/59506>

This thesis is made available online and is protected by original copyright.

Please scroll down to view the document itself.

Please refer to the repository record for this item for information to help you to cite it. Our policy information is available from the repository home page.

**The Regulatory Protein and
Component Interactions of Soluble
Methane Monooxygenase**

Anastasia J. Callaghan B.Sc.(Hons)

A thesis submitted for the degree of Doctor of Philosophy

Department of Biological Sciences

University of Warwick

Coventry

CV4 7AL

September 2000

To my loved ones.

Contents

List of Figures.....	vii
List of Tables.....	xiii
Acknowledgements.....	xiv
Declaration.....	xv
Abbreviations.....	xvi
Summary.....	xx

Chapter 1 Introduction 1

1.1 Methane to Methanol Conversion.....	1
1.2 Methane Utilising Bacteria.....	2
1.2.1 Methylotrophic Bacteria.....	2
1.2.2 Methanotrophic Bacteria.....	3
1.3 Methane Monooxygenase.....	5
1.4 Regulation of MMO Expression.....	6
1.5 Particulate Methane Monooxygenase (pMMO).....	7
1.6 Soluble Methane Monooxygenase (sMMO).....	9
1.6.1 The Hydroxylase Component.....	12
1.6.1.1 The Nature of the Iron Site.....	12
1.6.1.2 Sequence Studies.....	14
1.6.1.3 Crystal Structure.....	15
1.6.1.4 Activation by Hydrogen Peroxide.....	16
1.6.2 The Reductase Component.....	17
1.6.3 The Regulatory Component, Protein B.....	19
1.6.4 sMMO Reaction Mechanism.....	28
1.7 Objectives of the present work.....	32

Chapter 2 Materials and Methods 33

2.1 Organisms.....	33
2.2 Growth of <i>Mc. capsulatus</i> (Bath) and <i>Ms. trichosporium</i> OB3b.....	33
2.2.1 Media.....	33
2.2.2 Plate cultures.....	33
2.2.3 Batch cultures.....	34
2.2.4 Continuous cultures.....	34
2.2.5 Microscopy.....	34
2.2.6 Cell Harvesting.....	34
2.2.7 Whole cell assay.....	35
2.3 Purification of <i>Mc. capsulatus</i> (Bath) sMMO components - optimised protocols from this study.....	35
2.3.1 Preparation of soluble extract.....	35
2.3.2 Resolution of sMMO into its three constituent proteins.....	36
2.3.3 Purification of the hydroxylase component.....	36
2.3.4 Purification of the reductase component.....	37
2.3.5 Purification of the wild-type regulatory protein B'.....	37
2.4 Purification of the GST-fused regulatory proteins, WTB, G13Q, recombinant <i>Ms. trichosporium</i> OB3b protein B and M12A:G13Q.....	38

2.5 Purification of <i>Ms. trichosporium</i> OB3b protein B - optimised protocol from this study.....	38
2.6 Purification of His-tagged protein B truncates.....	39
2.7 Affinity chromatography.....	39
2.8 Chromatofocusing chromatography.....	40
2.9 Size exclusion chromatography.....	40
2.10 Determination of total protein concentration.....	40
2.10.1 Colorimetric Bradford assay.....	40
2.10.2 Extinction-coefficient values.....	41
2.11 Production of anti-sera.....	41
2.12 sMMO assays by gas chromatography.....	41
2.12.1 Propylene oxide assay – Type 1.....	42
2.12.2 Propylene oxide assay – Type 2 (C. Lesieur, personal communication).....	42
2.12.3 Peroxide shunt assay.....	43
2.13 Assay for monitoring the conversion of <i>p</i> -nitrophenylacetate to <i>p</i> -nitrophenol.....	43
2.14 Polyacrylamide gel electrophoresis (PAGE).....	44
2.14.1 SDS-PAGE.....	44
2.14.2 Native-PAGE.....	45
2.15 Western blotting.....	45
2.16 Mass spectrometry.....	46
2.16.1 Electrospray ionisation mass spectrometry (ESI-MS).....	46
2.16.2 Matrix assisted laser desorption ionisation time of flight mass spectrometry (MALDI-ToF MS).....	47
2.17 Fluorescence studies.....	47
2.18 Circular dichroism spectroscopy.....	48
2.19 FTIR Spectroscopy.....	48
2.19.1 Sample preparation.....	48
2.19.2 Data collection and analysis.....	48
2.20 Single particle analysis by electron microscopy.....	49
2.21 Analytical ultracentrifugation.....	49
2.21.1 Samples used.....	49
2.21.2 Experimental procedure.....	50
2.21.3 Data analysis.....	50
2.22 Crystallisation of the regulatory protein.....	51
2.23 Homology modelling studies.....	51
2.24 Secondary structure prediction.....	51
2.25 Small angle X-ray scattering.....	51
2.25.1 Sample preparation.....	51
2.25.2 X-ray scattering data acquisition and analysis.....	52
2.25.3 Modelling the scattering data.....	53
2.26 Atomic force microscopy (AFM).....	54
2.27 <i>E. coli</i> strains.....	55
2.27.1 Plasmids.....	55
2.27.2 Luria Bertani growth media for <i>E. coli</i>	57
2.27.3 Culture storage.....	57
2.27.4 Culturing conditions for <i>E. coli</i>	57
2.27.5 Antibiotics.....	58
2.28 Nucleic acids techniques.....	58
2.28.1 Plasmid extraction.....	58

2.28.2	Extraction of DNA with phenol and chloroform.....	58
2.28.3	Precipitation of nucleic acids	58
2.28.4	Determination of the concentration of nucleic acids.....	59
2.28.5	Agarose gel electrophoresis.....	59
2.29	Enzymatic modification of DNA	59
2.29.1	Restriction endonuclease digestion of DNA	59
2.29.2	Dephosphorylation of DNA	60
2.29.3	Ligation of DNA	60
2.29.4	Agarose gel purification of DNA	60
2.30	PCR	60
2.30.1	Design of oligonucleotides	60
2.30.2	PCR amplification	60
2.31	DNA sequencing	61
2.32	Transformation	61
2.33	Chemicals and gases.....	62

Chapter 3 Optimisation of Purification Protocols for Wild-Type, Recombinant and Mutant Forms of Protein B and the Reductase and Hydroxylase Components of sMMO **63**

3.1	Introduction	63
3.2	Purification of wild-type protein B/B' from <i>Mc. capsulatus</i> (Bath)	64
3.2.1	Optimisation of the published purification procedure.....	65
3.3	Preparation of anti-serum against proteins B and B'	69
3.4	Purification of recombinant <i>Mc. capsulatus</i> (Bath) protein B (WTB) and the single mutant G13Q.....	70
3.4.1	Transformation of constructs into protease negative cells for expression.....	71
3.4.2	Protein induction	71
3.4.3	Protein purification.....	72
3.5	Purification of wild-type protein B from <i>Ms. trichosporium</i> (OB3b).....	75
3.5.1	Optimisation of current protocols for <i>Ms. trichosporium</i> OB3b protein B purification.....	75
3.5.2	ESI-MS analysis of <i>Ms. trichosporium</i> OB3b protein B.....	78
3.6	Purification of recombinant <i>Ms. trichosporium</i> OB3b protein B.....	80
3.7	Determination of the extinction-coefficients of the regulatory proteins	80
3.8	Separation of protein B and truncate(s) by chromatofocusing chromatography	82
3.9	Determination of the purity of hydroxylase and reductase, as purified by the current published protocols	89
3.9.1	Purification of the hydroxylase and reductase proteins from <i>Mc. capsulatus</i> (Bath)	89
3.10	Conclusion.....	92

Chapter 4 The Cleavage of Protein B **94**

4.1	Introduction	94
4.2	Is the mechanism of cleavage of protein B autocatalytic?	96
4.2.1	Studying the mechanism of cleavage	96
4.2.2	How does protein B cleave?.....	98
4.3	ESI-MS analysis of the cleavage of protein B from various sources.....	103

4.4	The role of protein B' within the sMMO system	105
4.4.1	Sequence similarity searching	105
4.4.2	Can sMMO oxidise large substrate molecules when protein B' is used as the regulatory protein?	107
4.4.3	Does protein B' bind to the hydroxylase?	107
4.5	Does protein B' exist within sMMO-expressing cells?	109
4.6	Structural analysis of proteins B and B'	111
4.6.1	Secondary structure analysis of protein B and B'	111
4.6.1.1	Circular dichroism analysis	111
4.6.1.2	Fluorescence analysis	115
4.6.1.3	Fourier transform infrared spectroscopy (FTIR)	117
4.6.2	Crystallography studies	120
4.6.3	Dimer studies of proteins B and B'	121
4.6.3.1	PAGE analysis of protein B	122
4.6.3.2	Molecular size determination	123
4.6.3.3	MALDI-ToF MS analysis of protein B	124
4.6.3.4	Sedimentation equilibrium analysis	126
4.6.4	Biophysical characterisation of proteins B and B'	130
4.6.4.1	Small angle X-ray scattering (SAXS)	130
4.6.4.2	Atomic force microscopy (AFM)	132
4.7	Conclusion	135

Chapter 5 Stabilisation of Protein B by Biochemical Methods 139

5.1	Introduction	139
5.2	Effect of protein concentration and temperature on stability	140
5.2.1	Analysis by SDS-PAGE	141
5.2.2	Analysis of protein B' formation by activity measurement	144
5.2.3	Analysis of truncate formation by ESI-MS	146
5.3	Effect of additives on the stability of protein B	149
5.3.1	Effect of metals on protein B	153
5.3.2	Does protein B bind copper?	156
5.3.2.1	Copper affinity column studies	156
5.3.2.2	Fluorescence quenching studies	159
5.3.2.3	Is the secondary structure of protein B affected by copper binding?	165
5.4	Conclusion	167

Chapter 6 Effect of M12A:G13Q Double Mutation on the Stability and Structure of *Mc. capsulatus* (Bath) Protein B 170

6.1	Introduction	170
6.2	Construction of the double mutant M12A:G13Q of protein B from <i>Mc. capsulatus</i> (Bath)	170
6.2.1	PCR amplification and construction of vectors	171
6.2.2	Expression of pGEX-M12A:G13Q	174
6.2.3	Purification of M12A:G13Q	175
6.3	Characterisation of M12A:G13Q	177
6.3.1	Effect of mutation M12A:G13Q on the stability of protein B	177
6.4	ESI-MS analysis of M12A:G13Q	181

6.5	Affinity of M12A:G13Q for the hydroxylase	183
6.6	Theoretical modelling of the N-terminal region of M12A:G13Q, as compared to G13Q and wild-type <i>Mc. capsulatus</i> (Bath) protein B.....	184
6.7	Determination of the secondary structure of M12A:G13Q.....	186
6.8	Conclusion.....	190
Chapter 7 Expression, purification and characterisation of truncates of recombinant protein B from <i>Mc. capsulatus</i> (Bath)		193
7.1	Introduction	193
7.2	PCR amplification and construction of vectors.....	194
7.3	Expression of truncated proteins	199
7.4	Purification of the truncated proteins	201
7.5	Characterisation of the truncated proteins.....	204
7.5.1	Activities of the protein B truncates.....	204
7.5.2	Comparison of the cleavage sites that occur within the truncated proteins.....	205
7.5.3	Comparison of the molecular dimensions of the truncated proteins by size exclusion chromatography.....	210
7.5.4	Theoretical secondary structure determination of the N-terminus region of the protein B truncates	212
7.5.5	Secondary structure determination of the truncated proteins.....	213
7.6	Conclusion.....	214
Chapter 8 Component Interactions of sMMO		216
8.1	Introduction	216
8.2	Single particle analysis by electron microscopy	217
8.3	Atomic force microscopy	225
8.4	Small angle X-ray scattering (SAXS)	228
8.5	Conclusion.....	238
Chapter 9 General Discussion		245
References		257
Appendix		271

List of Figures

Figure 1.1: Sub-divisions of the major genera of methylotrophic bacteria.	3
Figure 1.2: Pathway of methane oxidation.	4
Figure 1.3: Model for the copper-dependent transcriptional regulation of pMMO and sMMO genes.	7
Figure 1.4: Schematic model of sMMO.	10
Figure 1.5: Schematic arrangement of the sMMO operon.	11
Figure 1.6: Structure of the hydroxylase from <i>Mc. capsulatus</i> (Bath) at 2.2 Å resolution (Rosenzweig <i>et al.</i> , 1993).	15
Figure 1.7: Order of electron flow from the reductase to the hydroxylase.	17
Figure 1.8: Regulation of the sMMO complex by protein B.	20
Figure 1.9: NMR derived structures of protein B from (i) <i>Mc. capsulatus</i> (Bath) (Walters <i>et al.</i> , 1999) and (ii) <i>Ms. trichosporium</i> OB3b (Chang <i>et al.</i> , 1999).	22
Figure 1.10: Surface diagram model for the docking of protein B into the hydroxylase.	24
Figure 1.11: Cleavage sites of protein B from <i>Mc. capsulatus</i> (Bath).	27
Figure 1.12: Proposed catalytic cycle of sMMO.	29
Figure 1.13: Representation of the active site structure of sMMO from <i>Mc. capsulatus</i> (Bath) in both the (i) oxidised and (ii) reduced states.	31
Figure 3.1: SDS-PAGE of protein B purified using the purification procedure developed by Pilkington <i>et al.</i> (1990).	65
Figure 3.2 Purification profile of protein B from <i>Mc. capsulatus</i> (Bath) on a Superdex 75 gel filtration column.	66
Figure 3.3 Purification profile of protein B' from <i>Mc. capsulatus</i> (Bath) on a MONO Q column.	67
Figure 3.4: SDS-PAGE of MONO Q purified protein B'.	68
Figure 3.5: ESI-MS of the pure protein.	68
Figure 3.6: Western blot analysis of purified protein B and B' from <i>Mc. capsulatus</i> (Bath) probing with antibodies to proteins B and B' from the first bleed.	70
Figure 3.7: SDS-PAGE analysis of samples of <i>E. coli</i> AD202 [pGEX-WTB] before and after IPTG induction.	71
Figure 3.8: Western blot analysis of <i>E. coli</i> AD202 [pGEX-WTB] 4 h after induction with IPTG, probing with antibodies to protein B/B'.	72
Figure 3.9: Purification profile of WTB on a Superdex 75 gel filtration column. ..	73
Figure 3.10: SDS-PAGE of the purification of WTB.	74

Figure 3.11: Purification profile of protein B from <i>Ms. trichosporium</i> OB3b on a MONO Q column.	76
Figure 3.12: Purification profile of protein B from <i>Ms. trichosporium</i> OB3b on a Superdex 75 column.	77
Figure 3.13: SDS-PAGE analysis of wild type <i>Ms. trichosporium</i> OB3b protein B at different stages of purification.....	78
Figure 3.14: ESI-MS of purified protein B from <i>Ms. trichosporium</i> OB3b.....	79
Figure 3.15: (i) MALDI-ToF MS of Sample 1 and (ii) ESI-MS of Sample 2.....	83
Figure 3.16: SDS-PAGE of Sample 2.	84
Figure 3.17: Chromatofocusing elution profiles for wild type protein B from <i>Mc. capsulatus</i> (Bath).....	85
Figure 3.18: SDS-PAGE of the protein B fraction obtained from chromatofocusing chromatography.....	86
Figure 3.19: Chromatofocusing elution profiles for WTB and G13Q.....	88
Figure 3.20: SDS-PAGE of the sMMO proteins purified by the method of Pilkington and Dalton, (1990).....	89
Figure 3.21: Western blot analysis of the sMMO proteins as purified by the method of Pilkington and Dalton, (1990), probing with antibodies to <i>Mc. capsulatus</i> (Bath) protein B/B'.....	90
Figure 3.22: sMMO activity assays of the hydroxylase and reductase purified by the method of Pilkington and Dalton (1990) and the effect of adding <i>Mc. capsulatus</i> (Bath) protein B/B' antibodies.	91
Figure 3.23: SDS-PAGE of purified hydroxylase and reductase proteins	92
Figure 4.1: Chromatofocusing elution profiles monitoring for the presence of protein B and its truncates.	97
Figure 4.2: Monitoring the formation of <i>p</i> -nitrophenol.....	102
Figure 4.3: Hit list from BLASTP report showing sequences producing significant alignments to (i) protein B' and (ii) protein B.....	106
Figure 4.4: The effect of proteins B and B' on the oxidation of propylene in the hydroxylase /H ₂ O ₂ system.....	108
Figure 4.5: Western blot of proteins B and B' in sMMO-expressing <i>Mc. capsulatus</i> (Bath) and <i>Ms. trichosporium</i> OB3b whole cells.....	110
Figure 4.6: Far UV CD spectra of (i) WTB and WTB', (ii) G13Q and G13Q B' and (iii) recombinant <i>Ms. trichosporium</i> OB3b protein B and recombinant <i>Ms. trichosporium</i> OB3b protein B'.....	112
Figure 4.7: Near UV CD spectra of (i) WTB and WTB', (ii) G13Q and G13Q B' and (iii) recombinant <i>Ms. trichosporium</i> OB3b protein B and recombinant <i>Ms. trichosporium</i> OB3b protein B'	113
Figure 4.8: Fluorescence spectra of (i) WTB and WTB', (ii) G13Q and G13Q B' and (iii) recombinant <i>Ms. trichosporium</i> OB3b protein B and recombinant <i>Ms. trichosporium</i> OB3b protein B'.....	116

Figure 4.9: Amide I band fitting results for the FTIR spectroscopy data for (i) WTB, (ii) G13Q and (iii) recombinant <i>Ms. trichosporium</i> OB3b protein B giving the secondary structure content for each protein after incubation at 20 °C at 0 h, 24 h and 48 h.	118
Figure 4.10: Photograph showing the crystalline entities of protein B/B'.	121
Figure 4.11: Size exclusion chromatography of G13Q, WTB, wild-type <i>Mc. capsulatus</i> (Bath) protein B and B', recombinant and wild-type <i>Ms. trichosporium</i> OB3b protein B.	123
Figure 4.12: Analysis of (i) recombinant <i>Ms. trichosporium</i> OB3b protein B and (ii) wild-type <i>Mc. capsulatus</i> (Bath) protein B by MALDI-ToF mass spectrometry.	125
Figure 4.13: Sedimentation equilibrium profiles for protein B' at (i) 1 mg/ml and (ii) 2 mg/ml.	128
Figure 4.14: Sedimentation equilibrium profiles for WTB at (i) 1 mg/ml and (ii) 2 mg/ml.	128
Figure 4.15 Sedimentation equilibrium profiles for G13Q at (i) 1 mg/ml and (ii) 2 mg/ml.	129
Figure 4.16: Solution scattering profiles ($I(Q)$ versus Q data) for G13Q (■) and protein B' (□).	131
Figure 4.17: Vector length distribution functions ($P(r)$ functions) for G13Q (■) and protein B' (□).	132
Figure 4.18: Tapping mode AFM images of (i) G13Q and (ii) protein B'.	133
Figure 4.19: Distribution of the observed volumes of (i) protein G13Q and (ii) protein B'.	134
Figure 5.1: SDS-PAGE analysis of G13Q and recombinant <i>Ms. trichosporium</i> OB3b protein B after incubation at (i) 20 °C, (ii) 45 °C and (iii) 60 °C for 0 h, 2 h, 4 h and 6 h.	141
Figure 5.2: SDS-PAGE analysis of (i) G13Q and recombinant <i>Ms. trichosporium</i> OB3b protein B and (ii) WTB after incubation at 6 mg/ml and 0.25 mg/ml for 24 h at 20 °C.	143
Figure 5.3: sMMO propylene oxidation assays of (i) WTB, (ii) G13Q and (iii) recombinant <i>Ms. trichosporium</i> OB3b protein B after incubation at 20 °C at concentrations of 0.25 mg/ml and 6 mg/ml.	145
Figure 5.4: SDS-PAGE of G13Q incubated for 24 h in different test solutions.	150
Figure 5.5: sMMO propylene oxidation assays of G13Q after incubation in different test solutions for 0 h and 24 h at 20 °C.	151
Figure 5.6: sMMO propylene oxidation assays conducted in the presence of NaCl and MgCl ₂ at various concentrations.	152
Figure 5.7: Native-PAGE analysis of (i) G13Q, (ii) WTB and (iii) protein B' in the presence of different metals.	154
Figure 5.8: Elution profile of G13Q run on a HiTrap® copper affinity column.	157

Figure 5.9: (i) SDS and (ii) Native-PAGE analysis of copper affinity column elution fractions	158
Figure 5.10: The effect of copper on the fluorescence spectra of (i) G13Q, (ii) WTB and (iii) protein B'	160
Figure 5.11: The effect of various metals on the fluorescence spectra of (i) G13Q, (ii) WTB and (iii) protein B'	162
Figure 5.12: Copper quenching of tryptophan fluorescence at 337nm for proteins G13Q, WTB and protein B'	164
Figure 5.13: Far UV CD spectra of (i) G13Q and (ii) WTB in both the metal-free and copper-complexed state	165
Figure 6.1: Construction of <i>Mc. capsulatus</i> (Bath) protein B double mutant vector.	172
Figure 6.2: Growth curve of <i>E. coli</i> AD202 expressing M12A:G13Q mutant protein B from <i>Mc. capsulatus</i> (Bath).	174
Figure 6.3: Western blotting of whole cell lysates of <i>E. coli</i> AD202 transformed with pGEX-M12A:G13Q.	175
Figure 6.4: SDS-PAGE of the purification of M12A:G13Q protein B from <i>E. coli</i> AD202 [pGEX-M12A:G13Q].	176
Figure 6.5: ESI-MS of pure M12A:G13Q.	176
Figure 6.6: SDS-PAGE of M12A:G13Q incubated at 20 °C for 48 h.	178
Figure 6.7: SDS-PAGE of two samples of M12A:G13Q at different concentrations incubated at 20 °C for 24 h.	179
Figure 6.8: sMMO propylene oxide stability assays of M12A:G13Q at two different concentrations of 0.5 mg/ml and 6 mg/ml, incubated at 20 °C.	179
Figure 6.9: Comparison of sMMO propylene oxide stability assays of (i) proteins WTB, G13Q and M12A:G13Q at ~0.5 mg/ml and (ii) proteins WTB, G13Q and M12A:G13Q at ~6 mg/ml incubated at 20 °C.	180
Figure 6.10: The effect of the double and single mutants of <i>Mc. capsulatus</i> (Bath) protein B and WTB on the oxidation of propylene in the hydroxylase/H ₂ O ₂ system.	184
Figure 6.11: The polypeptide chains of the models of the N-terminal regions (residues 1-33) of (i) G13Q and (ii) M12A:G13Q and (iii) the structure of the N-terminal region of protein B from <i>Mc. capsulatus</i> (Bath) (Walters <i>et al.</i> , 1999).	185
Figure 6.12: (i) Far UV CD and (ii) Near UV CD spectra of M12A:G13Q compared with those for WTB and G13Q.	187
Figure 6.13: Fluorescence spectra of M12A:G13Q after incubation at 20 °C for 0 h and 24 h.	189
Figure 6.14: Far UV CD spectra of M12A:G13Q after incubation at 20 °C for 0 h and 24 h.	189
Figure 6.15: Near UV CD spectra of M12A:G13Q after incubation at 20°C for 0 h	

and 24 h.	190
Figure 7.1: Schematic illustration of the numbering of the N-terminal of <i>Mc. capsulatus</i> (Bath) protein B single mutant G13Q.	194
Figure 7.2: Schematic representation of the <i>Mc. capsulatus</i> (Bath) G13Q protein B truncates produced.	194
Figure 7.3: Schematic representation of the control elements of the pET system (adapted from Novagen pET manual).	196
Figure 7.4: Construction of vectors for the expression of <i>Mc. capsulatus</i> (Bath) protein B truncates.	197
Figure 7.5: Growth curve of <i>E. coli</i> BL21(DE3) expressing the Q13-His-tag truncate of protein B from <i>Mc. capsulatus</i> (Bath).	199
Figure 7.6: (i) SDS-PAGE and (ii) Western blotting of truncated protein B expression in <i>E. coli</i> BL21(DE3).	200
Figure 7.7: SDS-PAGE of the purification of Q13 protein B truncate from <i>E. coli</i> BL21(DE3) [pET-3a-Q13-His-tag].	202
Figure 7.8: SDS-PAGE of purified 6-His-tagged protein B truncates from the various protein B truncate clones.	203
Figure 7.9: Activities of the protein B truncates.	204
Figure 7.10: Graphical representation of the change in the stability of protein B which occurs upon N-terminal truncation of the protein	209
Figure 7.11: Size exclusion chromatography of protein B truncates.	211
Figure 7.12: Secondary structure predictions of each of the truncated proteins of protein B from <i>Mc. capsulatus</i> (Bath) using the Jpred ² program.	212
Figure 7.13: Far UV CD spectra of the Y7 and D8 truncated proteins of protein B from <i>Mc. capsulatus</i> (Bath).	213
Figure 8.1: Typical electron micrographs of negatively stained (i) hydroxylase and (ii) sMMO complex.	218
Figure 8.2: Samples of the particles selected for SPA work from (i) the micrograph of the hydroxylase and (ii) the micrograph of the sMMO complex.	219
Figure 8.3: Dendrogram representation of groups of particle averages of (i) the hydroxylase protein and (ii) the sMMO complex.	220
Figure 8.4: Electron contour maps of the hydroxylase particle averages (i) 31 (Side View) and (ii) 40 (Front View) with the crystal structure (Rosenzweig <i>et al.</i> , 1993) in the same orientation.	221
Figure 8.5: Electron contour maps of the sMMO complex displayed with the crystal structure of the hydroxylase (Rosenzweig <i>et al.</i> , 1993) in the orientation in which it is thought to be present within the complex.	222
Figure 8.6: Activity assays for the sMMO complex formed at different ratios of hydroxylase:protein B:reductase.	224
Figure 8.7: Tapping mode AFM images of (i) the hydroxylase and (ii) the sMMO complex.	226

Figure 8.8: Distribution of the observed volumes of (i) hydroxylase and (ii) sMMO samples.	227
Figure 8.9: $I(Q)$ versus Q data for sMMO and its individual components.....	230
Figure 8.10: $P(r)$ functions for sMMO and its individual components.....	232
Figure 8.11: Hydroxylase crystal structure.....	233
Figure 8.12: Titration of hydroxylase with protein B and reductase.....	234
Figure 8.13: $P(r)$ functions for the hydroxylase, sMMO complex and sMMO complex formed with protein B' instead of protein B (1:10:10 mixture of hydroxylase:protein B':reductase).	235
Figure 8.14: Proposed model for the extended hydroxylase structure.	237
Figure 8.15: Model of the interaction between the three components of sMMO..	237
Figure 9.1: Orientation of the N- and C-terminal regions of <i>Mc. capsulatus</i> (Bath) protein B as determined by NMR analysis (Walters <i>et al.</i> , 1999)....	248
Figure 9.2: Schematic representation of the main features of protein B elucidated from the results obtained in this study.....	254

List of Tables

Table 3.1: ESI-MS data for purified protein B from <i>Ms. trichosporium</i> OB3b indicating the corresponding cleavage sites.	79
Table 3.2: Extinction -coefficient data	81
Table 4.1: ESI-MS of the cleavage products of (i) wild type protein B from <i>Ms. trichosporium</i> OB3b, (ii) recombinant protein B from <i>Ms. trichosporium</i> OB3b, (iii) G13Q and (iv) WTB.....	103
Table 4.2: Sedimentation equilibrium analysis data summary	129
Table 4.3: R_g , d_{max} , and molecular volumes for proteins G13Q and protein B' ...	132
Table 5.1: ESI-MS analysis of WTB samples at (i) 0.5 mg/ml and (ii) 6 mg/ml after incubation at 20 °C for various time periods.....	147
Table 5.2: ESI-MS analysis of G13Q samples at (i) 0.5 mg/ml and (ii) 6 mg/ml after incubation at 20°C for various time periods.....	147
Table 5.3: ESI-MS analysis of recombinant <i>Ms. trichosporium</i> OB3b protein B samples at (i) 0.5 mg/ml and (ii) 6 mg/ml after incubation at 20 °C for various time periods.	148
Table 6.1: PCR amplification of <i>mmoB</i> <i>Mc. capsulatus</i> (Bath) M12A:G13Q gene for the construction of the GST fusion protein.	173
Table 6.2: ESI-MS analysis of M12A:G13Q samples at (i) 0.5 mg/ml, and (ii) 6 mg/ml after incubation at 20 °C for various time periods	182
Table 7.1: PCR amplification of <i>mmoB</i> <i>Mc. capsulatus</i> (Bath) truncate genes for the construction of C-terminal 6-His-tag fusion proteins.....	198
Table 7.2: Soluble extract assays of the truncated proteins of protein B.....	201
Table 7.3: ESI-MS analysis of the purified <i>Mc. capsulatus</i> (Bath) protein B truncates.....	203
Table 7.4: ESI-MS of the cleavage products of the different truncate proteins	206
Table 8.1: Molecular Volumes for each sMMO component.....	234

Acknowledgements

My thanks go to Prof. Howard Dalton for his supervision of this work and the Biotechnology and Biological Sciences Research Council and the Society of General Microbiology for financial support.

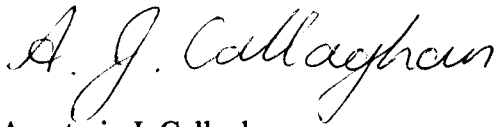
I would also like to thank Dr. Tom Smith, Dr. Claire Walker, Dr. John Lloyd, Prof. Tim Bugg, Prof. Keith Jennings, Sue Slade and Gez Chapman for guidance, useful discussions, technical advice and support during the course of this study. Particular thanks go to my collaborators for enabling me to be able to use such a wide variety of techniques in my research: Dr. Alan Wilkinson for his help with FTIR experiments; Dr. Neil Errington for assistance with analytical ultracentrifugation studies; Dr. Rob McKenna for help with protein crystallography studies; Bernie Sattin for AFM investigations; Drs. Jill Trehwella and Steve Gallagher for SAXS analysis; and Drs. Bob Ford and Mark Rosenberg for help with SPA by EM work. I would also like to thank Dr. Anne-Mette Hoberg for help with MALDI-ToF MS experiments and Sue Slade for help with ESI-MS experiments.

Special thanks go to my friends Piku, Dayo, Sue, Suki and Sarah for their encouragement and support during my time at Warwick. Ultimately this work would not have been possible without the love and care of Mam, Juliana, Alex and Lama. My unending thanks go to them.

Declaration

I declare that all of the work reported in this thesis is the result of original research conducted by myself (under the supervision of Professor H. Dalton FRS). Additional help and information, when obtained, has been referenced.

No work obtained within this thesis has been previously submitted for any other degree.

A handwritten signature in black ink, reading "A. J. Callaghan". The signature is written in a cursive style with a large, sweeping initial 'A'.

Anastasia J. Callaghan

Abbreviations

Å	Ångström
AFM	Atomic Force Microscopy
ai	arbitrary intensity
AMO	Ammonia Monooxygenase
Ap	Ampicillin
Ap ^R	Ampicillin Resistant
AMPS	Ammonium Persulphate
bp	base pairs
°C	degrees Celsius
CD	Circular Dichroism
cm	centimetre
Da	Dalton
DCM	Dichloromethane
DEAE	Diethylamino ethyl
DNA	Deoxyribonucleic acid
dNTP	déoxynucleotide triphosphate
DTT	D, L-dithiothreitol
ε	Extinction coefficient
EDTA	Ethylenediaminetetra-acetic acid
EM	Electron Microscopy
EPR	Electron Paramagnetic Resonance
ESI-MS	Electrospray Ionisation-Mass Spectrometry
EXAFS	Extended X-ray Absorption Fine Structure
FAD	Flavin-adenine dinucleotide
Fe-OH-Fe	sMMO hydroxylase diiron site
FDH	Formate Dehydrogenase
FADH	Formaldehyde Dehydrogenase
FPLC	Fast Protein Liquid Chromatography
FTIR	Fourier Transform Infrared Spectroscopy
g	gram
G13Q	recombinant <i>Methylococcus capsulatus</i> (Bath) protein B with Gly ¹³ to Gln mutation
GC	Gas Chromatography
GHz	Giga Hertz
GST	Glutathione S-transferase
h	hour
H ₂ O ₂	Hydrogen peroxide
H _{ox}	sMMO hydroxylase diiron site oxidised
H _{red}	sMMO hydroxylase diiron site reduced
Hz	Hertz
IPTG	Isopropyl β-D-thiogalactopyranoside
IR	Infrared
K or k	Thousand
kb	kilo base
kDa	kilo Daltons
kHz	kilo Hertz
kV	kilo Volts

l	litre
LB	Luria Bertani media
lb/in ²	pounds per square inch
M	Molar
mA	milli-Amps
MALDI-ToF MS	Matrix Assisted Laser Desorption Ionisation Mass Spectrometry
<i>Mb.</i>	<i>Methylobacter</i>
<i>Mc.</i>	<i>Methylococcus</i>
MCD	Magnetic Circular Dichroism
<i>Mcy.</i>	<i>Methylocystis</i>
MDH	Methanol Dehydrogenase
mg	milligram
MHz	Mega Hertz
min	minute
ml	millilitre
<i>Mm.</i>	<i>Methylomicrobium</i>
mM	millimolar
mm	millimetres
MMO	Methane Monooxygenase
mol	mole
MOPS	3-[N-Morpholino] propanesulphonic acid
MPa	Mega Pascals
<i>Ms.</i>	<i>Methylosinus</i>
m/z	mass to charge ratio
NAD/NADH	Nicotinamide Adenine Dinucleotide (oxidised/reduced)
ng	nanogram
nm	nanometres
nmol	nanomole
NMR	Nuclear Magnetic Resonance
NMS	Nitrate Minimal Salts
ns	nanoseconds
%	Percentage
OD	Optical Density
-OH	hydroxyl group
ORF	Open Reading Frame
PAGE	Polyacrylamide Gel Electrophoresis
PCR	Polymerase Chain Reaction
PEG	Polyethylene glycol
pH	hydrogen-ion concentration
pI	isoelectric point
pMMO	Particulate Methane Monooxygenase
pmol	picomole
PQQ	Pyrrloquinoline quinone
Rec. or rec.	Recombinant
RNA	Ribonucleic acid
RNR	Ribonucleotide Reductase
rpm	revolutions per minute
RuMP	Ribulose Monophosphate
s	second

SAXS	Small Angle X-ray Scattering
SDS	Sodium dodecyl sulphate
sMMO	Soluble Methane Monooxygenase
sp.	species
SPA	Single Particle Analysis
SPR	Surface Plasmon Resonance
TAE	Tris-acetate EDTA buffer
TBE	Tris-borate EDTA buffer
TBS	Tris-buffered saline
TBST	Tris-buffered saline with 0.1 % Tween 20
TEMED	<i>N, N, N', N'</i> -tetramethylethylenediamine
TESP	Tapping Mode Etched Silicon Probe
TOD	Tetrazotised-O-dianisidine
Tris	Tris-(hydroxymethyl)-aminomethane
µg	microgram
µl	microlitre
µM	micromolar
µmol	micromole
UV	Ultra Violet
v/v	concentration, volume by volume
WTB	recombinant <i>Methylococcus capsulatus</i> (Bath) protein B
w/v	concentration, weight by volume

Single and Triple Letter Codes for Amino Acids

Alanine	A	Ala
Arginine	R	Arg
Asparagine	N	Asn
Aspartate	D	Asp
Cysteine	C	Cys
Glutamate	E	Glu
Glutamine	Q	Gln
Glycine	G	Gly
Histidine	H	His
Isoleucine	I	Ile
Leucine	L	Leu
Lysine	K	Lys
Methionine	M	Met
Phenylalanine	F	Phe
Proline	P	Pro
Serine	S	Ser
Threonine	T	Thr
Tryptophan	W	Trp
Tyrosine	Y	Tyr
Valine	V	Val

Summary

The purpose of this study was to investigate the regulatory protein (protein B) and component interactions of soluble methane monooxygenase (sMMO). sMMO is a multi-component enzyme which catalyses the oxidation of methane to methanol. It consists of three proteins, a hydroxylase, a reductase and protein B (Colby and Dalton, 1978). Protein B contains no metals, cofactors or prosthetic groups and has a molecular mass of 16 kDa. It has been shown that protein B is absolutely necessary for the hydroxylase activity of the sMMO complex and is a powerful regulator of the enzyme (Green and Dalton, 1985). It has also been found that 12 amino acids are cleaved from the N-terminus of protein B from *Mc. capsulatus* (Bath) to form an inactive truncate, known as protein B' and mutation of the Met¹²-Gly¹³ cleavage site to Met¹²-Gln¹³ to give the single mutant protein G13Q, improved the stability of the protein (Lloyd *et al.*, 1997).

Much of this work has concentrated on the study of the catalytic and regulatory significance of the 12 amino acids cleaved from protein B. *Mc. capsulatus* (Bath) protein B appears to cleave autocatalytically, generating the inactive protein B' truncate. The secondary structures of proteins B and B' were seen to be the same, although the overall structure was identified as differing slightly and protein B was shown to be capable of existing in a monomer-dimer equilibrium, whereas protein B' was identified as existing in a monomer form. An homologous protein B from *Ms. trichosporium* OB3b, identified as being more α -helical in character, has been shown to be more stable than *Mc. capsulatus* (Bath) protein B but still undergoes the inactivating cleavage reaction to form truncates, although the cleavage sites differ between the two proteins.

The construction, expression and purification of N-terminal truncates of *Mc. capsulatus* (Bath) protein B identified that the presence of the first 7 amino acids was essential for protein B activity within the sMMO system and a decrease in specific activity was observed as each amino acid from 1 to 7 was lost. Upon loss of the 7th amino acid, tyrosine, the truncate protein was observed to be totally inactive and also much more prone to cleavage, but unchanged in terms of secondary structure.

Protein concentration was observed as having an effect on the stability of *Mc. capsulatus* (Bath) protein B and the single mutant G13Q, with increased concentrations improving stability. This effect was not observed for the double mutant M12A:G13Q, although it was shown to be more stable than the other proteins under more dilute conditions. The addition of a magnesium salt also improved the stability of protein B.

Studies into the interactions of protein B with the other proteins within the sMMO complex have also been performed. Evidence that the hydroxylase undergoes a large conformational change upon the binding of the reductase and protein B has been obtained and modelled to suggest that one trimer of the hydroxylase dimer rotates by 180° relative to the other upon complex formation. It also showed the sMMO complex to form in a stoichiometry of 1:2:2 hydroxylase:reductase:protein B. Other data suggest that sMMO component binding occurs on only one trimer of the hydroxylase dimer under different conditions.

Chapter 1

Introduction

1.1 Methane to Methanol Conversion

Methane is a colourless, odourless gas with a boiling point of $-164\text{ }^{\circ}\text{C}$ and is the most abundant organic gas in the atmosphere (Crutzen, 1991). Over the past 300 years, as a consequence of human activity, atmospheric methane levels have increased. Terrestrial radiation in the infrared region is absorbed by atmospheric methane, with the re-emission of the absorbed radiant energy causing global warming. Because methane absorbs the radiation more efficiently than carbon dioxide, it is estimated to contribute about 26 times that of carbon dioxide (mole for mole) to climatic change (Lelieveld *et al.*, 1993). Therefore, a reduction in atmospheric methane concentrations is important in reducing the global warming effect (Hogan *et al.*, 1991). Bacteria that can utilise methane provide a means of removing it from the environment, although it is necessary to define the sources and sinks of environmental methane in order to identify accurately which steps have practical value in reducing the effects of global warming (Hanson and Hanson, 1996).

Methane is the chief constituent of natural gas. Chemically, it is fairly inert and thus its activation has attracted increased attention in recent years because of its scientific and industrial importance as a source of chemicals and fuels. In particular, the conversion of methane to methanol is of great interest as an important energy source for the 21st century to replace projected dwindling petroleum reserves (Yoshizawa *et al.*, 1998). Current chemical methods for the conversion of methane to methanol involves indirect processes which are energy intensive and often result in other oxidation products besides methanol being formed (Gesser *et al.*, 1985). For, example, most chemicals derived from methane, including methanol, are indirectly converted via a syngas intermediate. Thus, methane and water are converted to carbon monoxide and hydrogen based on high temperature ($700\text{-}900\text{ }^{\circ}\text{C}$) energy intensive processes. Several other catalytic steps are then required to convert the

syngas intermediate, the carbon monoxide and hydrogen mixture, into methanol (Dalton, 1991). The use of Hg(II) to catalyse the selective oxidation of methane to methanol was described by Periana *et al.* (1993). The reaction was shown to occur at 180 °C with reagents that could be used on a large scale. However, a yield of only 40 % was achieved and carbon dioxide was produced as the main side product. Therefore, the methane monooxygenase (MMO) enzyme, for which is observed the direct oxidation of methane at ambient temperature and pressure with 100 % selectivity of methanol as the product, provides an ideal model for the development of direct methane oxidation catalysts (Dalton, 1992).

The conversion of methane into more valuable chemical products has also been well researched (Cover and Peterson, 1988; Green and Ramanathan, 1988). Methane can be chemically converted to produce base, intermediate and fine chemicals. In some cases the conversion process is direct, such as in the production of halomethane, hydrogen cyanide and acetylene, in which methane is activated either at very high temperatures or by the halogen radicals, but in many cases it is much more complicated. Although much research has focused on developing a convenient chemical method for converting methane into other useful organic chemicals, none has been significantly successful. Methane is the end product of degradation of most organic materials. Thus there is a need to be able to use this resource. The discovery of the unique abilities of the MMOs of methane-utilising bacteria to catalyse reactions of such commercial and environmental importance has opened up a whole new field for scientific research.

1.2 Methane Utilising Bacteria

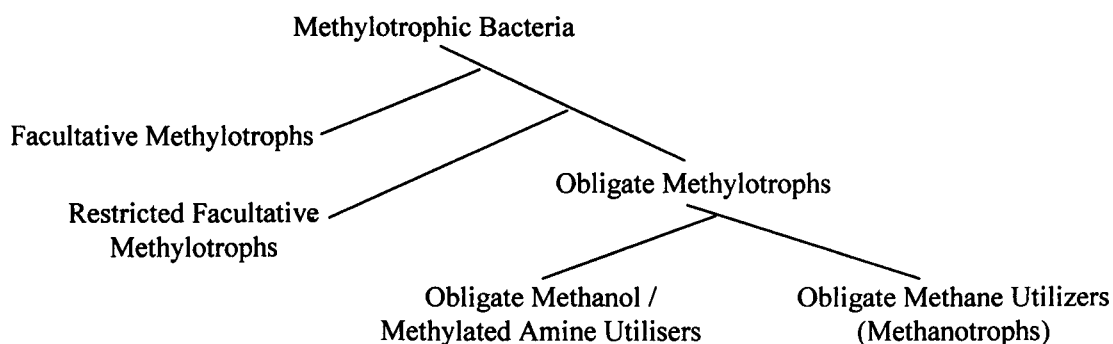
1.2.1 Methylotrophic Bacteria

The first methylotrophic bacterium was identified by Leow in 1892 (Quayle, 1987). Since then, many methylotrophic bacteria have been isolated and characterised. Methylotrophic bacteria are a diverse group of microorganisms that have the common ability to generate energy by the utilisation of one-carbon (C₁) compounds

for growth. The C₁ primary substrate can take the form of methane, methanol, formic acid, methylamines, carbon monoxide, cyanide or methylated sulphur species. (Colby and Zatman, 1973). Sub-divisions of the major genera of methylotrophic bacteria are as shown in Figure 1.1.

Figure 1.1: Sub-divisions of the major genera of methylotrophic bacteria.

Adapted from Green (1992).



The facultative methylotrophs have the ability to be able to grow on multicarbon substrates, whereas the restricted facultative methylotrophs can only utilise a narrow range of these compounds. In contrast, however, obligate methylotrophs can only grow on C₁ compounds as their sole carbon and energy source (Colby *et al.*, 1979). These bacteria are rod shaped Gram-negative organisms and can be sub-divided into the methanol/methylated amine utilisers and the methane utilisers, which can also grow on limited amounts of methanol and are known as Methanotrophs.

1.2.2 Methanotrophic Bacteria

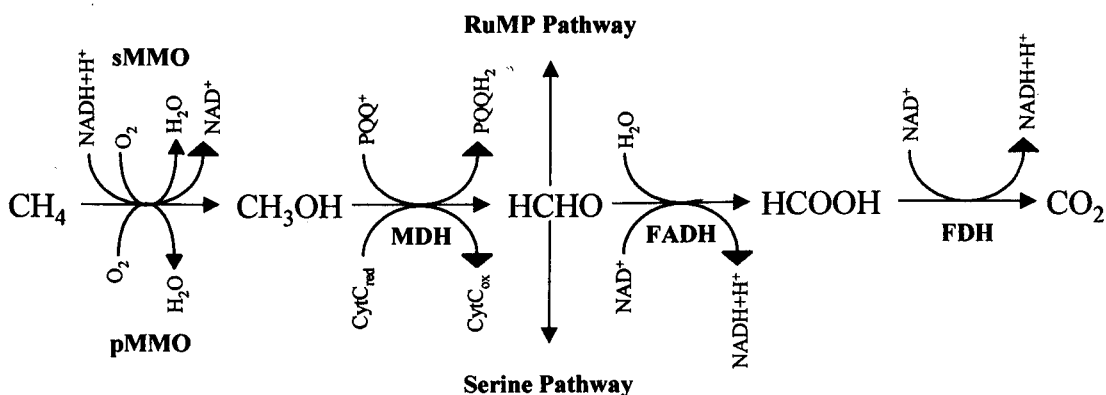
The first methanotrophic bacterium was isolated in 1906 by Sohngen (Quayle, 1972). Further isolation and characterisation studies were conducted by Whittenbury *et al.* (1970) and led to over 100 different strains being identified. Analysis of their morphology, resting structures, intracytoplasmic structures and physiological characteristics formed the basis for the current classification schemes. The generic groups identified included *Methylomonas* (*Mm.*), *Methylobacter* (*Mb.*), *Methylococcus* (*Mc.*), *Methylocystis* (*Mcy.*), and *Methylosinus* (*Ms.*) (Whittenbury

and Dalton, 1981) and the recent addition of the new genus *Methylomicrobium* (*Mm.*) (Bowman *et al.*, 1993, 1995). These organisms can be further subdivided into Type I, Type II, and Type X organisms based on various characteristics including DNA base composition, and the major carbon assimilation pathway. Type II organisms, *Ms.* and *Mcy.*, utilise the serine pathway to assimilate formaldehyde (Lawrence and Quayle, 1970), whereas Type I, *Mm.* and *Mb.*, and Type X, *Mc.*, organisms assimilate formaldehyde via the ribulose monophosphate (RuMP) pathway. Type X methanotrophs are distinguishable from the Type I organisms as they possess, amongst other differences, DNA with a higher mol % G + C content (Green, 1992; Hanson and Hanson, 1996).

A defining characteristic of methanotrophs is their use of enzymes known as methane monoxygenases (MMOs) to catalyse the oxidation of methane to methanol. The methanol is then further oxidised to formaldehyde, catalysed by a second enzyme known as methanol dehydrogenase (MDH). The formaldehyde can then either be assimilated into cellular biomass or further oxidised by the enzymes formaldehyde dehydrogenase (FADH) and formate dehydrogenase to carbon dioxide (CO₂). Figure 1.2 illustrates the methane oxidation pathway.

Figure 1.2: Pathway of methane oxidation.

The enzymes catalysing the reactions are: sMMO, soluble methane monoxygenase; pMMO, particulate methane monoxygenase; MDH, methanol dehydrogenase; FADH, formaldehyde dehydrogenase; and FDH, formate dehydrogenase. [Modified from Hanson and Hanson, (1996)].



1.3 Methane Monooxygenase

The oxidation of methane to methanol occurs efficiently when catalysed enzymatically by methane monooxygenase (MMO), the first enzyme in the methane oxidation pathway of methanotrophs (Lipscomb, 1994; Wallar and Lipscomb, 1996). Leadbetter and Foster (1959) first proposed the involvement of an oxygenase enzyme in the initial attack on methane by methanotrophs, based on the incorporation of ^{18}O from $^{18}\text{O}_2$ into its cellular biomass. Observations of methane oxidation catalysed by cell extracts of some methanotrophs suggested that a monooxygenase, which catalysed the incorporation of one oxygen atom into the substrate, was the form of the oxygenase responsible for methane oxygenation (Ribbons and Michalover, 1970; Ferenci, 1974). Colby *et al.* 1975, devised a convenient and rapid method for assaying for MMO in which the disappearance of bromomethane, a soluble derivative of methane and substrate analogue, was monitored via gas chromatography. Further studies (Colby and Dalton, 1976) confirmed that MMO activity could also be measured by monitoring for methanol accumulation using the same technique and in 1977 it was reported that propylene could also be oxidised by MMO, forming epoxypropane, which could be similarly monitored by gas chromatography. Epoxypropane was not susceptible to further oxidation by MMO and, therefore, monitoring epoxypropane formation has become the standard method for the monitoring of MMO activity (Colby *et al.*, 1977).

Studies of MMO from several methanotrophs during the 1970s revealed that the enzyme existed in two forms differing in cellular location. Particulate MMO (pMMO) is membrane-associated and thus enzyme activity is identified in the cellular membrane fraction of the cell free extracts. Soluble MMO (sMMO) is identified in the cytosolic fraction of the cell free extracts (Colby *et al.*, 1975; Ferenci *et al.*, 1975; Tonge *et al.*, 1975; 1977; Patel *et al.*, 1979; Dalton *et al.*, 1984).

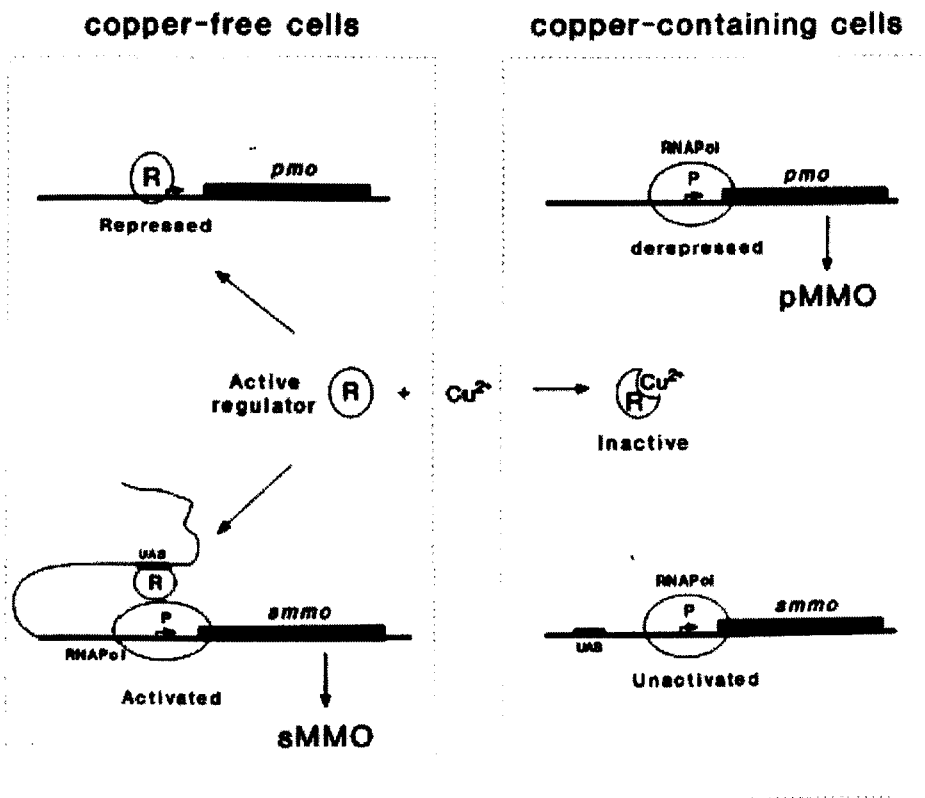
1.4 Regulation of MMO Expression

The determination of the form of MMO expressed is as a response to different copper-to-biomass ratios achieved under different growth conditions (Stanley *et al.*, 1983). sMMO is expressed at low copper-to-biomass ratios, whereas pMMO is expressed at higher ratios. The presence of a copper-regulated promoter was subsequently proposed to be involved (Neilsen *et al.*, 1996). In both *Mc. capsulatus* (Bath) and *Ms. trichosporium* OB3b transcription of the sMMO gene cluster was seen to be negatively regulated by copper ions and data suggested that transcription was directed from a σ^{54} -like and σ^{70} -like promoter, both regulated by copper ions. The synthesis of polycistronic mRNA transcribed from the pMMO genes was identified as being activated by copper ions and this was concomitant with repression of sMMO gene transcription (Neilsen *et al.*, 1997). A hypothetical model for the transcriptional regulation of MMO genes was therefore proposed (Figure 1.3).

The expression of sMMO genes was proposed to be subject to positive control, such that copper ions would regulate sMMO expression by inactivation of an, as yet, unidentified activator protein. In copper-free cells, transcription of pMMO genes would be repressed by the binding of a regulator to the pMMO operator. Transcription of sMMO genes would be brought about by the binding of the same (or another) regulator to the activator sequence upstream of the sMMO promoter. In copper-containing cells, copper ions would bind to the regulator, inducing a conformational change preventing it from binding to the pMMO promoter, resulting in transcription of the pMMO genes whilst transcription of the sMMO genes was repressed.

Figure 1.3: Model for the copper-dependent transcriptional regulation of pMMO and sMMO genes.

pMMO and sMMO genes are indicated by the black boxes labelled *pmo* and *smmo* respectively. The putative promoter regions are labelled P. In copper-free cells the regulator protein, labelled R, binds to the *pmo* operator and represses its transcription. The same, or another regulator protein, also labelled R, binds to an upstream activator site, labelled UAS, 5' of the *smmo* promoter and contacts the RNA polymerase, labelled RNAPol, leading to the *smmo* genes being transcribed. In copper-containing cells, copper-binding to the regulator protein induces a conformational change in the protein preventing its binding to the *pmo* promoter or the *smmo* UAS. This leads to derepression and the subsequent transcription of the *pmo* genes and the *smmo* genes become unactivated. [Reproduced from Neilsen *et al.* (1997), with permission.]



1.5 Particulate Methane Monooxygenase (pMMO)

The particulate membrane associated methane monooxygenase (pMMO) is present in all known methanotrophs. In methanotrophs capable of sMMO and pMMO expression, pMMO appears to be produced at the same time as the extensive formation of membranes is observed when cells are grown in copper containing media. Under copper limitation the internal membranes are observed as being fewer

in number and less well organised in nature and also the sMMO enzyme is produced. However, it still remains unclear whether these two events are interrelated or not (Prior and Dalton, 1985). The ability to switch from particulate to soluble MMO during copper limitation conditions is advantageous to the organisms. Methanotrophs that only express pMMO, such as *Methylomonas album* BG8, are incapable of avoiding copper stress and so these organisms experience copper limited growth at a cell density dependent on the available copper concentration (Dalton *et al.*, 1984). Three new polypeptides are observed in membrane fractions of *Mc. capsulatus* (Bath) cells switched from sMMO to pMMO expression. Their apparent molecular masses are 45, 35, and 26 kDa and, therefore, they are proposed to be involved in pMMO activity (Stanley *et al.*, 1983).

The purification of pMMO has proved to be particularly problematic. Tonge *et al.* (1975) reported that pMMO from *Ms. trichosporium* OB3b could be resolved from the membrane using a variety of techniques including detergent treatment and sonication, although subsequent attempts to solubilise pMMO from the membranes proved unsuccessful (Burrows *et al.*, 1984). Work by Smith and Dalton (1989) achieved pMMO activity after solubilisation of the enzyme from *Mc. capsulatus* (Bath) using the non-ionic detergent dodecyl- β -D-maltoside and treatment with either egg or soybean lipids. Further purification of the protein into its component polypeptides was unsuccessful and complete enzyme activity was lost. Recently work by Zahn and DiSpirito (1996) and Nguyen *et al.* (1998) has provided procedures for the solubilisation and isolation of pMMO from *Mc. capsulatus* (Bath) and identified the active polypeptides as having molecular masses of 47, 27, and 25 kDa. Acetylene has been identified as a suicide substrate of pMMO (Prior and Dalton, 1985) and the 27 kDa polypeptide was identified as the acetylene-binding protein. The active enzyme complex was shown to contain 2.5 iron atoms and 14.5 copper atoms per 99 kDa (Zahn and DiSpirito, 1996). However, Nguyen *et al.* (1998) found pMMO to be a copper-containing protein only, which showed a requirement for Cu(I) ions.

pMMO has been shown to be capable of functioning with several electron donors including NADH, ethanol and succinate (Stanley *et al.*, 1983). More recently, studies

by Shiemke *et al.* (1995) have suggested that the enzyme obtains reducing equivalents directly from quinol (probably plastoquinol) *in vivo* and Zahn and DiSpirito (1996) identified pMMO as containing non-stoichiometric concentrations of cytochrome b-559/569, which, it is suggested, could function as the initial electron donor. The range of substrates that pMMO will oxidise is limited to a number of alkanes and alkenes of up to 4 carbons only or less and suggests pMMO has a rather restricted active site (Smith and Dalton, 1989).

The mixed reports about pMMO present conflicting information and have created confusion concerning the nature of the complex, particularly the discrepancies between the findings of Zahn and DiSpirito (1996) and Nugyen *et al.* (1998) regarding the composition of the active site metal(s). Work by Semrau *et al.* (1995) succeeded in cloning and sequencing genes from *Mc. capsulatus* (Bath) that encode polypeptides proposed to be the 45 and 27 kDa subunits of pMMO, known as *pmoA* and *pmoB* respectively, and have a high similarity to the subunits of ammonia monooxygenase (AMO), implying that the enzymes are related. The work also suggested that the two genes were present in duplicate copies and that the duplicate genes were closely related in DNA sequence. Costello *et al.* (1995) identified a third open reading frame, designated *pmoC*, which encodes the 25 kDa polypeptide of pMMO, and was also present in duplicate copies. This raises the possibility that two different copies of pMMO could be present in methanotrophs and might be expressed differentially depending upon cellular needs (Lidstrom and Semrau, 1995). Nevertheless, these genetic findings along with the biochemical information available for the enzyme itself show pMMO and sMMO to be genetically and structurally distinct.

1.6 Soluble Methane Monooxygenase (sMMO)

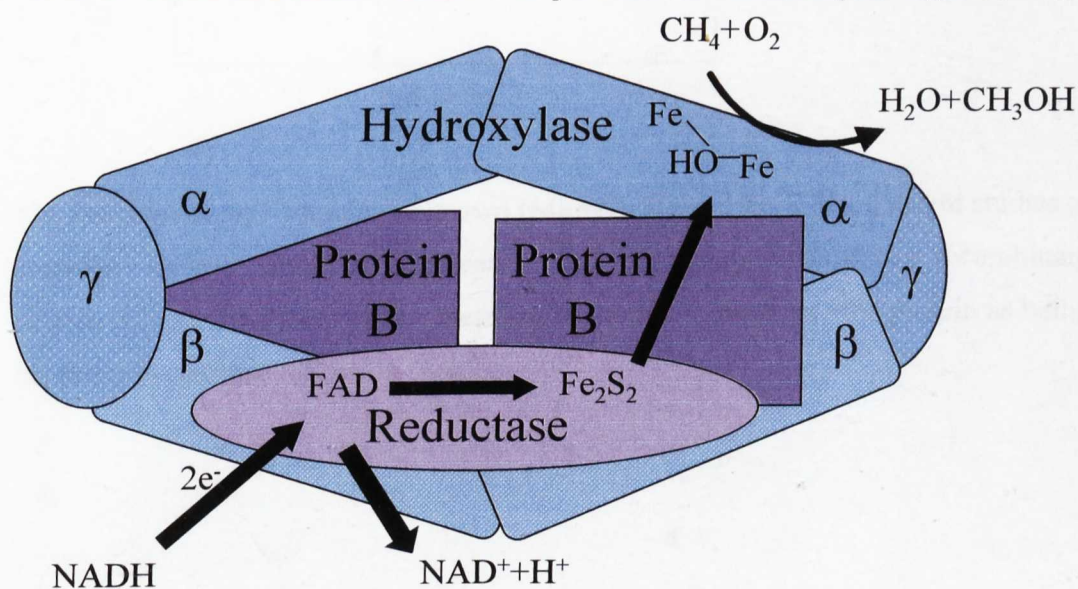
sMMO was first identified by Colby and Dalton in 1976. The work demonstrated that that supernatant from a cell free extract of *Mc. capsulatus* (Bath) catalysed the NADH and O₂-dependent oxidation of methane. They further identified the multi-component nature of the enzyme system by resolving the extract into two fractions

by ion exchange chromatography, both of which were essential for reconstitution of activity. sMMO was demonstrated to have a very broad substrate range and to be capable of catalysing a number of different oxygen incorporation reactions (Colby *et al.*, 1977).

sMMO was first purified from *Mc. capsulatus* (Bath) by Colby and Dalton (1978). Since then sMMO has been purified from various methanotrophs including *Methylobacterium* sp. CRL-26 (Patel and Savas, 1987), *Ms. sporium* 5 (Pilkington and Dalton, 1991), *Methylocystis* sp. Strain M (Nakajima *et al.*, 1992) and *Ms. trichosporium* OB3b (Fox *et al.*, 1989). sMMO has been shown to consist of three distinct component proteins known as the hydroxylase (formally protein A), the regulatory protein which is also known as protein B, and the reductase (formally protein C) (Figure 1.4). Interestingly, the sMMO from *Methylobacterium* sp. Strain CRL-26 does not appear to contain the protein B component (Patel and Savas, 1987).

Figure 1.4: Schematic model of sMMO.

The hydroxylase is shown in blue, reductase in mauve and protein B in purple. α , β and γ refer to the subunits of the hydroxylase. Fe-OH-Fe represents the di-iron site at the active site of the hydroxylase. The arrows indicate the direction of electron flow. [Modified from Rosenzweig and Lippard, (1994)].



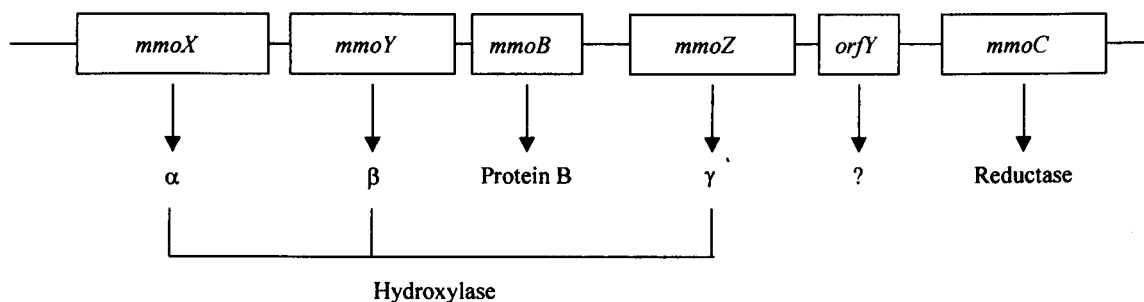
The hydroxylase is a large non-haem iron containing protein comprising six subunits, forming an $\alpha_2\beta_2\gamma_2$ arrangement. The reductase is a single subunit protein and contains one flavin adenine dinucleotide (FAD) and one Fe_2S_2 (iron-sulphur)

centre per molecule. Protein B is similarly a single subunit protein but contains no metals, cofactors or prosthetic groups.

The identification and cloning of the structural genes of sMMO have given complete sequence information for the hydroxylase, reductase and protein B from *Mc. capsulatus* (Bath), *Ms. trichosporium* OB3b and *Methylocystis* sp. Strain M (Stainthorpe *et al.*, 1989, 1990; Cardy *et al.*, 1991a, 1991b; McDonald *et al.*, 1997). DNA sequencing of the sMMO operon revealed that the genes encoding the α , β and γ subunits of the hydroxylase (known as *mmoX*, *mmoY* and *mmoZ* respectively), protein B (known as *mmoB*) and the reductase (known as *mmoC*) are all linked on the chromosome (Figure 1.5).

Figure 1.5: Schematic arrangement of the sMMO operon.

Details are shown of the proteins encoded by the various genes. [Modified from Murrell (1992)].



The function of *orfY* remains unknown (Murrell, 1992, 1994). More recent studies to elucidate its role involved purification and characterisation of the recombinant protein (Lloyd, 1997). However, these studies failed to implicate the protein as being involved in methane oxidation.

1.6.1 The Hydroxylase Component

The purification and characterisation of the hydroxylase component of sMMO from *Mc. capsulatus* (Bath) was first achieved by Woodland and Dalton (1984). It was identified as having a molecular mass of approximately 210 kDa and being comprised of three subunits α , β , and γ of 54, 42 and 17 kDa respectively. These were present in stoichiometric amounts suggesting an $\alpha_2\beta_2\gamma_2$ arrangement. The studies also revealed the presence of 2 moles of non-haem iron per mole of protein. Similarly, the hydroxylase component of *Ms. trichosporium* OB3b comprises three subunits α , β , and γ of 54, 43 and 23 kDa respectively, arranged in an $\alpha_2\beta_2\gamma_2$ configuration, forming a complex of about 245 kDa (Fox *et al.*, 1989). However, the protein was calculated as containing 4.3 moles of non-haem iron per mole protein. The hydroxylase proteins of the sMMO systems of *Methylobacterium* sp. CRL-26 (Patel and Savas, 1987), *Methylosinus sporium* 5 (Pilkington and Dalton, 1991), *Methylomonas* GYJ3 (Liu *et al.*, 1991) and *Methylocystis* sp. M (Nakajima *et al.*, 1992) have been observed as exhibiting the same $\alpha_2\beta_2\gamma_2$ subunit structure, and the iron content in the first three was identified as being the same as that in *Mc. capsulatus* (Bath) hydroxylase, whereas the latter gave an iron content similar to that reported for *Ms. trichosporium* OB3b. Interestingly, a direct correlation between the amount of iron in the protein and its specific activity was noted (Dalton, 1992). The difference in iron content could therefore be a reflection of varying extents of iron loss occurring during the purification procedure of the hydroxylase.

1.6.1.1 The Nature of the Iron Site

The requirement of iron for catalysis was illustrated by the reactivation of iron-depleted hydroxylase upon the addition of iron-EDTA and DTT (Green and Dalton, 1988). Work by Atta *et al.* (1993) illustrated that Mn(II) could be incorporated into the apo-hydroxylase of *Mc. capsulatus* (Bath), although this gave rise to inactive hydroxylase. Nevertheless, it was concluded that two Mn(II) ions had been incorporated and two Fe(II) ions lost per mole protein, suggesting that hydroxylase contained a single di-iron site. Interestingly, only iron could re-introduce functionality to the iron-depleted protein; neither Ni(II), Co(II), Zn(II), Mo(VI), nor

V(III) could give rise to active protein (Green and Dalton, 1988). This emphasised the importance of the iron atoms being essential for the functioning of the hydroxylase of sMMO. Furthermore, *in vitro* translation of total RNA isolated from *Mc. capsulatus* (Bath) produced hydroxylase subunits with molecular masses equal to the wild-type suggesting no post translational processing occurred, but they were inactive within the sMMO system. Functionally-active protein was only obtained upon the addition of iron to the translated hydroxylase. This suggested that the subunits of the hydroxylase were synthesised in their native form and self-assembled into an apo-protein into which iron was inserted (Green and Dalton, 1988).

Woodland and Dalton (1984) used electron paramagnetic resonance (EPR) to show that the hydroxylase contained Fe(III) and that Fe(II) could be identified upon reduction with DTT. This illustrated that sMMO contained a novel iron-containing prosthetic group. EPR evidence by Woodland *et al.* (1986) provided the first evidence that the two iron atoms within the proteins were coupled via a μ -oxo bridge. Extended x-ray absorption fine structure (EXAFS) confirmed the presence of a μ -oxo binuclear-type bridge structure in the hydroxylase of *Mc. capsulatus* (Bath) (Ericsson *et al.*, 1988). This was also confirmed to be the case for the hydroxylase of *Ms. trichosporium* OB3b (Fox *et al.*, 1988) for which the technique of Mössbauer was also used. This remains an unusual finding for an oxygenase, as similar structures have only been reported in hemerythrin (Wilkins and Wilkins, 1987), purple acid phosphatase (Que and True, 1990) and ribonucleotide reductase (RNR) (Nordlund *et al.*, 1990), all of which have quite different functions (Wilkins, 1992). In hemerythrin, the di-iron centre is involved in oxygen transport and storage (Wilkins and Wilkins, 1987), whereas in ribonucleotide reductase (RNR) R2-protein the di-iron centre and oxygen generate a tyrosyl radical that is involved in the reduction of ribonucleoside diphosphate to deoxyribonucleoside diphosphate for DNA synthesis (Stubbe, 1990). The di-iron site in purple acid phosphatase is thought to be the catalytic site for phosphate ester hydrolysis (Doi *et al.*, 1988). A proton electron nuclear double resonance (ENDOR) study finally identified the nature of the monoatomic bridge in the mixed valent di-iron centre of the hydroxylase of *Mc. capsulatus* (Bath) as a hydroxo-bridge. It was suggested that this was probably also present in the oxidised hydroxylase (DeRose *et al.*, 1993). Similar experiments for

the hydroxylase of *Ms. trichosporium* OB3b gave the same result (Thomonn *et al.*, 1993).

The iron atoms at the active site can exist in one of three states; oxidised Fe(III)/Fe(III), half-reduced Fe(II)/Fe(III) or fully reduced Fe(II)/Fe(II). The native hydroxylase was EPR silent, whereas the mixed valent state was EPR active. Studies indicated that the mixed valent state was unreactive towards oxygen, whereas the fully reduced state interacts with oxygen, returning the enzyme to its oxidised state (Woodland *et al.*, 1986; Fox *et al.*, 1988; Dalton, 1992). Single turnover experiments have also been used to show that chemically reduced hydroxylase is able to effect the oxidation of the MMO substrates propane and propene (Fox *et al.*, 1988).

1.6.1.2 Sequence Studies

Comparisons of the deduced amino acid sequences for the sMMO proteins of the hydroxylase from *Mc capsulatus* (Bath), *Ms. trichosporium* OB3b and *Mcy. sp.* Strain M showed the α -subunit to exhibit the highest sequence similarity (88.9 - 97.3 %) and identity (80.2 - 95.4 %) among the three methanotrophs (McDonald *et al.*, 1997). Amino acid sequence homologies further revealed that the active site structures of the hydroxylases of the sMMO systems were similar to the R2 subunit of ribonucleotide reductase. A sequence motif of Glu-X-X-His was shown to coordinate the ions within the binuclear iron-binding site of the R2 subunit of the protein by X-ray crystallography (Nordlund *et al.*, 1990). The α -subunits of the hydroxylase were identified as having the same sequence motif implying the principle ligands of the di-iron centres to be similar and that the active site resides on the α -subunit. This result was in agreement with the studies of Prior and Dalton (1985) where it had been shown that the ketene product formed from radioactive acetylene, a suicide substrate for sMMO, closely associated with the α -subunit of the hydroxylase. The sequence homology work was further used to create a model of the active site structure based on that of RNR, which was later verified by X-ray structure analysis (Figure 1.13). It identified the principal ligands at the active site and was consistent with the findings that two histidine ligands were present (DeWitt *et al.*, 1991; Smith and Dalton, 1992).

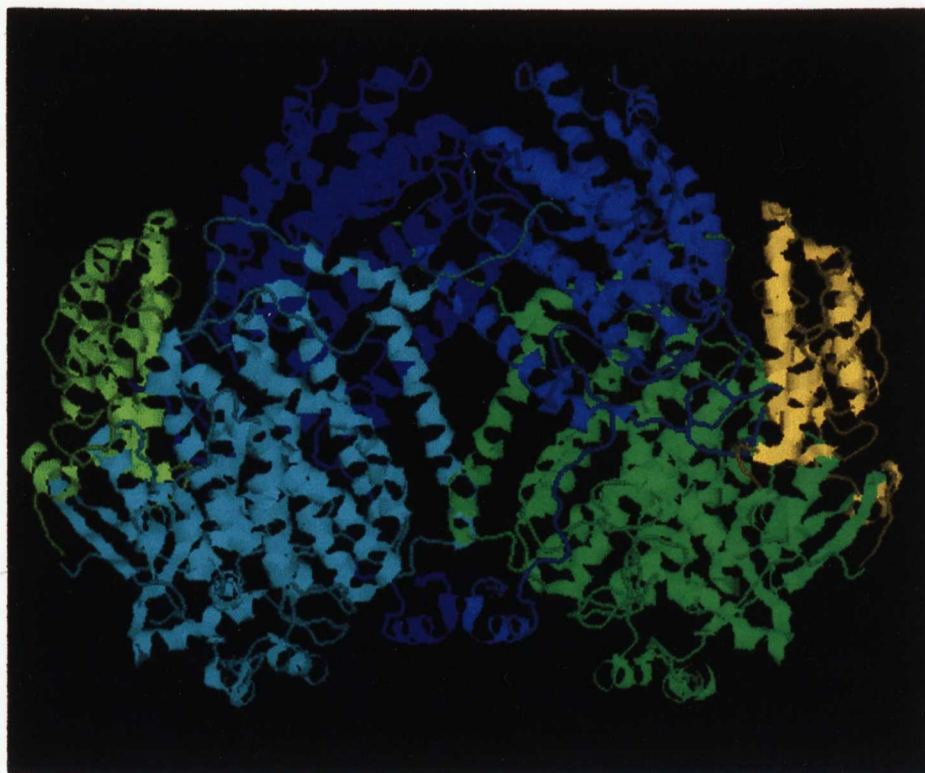
Circular dichroism (CD) studies by Smith and Dalton (1992) suggested the hydroxylase to have a high α -helical content, a result which supported the prediction that the di-iron site was situated in a four helix bundle, based on the RNR structure. A further model proposed the arrangement of the three subunits of the hydroxylase based on chemical cross-linking studies. No cross-linking was observed for the γ subunits, only cross-linking products of the α and β subunits and a dimer of the β subunits were identified (Fox *et al.*, 1991).

1.6.1.3 Crystal Structure

The crystal structure of the hydroxylase of *Mc. capsulatus* (Bath) was determined in 1993 by Rosenzweig *et al.* (Figure 1.6) and a few years later the structure of the hydroxylase from *Ms. trichosporium* OB3b was also elucidated (Elango *et al.*, 1997). The structures were found to be very similar and were in agreement with the previous structural studies and models of the two proteins.

Figure 1.6: Structure of the hydroxylase from *Mc. capsulatus* (Bath) at 2.2 Å resolution (Rosenzweig *et al.*, 1993).

The subunits are as follows: α are pale blue and green coloured, β are royal blue and mid-blue coloured and γ are yellow-green and yellow coloured.



The two $\alpha\beta$ protomers were found to be related by a two-fold symmetry axis with a wide canyon running along the dimer interface and an opening in the centre of the molecule. The structure illustrates there to be two di-iron sites, one on each of the α -subunits. The three subunits were determined to be primarily α -helical in secondary structure with a small region of β -structure in the α -subunit. Interactions between the two protomers involve helices from the α and β subunits with no participation from the two γ subunits. The structure also revealed the possible binding sites for the regulatory protein B and the reductase as being in the extended canyon formed between the $\alpha\beta$ pairs of the dimer. Two of the iron-binding helices are exposed in this canyon and could interact with the coupling protein resulting in a conformational change near the active site. The structure also reveals a cavity at the iron centre where the two iron atoms and the coordinating ligands are located on one internal surface of the cavity and the rest is filled with the hydrophobic side chain residues; Ile²¹⁷, Ile²³⁹, Phe²³⁶, Leu¹¹⁰, Phe¹⁸⁸, Ala¹¹⁷, Phe¹⁹², Leu²⁰⁴; and Gly²⁰⁸, with the exception of Thr²¹³. This is ideal for binding the non-polar substrate, methane, and is close to the di-iron core where dioxygen is activated (Rosenzweig *et al.*, 1993). This proposal was verified by the findings of George *et al.* (1996) where computational investigation of the possible substrate binding sites identified methane as binding to the hydrophobic residues described. However, no direct path to the active site exists from the surface of the protein, but hydrophobic pockets occur in the α -subunit leading to the catalytic centre, which may provide a route for substrate access to the di-iron site (Rosenzweig *et al.*, 1993).

1.6.1.4 Activation by Hydrogen Peroxide

The catalysis of oxidation of methane and other sMMO substrates can occur via the activation of the hydroxylase by hydrogen peroxide. In the normal sMMO reaction protein B, the reductase, oxygen and NADH are required for catalytic activity, but can be replaced by hydrogen peroxide which serves as a source of both oxygen and electrons for the reaction. The 'peroxide shunt' mechanism has been observed to occur for the hydroxylases of both *Mc. capsulatus* (Bath) (Jiang *et al.*, 1993) and *Ms. trichosporium* OB3b (Andersson *et al.*, 1991). Interestingly, protein B was found to

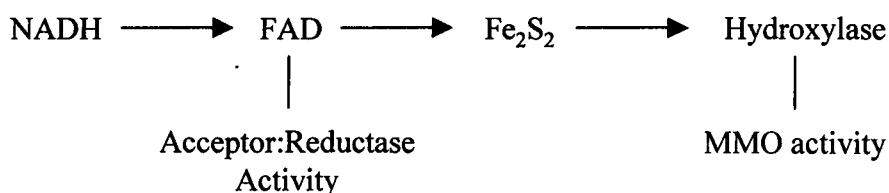
affect the selectivity of C-hydroxylation for the hydroxylase functioning via the peroxide shunt reaction. It was also observed to be an inhibitor of the hydroxylase/hydrogen peroxide system (Jiang *et al.*, 1993) (See also Section 1.6.3).

1.6.2 The Reductase Component

The isolation of the reductase component, previously named Protein C, was first accomplished in 1978 by Colby and Dalton and identified as the protein responsible for electron transport from NADH to the hydroxylase. It was found to be very unstable unless kept in the presence of reducing agents such as thioglycollate or dithiothreitol. The protein was identified as a single subunit protein of 38.5 kDa and contained, per molecule, an FAD group identified from its absorption and fluorescence spectra and by thin layer chromatography (Colby and Dalton, 1979) and an Fe_2S_2 cluster confirmed by its absorbance and EPR spectra (Lund and Dalton, 1985) and Mössbauer spectroscopy (Solomon *et al.*, 2000). Experiments involving the removal and reconstitution of the redox centres of the reductase suggested a correlation between the presence of the FAD and Fe_2S_2 redox centres and NADH acceptor : reductase activity and MMO activity respectively. The FAD redox centre was identified as interacting directly with NADH and the Fe_2S_2 centre was not required for its oxidation. However, the Fe_2S_2 centre was shown to be required for MMO activity, as it was observed as being necessary for electron transfer from the reductase to the hydroxylase component (Lund *et al.*, 1985). Therefore, the pathway of electron flow between NADH and the two redox centres was identified, as shown in Figure 1.7.

Figure 1.7: Order of electron flow from the reductase to the hydroxylase.

FAD and Fe_2S_2 are the redox centres of the reductase. The arrows indicate the order or electron flow. [Modified from Lund *et al.* (1985)].



Work by Green and Dalton (1989) illustrated that the reductase undergoes a $3e^-1e^-$ catalytic cycle. Initially, the FAD centre is fully reduced by the addition of 2 electrons from NADH. The electrons are then transferred singly to the Fe_2S_2 centre, which is only capable of carrying one electron at a time and provides single constant-potential electrons to the acceptor, the hydroxylase component (Lund and Dalton 1985; Lund *et al.*, 1985).

Copper, which plays a fundamental role in the regulation of MMO, has been shown to inhibit the reductase by causing the loss of the Fe_2S_2 , thus preventing transfer of electrons from the reductase to the hydroxylase. At higher concentrations the FAD centre was rendered inactive as observed by the loss of NADH : acceptor reductase activity (Green *et al.*, 1985). Increased copper levels induce expression of the energetically more favourable pMMO and through interaction with the reductase irreversibly inhibits the less efficient sMMO (Colby and Dalton, 1979; Green *et al.*, 1985). This, therefore, provides the organism with a rapid method of switching to a more efficient growth pattern in response to a change in environmental conditions (Green *et al.*, 1985).

The reductase has been shown to be present at only 10 % of the molar concentration of the other sMMO components (Fox *et al.*, 1989; Liu *et al.*, 1997). It has been shown to be capable of transferring electrons to several hydroxylase molecules in the time it takes the hydroxylase to complete a single turnover. This has been suggested to be the reason for the low levels of the reductase present as one molecule can activate many hydroxylase molecules (Gassner and Lippard, 1999).

The reductase component has been purified from a number of sMMO systems, including those of *Ms. trichosporium* OB3b (Fox *et al.*, 1989), *Methylobacterium* sp. CRL-26 (Patel and Savas, 1987), *Methylosinus sporium* strain 5 (Pilkington and Dalton, 1991) and *Methylocystis* sp. M (Nakajima *et al.*, 1992). They have all been found to be very similar containing an FAD and Fe_2S_2 cluster and having molecular weights between 38-40 kDa.

The reductase from *Ms. trichosporium* OB3b has been shown to bind to the β subunit of the hydroxylase (Fox *et al.*, 1991). The reductase from *Mc. capsulatus* (Bath) has been identified as having a binding site on domain 2 of the α subunit of the hydroxylase. Modelling studies proposed that binding to this region would result in the reductase also contacting the β subunit of the hydroxylase (Rosenzweig *et al.*, 1997). Regulatory functions have also been proposed for the reductase in addition to its role as an electron supplier (Liu *et al.*, 1997). Work by Froland *et al.* (1992) observed the reductase to cause a shift in the distribution of products. Studies by Paulsen *et al.* (1994) identified the reductase as altering the redox potential of the hydroxylase. Liu *et al.* (1997) expanded this finding to show that little change was observed in the potential for the first electron transfer to the di-iron site, at the active site of the hydroxylase, whereas the potential for the second electron transfer increased. This provided a larger driving force for electron transfer from the reductase to the hydroxylase, and favoured the transfer of 2 electrons rather than 1, as required for catalysis.

1.6.3 The Regulatory Component, Protein B

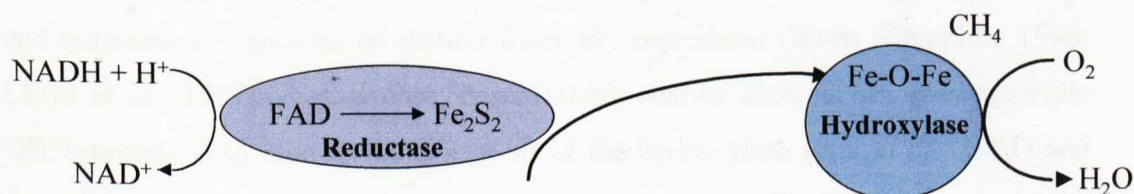
The regulatory component is also known as protein B. It was first identified in 1978 by Colby and Dalton during the purification of sMMO from *Mc. capsulatus* (Bath) as the fraction capable of stimulating sMMO activity. Later, it was purified by Green and Dalton (1985) and shown to be comprised of a single 16 kDa subunit and devoid of prosthetic groups or metal co-factors. It was also found to be a powerful regulator of sMMO activity, converting it from an oxidase to an oxygenase or *vice versa*, possibly in response to environmental conditions. In the absence of protein B, uncoupling occurs, whereby NADH is oxidised and the hydroxylase and reductase catalyse the 4 electron reduction of oxygen to water in both the presence and absence of substrate. The enzyme is recoupled and switched from an oxidase to an oxygenase upon addition of protein B, and oxygen is no longer reduced to water. In the absence of substrate, electron transfer between the hydroxylase and reductase is shut down. Substrate addition to the sMMO complex restores electron transfer between the hydroxylase and reductase and the oxygenase reaction catalyses the oxidation of substrate (Green and Dalton, 1985). Therefore, in the presence of protein B,

electrons are readily transferred to the hydroxylase when substrate is present, but shut down in its absence (Dalton, 1992) (Figure 1.8).

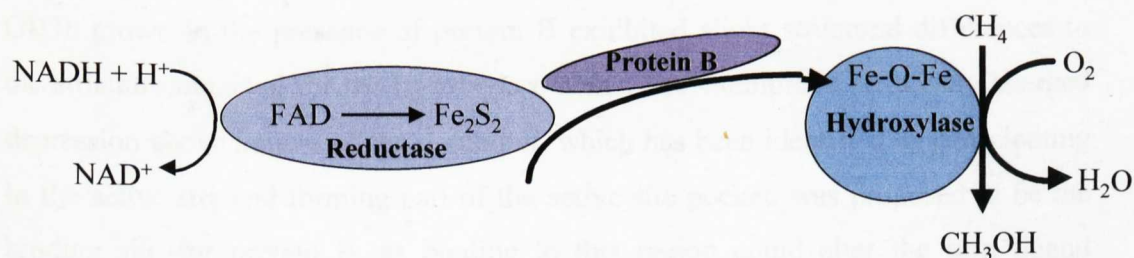
Figure 1.8: Regulation of the sMMO complex by protein B.

The hydroxylase is shown in blue, reductase in mauve and protein B in purple. Fe-OH-Fe represents the di-iron site at the active site of the hydroxylase. The arrows indicate the direction of electron flow and the widths of the arrows indicate the relative rates of reaction. [Modified from Green and Dalton, (1985)].

- In the absence of protein B, the enzyme functions as an oxidase



- In the presence of protein B, the enzyme functions as an oxygenase



Protein B from *Ms. trichosporium* OB3b was first purified by Fox *et al.* in 1989. It existed as a dimer under certain conditions and was shown to be none essential for activity. Therefore, in the *Ms. trichosporium* OB3b sMMO system the 4 electron reduction of oxygen to water was not observed in the absence of protein B, as the hydroxylase and reductase components were capable of directly catalysing oxygen activation, unlike in the *Mc. capsulatus* (Bath) sMMO system. However, protein B was seen to increase the reaction rate 150 fold, showing it to fulfil a necessary and specific role in catalysis. Similarly, protein B purified from *Methylocystis* sp. M was observed as a dimer (Shinohara *et al.*, 1998) and identified as being non-essential for activity, but having only a stimulatory effect (Nakajima *et al.*, 1992). During the purification of the hydroxylase and reductase components of the sMMO from

Methylosinus sporium 5, a component was lost, thought to be equivalent to protein B, which was identified as being essential for activity (Pilkington and Dalton, 1991). In contrast, the sMMO of *Methylobacterium* sp. CRL-26 was shown to be lacking the presence of a protein B component and such a component was not required for sMMO activity. Although it has been proposed that the protein remains tightly bound to the hydroxylase during purification and because of its small size and lack of prosthetic groups, it remains undetected (Patel and Savas, 1987).

Surface plasmon resonance studies indicated that protein B bound to the hydroxylase and reductase components of sMMO from *Mc. capsulatus* (Bath) (Bhambra, 1996; Lloyd *et al.*, 1997). Furthermore, cross-linking studies showed *Ms. trichosporium* OB3b protein B to bind to the α subunit of the hydroxylase (Fox *et al.*, 1991) and crystal structure data of the hydroxylase of *Mc. capsulatus* (Bath) have proposed the binding site of protein B to be in the canyon formed between the $\alpha\beta$ pairs of the protein (Rosenzweig *et al.*, 1993). Crystals for the hydroxylase of *Ms. trichosporium* OB3b grown in the presence of protein B exhibited slight structural differences to the structure obtained for the hydroxylase alone. For example, a negatively charged depression above helices of the α subunit, which has been identified as participating in the active site and forming part of the active site pocket, was proposed to be the binding site for protein B, as binding to this region could alter the iron ligand geometry as well as the active site volume, thus modulating activity (Elango *et al.*, 1997).

Very recently the nuclear magnetic resonance (NMR) structures of protein B from both *Mc. capsulatus* (Bath) and *Ms. trichosporium* OB3b were published, as shown in Figure 1.9 (Chang *et al.*, 1999; Walters *et al.*, 1999).

Figure 1.9: NMR derived structures of protein B from (i) *Mc. capsulatus* (Bath) (Walters *et al.*, 1999) and (ii) *Ms. trichosporium* OB3b (Chang *et al.*, 1999).

(i) Shown is one of 14 structures derived for protein B from the NMR data. All residues are displayed.



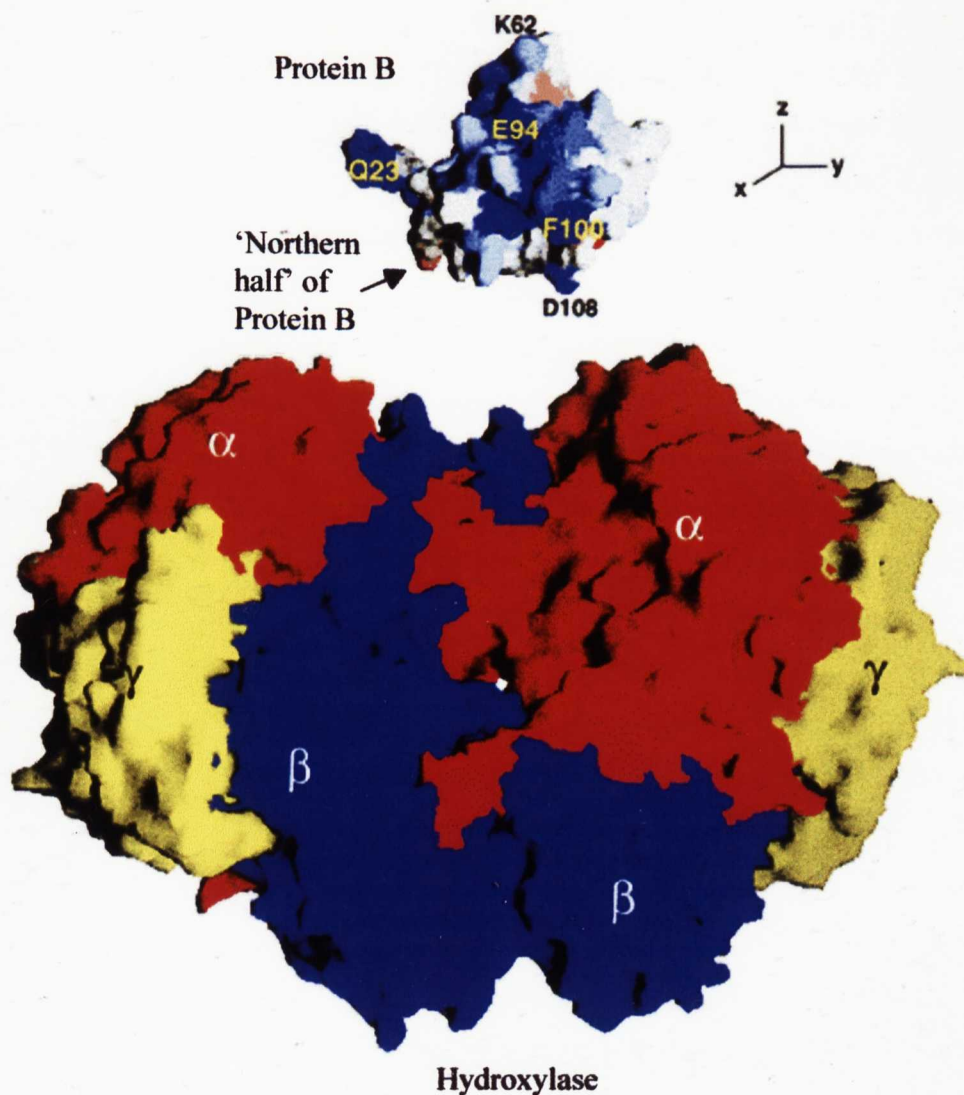
(ii) Shown is one of 15 structures derived for protein B from the NMR data. Only residues 35-128 are shown which form the well-structured part of the protein. The N- and C-terminal segments are omitted as their structures were ill-defined.



In the case of the *Mc. capsulatus* (Bath) protein B, the N-terminal region contained two partially folded helices, but their orientation relative to the protein core was unidentified. Similarly, protein B from *Ms. trichosporium* OB3b consisted of an aperiodic N-terminus and in both cases the C-terminal region was unstructured. Protein B of *Mc. capsulatus* (Bath) was considered to have a novel fold, as the DALI server (Holm and Sander, 1993) failed to identify similar folds in other proteins. The NMR studies indicated that substrates did not bind to or associate with protein B of *Ms. trichosporium* OB3b, as no chemical shift changes were observed for the protein in the presence of substrates (Chang *et al.*, 1999). The NMR studies of *Mc. capsulatus* (Bath) protein B indicated that the reductase and protein B do not interact in either the presence or absence of the hydroxylase. The studies identified the 'northern half' of protein B (Figure 1.10) as forming hydrophobic interactions with the hydroxylase in contrast to the 'southern half' containing the terminal regions. The residues, Leu⁹⁶, Gly⁹⁷, Phe¹⁰⁰, and Asp¹⁰⁸, identified as conserved within the protein B and related hydroxylase cofactor proteins, were observed as being involved in binding to the hydroxylase. Residues Trp⁷⁸, Arg¹¹⁵, and Tyr¹¹⁷ were also identified as being involved. The unstructured N-terminus was observed to experience greater flexibility than the core, a property apparently maintained in the presence of the hydroxylase. Modelling studies, to dock protein B into its proposed binding site in the hydroxylase cleft formed between the $\alpha_2\beta_2$ interface of the hydroxylase (Rosenzweig *et al.*, 1993), showed that the structure could be easily positioned into the region and its mainly hydrophobic surface was ideally suited for binding in this site (Walters *et al.*, 1999) (Figure 1.10).

Figure 1.10: Surface diagram model for the docking of protein B into the hydroxylase.

The hydroxylase and protein B are labelled. The α subunits of the hydroxylase are shown in red, β in blue and γ in yellow. Protein B has been translated away from its proposed docking site on the surface of the hydroxylase and rotated 90° clockwise about the y -axis to expose the residues most involved in binding, identified as the 'northern half' of the protein. The residues coloured blue are those most affected by binding. [Reproduced from Walters *et al.* (1999) with permission].



Protein B is not thought to participate directly in the electron transfer pathway as it contains no metal ions or cofactors (Fox *et al.*, 1989). However, the protein has been shown to decrease the redox potentials for the oxidation of the di-iron site of the hydroxylase in *Ms. trichosporium* OB3b (Paulsen *et al.*, 1994) and *Mc. capsulatus* (Bath) (Liu and Lippard, 1991; Kazlauskaite *et al.*, 1996) such that the di-ferrous state is made more reactive to oxygen. It has been suggested that the negative shift in

the redox potentials caused by protein B binding to the hydroxylase is due to a change in the first coordination sphere of the iron(s) or a change in the protonation state of the hydroxo bridge (Paulsen *et al.*, 1994). Other effects which could account for the changes in potentials involve a change in the solvent accessibility or the structure of the active site environment as a result of a conformational change occurring upon protein B binding (Kazlauskaite *et al.*, 1996).

Further evidence that the binding of protein B results in an alteration of the iron environment of the hydroxylase has been provided by EPR spectroscopy. For the *Ms. trichosporium* OB3b system, protein B was also observed to cause a change in the conformation of the di-ferric hydroxylase and it is hypothesised that the structural changes observed may involve the conversion of the di-hydroxo-bridged diamond core structure to one with more readily dissociable bridging oxygen ligands to facilitate reaction with oxygen following di-iron site reduction (Davydov *et al.*, 1997). However, for the *Mc capsulatus* (Bath) system similar studies concluded that protein B complex formation induced only minor alterations in ligand binding at the di-iron centre of di-ferric hydroxylase, although in the presence of alcohols, major perturbations were observed (Davydov *et al.*, 1999). This suggested protein B to play a role in the catalytic cycle by providing favourable active site geometry for substrate conversion and product release. Protein B binding to the mixed-valent or fully-reduced hydroxylase caused a major alteration in the environment of the di-iron cluster (Fox *et al.*, 1991; Froland *et al.*, 1992; DiWitt *et al.*, 1995). The EPR spectrum of the mixed valent hydroxylase was found to be progressively altered until a stoichiometric complex was formed with protein B. Analogous changes in the EPR spectrum of the reduced hydroxylase were maximised at 0.3 protein B per hydroxylase di-iron cluster. Therefore, it was proposed that this observation results from hysteresis in the relaxation of the altered hydroxylase structure in solution after weakly bound protein B dissociated. Thus, a small amount of protein B was able to affect a larger reduced hydroxylase population (Paulsen *et al.*, 1994). On the basis of these observations, proposals as to the regulatory effect of protein B from both *Mc capsulatus* (Bath) and *Ms. trichosporium* OB3b systems were suggested. For example the cyclic dissociation and reassociation at appropriate points in the catalytic cycle could be involved in restricting substrate access to the di-iron site

until it is reduced or oxygen is activated and product release could be promoted by protein B reassociation.

CD and magnetic circular dichroism (MCD) were used to provide insights into the effect of protein B on the hydroxylase (Coates-Pulver *et al.*, 1997). It was found that the formation of the di-ferrous hydroxylase-protein B complex caused changes in the conformation of the active site so that substrates interacted more strongly with the di-iron metal centre than in uncomplexed hydroxylase. The CD and MCD spectral changes arising from protein B binding suggested that the protein effects both Fe(II) active site atoms, but one more directly while substrate binding perturbs the other.

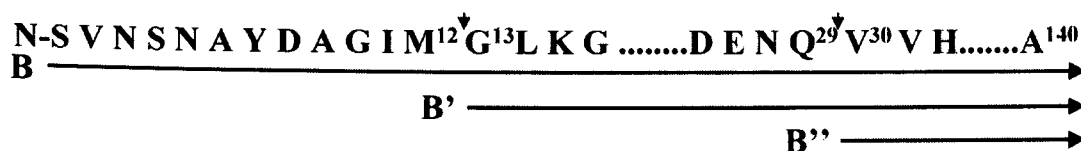
Protein B has been shown to alter the product distribution for complex substrates that can be hydroxylated in more than one position (Froland *et al.*, 1992; Jiang *et al.*, 1993). It is proposed that this occurs as a result of changes in the hydroxylase structure occurring upon complex formation with protein B causing substrates to be presented differently to the activated oxygen species at the active site. Similarly, protein B was shown to affect the selectivity of carbon hydroxylation when the hydroxylase was activated via the peroxide shunt mechanism and was also able to inhibit the hydrogen peroxide-driven oxidations. Protein B was, therefore, clearly seen to be able to interact with the hydroxylase to significantly affect the hydroxylase/hydrogen peroxide system (See also Section 1.6.1.4).

Protein B has also been shown to play a specific role in catalysis by exerting a 'gating' effect on oxygen reactivity by increasing the rate of Compound P (an MMO reaction intermediate) by as much as 1000 fold and that the rate of conversion of Compound P to Compound Q (another MMO reaction intermediate) (Section 1.6.4; Figure 1.12) is also increased by at least 40 fold (Liu *et al.*, 1995). The rate limiting step in catalysis is, therefore, shifted to either the enzyme-bound product or product release step. The method by which protein B enhances the reaction rate with oxygen has been proposed to be as a result of the protein lowering the redox potential of the hydroxylase-protein B complex or derived from an increase in oxygen accessibility of the active site or the di-iron cluster by means of a conformational change, proposals discussed previously.

Protein B from *Mc. capsulatus* (Bath) has been observed as being particularly sensitive to proteases (Green and Dalton, 1985). Work by Pilkington *et al.* (1990) purified two forms of the protein, the intact protein B and a truncated version, B'. Later studies by Bhambra (1996) and Lloyd *et al.* (1997) identified a second truncated protein, B''. ESI-MS analysis indicated that the cleavage of protein B to give B' occurs between Met¹²-Gly¹³ residues, resulting in 12 amino acids being lost from the N-terminus, and Gln²⁹-Val³⁰ cleaves to form B'' with the loss of 29 amino acids from the N-terminus (Figure 1.11).

Figure 1.11: Cleavage sites of protein B from *Mc. capsulatus* (Bath).

The N-terminal amino acids of protein B are shown with arrows indicating the sites of cleavage and the truncate proteins produced. [Modified from Lloyd *et al.*, 1997].



Cleavage to form B'' has also been observed in *Methylocystis* sp. M (Shinohara *et al.*, 1998). Studies have shown that the 12 amino acid fragment cleaved from protein B to give B' had no effect on sMMO activity, in either the presence or absence of protein B' (Bhambra, 1996). B' was shown to have no effect on the redox behaviour of the hydroxylase (Kazlauskaitė *et al.*, 1996). It has also been shown to form a complex with the oxidised hydroxylase which is 3 times less stable than the corresponding protein B complex and the strength of binding of protein B to the hydroxylase becomes reduced in the presence of protein B'. This suggested that protein B' bound at the same site as protein B, but the former did not affect the hydroxylase in the manner protein B itself did to bring about activity (Kazlauskaitė *et al.*, 1996).

Proteins B' and B'' were seen to co-purify with protein B from *Mc. capsulatus* (Bath) and the addition of protease inhibitors failed in reducing the level of cleavage observed (Bhambra, 1996; Lloyd *et al.*, 1997). Expression of protein B has been achieved in *E. coli* (West *et al.*, 1992), although cleavage to form B' was still seen to occur. Expression of protein B in protease deficient strains also failed to prevent cleavage (Bhambra, 1996; Lloyd *et al.*, 1997).

Alteration of the Met¹²-Gly¹³ cleavage site to Met¹²-Gln¹³, equivalent to the site found in *Ms. trichosporium* OB3b protein B and for which truncation had not been reported, enhanced the stability of recombinant protein B preparations (Lloyd *et al.*, 1997). Similarly, a triple mutant protein B in which Gly¹⁰ and Gly¹⁶ were mutated to Ala residues and Gly¹³ was mutated to Gln, was also resistant to truncation, but exhibited only about half the activity of the native and single mutant proteins (Brandstetter *et al.*, 1999).

The existence of three forms of protein B has been proposed to be a mechanism to control the amount of active protein B within the cell since the occurrence of the cleavage reaction rapidly inactivates the protein, thus preventing sMMO activity. It remains unclear whether cleavage occurs due to activation of an autocatalytic process as a response to specific conditions, or due to proteolysis. Nevertheless, the production of an inactive form of protein B is potentially useful to the cell. Substrate oxidation does not occur in the presence of protein B' or B'', so their formation may be a mechanism of shutting down enzyme activity, possibly as a response to substrate absence. This process would prevent the wasteful oxidation of NADH, and so conserve the cell's energy (Kazlauskaitė *et al.*, 1996; Lloyd *et al.*, 1997; Shinohara *et al.*, 1998).

1.6.4 sMMO Reaction Mechanism

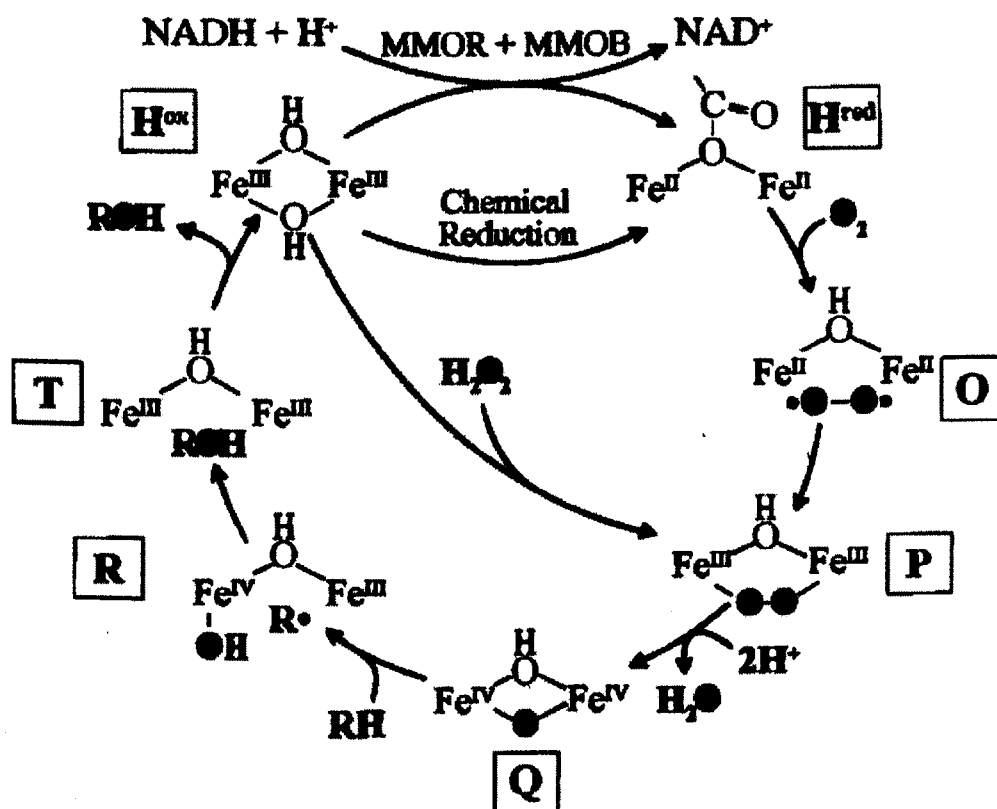
The reaction mechanism of sMMO was identified in 1986 by Green and Dalton from steady-state kinetic analysis studies. Methane was identified as binding to the enzyme first, followed by NADH, which reacts to yield the reduced form of the enzyme with the release of NAD⁺. The reduced form then binds oxygen to form a second ternary complex, which breaks down to release the products water and methanol. The enzyme was, therefore, seen to control the supply of electrons to the active site to coincide with the arrival of methane.

Progress has subsequently been made towards improving understanding of the mechanism of dioxygen and methane activation by MMO. In particular, current

insights have been greatly advanced since the spectroscopic characterisation of reactive sMMO intermediates has been possible. Figure 1.12 illustrates a current proposal for the catalytic cycle of sMMO.

Figure 1.12: Proposed catalytic cycle of sMMO.

Boxed letters O-T refer to reaction intermediates. H_{ox} and H_{red} refer to oxidised and reduced hydroxylase respectively. MMOR refers to the reductase and MMOB refers to protein B. The states of the di-iron site at the active site of the hydroxylase is illustrated at each stage of the reaction cycle with the arrows indicating the reaction cycle flow. Oxygen atoms derived from O_2 are filled. [Reproduced from Wallar and Lipscomb, (1996), with permission].



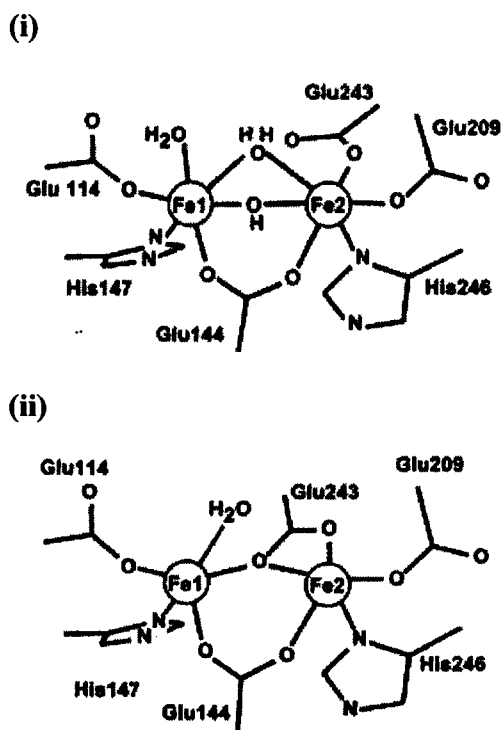
The initial step in the catalytic cycle involves dioxygen activation by the di-ferrous site in the presence of protein B but independent of substrate (Liu *et al.*, 1995). It has been proposed that oxygen binds in the active site prior to association with the di-ferrous cluster, forming intermediate O, an oxygen adduct (Froland *et al.*, 1992). Compound O spontaneously converts to a peroxo-intermediate termed Compound P, which has been characterised by Mössbauer spectroscopy (Liu *et al.*, 1995), which showed both iron atoms to be in a high spin ferric state and to be similar to end-on

peroxo-bridged biferric model complexes. Raman spectroscopy (Wallar and Lipscomb, 1996) gave data consistent with peroxide-stretching frequencies and suggested that both oxygens were bound symmetrically to the irons. Compound P spontaneously converts to a high-valent ferryl species termed Compound Q. Mössbauer spectroscopy has identified the intermediate as containing 2 antiferromagnetically coupled high spin Fe(IV) atoms and in combination with EXAFS, has identified Compound Q as having a diamond core structure (Shu *et al.*, 1997). Upon formation of this intermediate, methane enters the reaction cycle and substrate oxygenation occurs. It remains unclear whether cleavage of the O-O bond occurs via homolytic or heterolytic cleavage (Lee and Lipscomb, 1999). The Compound R intermediate is formed by reaction of Compound Q with substrate. This intermediate does not live long enough to be trapped, so it has not been possible to characterise it spectroscopically. Nevertheless, attempts to elucidate the possible steps within the reaction pathway have been made, but it remains controversial whether methane C-H bond activation occurs via a mechanism involving a radical step or a concerted oxygen atom insertion process. Product analysis in the oxygenation of substrates that include radical traps within their structures have provided experimental evidence supporting both mechanisms (Wilkins *et al.*, 1992; Liu *et al.*, 1993; Wilkins *et al.*, 1994; Nesheim and Lipscomb, 1996; Frey, 1997; Valentine *et al.*, 1997, 1999). Also these studies give differing results for the sMMOs of *Ms. trichosporium* OB3b and *Mc. capsulatus* (Bath), despite their similar structures and reaction cycle intermediates. Recent work by Jin and Lipscomb (1999) using methylcubane, the reaction clock substrate, has provided data which supports a radical-based mechanism for *Ms. trichosporium* OB3b sMMO. They propose that subtle differences in the accessibility to the reactive species in the active site of sMMOs from *Ms. trichosporium* OB3b and *Mc. capsulatus* (Bath) mask inherently similar radical-based chemical mechanisms. Nevertheless, the terminal adduct, Compound T, is the final product complex of the enzyme. The decay of Compound T yields diferric hydroxylase, thus completing the reaction cycle.

Amino acids which have key roles in the MMO mechanism have been identified from the crystal structure of the hydroxylase, particularly the comparison of the crystal structures of *Mc. capsulatus* (Bath) hydroxylase in the oxidised and reduced states (Figure 1.13) (Rosenzweig *et al.*, 1995).

Figure 1.13: Representation of the active site structure of sMMO from *Mc. capsulatus* (Bath) in both the (i) oxidised and (ii) reduced states.

Illustration of the coordination of the two iron atoms, labelled Fe1 and Fe2, at the active site of the hydroxylase. [Reproduced from Solomon *et al.* (2000), with permission].



Glu²⁴³ was identified as undergoing a carboxylate shift, which is a structural variation in the binding of RCO₂⁻ fragments to polymetallic centres and maintains a constant coordination level on the iron species. The flexible nature of the carboxylate ligand is suggested to be important for the formation of the di-iron(II) centre and may facilitate the binding of dioxygen and the formation of the high valent iron-oxo intermediates. Thr²¹³ is hydrogen-bonded through a water molecule in the reduced hydroxylase to the proposed site of chemical reactivity and has been proposed to function as a proton donor in the hydroxylation reaction. It may also cause changes in the active site upon binding of protein B since it is positioned on the helix thought to be the binding domain of protein B. Therefore, protein B would affect the di-iron centre by perturbing the hydrogen-bonding network involving Thr²¹³. Residues Phe¹⁸⁸ and Phe¹⁹² have been identified as ‘clamping’ the acetate ion into the active site of the oxidised hydroxylase. These residues may, therefore, play a role in facilitating methane and oxygen binding to the active site (Rosenzweig *et al.*, 1995).

The reduced hydroxylase structure identified an altered side chain conformation for Leu¹¹⁰ at the active site cavity. It has been suggested that this conformational shift in Leu¹¹⁰ served as a gate controlling access of substrates and products to and from the active site. Furthermore, it was proposed that protein B may affect the hydroxylase by means of the 'Leucine gate', thus controlling the reactivity of the MMO complex (Rosenzweig *et al.*, 1997).

1.7 Objectives of the present work

The sMMO of *Mc. capsulatus* (Bath) is functionally inactive in the absence of the regulatory protein, protein B, although protein B itself undergoes an inactivatory cleavage reaction to form the inactive truncates, proteins B' and B'', about which knowledge is limited. Also, in the absence of a crystal structure of the sMMO complex, the interactions of protein B with the other sMMO components is not well defined. Gaining an insight into the reasons behind the cleavage reaction and information on the component interactions of the complex are fundamental to obtaining a full understanding of the sMMO system.

Therefore, the main aims of the work presented in this thesis were:

- 1) To investigate further the mechanism of protein B cleavage, the reason for its occurrence and establish the individual roles of the truncate proteins B' and B''.
- 2) To devise methods which minimise or prevent truncate formation of protein B, necessary for biochemical and structural studies to be possible.
- 3) To identify the reason(s) for the inactivity of the protein B' truncate and determine specifically how many of the protein B amino acids are required for its activity.
- 4) To study the component interactions of the sMMO system.

Chapter 2

Materials and Methods

2.1 Organisms

The organisms used in this study were the obligate methanotrophs *Methylococcus capsulatus* (Bath) (*Mc. capsulatus* (Bath) (Whittenbury *et al.*, 1970; Stanley *et al.*, 1983) and *Methylosinus trichosporium* OB3b (*Ms. trichosporium* OB3b) (Whittenbury *et al.*, 1970), obtained from the culture collection of the University of Warwick, UK.

2.2 Growth of *Mc. capsulatus* (Bath) and *Ms. trichosporium* OB3b

2.2.1 Media

Methanotrophs were routinely grown in sterile low copper Nitrate Minimal Salts (NMS) media for the expression of sMMO. The constitution of the media was as follows; 1 g/l MgSO₄, 1 g/l KNO₃, 0.2 g/l CaCl₂.2H₂O, 0.5 mg/l NaMoO₄.2H₂O, 3.8 mg/l FeNaEDTA, 1 ml/l Trace Element Solution containing 0.5 g/l FeSO₄.5H₂O, 0.4 g/l ZnSO₄.7H₂O, 0.015 g/l H₃BO₃, 0.05 g/l CoCl₂.6H₂O, 0.25 g/l Na₂EDTA, 0.02 g/l MnCl₂.4H₂O, 0.001 g/l NiCl₂.6H₂O and 0.1 g/l CuSO₄.5H₂O and 15 ml 6.5 % Na₂HPO₄/KH₂PO₄ phosphate buffer pH 6.8. The phosphate buffer was sterilised separately and mixed with the rest of the media once both were cool in order to prevent precipitation. Solid media was prepared by the addition of 1.5 % (w/v) Bacto-agar (Difco, Michigan, USA) to the NMS (minus the phosphate) prior to sterilisation.

2.2.2 Plate cultures

Plate cultures were grown on NMS agar media in plastic Tupperware™ boxes in an atmosphere of air supplemented with ~ 50 % (v/v) methane/CO₂ mix (95 % and 5 % v/v respectively) and incubated at 30 °C in the case of *Ms. trichosporium* OB3b plates and at 45 °C in the case of *Mc. capsulatus* (Bath) plates.

2.2.3 Batch cultures

Growth of cells by batch culture was performed in 250 ml flasks containing 50 ml of NMS media. Flasks were sealed with rubber Suba seals (W.H Freeman, Barnsley, UK) and cultures were gassed by removal of 50 ml air from the flask and replacing it with 60 ml of a methane/CO₂ mix (95 % and 5 % v/v respectively). Cultures were incubated, with shaking at 200 rpm, at 30 °C in the case of *Ms. trichosporium* OB3b cultures and at 45 °C in the case of *Mc. capsulatus* (Bath) cultures.

2.2.4 Continuous cultures

Growth of cells in continuous culture was performed in 4.5 l fermenters (L.H. Engineering Ltd., Stoke Poges, Bucks, UK) in NMS medium with an agitation speed of 500 rpm and gas flow rates of 60-80 ml/min for methane and 80-100 ml/min for air. The temperature was maintained at 30 °C for the growth of *Ms. trichosporium* OB3b and at 45 °C for the growth of *Mc. capsulatus* (Bath). The medium flow rate was maintained at approximately 1.5 ml/min and the pH was maintained at 6.8 by automatic titration with 1 M HCl and/or 1 M NaOH. The oxygen tension of the cultures was maintained below 5 %. A 10 % (v/v) inoculum of culture that had grown to an OD₅₄₀ of 0.6 in 50 ml batch cultures was used and the chemostat conditions were only initiated once the culture had grown to OD₅₄₀ of 7-9 within the fermenter.

2.2.5 Microscopy

Light microscopy was conducted using a Kyoga-Unilix II (Tokyo) phase contrast microscope. Microbial cultures were examined using 1000 × magnification under oil immersion to check for culture contamination.

2.2.6 Cell Harvesting

Harvesting of 20 l of cells from the chemostat overflow was conducted using a Westfalia continuous centrifuge (Westfalia Separator Ltd., Wolverton, Bucks, UK). The resulting cell paste was washed with 25 mM MOPS buffer pH 7 containing 1mM benzamidine and then re-suspended in the same buffer containing 5 mM DTT. At this point the cell suspension could be frozen and stored at – 80 °C.

2.2.7 Whole cell assay

The method used was a modification of that of Brusseau *et al.* (1990). 1 ml samples of methanotroph cultures were incubated in the presence of a naphthalene crystal for 30 min, with agitation, at 30 °C in the case of *Ms. trichosporium* OB3b cultures and at 45 °C in the case of *Mc. capsulatus* (Bath) cultures. Oxidation of naphthalene to 1-naphthol and 2-naphthol in the presence of sMMO was then detected by the addition of 100 µl of a fresh solution of TOD (0.2 % w/v), which resulted in the formation of a purple diazo dye. Lack of such a colour change indicated a lack of sMMO expression within the cells. The naphthalene assay was not quantitative (Martin, 1994).

2.3 Purification of *Mc. capsulatus* (Bath) sMMO components - optimised protocols from this study

The purification of the sMMO components was performed by modification of the published protocols (Colby and Dalton, 1978; Pilkington and Dalton, 1990; Pilkington *et al.*, 1990). Protein purification chromatography procedures were conducted using Fast Protein Liquid Chromatography (FPLC) equipment (Amersham Pharmacia Biotech, Bucks., UK). The 'FPLC Basic' system was used which consists of two P-500 pumps, an LCC 500 programmable pump controller, a monitor UV-M detector system and a FRAC-100 fraction collector.

2.3.1 Preparation of soluble extract

Thawed cell paste was diluted with 25 mM MOPS buffer pH 7 containing 1 mM benzamidine, 5 mM dithiothreitol, 5 mM sodium thioglycolate and 0.01 mg/ml deoxyribonuclease I. Cells were broken by 2 passages through a cell disrupter (Constant Systems Ltd, Honiley, Warwickshire, UK) at 170 MPa and centrifuged at $48,000 \times g$ for 1.5 hours to separate the extract into soluble and particulate fractions. The supernatant was used as soluble extract or directly resolved into the three constituent sMMO proteins.

2.3.2 Resolution of sMMO into its three constituent proteins

To the soluble extract, NaCl was added to a final concentration of 50 mM and then loaded onto a DEAE cellulose FPLC column (2.6 cm × 13.5 cm; 70 ml) (Amersham Pharmacia Biotech, Bucks., UK) equilibrated in 25 mM MOPS buffer pH 7 containing 50 mM NaCl, 1 mM benzamidine, 5 mM DTT and 5 mM thioglycolate. The hydroxylase was eluted at 50 mM NaCl. Protein was then eluted successively with 500 ml batches of the same buffer containing 200 mM and 500 mM NaCl to elute the protein B and reductase containing fractions respectively.

Further purifications of the separate fractions containing the sMMO components were undertaken separately.

2.3.3 Purification of the hydroxylase component

Step 1: After the initial ion exchange step, the hydroxylase was applied to a pre-packed Q-sepharose ion exchange FPLC column (2.6 cm × 14.5 cm; 77 ml) (Amersham Pharmacia Biotech, Bucks., UK) equilibrated with 25 mM MOPS buffer pH 7. Protein was eluted with a 100-400 mM linear gradient of NaCl over 3 column volumes. The hydroxylase was eluted from the column at 240 mM NaCl.

Step 2: The hydroxylase from step 1 was applied to a Superdex 200 gel filtration FPLC column (2.6 cm × 68 cm; 360 ml) (Amersham Pharmacia Biotech, Bucks., UK). The hydroxylase was eluted with 25 mM MOPS buffer pH 7.

Step 3: Final purification of the hydroxylase was achieved by elution from a MONO Q ion exchange FPLC column (HR16/10; 20 ml) (Amersham Pharmacia Biotech, Bucks., UK) using a NaCl gradient of 100-400 mM over 5 column volumes. The hydroxylase eluted at 120 mM NaCl.

2.3.4 Purification of the reductase component

Step 1: After the initial ion exchange step, the reductase was desalted and applied to a Q-Sepharose high performance ion exchange FPLC column (2.6 cm × 14.5 cm; 77 ml) (Amersham Pharmacia Biotech, Bucks., UK). The reductase was eluted with a 300-700 mM linear gradient of NaCl over 4 column volumes. The reductase eluted at 450 mM NaCl.

Step 2: Fractions containing active reductase from step 1 were applied to a Superdex 75 gel filtration FPLC column (2.6 cm × 61 cm; 325 ml) (Amersham Pharmacia Biotech, Bucks., UK). The reductase was eluted with 25 mM MOPS buffer pH 7 containing 5 mM DTT.

Step 3: Final purification was achieved by elution of the reductase from a MONO Q ion exchange FPLC column (HR10/10; 10 ml) (Amersham Pharmacia Biotech, Bucks., UK) using a 300-700 mM NaCl gradient over 10 column volumes. The reductase eluted at 500 mM NaCl.

2.3.5 Purification of the wild-type regulatory protein B'

Step 1: Ammonium sulphate was added directly to the DEAE fraction containing regulatory protein B/B' to make a 50 % saturated solution. The mixture was stirred at 4 °C for 30 mins. Centrifugation at 48,000 × g for 30 mins pelleted the precipitated protein fraction, which was subsequently re-suspended in a minimum volume of 25 mM MOPS buffer pH 7. The sample was concentrated in an ultra filtration cell (Amicon, Danvers, MA, USA) using a membrane with a 3 kDa molecular weight cut-off size (YM3, Amicon, Danvers, MA, USA) ready for the next purification step.

Step 2: The ammonium sulphate precipitated regulatory protein from step 1 was applied to a Superdex 75 gel filtration FPLC column (2.6 cm × 61 cm; 325 ml) (Amersham Pharmacia Biotech, Bucks., UK). The regulatory protein was eluted with 25 mM MOPS buffer pH 7.

Step 3: Final purification was achieved by elution of the regulatory protein from a MONO Q ion exchange FPLC column (HR10/10; 10 ml) (Amersham Pharmacia Biotech, Bucks., UK) using a 0-350 mM NaCl gradient over 10 column volumes. The regulatory protein eluted at 220-250 mM NaCl.

2.4 Purification of the GST-fused regulatory proteins, WTB, G13Q, recombinant *Ms. trichosporium* OB3b protein B and M12A:G13Q

Plasmids containing the *mmoB* gene from *Mc. capsulatus* (Bath) and *Ms. trichosporium* OB3b and the single mutant version of *Mc. capsulatus* (Bath) protein B (G13Q) were derived from pGEX-2T and the method of cloning (Lloyd, 1997) was such that the genes were expressed as GST-fusion proteins under the control of an inducible *tac* promoter. This strategy was also adopted for the M12A:G13Q double mutant (Chapter 6). The plasmids also contained the *bla*, β -lactamase gene encoding ampicillin resistance. .

The proteins encoded were purified with the following modifications to the published protocol of Lloyd *et al.* (1997). After elution of the fusion protein from the GST-affinity column, the GST affinity tag was cleaved from the recombinant protein by addition of thrombin (2 ng thrombin/ μ g fusion protein). After 5-10 mins at room temperature the mixture was applied to a Superdex 75 gel filtration FPLC column (2.6 cm \times 61 cm; 325 ml) (Amersham Pharmacia Biotech, Bucks., UK). The recombinant protein of interest was eluted with 25 mM MOPS buffer pH 7.

2.5 Purification of *Ms. trichosporium* OB3b protein B - optimised protocol from this study

The purification of the protein B was carried out by modification of the published protocol (Fox *et al.*, 1989).

Step 1: After ammonium sulphate precipitation of the regulatory protein (Fox *et al.*, 1989), the sample was concentrated and desalted into 25 mM MOPS buffer, pH 7 by ultra-filtration using a membrane with a molecular cut-off size of 3 kDa (YM3, Amicon, Danvers, MA, USA).

Step 2: The sample of protein B was applied to a MONO Q ion exchange FPLC column (HR10/10; 10 ml) (Amersham Pharmacia Biotech, Bucks., UK). Protein B was eluted over a linear gradient of 25 mM MOPS buffer, pH 7 containing 150 mM to 350 mM NaCl over 8 column volumes. Protein B eluted at 260-270 mM NaCl.

Step 3: Fractions containing active protein B from step 2 were concentrated and applied to a Superdex 75 gel filtration FPLC column (2.6 cm × 61 cm; 325 ml) (Amersham Pharmacia Biotech, Bucks., UK). Protein B was eluted with 25 mM MOPS buffer pH 7 in a size dependent manner.

2.6 Purification of His-tagged protein B truncates

Various *E. coli* BL21(DE3) clones containing plasmids with genes encoding the truncated forms of protein B fused to 6-His-tags, under the control of isopropyl β -D-thiogalactopyranoside (IPTG)-inducible promoters were constructed (as detailed in Chapter 7). Each clone was grown in LB broth, induced and harvested and re-suspended in 20 mM phosphate buffer containing 0.5 M NaCl and 10 mM imidazol, pH 7.4-7.6. Purification was accomplished using the HisTrap™ kit for the purification of histidine-tagged proteins (Amersham Pharmacia Biotech, Bucks., UK) according to the manufacturers instructions. After elution of the 6-His-tagged truncate proteins using 500 mM imidazol, the samples were concentrated using an ultra-filtration cell (Amicon, Danvers, MA, USA) and applied to a Superdex 75 gel filtration FPLC column (2.6 cm × 61 cm; 325 ml) (Amersham Pharmacia Biotech, Bucks., UK). Pure 6-His-tagged truncate proteins were eluted with 25 mM MOPS buffer pH 7 in a size dependent manner.

2.7 Affinity chromatography

A HiTrap® affinity column (Amersham Pharmacia Biotech, Bucks., UK) was used for affinity chromatography. The chelating sepharose media within the pre-packed 5 ml FPLC column was charged with copper. The column was equilibrated with 0.02 M Na₂HPO₄ containing 1 M NaCl, pH 7 before loading the protein sample in the same buffer and washing in the same buffer over 1 column volume. A linear gradient from 0-100 % elution buffer of 0.02 M Na₂HPO₄ containing 1 M NH₄Cl, pH7.2 was used to elute the copper-bound proteins from the column over 3 column volumes. Column regeneration was achieved by elution of the column-bound copper by washing with 0.02 M Na₂HPO₄ containing 1 M NaCl and 0.05 M EDTA, pH 7.2 over 1 to 2 column volumes.

2.8 Chromatofocusing chromatography

Chromatofocusing chromatography was achieved using a MONO P FPLC column (HR 5/20) (Amersham Pharmacia Biotech, Bucks., UK). The column was equilibrated with Start Buffer A (25 mM methylpiperazine, either pH 5.64 or 5.7) before loading the protein in the same buffer. Application of Buffer B (1 in 10 dilution of PolyBuffer 74TM (Amersham Pharmacia Biotech, Bucks., UK) either pH 3.5 or 4) at 0.3 ml/min to 1 ml/min over ~ 15 column volumes eluted the proteins in a pH dependent manner.

2.9 Size exclusion chromatography

Size exclusion chromatography was achieved using a Superdex 75 gel filtration FPLC column (2.6 cm × 61 cm; 325 ml) (Amersham Pharmacia Biotech, Bucks., UK). The column was equilibrated in 25 mM MOPS buffer, pH 7. The column was calibrated using a Gel Filtration LMW Calibration Kit (Amersham Pharmacia Biotech, Bucks., UK) containing ribonuclease A, chymotrypsinogen A, ovalbumin, bovin serum albumin and blue dextran, of apparent molecular weights 13,700 kDa, 25,000 kDa, 43,000 kDa, 67,000 kDa and ~ 2,000,000 kDa respectively. The protein sample for analysis was loaded onto the column in 25 mM MOPS buffer, pH 7. Proteins were eluted in a size dependent manner.

2.10 Determination of total protein concentration

2.10.1 Colorimetric Bradford assay

Total protein concentrations were determined colourimetrically by the method of Bradford (1976) using bovine serum albumin as standard and using commercially available Bio-Rad reagent (BioRad Ltd., Watford, Herts, UK).

2.10.2 Extinction-coefficient values

The concentrations of hydroxylase and protein B samples could also be determined using the extinction-coefficient values calculated for each of the proteins by the methods of Whittaker and Granum (1980) and Scopes (1974). The extinction-coefficient value of the hydroxylase was identified as being $550,814 \text{ M}^{-1} \text{ cm}^{-1}$ at 280nm (C. Lesieur, personal communication). The extinction-coefficient values for the protein B samples are detailed in Chapter 3, Section 3.7.

In order to identify the protein concentration the absorbance of the protein of interest at 280 nm was elucidated and thus protein concentration determined using the equation: $A = \epsilon cl$ where A is the absorbance of the protein at 280nm, ϵ is the extinction-coefficient value of the protein, c is the concentration of the protein in molar units, and l is the pathlength in cm.

2.11 Production of anti-sera

Anti-sera to the regulatory protein of sMMO was raised in a New Zealand White rabbit by subcutaneous injection of 1.5 mg/ml aliquots of regulatory protein homogenised with Freund's adjuvant by V. Cooper (University of Warwick, UK). At four weekly intervals, bleeds were taken and stored for 16 hours at 4 °C. After this time the clear supernatant was obtained and stored in 50 μl aliquots at -20 °C.

2.12 sMMO assays by gas chromatography

Measurement of enzyme assay reaction products were performed by gas chromatography analysis using a Pye Unicam Series 104 gas chromatograph (Pye Unicam, Cambridge, UK). The machine was fitted with a flame ionisation detector and a 'Porapack Q' column (1 m \times 4 mm internal diameter; Waters Associates, Milford, MA, USA) which was maintained at 190 °C, with nitrogen as the carrier gas at a flow rate of 30 ml/min. Peak areas were determined by a 3390A Integrator (Hewlet Packard, Berkshire, UK) to which the system was linked. The gas

chromatograph was calibrated by injection of 5 μ l aliquots of a freshly prepared 2 mM solution of propylene oxide in water.

2.12.1 Propylene oxide assay – Type 1

Assays were performed by modifications to the method of Pilkington and Dalton (1990). 5 ml conical flasks sealed with Suba Seals (W. H. Freeman, Barnsley, UK) were used. Each reaction contained 8 μ M of purified hydroxylase, reductase, and protein B or 5 mg of soluble extract (concentrations determined by the colourimetric Bradford assay) in a total volume of 475 μ l, made up with 25 mM MOPS buffer, pH 7. 3 ml of the gas phase of the reaction flask were removed and replaced with 3 ml of propylene. The flask was incubated for 1 min at 45 °C in a gyratory water bath. Initiation of the reaction was by the addition of 25 μ l of 100 mM ethanol-free NADH (courtesy of S. Slade, Department of Biological Sciences, University of Warwick, UK). The reaction mix was incubated for a further 3 min at 45 °C in the gyratory water bath before removal of 5 μ l of the liquid phase of the reaction mix for GC analysis. MMO activities were expressed as nmol of propylene oxide produced per min, per mg of protein. This method was used in the calculation of the activity values quoted in Chapter 3.

2.12.2 Propylene oxide assay – Type 2 (C. Lesieur, personal communication)

Further modifications to the method of Pilkington and Dalton (1990) were performed to reduce the quantity of proteins required for the assay procedure. 1.5 ml crimp top vials were sealed with crimp tops (Sigma-Aldrich Chemical Company, Dorset, UK). The reactions contained 8 μ M of each of the sMMO proteins (concentrations of hydroxylase and protein B calculated using their extinction-coefficients) or 5 mg of soluble extract protein in MOPS buffer pH 7 in a total volume of 100 μ l. 1 ml of the gas phase of the reaction vessel was removed and replaced with 1 ml of propylene. The flask was incubated for 30 s at 45 °C in a gyratory water bath and the reaction initiated by addition of 5 μ l of 100 mM ethanol-free NADH. The reaction mix was incubated for a further 3 min at 45 °C in the gyratory water bath before removal of 5 μ l of the liquid phase of the reaction mix or 500 μ l of the gas phase for GC analysis.

MMO activities were expressed as nmol of propylene oxide produced per min, per mg of protein. This method gave lower activity values (~ 60 % lower) than those obtained by the Type 1 propylene oxide assay (Section 2.12.1), but the method changes were justified as they incorporated an improved means of obtaining more accurate and reproducible values for the protein concentrations of the hydroxylase and protein B, and the reduction in assay size enabled the large number of experiments reported in this thesis to be performed. The type 2 propylene oxide assays were used in the calculation of the activity values quoted in Chapters 4-8, and have not been compared to the results obtained by the Type 1 assays.

2.12.3 Peroxide shunt assay

Assays were carried out by modifications to the method of Jiang *et al.* (1993). 24 μ M hydroxylase in 25 mM MOPS buffer, pH 7 with varying concentrations of WTB, G13Q, recombinant *Ms. trichosporium* OB3b protein B, B' or M12A:G13Q from 0-50 μ M in a total volume of 100 μ l, were sealed in 1.5 ml crimp topped vials. 1 ml of the gas phase of the reaction vessel was removed and replaced with 1 ml of propylene. The flask was incubated for 1 min at 45 °C in a gyratory water bath and the reaction initiated by addition of hydrogen peroxide to a concentration of 100 mM. The reaction mix was incubated for a further 10 mins at 45 °C in the gyratory water bath before removal of 500 μ l of the gas phase of the assay mix for GC analysis to monitor for propylene oxide formation.

2.13 Assay for monitoring the conversion of *p*-nitrophenylacetate to *p*-nitrophenol

The enzymatic conversion of *p*-nitrophenylacetate to *p*-nitrophenol was monitored spectrophotometrically by modifications to the method of Balls and Wood (1956). The reaction mixture (600 μ l total volume) contained 500 μ l of protein in 25 mM MOPS buffer, pH 7, and 100 μ l of 10 mg/ml *p*-nitrophenylacetate dissolved in ethanol. The reaction was started by addition of the *p*-nitrophenylacetate to the protein. After 30 s incubation at 20 °C, the solution was examined for *p*-nitrophenol formation by monitoring absorbance changes at 400nm over time.

2.14 Polyacrylamide gel electrophoresis (PAGE)

2.14.1 SDS-PAGE

The protein containing samples were boiled for 5 min in an equal volume of SDS sample buffer (100 mM Tris-HCl, pH 6.8 supplemented with SDS (2 % w/v), DTT (200 mM), glycerol (10 % (v/v)) and bromophenol blue (0.2 % (v/v))). A whole cell extraction method was used for the rapid analysis of proteins from whole cells of both methanotrophs and *E. coli*. Cultures were diluted in 25 mM MOPS buffer pH 7 to an OD₅₄₀ of 1. Harvesting of 1 ml of the culture was then carried out and the cells were re-suspended in 100 µl SDS sample buffer and boiled for 5 min. 10 µl of the boiled samples were then analysed by SDS-PAGE.

A discontinuous system of SDS-PAGE was used, as described by Laemmli (1970). It comprised a 4 % w/v stacking gel (1 ml 50 % (w/v) acrylamide/*N*, *N*'-Methylene bis-acrylamide (29:1 v/v), 4.2 ml stacking gel buffer (0.375 M Tris-HCl, pH 6.8), 125 µl 10 % (w/v) SDS, 6.3 ml H₂O, 5 µl TEMED, 1 ml catalyst (5 % (w/v) AMPS)), a 12% w/v separating gel (6 ml 50 % (w/v) acrylamide/*N*, *N*'-Methylene-bis-acrylamide (29:1 w/v), 9.4 ml separating gel buffer (1 M Tris-HCl, pH 8.8), 250 µl 10 % SDS (w/v), 4 ml 50 % (w/v) sucrose, 4.8 ml H₂O, 6.25 µl TEMED, 625 µl catalyst (5 % (w/v) AMPS), and a reservoir buffer (2.9 g/l Tris-base, 14.4 g/l glycine, 1 g/l SDS). Electrophoresis was carried out using the MINI protean system (Amersham Pharmacia Biotech, Bucks., UK). Gels were stained using Coomassie Brilliant Blue (0.5 g Coomassie Blue R-250, 225 ml methanol, 45 ml glacial acetic acid, 225 ml water) and de-stained with a solution of methanol (40 % v/v) and glacial acetic acid (10 % v/v) to visualise the protein. SDS-PAGE gels were calibrated with Dalton Mark VII-L molecular mass markers which contained bovine albumin, 66 kDa; egg albumin, 45 kDa; glyceraldehyde-3-P-dehydrogenase, 36 kDa; bovine carbonic anhydrase, 29 kDa; bovine pancreas trypsinogen, 24 kDa; soybean trypsin inhibitor, 20 kDa; and bovine milk α-lactalbumin, 14.2 kDa (Sigma-Aldrich Chemical Company, Dorset, UK).

2.14.2 Native-PAGE

For native-PAGE, the method of gel preparation and electrophoresis was the same as that for SDS-PAGE except that SDS was omitted from all the solutions and replaced with water. DTT was also omitted from the sample buffer and samples were not boiled prior to loading on the gel. Native-PAGE gels were calibrated using molecular weight markers for non-denaturing PAGE which contained bovine milk α -lactalbumin, 14.2 kDa; bovine carbonic anhydrase, 29 kDa; chicken egg albumin, 45 kDa; bovine serum albumin, 66 kDa (monomer) and 132 kDa (dimer); and jack bean urease, 272 kDa (trimer) and 545 kDa (hexamer) (Sigma-Aldrich Chemical Company, Dorset, UK).

2.15 Western blotting

Following electrophoresis, the polyacrylamide gel was soaked for 30 min in Western Transfer Buffer (20 mM Tris-HCl pH 8, 150 mM glycine, 20 % v/v methanol) Electroblotting of proteins onto Hybond-C nitrocellulose membrane (Amersham, UK) was then performed in a X-Cell I blot module (Novex) at constant voltage (30 V) for 2 hours. The membrane was blocked by soaking at 4 °C overnight in 20 ml TBST buffer (50 mM Tris-HCl pH 8, 150 mM NaCl, 0.1 % (v/v) Tween 20) containing 2 % milk (Marvel skimmed milk powder) to block non-specific protein-binding sites on the membrane. The membrane was then removed and a fresh 20 ml of TBST buffer containing 2 % milk was added, containing 50-100 μ l of anti-serum. After 2 hours shaking the anti-serum was removed by washing three times in 20 ml TBS buffer (TBST buffer without Tween 20). 20 ml of TBS buffer were then mixed with 50 μ l anti-rabbit IgG peroxidase conjugate (Sigma Immuno Chemicals, Dorset, UK) and added to the membrane and shaken for a further 2 hours. The membrane was subsequently washed twice in TBST buffer and twice in TBS buffer before visualising the bound antibody-peroxide conjugate by soaking the membrane in staining solution for 10 min. The staining solution comprised NaCl 1.5 g and 1 ml of 1 M Tris-HCl pH 7.5 dissolved in 50 ml distilled water, known as solution A, and 30 mg chloronaphthol tablet dissolved in 10 ml methanol and diluted to 50 ml with distilled water, known as solution B. 50 μ l of 8 M hydrogen peroxide were added to

solution B which was then mixed with solution A immediately prior to use. After the blot had been developed to the desired extent, the membrane was rinsed in distilled water and left to dry for 30 min at room temperature.

2.16 Mass spectrometry

Mass spectrometry was used to analyse various protein samples.

2.16.1 Electrospray ionisation mass spectrometry (ESI-MS)

ESI-MS was performed using a Quattro II QhQ tandem mass spectrometer (Micromass, UK) equipped with an electrospray ionisation (ESI) source operated with nitrogen as the nebulising gas in nebuliser assisted mode. Applied to the capillary of the ESI source was a potential difference of 2.5 - 3.5 kV relative to the counter electrode. A voltage ramp was applied to the extraction cone such that the voltage across the cone varied linearly from 30 V at 600 m/z to 90 V at 2600 m/z at a source temperature of 60 °C.

For accurate determination of molecular masses, calibration was carried out using horse heart myoglobin (Sigma-Aldrich Chemical Company, Dorset, UK) 20 pmol/ μ l. The carrier solvent was water/acetonitrile (1:1 v/v) containing 1 % formic acid, and was applied at a flow rate of 5 μ l/min. Mass spectra were acquired over the range m/z 600-1700 during a 10 s scan and data were collected in multichannel analyser mode. Processing of data was accomplished using the MassLynx (VG Biotech) software. Deconvolution of the ESI-spectrum was carried out using the maximum entropy 'MaxEnt' algorithm incorporated in the VG MassLynx software.

The ExPASy world wide web molecular biology server of the University of Geneva was used for the calculation of theoretical molecular mass values (<http://www.expasy.ch/>)

2.16.2 Matrix assisted laser desorption ionisation time of flight mass spectrometry (MALDI-ToF MS)

Matrix assisted laser desorption ionisation time of flight analysis was performed using a linear Proflex II MALDI-ToF mass spectrometer (Bruker, Analytical Systems Inc., Billerica, MA, USA) operated in a delayed ion extraction mode. A 333 nm nitrogen laser (VS-337I, Laser Science Inc., Newton, MA) with a 3 ns pulse duration and a 3 Hz repetition rate was focused onto a stainless steel multiproBE utilising a 10-spot circular sample plate.

The voltage applied to the sample was typically 20 kV. After a delaytime 17.7 kV were applied to a pulseplate and the ions were extracted from the source and accelerated into a 125 cm linear flight tube and subsequently detected by an electron multiplier. Data was recorded by a 1 cm linear LeCroy digitiser and analysed by Bruker Xtof 3.1.0 software.

The MALDI-spectrum was recorded by averaging data over 60 laser shots with a laser power just above threshold for ion formation.

Sinapinic acid (Sigma-Aldrich Chemical Company, Dorset, UK) was used as the matrix. 100 µl of a saturated solution of sinapinic acid in acetonitrile/water 2:1 and 0.1 % TFA were mixed with 25 µl of the protein solution (3 mg/ml) in ammonium acetate buffer. 0.4 µl of the mixture was applied to each sample spot and the sample droplet was dried under a stream of cold air to give a uniform crystalline layer ready for MALDI-ToF analysis.

2.17 Fluorescence studies

Protein samples in 25 mM phosphate buffer pH 7 were placed in a 3 ml quartz cuvette with a 10 mm pathlength. Fluorescence measurements were made using a Perkin Elmer LS-50 fluorimeter at room temperature with a scan speed of 500 nm/min, excitation wavelength of 280 nm, and scanned over a range from 300-450

nm. An accumulation of 8 scans were taken for each sample and scans were blanked against buffer data collected under the same conditions.

2.18 Circular dichroism spectroscopy

Protein samples for CD analysis were buffer exchanged in 25 mM phosphate buffer. CD measurements were collected on a Jasco J715 spectropolarimeter. Samples for far UV CD analysis were placed in a quartz cuvette with a pathlength of 1 mm and scanned from 190 nm - 250 nm whereas for near UV CD analysis samples were placed in a quartz cuvette with a 1 cm pathlength and scanned from 260 nm – 300 nm. In all cases the response time was 0.25 s, and the scan speed was 100 nm/min and 10 scans were accumulated. The scans were blanked against fresh buffer recorded under the same conditions.

2.19 FTIR Spectroscopy

2.19.1 Sample preparation

Pure protein was buffer exchanged into 25 mM ammonium bicarbonate buffer pH 7. The protein solutions were then frozen using liquid nitrogen and lyophilised under reduced pressure (1 mm Hg) before re-suspending in 50 mM deuterated phosphate buffer pH 7.

2.19.2 Data collection and analysis

FTIR spectra were obtained at protein solution concentrations of ~ 8 mg/ml. Spectra were recorded at room temperature using a Bruker IFS 66 FTIR spectrometer equipped with a MCT detector (Graseby infrared) operated at liquid nitrogen temperatures. Single beam spectra were collected which consisted of 256 scans, equivalent to 40 s collection time and using a 180 MHz scanning mirror frequency. The spectra collected were then converted to an absorbance spectrum by ratioing against a single beam spectrum of the appropriate buffer collected under identical conditions. Data were collected at 2 cm⁻¹ wavenumber resolution. Wavenumbers collected were from 2000-1000. As water absorbs strongly in the amide I region of

the spectrum, all experiments were performed in D₂O. Further reductions in solvent absorbance were obtained by using a 50 µm path length cell fitted with calcium fluoride windows. Band fitting to amide I absorbance was performed using the Opus version 2.2 analysis program running under the OS2 operating system (Bruker).

2.20 Single particle analysis by electron microscopy

The proteins (hydroxylase 0.05 mg/ml; sMMO complex at 1:2:2, 1:5:5 molar ratios at 0.1 mg/ml) were incubated with a glow-discharged (under air) electron microscope grid coated with a continuous carbon film. Samples were negatively stained in 4 % (w/v) uranyl-actetate. Micrographs were recorded under low-dose conditions on Phillips CM 100 and EM 301 electron microscopes. Images were scanned using a Zeiss SCAI scanner at 5.4 Å scan step. Analysis of the single particle data was undertaken using SPIDER (Frank, *et al.*, 1996). Particles were selected using Ximdisp (MRC Cambridge, UK) and aligned by a reference-free alignment based algorithm (Penczek, *et al.*, 1992) and finally classified into groups and averaged.

2.21 Analytical ultracentrifugation

2.21.1 Samples used

WTB (2 mg/ml in MOPS + 150 mM NaCl), Protein B' (2 mg/ml in H₂O + 150 mM NaCl) and G13Q (2 mg/ml in MOPS + 150 mM NaCl).

Values calculated: partial specific volume from amino acid composition:

$$\text{WTB } \bar{v} \text{ @ } 4^\circ \text{ C} = 0.7256 \text{ ml/g}$$

$$\text{G13Q } \bar{v} \text{ @ } 4^\circ \text{ C} = 0.7253 \text{ ml/g}$$

$$\text{Protein B' } \bar{v} \text{ @ } 4^\circ \text{ C} = 0.7288 \text{ ml/g}$$

$$\text{density of 150mM NaCl} = 1.006 \text{ g/ml}$$

2.21.2 Experimental procedure

Solutions of 1 and 2 mg/ml of each peptide were run, with absorbance blanks, to sedimentation equilibrium at 4 °C in 12 mm path length cells in the Beckman XL-A analytical ultracentrifuge using an An-60-Ti rotor. The rotor speeds employed were 30,000 and 42,000 rpm. The concentration distribution of the peptides was monitored using scanning absorption optics at 290 nm wavelength. The achievement of sedimentation equilibrium was determined by subtraction of scans of at least 2 hours difference in time until no difference in distribution was observed. This was done for both rotor speeds used. A baseline value of absorbance was not obtained, as the upper limit for the epoxy resin centrepieces used is 42,000 rpm.

2.21.3 Data analysis

The data obtained were analysed using WinNONLIN3 program (David A. Yphantis, Michael L. Johnson & Jeffrey W. Lary, available over the internet from <ftp://spin6.mcb.uconn.edu/pc/win95/winnonln/>). The program fits multiple data sets simultaneously accounting for speed and concentration differences. The program fits

for sigma (the reduced molecular weight which is equal to $\frac{M(1 - \bar{v}\rho)\omega^2}{RT}$) knowing

rotor speed, \bar{v} , temperature and density, can then be converted to molecular weight. The data for each peptide were fit firstly to a single ideal species model, and then, if appropriate, a self-association model using sigma calculated from monomer molecular weight. With self-association models the program fits for $\ln K_a$ in absorbance units, which were converted to per molar units using the molar extinction coefficient of the peptide, were then converted to K_d .

2.22 Crystallisation of the regulatory protein

Crystallisation of the regulatory protein was performed using the hanging drop and oil immersion methods. For the hanging drop method the protein (13-26 mg/ml) was suspended in a droplet (2 μ l) on a glass cover slip mixed with 2 μ l of the precipitant. This was placed and sealed over a 2.5 ml well containing 1 ml of precipitant. In the case of the oil immersion method the droplet of protein mixed with precipitant was immersed under oil. The precipitant that resulted in the formation of quasi-crystals was 25 mM Tris-HCl, pH 7 containing 25 mM lithium sulphate and 18 % PEG 8 K. Seeding of the quasi-crystals into a fresh preparation of regulatory protein was attempted to obtain large crystals.

2.23 Homology modelling studies

All sequence alignments were performed using the Blast alignment tool available on the ExPASy server (<http://www.expasy.ch/>). Modelling of the N-terminal region of the regulatory protein and mutants was performed using the Swissmodel program available on the same server (Peitsch, 1995).

2.24 Secondary structure prediction

Secondary structure was predicted using the Jpred² program available on the internet at <http://jura.ebi.ac.uk:8888/>. Using the single protein sequence of interest, it combines a number of modern, high quality prediction methods to form a consensus. The accuracy of the method is approximately 72.9 % (Cuff and Barton, 1999).

2.25 Small angle X-ray scattering

2.25.1 Sample preparation

Prior to the collection of scattering measurements the sMMO proteins were dialysed against 25 mM MOPS buffer pH 7. A sample of the dialysis buffer was retained and

used as a blank to subtract the effect of the scattering contribution from the solvent. Each protein (A, mB, B' and C) was analysed individually as well as various ratios of components A:B:C ranging from 1:2:2 to 1:10:10. Protein samples were centrifuged into a 1 mm glass capillary that was glued into the brass sample holder.

2.25.2 X-ray scattering data acquisition and analysis

X-ray data were collected using the small-angle X-ray scattering station at Los Alamos, USA, using X-rays generated from a copper anode at a frequency of 1.54 Å over a Q range of 0.01-0.3 Å, as described by Heidorn and Trewella (1988). Samples were maintained at 16 °C during data acquisition. Typical data collection times were 10 min to 2 h, depending on protein concentration and molecular mass. All scattering experiments were repeated at least twice using samples from independent preparations.

Scattering data were reduced and analysed as detailed in Heidorn and Trewella (1988). Parameters used in the interpretation of the scattering data included radius of gyration, R_g , forward (or zero-angle) scattering intensity, I_0 , and the pairwise length distribution function, $P(r)$. $P(r)$ is the probable frequency of vector lengths connecting small-volume elements within the scattering particle. $P(r)$, therefore, goes to zero at the maximum linear dimension of the particle, d_{max} . For a dilute solution of monodisperse, identical particles the scattering intensity, $I(Q)$, and $P(r)$ are related by a Fourier transformation:

$$\text{Equation 2.1: } P(r) = r^2/2\pi^2 \int I(Q)Q^2(\sin(Qr)/Qr) dQ$$

where $Q = (4\pi \sin\theta)/\lambda$ is the amplitude of the scattering vector, θ is half the scattering angle, and λ the wavelength of the scattered radiation (1.54 Å). $P(r)$ is calculated from the experimental scattering profile using an indirect Fourier transform method (Moore, 1980). R_g and I_0 are calculated as the second and zeroth moments of $P(r)$, respectively.

I_0 , when normalized to molar concentration, is proportional to the square of the molecular weight for particles with the same mean scattering densities. By using a standard protein of known molecular weight (lysozyme in this study), one can determine the molecular weight of another monodisperse protein sample by taking

ratios of the I_0 values. An I_0 analysis can thus be used to check the monodispersity in samples of known protein concentration or to determine accurate protein concentrations for solutions known to be monodisperse (Krueger *et al.*, 1998). In addition, I_0 is highly sensitive to complex formation (Krueger *et al.*, 1998). For a three component system with component molecular weights M_a , M_b , and M_c , I_0 is proportional to $(M_a + M_b + M_c)^2$ for the 1:1:1 complex but to the much smaller $M_a^2 + M_b^2 + M_c^2$ if the components do not form a complex. For a mixture of partially complexed components, I_0 is proportional to the concentration-weighted average of the I_0 values for the complexed and uncomplexed components.

Molecular volumes were calculated from the scattering data using the equation:

Equation 2.2: $V=2\pi^2I_0/Q_i$

where Q_i is the scattering invariant (Porod, 1982):

Equation 2.3: $Q_i = \int Q^2 dQ I(Q)$

Because the scattering data are measured only over a finite Q -range, the scattering invariant, and hence molecular volume, calculations are subject to systematic error. These errors vary for different experiments and in our case are of the order of 10 %, based on comparison of the expected volumes with those calculated from the scattering data.

2.25.3 Modelling the scattering data

In the absence of high-resolution crystal structure data, the scattering from globular proteins can be effectively modelled using uniform-density ellipsoid shapes (Henderson *et al.*, 1992; Zhao *et al.*, 1998). Protein B and the reductase were each modelled as uniform density ellipsoids, and model scattering profiles were calculated using a Monte Carlo simulation program [SASMODEL (Zhao *et al.*, 1998)]. SASMODEL generates models using one or more ellipsoid shapes with dimensions constrained within a range given by the user. Large numbers of models are generated by an algorithm that assigns random values (within the defined constraints) to the lengths of each semi-axis. For each model generated, a $P(r)$ function is calculated using a rapid Monte Carlo integration method (Heidorn and Trewhella, 1988) in which the ellipsoids are filled with random points and all possible vector lengths between the points are summed to give $P(r)$. Model $P(r)$ functions based on the

hydroxylase crystal structure [Protein Data Bank (PDB) accession no. P22869], as well as for the sMMO complex, were calculated using a program (PRPDB) that utilizes a rapid Monte Carlo integration method similar to that used by SASMODEL. The atomic co-ordinates from the crystal structure are placed in a box with a three-dimensional grid. An option to include a hydration layer, in which the solvent layer at the surface of the protein is assigned a different mean scattering density to the bulk solvent, is included. The thickness and contrast of the hydration layer are parameters that can be chosen by the user. The volume elements of the grid are assigned scattering density values based on the number of electrons that fall within the volume element (from either the protein or hydration layer components). Alternatively, a uniform density can be assigned to grid elements occupied by the structure. The model $P(r)$ is calculated by filling each volume element occupied by the molecular shape with 4,000 random points and summing all vector-lengths between pairwise combinations of the saved points. PRPDB can also use the output from SASMODEL and calculate $P(r)$ profiles from uniform density ellipsoid shapes as well as composite models made up from uniform density ellipsoids combined with crystal structure coordinates. Typically, 4,000 points were used in our model $P(r)$ calculations, which gave smooth well-determined profiles. Both SASMODEL and PRPDB calculate model scattering profiles for comparison with experiment by Fourier transformation of $P(r)$. Model fits are evaluated using least-squares methods and saved in PDB format for ease of viewing.

2.26 Atomic force microscopy (AFM)

The protein samples to be analysed were placed in a Nanoscope III fluid cell (Digital Instruments, Santa Barbara, CA) and imaged under 50 mM Tris buffer pH 7 which was flown over the cells to remove any non-adsorbed protein material. The samples were imaged using tapping mode AFM in fluid, using a triangular cantilever of nominal spring constant 0.3-0.6 N/m. The cantilever was oscillated at a resonance frequency between 16 and 32 kHz. The imaging parameters were set to obtain a high-resolution image with minimal tip-sample interactions. Particle volumes were determined using custom built software (C. Goh Group, University of Toronto, Canada).

2.27 *E. coli* strains

<i>E. coli</i> strain	Source
AD202	Nakano <i>et al.</i> (1994)
DH5 α	Hanahan (1983)
BL21(DE3)	Novagen, Abingdon, UK

2.27.1 Plasmids

Plasmid	Characteristics	Source
pGEX-2T	Ap ^R translational fusion expression vector containing the <i>Shistosoma japonicum</i> GST gene under the control of the <i>tac</i> promoter (5 kb)	Amersham Pharmacia Biotech, Bucks., UK
pGEX-WTB	pGEX-2T containing <i>mmoB</i> from <i>Mc. capsulatus</i> (Bath) as a <i>Bam</i> HI/ <i>Eco</i> RI fragment (5.5 kb)	Lloyd <i>et al.</i> , (1997)
pGEX-G13Q	pGEX-WTB containing a Gly ¹³ to Gln ¹³ mutation in <i>mmoB</i>	Lloyd <i>et al.</i> , (1997)
pGEX-MTB	pGEX-2T containing <i>mmoB</i> from <i>Ms. trichosporium</i> OB3b as a <i>Bam</i> HI/ <i>Eco</i> RI fragment (5.5 kb)	S. Harris, unpublished
pGEX-M12AG13Q	pGEX-WTB containing Gly ¹³ to Gln ¹³ and Met ¹² to Ala ¹² mutations in <i>mmoB</i>	This study
pET-3a	Ap ^R expression vector containing the T7 RNA polymerase promoter (4.6kb)	Novagen Inc., Madison, WI, USA

pET-G13Q	pET-3a containing a Gly ¹³ to Gln ¹³ mutation in <i>mmoB</i> and a 6-His-tag at the C-terminal	This study
pET-S4-His-tag	pET-3a containing a Gly ¹³ to Gln ¹³ mutation in <i>mmoB</i> , a deletion in the first 12 bases of <i>mmoB</i> and a 6-His-tag at the C-terminal	This study
pET-N5-His-tag	pET-3a containing a Gly ¹³ to Gln ¹³ mutation in <i>mmoB</i> , a deletion in the first 15 bases of <i>mmoB</i> and a 6-His-tag at the C-terminal	This study
pET-A6-His-tag	pET-3a containing a Gly ¹³ to Gln ¹³ mutation in <i>mmoB</i> , a deletion in the first 18 bases of <i>mmoB</i> and a 6-His-tag at the C-terminal	This study
pET-Y7-His-tag	pET-3a containing a Gly ¹³ to Gln ¹³ mutation in <i>mmoB</i> , a deletion in the first 21 bases of <i>mmoB</i> and a 6-His-tag at the C-terminal	This study
pET-D8-His-tag	pET-3a containing a Gly ¹³ to Gln ¹³ mutation in <i>mmoB</i> , a deletion in the first 24 bases of <i>mmoB</i> and a 6-His-tag at the C-terminal	This study
pET-A9-His-tag	pET-3a containing a Gly ¹³ to Gln ¹³ mutation in <i>mmoB</i> , a deletion in the first 27 bases of <i>mmoB</i> and a 6-His-tag at the C-terminal	This study

pET-G10-His-tag	pET-3a containing a Gly ¹³ to Gln ¹³ mutation in <i>mmoB</i> , a deletion in the first 30 bases of <i>mmoB</i> and a 6-His-tag at the C-terminal	This study
pET-Q13-His-tag	pET-3a containing a Gly ¹³ to Gln ¹³ mutation in <i>mmoB</i> , a deletion in the first 39 bases of <i>mmoB</i> and a 6-His-tag at the C-terminal	This study

Ap, Ampicillin; GST, glutathione S-transferase; His-tag, 6 histidine residues.

2.27.2 Luria Bertani growth media for *E. coli*

Luria Bertani medium (LB) was used routinely for the culturing of *E. coli*, as detailed in Sambrook *et al.* (1989) and Maniatis *et al.* (1982). Solid media was prepared by the addition of 2 % (w/v) Bacto-agar (Difco, Michigan, USA) prior to sterilisation. All media were made using distilled water and sterilised by autoclaving at 120 °C, 15 lb/in² for 15 min. Sterile disposable filter units with a pore size of 0.2 µm (Millipore, Watford, UK) were used to sterilise water soluble, heat labile solutions.

2.27.3 Culture storage

For long-term storage, 500 µl of *E. coli* overnight cultures were mixed with 500 µl of sterile glycerol (50 %) and frozen in liquid nitrogen for storage at – 70 °C. To re-culture the *E. coli* strain, 10ml LB, containing antibiotic as appropriate, was inoculated with 50 µl of the glycerol stock.

2.27.4 Culturing conditions for *E. coli*

E. coli strains were routinely grown in batch cultures of 10 ml, 50 ml or 1 l volumes at 37 °C with shaking at 200 rpm. Antibiotics appropriate to the *E. coli* strain and

plasmid were included in the growth medium. This ensured plasmid maintenance and strain purity.

2.27.5 Antibiotics

Stock solution was prepared by dissolving ampicillin in water to a concentration of 100 mg/ml, sterilised by filtration using a sterile disposable filter unit with a pore size of 0.2 μm (Millipore, Watford, UK) and stored in 1 ml aliquots at $-20\text{ }^{\circ}\text{C}$. Ampicillin was added to LB media to give a working concentration of 100 $\mu\text{g/ml}$.

2.28 Nucleic acids techniques

2.28.1 Plasmid extraction

Plasmid DNA was extracted using a QIAGEN MINIPREP kit (QIAGEN, Crawley, West Sussex, UK) according to the instructions of the manufacturer.

2.28.2 Extraction of DNA with phenol and chloroform

DNA was extracted from solutions containing proteins by the addition of an equal volume of a phenol chloroform mix (containing phenol and chloroform in a 1:1 ratio). After vigorous mixing by vortexing and subsequent centrifugation at $20800 \times g$, $4\text{ }^{\circ}\text{C}$, the DNA was recovered by ethanol precipitation (Section 2.28.3) of the upper aqueous phase.

2.28.3 Precipitation of nucleic acids

To a specified volume of a solution containing nucleic acids was added $1/10^{\text{th}}$ of the original volume of 3 M sodium acetate (pH 5.2) and 2 times the original volume of ethanol and incubated for 30 mins at $-20\text{ }^{\circ}\text{C}$. Centrifugation at $20,800 \times g$, $4\text{ }^{\circ}\text{C}$ for 20 min pelleted the nucleic acids, which were then washed in 70 % (v/v) ethanol and air-dried before re-suspension in an appropriate volume of sterile water or TE buffer pH 8 (Tris-HCl 10 mM, di-sodium EDTA 1 mM).

2.28.4 Determination of the concentration of nucleic acids

The concentration of nucleic acids was determined from the absorbance at 260 nm, measured using quartz cuvettes with a 1 cm path length in a Beckmann DU-70 spectrophotometer. Assuming an A_{260} of 1 for the following nucleic acid concentrations: oligonucleotides, $20 \mu\text{g ml}^{-1}$; RNA, $40 \mu\text{g ml}^{-1}$ and double stranded DNA, $50 \mu\text{g ml}^{-1}$ (Sambrook *et al.*, 1989), the concentration could be calculated.

2.28.5 Agarose gel electrophoresis

The Minigel apparatus (Flowgen Instruments Ltd., Sittingbourne, UK) was used for agarose gel electrophoresis. Gels containing 1 % agarose (w/v) were prepared and run in $1 \times$ Tris-borate EDTA (TBE) buffer pH 8 (Tris-base 90 mM, Boric acid 90 mM, EDTA 2.5 mM). $0.5 \mu\text{g/ml}$ ethidium bromide was added directly to the gel before casting. DNA samples ($10 \mu\text{l}$) were mixed with one-fifth volume marker dye ($2 \mu\text{l}$) (0.25 % (w/v) bromophenol blue, 0.25 % (w/v) xylene cyanol, 30 % glycerol). Gels were run at a constant current of 50 mA for 1-2 hours. DNA was visualised on a UV transilluminator and photographed using an instant camera (CU5 Land Camera, loaded with Polaroid 665 positive/negative film). The agarose gels were calibrated with a 1 kb ladder (Gibco BRL, Life Technologies Ltd., Paisley, UK).

2.29 Enzymatic modification of DNA

2.29.1 Restriction endonuclease digestion of DNA

Restriction endonucleases and buffer solutions were supplied by Gibco BRL (Life Technologies Ltd., Paisley, UK) and New England Biolabs (Beverly, MA, USA). DNA was digested according to the instructions of the manufacturer.

2.29.2 Dephosphorylation of DNA

DNA was dephosphorylated using alkaline phosphatase obtained from Boehringer Mannheim (East Sussex, UK) and used according to the instructions of the manufacturer.

2.29.3 Ligation of DNA

T4 DNA ligase was used to ligate DNA. It was obtained from Gibco BRL (Life Technologies Ltd., Paisley, UK) and used according to the instructions of the manufacturer.

2.29.4 Agarose gel purification of DNA

Agarose gels were made and run as detailed in section 2.27.5, except that TAE buffer pH 8 (0.04 M Tris-acetate, 0.001 M EDTA) was used instead of TBE buffer. The DNA fragments separated were removed from the gel by excision of the DNA bands and purified using the GeneClean™ Kit (Bio101 Vista, California, USA) according to the protocol of the manufacturer.

2.30 PCR

2.30.1 Design of oligonucleotides

Oligonucleotides used for PCR and sequencing were synthesised and purified by Gibco BRL (Life Technologies Ltd., Paisley, UK).

2.30.2 PCR amplification

PCR amplification was performed in a total volume of 50 µl in 0.5 ml Eppendorf tubes in a TouchDown Thermal Cycling System (Hybaid, Tennington, Middlesex, UK). Reaction mixtures were composed of 1.5 mM MgCl₂, 50 mM KCl, 10 mM Tris-HCl pH 9, 100 µM of each dNTP, 50 pmol of each primer, 2.5 units of *Taq* polymerase (Gibco BRL, Life Technologies Ltd., Paisley, UK) and approximately 1

ng template DNA. The reaction conditions were as follows; 30 cycles consisting of denaturation at 94 °C for 1min, annealing at 50 °C for 1min, polymerisation at 72 °C for 1 min and then a final step of 72 °C for 10 min.

2.31 DNA sequencing

DNA sequencing reactions were performed by cycle sequencing with the Dye Terminator Kit (PE Applied Biosystems, Warrington, Cheshire, UK). The primers used are detailed in the relevant sections (Chapter 6, Table 6.1; Chapter 7, Table 7.1). The nucleotide sequences obtained were manually aligned with the expected sequences to identify if the desired sequence had been cloned.

2.32 Transformation

A 10 ml overnight culture of the appropriate *E. coli* strain was grown and 200 µl of it was used to inoculate a second 10 ml culture which was left to grow for ~3 h or to an OD of ~0.5-0.6. The second culture was then centrifuged at 2,000 × g for 5 min at 4 °C. The pellet was re-suspended in 0.1 M MgCl₂ at 4 °C to half the original volume (5 ml) and the centrifuged immediately at 2,000 × g for 10 min at 4 °C. The pellet formed was re-suspended in 0.1 M CaCl₂ at 4 °C in half the original volume (5ml) and centrifuged immediately at 2,000 × g for 10 min at 4 °C. The resultant pellet was then re-suspended in 0.1 M CaCl₂ at 4 °C in 1/20th of the original volume (0.5 ml) and incubated on ice for 90 min. After incubation, 100 µl of the cells were added to either ligated DNA or purified plasmid and left on ice for 30 min before a 1.5 min heat shock at 42 °C followed by a further 10 min incubation at 4 °C. The resultant suspension was added to 800 µl SOC (2 % (w/v) bacto-tryptone, 0.5 % (w/v) yeast extract, 10 mM NaCl, 2.5 mM KCl, 10 mM MgCl₂, 10 mM MgSO₄, 20 mM glucose) and incubated at 37 °C for 1 h with shaking. This time allowed for the plasmid-encoded antibiotic resistance genes to be expressed. Cells were then plated onto LB agar containing the appropriate antibiotic for plasmid selection and incubated overnight at 37 °C.

2.33 Chemicals and gases

Gases, including methane, oxygen, propene, argon, oxygen free nitrogen and air were obtained from either BOC (London, UK) or Linde Gas Ltd. (Stoke on Trent, UK). All chemicals and biochemicals were of analytical grade and obtained from Sigma-Aldrich Chemical Company (Dorset, UK) and BDH Chemicals Ltd. (Dorset, UK). Restriction endonucleases and DNA modifying enzymes were obtained from Gibco BRL (Life Technologies Ltd., Paisley, UK) and New England Biolabs (Beverly, MA, USA)

Chapter 3

Optimisation of Purification Protocols for Wild-Type, Recombinant and Mutant Forms of Protein B and the Reductase and Hydroxylase Components of sMMO

3.1 Introduction

The isolation of the pure form of a protein is a vital step in the advancement of understanding biological structure and function. Isolation of the catalytic species is essential for the understanding of an enzyme's mechanism of action and would be impossible without techniques that allow its separation from other proteins and cellular components.

The purification of protein B (the regulatory protein) from *Mc. capsulatus* (Bath) to homogeneity was reported by Green and Dalton (1985) and was achieved by the use of ion exchange- and gel filtration-chromatography followed by a final hydroxylapatite step. Subsequent purification attempts proved unsuccessful and resulted in the isolation of at least two forms of the protein (Pilkington *et al.*, 1990; Bhambra, 1996). Recently these forms of the protein have been identified as active, full-length protein B and inactive N-terminally truncated cleavage products known as B' and B'' (Bhambra, 1996; Lloyd *et al.*, 1997). Efforts to prevent truncate formation focused on the addition of protease inhibitors at the time of cell lysis and in the subsequent purification buffers. However, prevention of cleavage was not achieved. Attempts to separate proteins B and B' in order to obtain pure, active protein B for further studies involved the use of various combinations of reverse phase-, hydrophobic interaction- and gel filtration- chromatography, all of which proved unsuccessful (Bhambra, 1996).

In order for studies of protein B of sMMO to continue, it was essential that the full length, active protein species could be purified to homogeneity. Similarly, if the mechanism of cleavage to form the inactive truncates B' and B'' was to be

understood, and structural comparisons between the active and inactive species were to be possible, then it was necessary to be able to purify the truncated forms.

It is not known whether the regulatory protein from other methanotrophs such as *Ms. trichosporium* OB3b undergoes a similar cleavage reaction to that observed for protein B from *Mc. capsulatus* (Bath). However, recent studies by Lloyd (1997) on the recombinant form of *Ms. trichosporium* OB3b protein B, identified the occurrence of truncate formation. Purification of wild-type protein B from *Ms. trichosporium* OB3b to homogeneity was necessary to determine the possible presence of truncate formation in protein B from the native host.

The work in this chapter concentrates on the optimisation of previously published protocols for the purification of large quantities of > 90 % pure wild-type and recombinant protein B from both *Mc. capsulatus* (Bath) and *Ms. trichosporium* OB3b, and hydroxylase and reductase proteins from *Mc. capsulatus* (Bath). This was conducted in order that further characterisation of the regulatory proteins and sMMO components was possible, using techniques for which optimal purity was essential.

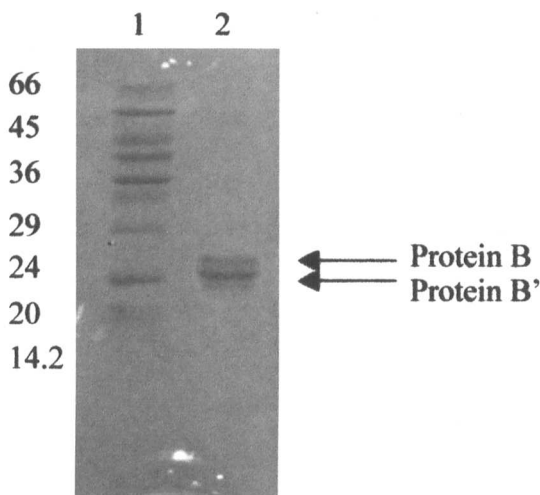
3.2 Purification of wild-type protein B/B' from *Mc. capsulatus* (Bath)

Protein B purified in this study using the protocol developed by Pilkington *et al.* (1990) was analysed by SDS-PAGE (Chapter 2, Section 2.14.1) and shown to consist of a mixture of intact and truncated versions of the protein (Figure 3.1). This observation highlighted the need to optimise the purification protocol in order to obtain pure protein B devoid of the cleavage products.

Figure 3.1: SDS-PAGE of protein B purified using the purification procedure developed by Pilkington *et al.* (1990).

Lane 1: Molecular weight markers (bovine albumin, 66 kDa; egg albumin, 45 kDa; glyceraldehyde-3-P-dehydrogenase, 36 kDa; bovine carbonic anhydrase, 29 kDa; bovine pancreas trypsinogen, 24 kDa; soybean trypsin inhibitor, 20 kDa; bovine milk α -lactalbumin, 14.2 kDa).

Lane 2: Protein B purified by the method of Pilkington *et al.* (1990) indicating the presence of 2 protein bands at ~ 16 kDa and ~ 15 kDa, corresponding to protein B and protein B' respectively.

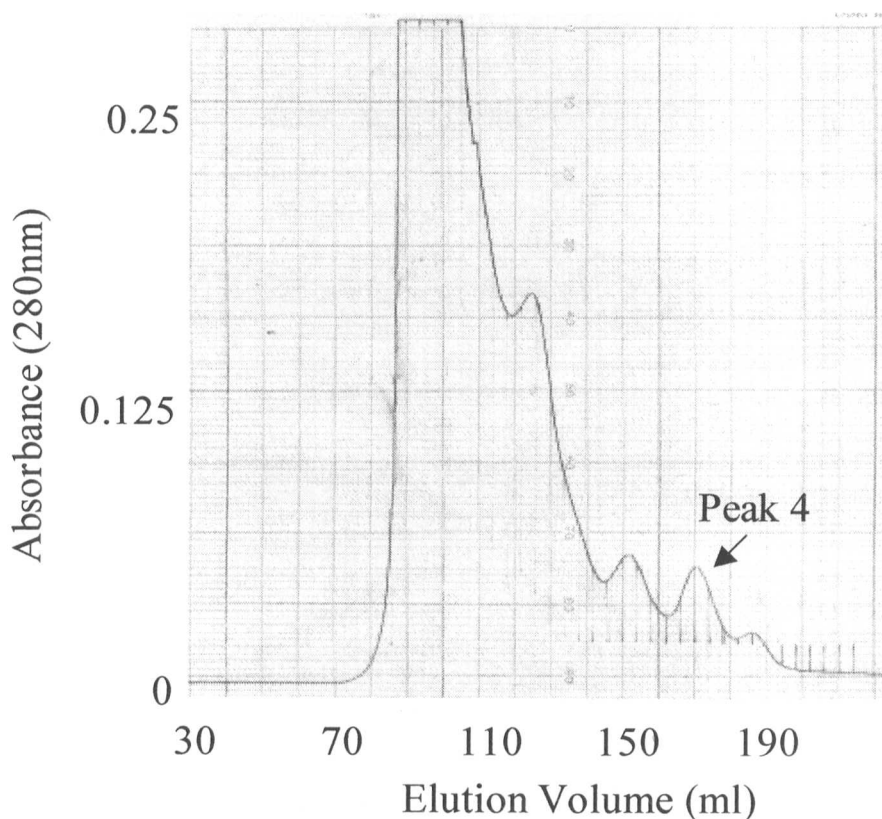


3.2.1 Optimisation of the published purification procedure

Protein B cleaves to form inactive protein B' and B'' over time (Bhambra, 1996; Lloyd *et al.*, 1997). Therefore, efforts were made to increase the speed of purification in an attempt to minimise the time available for this occurrence. Ammonium sulphate precipitation was undertaken as a possible method of achieving this (Chapter 2, Section 2.3.5, Step 1). Subsequent gel filtration chromatography of the ammonium sulphate treated sample using a Superdex 75 FPLC column (2.6 cm by 61 cm; 325 ml) (Amersham Pharmacia Biotech, Bucks., UK) equilibrated with 25 mM MOPS buffer, pH 7 (Chapter 2, Section 2.3.5, Step 2) further purified the protein. The protein was eluted in a size dependent manner (Figure 3.2).

Figure 3.2 Purification profile of protein B from *Mc. capsulatus* (Bath) on a Superdex 75 gel filtration column.

The column was equilibrated in 25 mM MOPS buffer, pH 7. The elution rate was 1 ml/min. Peak 4 eluted after approximately 170 ml over 3 fractions of 4 ml each.

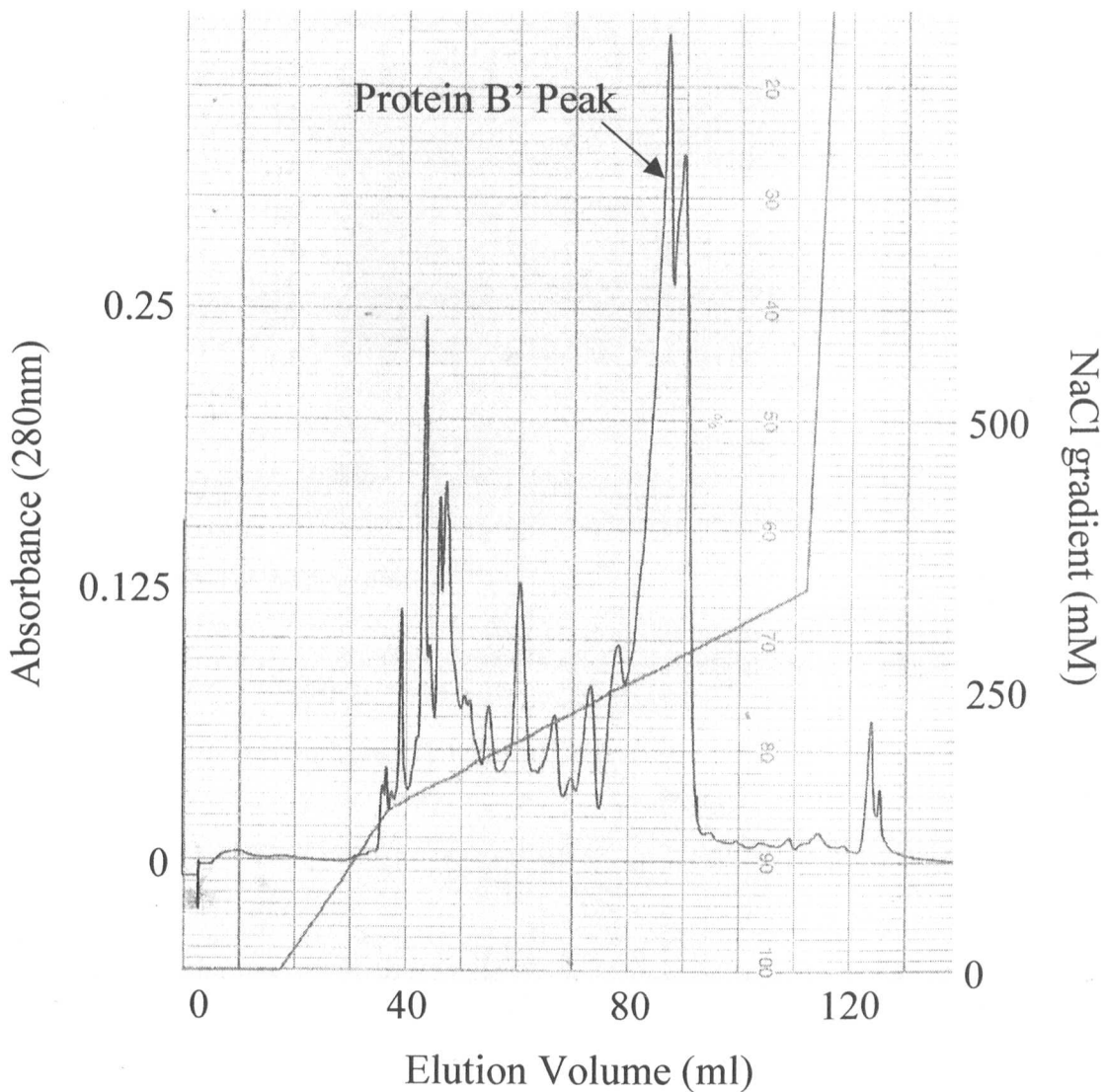


Peak 4 (Figure 3.2) was proposed to correspond to protein B due to its position of elution from the gel filtration column. However, the protein was found to be inactive, which suggested that it had already undergone the cleavage reaction to form protein B'. The final purification step of anion exchange chromatography was conducted such that pure protein B' would be obtained for further analysis.

The peak 4 fraction from the gel filtration purification step was loaded onto a MONO Q anion exchange FPLC column (HR10/10; 10ml) (Amersham Pharmacia Biotech, Bucks., UK) equilibrated with 25 mM MOPS, pH 7. The protein eluted over a linear gradient of 150 to 350 mM NaCl over 10 column volumes (Chapter 2, Section 2.3.5, Step 3), and the protein of interest at 275 mM NaCl (Figure 3.3).

Figure 3.3 Purification profile of protein B' from *Mc. capsulatus* (Bath) on a MONO Q column.

The column was equilibrated in 25 mM MOPS buffer, pH 7. Protein was eluted over a linear NaCl gradient of 150-350 mM NaCl. The peak indicated corresponds to protein B', eluted at 275 mM NaCl.



SDS-PAGE analysis indicated the protein to be ~ 95 % pure B' (Figure 3.4). Mass spectrometry analysis identified the purified protein to have a mass of 14629.7 Da (Figure 3.5). This confirmed the nature of the protein as that of protein B' and not that of protein B, which would have given a mass value of ~15852 Da, or protein B'', which would have given a mass value of ~12717 Da, based on the known DNA sequence of protein B.

Figure 3.4: SDS-PAGE of MONO Q purified protein B'.

Lane 1: Molecular weight markers (bovine albumin, 66 kDa; egg albumin, 45 kDa; glyceraldehyde-3-P-dehydrogenase, 36 kDa; bovine carbonic anhydrase, 29 kDa; bovine pancreas trypsinogen, 24 kDa; soybean trypsin inhibitor, 20 kDa; bovine milk α -lactalbumin, 14.2 kDa).

Lane 2: Protein B' after the final purification step identified as a single band at ~ 15 kDa so showing it to be ~ 95 % pure and containing no protein B or protein B".

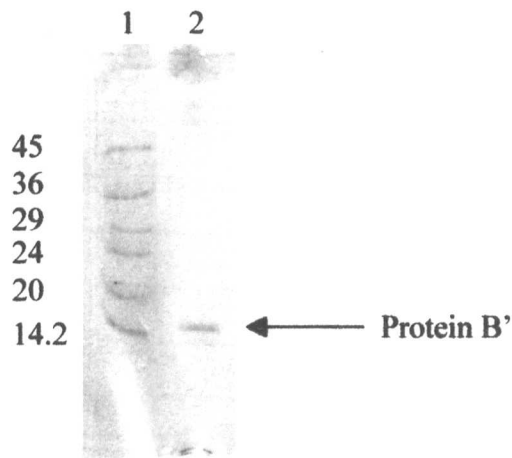
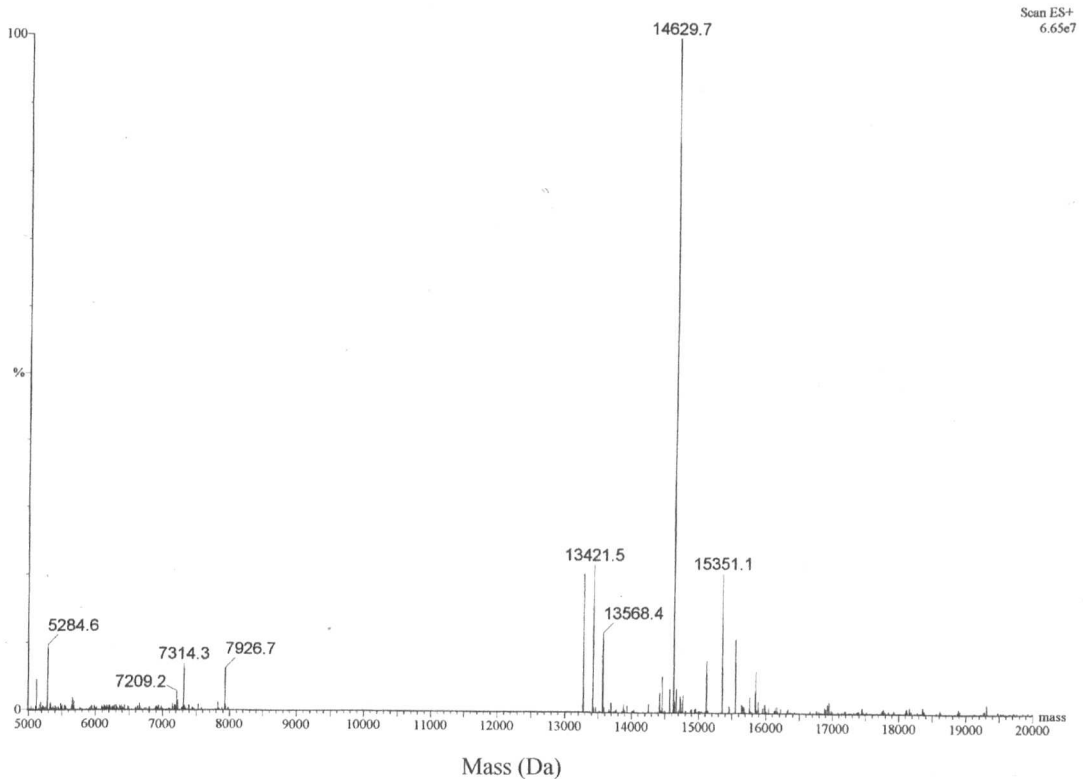


Figure 3.5: ESI-MS of the pure protein.

The ESI-MS spectrum of the *Mc. capsulatus* (Bath) protein B/B' was recorded on a Quattro II tandem mass-spectrometer with an electrospray ion source and the data were processed using the MassLynx program (VG Biotech) (Chapter 2, Section 2.16.1).

Relative Abundance



The determination of molecular masses by mass spectrometry was reported as far back as 1912. However, only more recently, in the 1960s-1970s has its use in bio-molecular research been possible (Barber *et al.*, 1981; Meng *et al.*, 1988). Electrospray ionisation mass spectrometry is a powerful analytical technique for the analysis of proteins and peptides (Smith *et al.*, 1990; Chait and Kent, 1992). ESI-MS has been used successfully for the measurement of molecular masses up to 100,000 Da at resolutions of ~ 1 unit (Covey *et al.*, 1988). Thus ESI-MS was the ideal technique for use in determining the exact molecular masses of the protein(s) within the purified *Mc. capsulatus* (Bath) protein B sample.

Overall, a reproducible purification procedure for obtaining homogeneous protein B' had been devised, although the initial objective of devising a method for isolating protein B had not been accomplished. The observation that protein B degraded so rapidly to protein B' during the purification procedure emphasised the highly sensitive nature of the protein.

3.3 Preparation of anti-serum against proteins B and B'

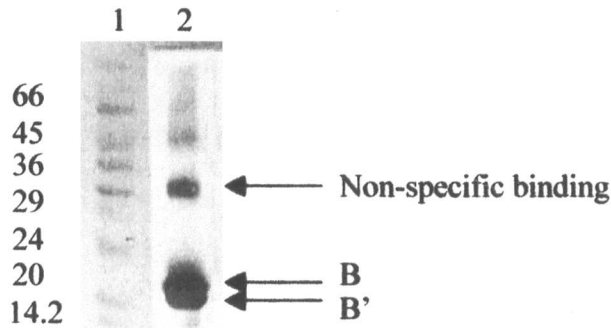
Antibodies to protein B and B' were required for use as an assay for detection of their production in cell samples. The purification of protein B by the method of Pilkington *et al.* (1990) yielded a mixture of proteins B and B' (Figure 3.1), and was identified as being free from contaminating proteins and was, therefore, suitable for raising antibodies. Antiserum was raised (Chapter 2, Section 2.11) using the wild type *Mc. capsulatus* (Bath) protein B and B' mixture as the immunogen. SDS-PAGE of proteins B and B' from *Mc. capsulatus* (Bath) was performed followed by Western blotting with ~ 100 μ l of the first bleed of antiserum against the proteins (Chapter 2, Section 2.15). Binding was observed in each case (Figure 3.6). The control reaction with pre-immune serum proved that the binding was not a non-specific event (data not shown). The antiserum produced was found to bind to both proteins B and B'.

Figure 3.6: Western blot analysis of purified protein B and B' from *Mc. capsulatus* (Bath) probing with antibodies to proteins B and B' from the first bleed.

Specific binding of the antibodies to proteins B and B' is illustrated.

Lane 1: Molecular weight markers (bovine albumin, 66 kDa; egg albumin, 45 kDa; glyceraldehyde-3-P-dehydrogenase, 36 kDa; bovine carbonic anhydrase, 29 kDa; bovine pancreas trypsinogen, 24 kDa; soybean trypsin inhibitor, 20 kDa; bovine milk α -lactalbumin, 14.2 kDa).

Lane 2: Proteins B and B'.



3.4 Purification of recombinant *Mc. capsulatus* (Bath) protein B (WTB) and the single mutant G13Q

Plasmids containing the genes encoding wild-type protein B from *Mc. capsulatus* (Bath) [pGEX-WTB] and the mutant version [pGEX-G13Q] (Lloyd, 1997; Lloyd *et al.*, 1997) were available. These produced the proteins with GST affinity tags at the N-terminus and provided an alternative method for the rapid purification of protein B. The system had been engineered such that the removal of the tag with thrombin protease was possible (Lloyd, 1997). However, subsequent purification of the protein from the cleaved GST protein as well as any uncleaved protein and the thrombin protease was important. Also, as the G13Q mutant had been shown to have increased stability (Lloyd *et al.*, 1997), it provided a viable alternative active protein B for use in experiments in place of the wild-type form which is sensitive to cleavage. Efforts, therefore, were concentrated on optimising a purification method for both proteins in order to obtain highly pure protein samples of each for characterisation studies.

3.4.1 Transformation of constructs into protease negative cells for expression

pGEX-WTB and pGEX-G13Q were provided as glycerol stocks in *E. coli* Inv α F' cells (Chapter 2, Section 2.27.1). Cultures of them were grown and the plasmids purified. The protease-negative *E. coli* AD202 strain (Nakano *et al.*, 1994) was chosen for improving protein expression levels. Thus, transformation of [pGEX-WTB] and [pGEX-G13Q] into competent *E. coli* AD202 cells was conducted and cells containing the plasmids selected by the ampicillin resistance conveyed.

3.4.2 Protein induction

Protein induction was controlled by an isopropyl β -D-thiogalactopyranoside (IPTG) promoter. Protein expression was induced for both pGEX-WTB and pGEX-G13Q at an OD₅₄₀ of \sim 0.5 by addition of 1 mM IPTG at 37 °C. Samples were taken for SDS-PAGE and Western blot analysis, probing with antibodies to protein B/B', before IPTG induction and at 1, 2, 3 and 4 hours after induction. Figures 3.7 and 3.8 show the results obtained for WTB, which were the same as those observed for the G13Q samples.

Figure 3.7: SDS-PAGE analysis of samples of *E. coli* AD202 [pGEX-WTB] before and after IPTG induction.

Lane 1: Molecular weight markers (bovine albumin, 66 kDa; egg albumin, 45 kDa; glyceraldehyde-3-P-dehydrogenase, 36 kDa; bovine carbonic anhydrase, 29 kDa; bovine pancreas trypsinogen, 24 kDa; soybean trypsin inhibitor, 20 kDa; bovine milk α -lactalbumin, 14.2 kDa).

Lane 2: AD202 [pGEX-WTB] before induction with IPTG.

Lane 3: AD202 [pGEX-WTB] 1 h after induction with IPTG.

Lane 4: AD202 [pGEX-WTB] 2 h after induction with IPTG.

Lane 5: AD202 [pGEX-WTB] 3 h after induction with IPTG.

Lane 6: AD202 [pGEX-WTB] 4 h after induction with IPTG.

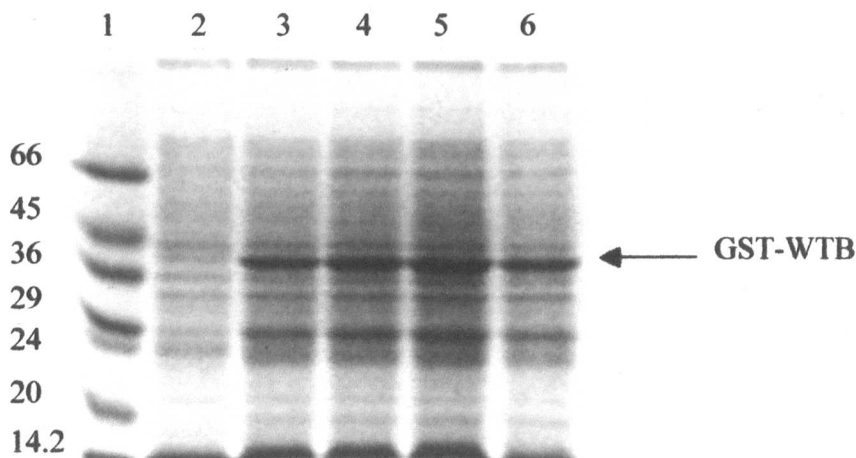
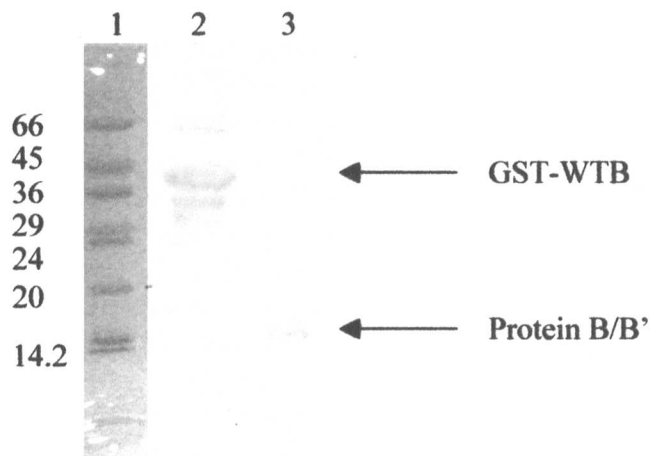


Figure 3.8: Western blot analysis of *E. coli* AD202 [pGEX-WTB] 4 h after induction with IPTG, probing with antibodies to protein B/B'.

Lane 1: Molecular weight markers (bovine albumin, 66 kDa; egg albumin, 45 kDa; glyceraldehyde-3-P-dehydrogenase, 36 kDa; bovine carbonic anhydrase, 29 kDa; bovine pancreas trypsinogen, 24 kDa; soybean trypsin inhibitor, 20 kDa; bovine milk α -lactalbumin, 14.2 kDa).

Lane 2: AD202 [pGEX-WTB] 4h after induction with IPTG.

Lane 3: Protein B/B' control.



The gel (Figure 3.7) identified an increase with time in the expression level of a protein at ~ 43 kDa corresponding to GST-WTB induction. The blot (Figure 3.8) confirmed that the protein induced was probably GST-WTB by its cross-reaction with the *Mc. capsulatus* (Bath) protein B/B' antibodies.

3.4.3 Protein purification

The GST fusion proteins were rapidly purified from the soluble extract of *E. coli* AD202 cells using the GST affinity purification system (Amersham Pharmacia Biotech, Bucks., UK) (Chapter 2, Section 2.4). GST-WTB or GST-G13Q was eluted from the Glutathione Sepharose 4B affinity column using Tris-HCl buffer pH 8 containing 10 mM glutathione. Cleavage of the GST tag from the protein of interest was achieved by incubation of the protein for 10 min at room temperature with thrombin protease at a concentration of 10 units/mg of fusion protein. The sample was loaded directly onto a Superdex 75 FPLC gel filtration column equilibrated with 25 mM MOPS buffer, pH7. This procedure successfully separated all the proteins contained within the mixture, and eluted uncleaved GST fusion protein, thrombin protease, GST, and the protein of interest, respectively (Figure 3.9). SDS-PAGE analysis (Figure 3.10) verified the clean separation of uncleaved GST-fusion protein,

GST and the protein of interest, and indicated that the protein of interest was obtained at a purity of ~ 95 %. The figures are shown for WTB but the same results were obtained for G13Q. The protein samples were tested for propylene oxidation activity (Chapter 2, Section 2.12.1) and found to be active, indicating that the protein had not completely degraded to protein B'.

Figure 3.9: Purification profile of WTB on a Superdex 75 gel filtration column.

The column was equilibrated in 25 mM MOPS buffer, pH 7. Protein was eluted in a size dependent manner. Peak 4 corresponds to WTB.

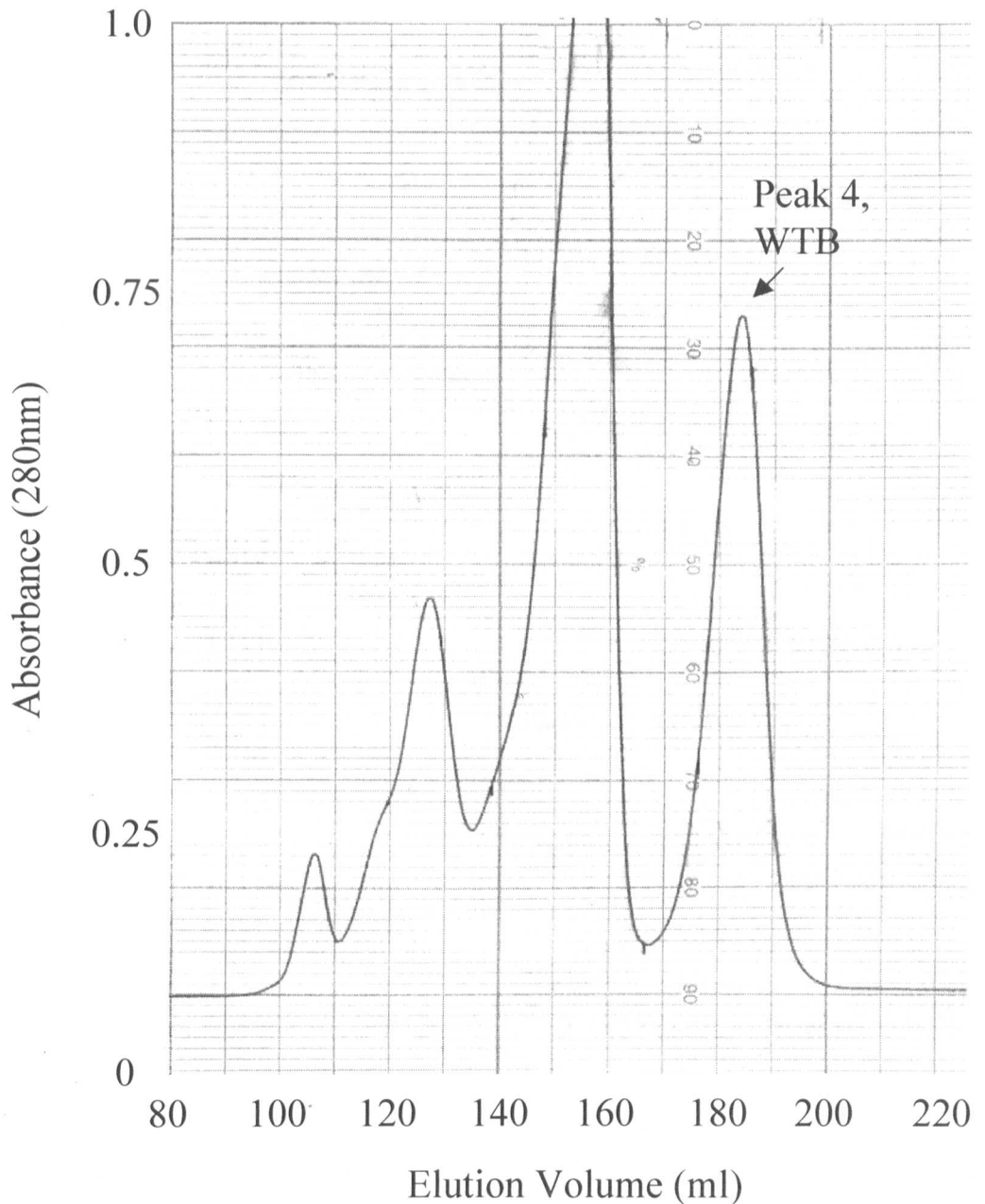


Figure 3.10: SDS-PAGE of the purification of WTB.

Lane 1: Molecular weight markers (bovine albumin, 66 kDa; egg albumin, 45 kDa; glyceraldehyde-3-P-dehydrogenase, 36 kDa; bovine carbonic anhydrase, 29 kDa; bovine pancreas trypsinogen, 24 kDa; soybean trypsin inhibitor, 20 kDa; bovine milk α -lactalbumin, 14.2 kDa).

Lane 2: GST-WTB eluted from Glutathione Sepharose 4B affinity column.

Lane 3: GST-WTB after incubation with thrombin for 10 mins at room temperature.

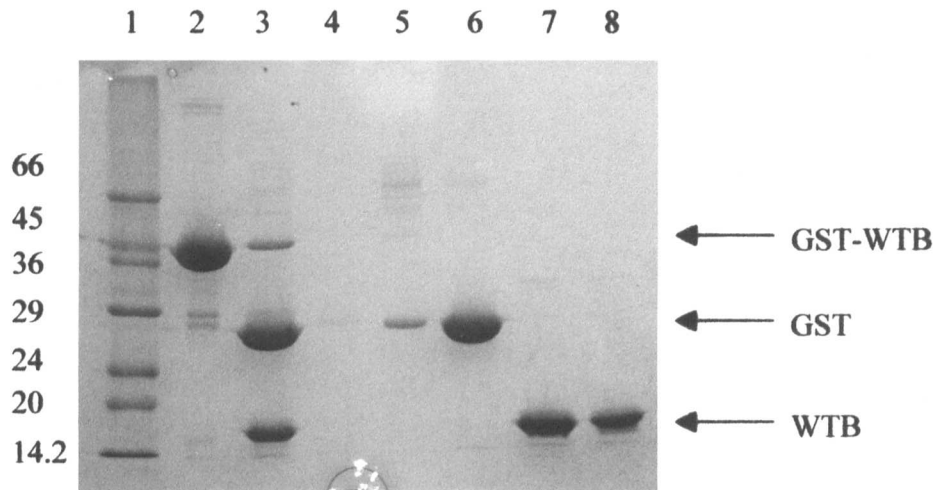
Lane 4: Blank.

Lane 5: GST protein after S75 step, under loaded.

Lane 6: GST protein after S75 step, overloaded.

Lane 7: WTB after S75 step, overloaded.

Lane 8: WTB after S75 step, under loaded.



WTB and G13Q purified by the protocol outlined were of a pure enough quality for further studies to be conducted on the samples. Also, as the purification procedure was faster than that undertaken for wild-type protein from *Mc. capsulatus* (Bath), only minimal cleavage was observed for WTB (Figure 3.10, Lanes 7 and 8). Therefore, this method of purification was successful in isolating uncleaved and minimally cleaved recombinant wild-type *Mc. capsulatus* (Bath) protein B (WTB) and the single mutant version, G13Q.

3.5 Purification of wild-type protein B from *Ms. trichosporium* OB3b

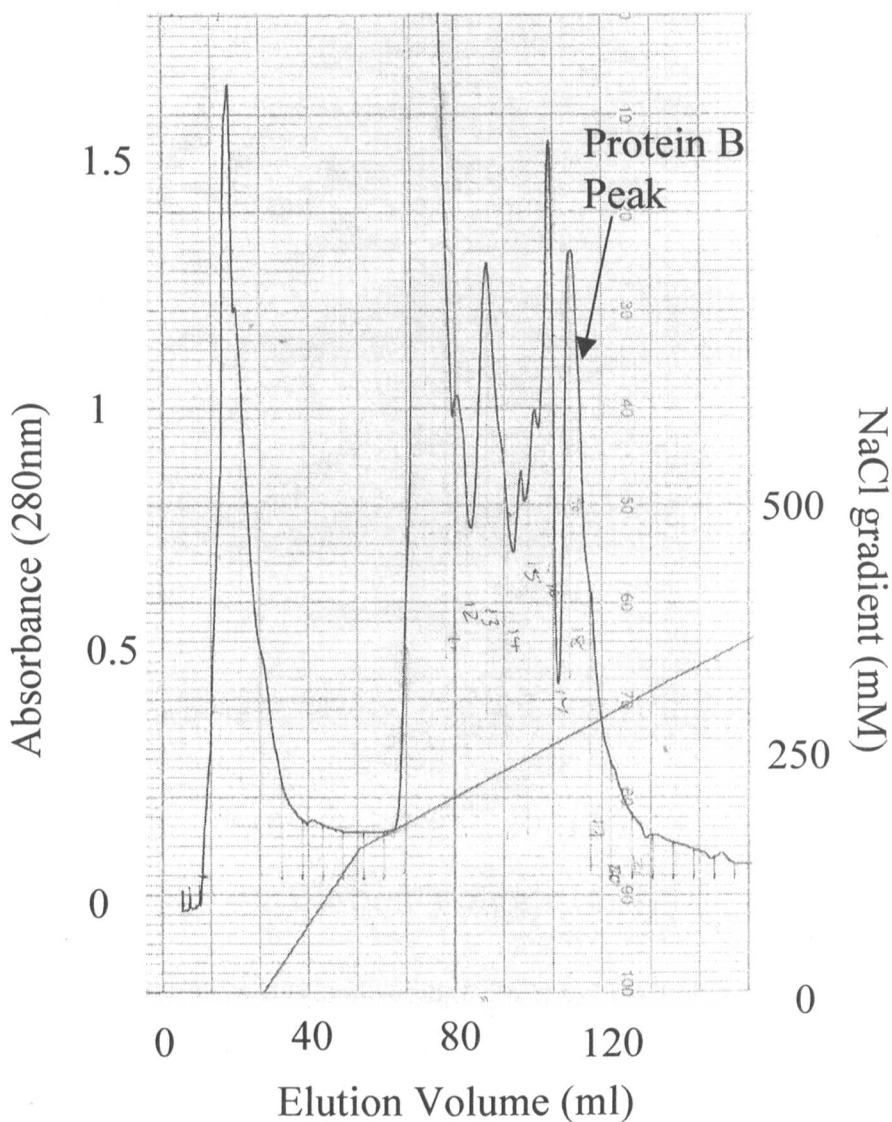
It was important to undertake studies to confirm the sequence of *Ms. trichosporium* OB3b protein B by accurately determining the molecular mass of the protein and also to elucidate whether the protein underwent a similar cleavage reaction to that observed for *Mc. capsulatus* (Bath) protein B. It was, therefore, necessary to purify protein B from *Ms. trichosporium* OB3b to a high enough purity for mass spectrometry analysis. Thus, the purification procedure developed by Fox *et al.* (1989) was modified to achieve this.

3.5.1 Optimisation of current protocols for *Ms. trichosporium* OB3b protein B purification

The modified protocol (Chapter 2, Section 2.5) involved the separation of the sMMO components from the soluble extract by ion exchange chromatography on a Sepharose CL-6B (Amersham Pharmacia Biotech, Bucks., UK) FPLC column followed by ammonium sulphate precipitation of the protein B fractions. Subsequent anion exchange chromatography on a MONO Q FPLC column was then carried out, after a buffer exchange procedure had transferred the protein into 25 mM MOPS buffer, pH 7. The protein was eluted over a linear gradient of 150 mM to 350 mM NaCl over 8 column volumes. Protein B eluted at 260-270 mM NaCl (Figure 3.11), as determined by activity assays of each fraction.

Figure 3.11: Purification profile of protein B from *Ms. trichosporium* OB3b on a MONO Q column.

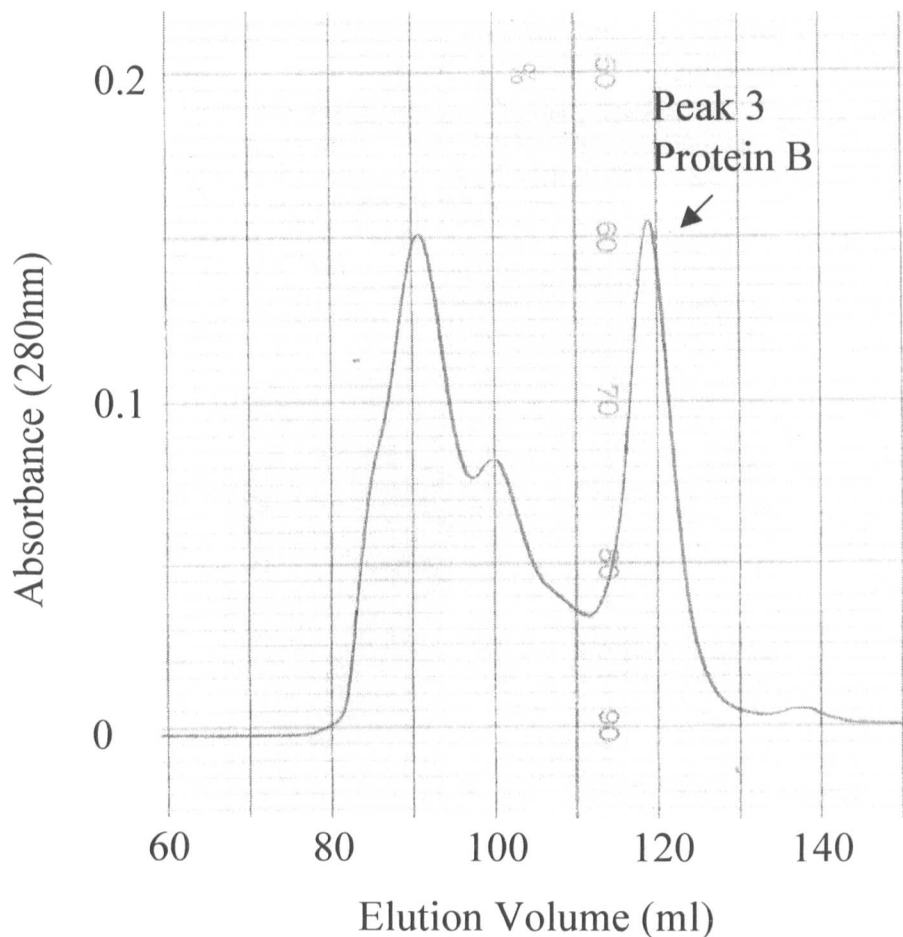
The column was equilibrated in 25 mM MOPS buffer, pH 7. The protein was eluted with a 150-350 mM NaCl gradient. The protein eluted at 260-270 mM NaCl.



SDS-PAGE analysis of the protein B fraction (Figure 3.13, Lane 2) identified an additional band of ~ 30 kDa. Therefore, a gel filtration step was included to separate protein B from this contaminating protein. Protein from the anion exchange step was concentrated before loading onto a Superdex 75 gel filtration FPLC column equilibrated with 25 mM MOPS buffer, pH 7. Protein was eluted in a size dependent manner (Figure 3.12).

Figure 3.12: Purification profile of protein B from *Ms. trichosporium* OB3b on a Superdex 75 column.

The column was equilibrated in 25 mM MOPS buffer, pH 7. Peak 3 corresponds to protein B.



Peak 3 was found to be active, indicating it to be the protein B fraction. SDS-PAGE analysis (Figure 3.13, Lane 3) indicated that the ~ 30 kDa band remained after the gel filtration step and was, therefore, presumed to correspond to a dimer of the protein. This is in agreement with the findings of Fox *et al.* (1991) and Chang *et al.* (1999) where *Ms. trichosporium* OB3b protein B was also observed as existing as a dimer under certain conditions. However, the dimer band was observed as being slightly weaker for the protein B eluted from the S75 column (Figure 3.13, Lane 3) compared to the protein prior to this purification step (Figure 3.13, Lane 2). Therefore, it is possible that some contaminating proteins visible at ~ 30 kDa were separated from the protein of interest. This is clearly indicated on the purification profile (Figure 3.12) where the protein B peak was observed to be separated from some higher molecular weight contaminating proteins, which eluted prior to the

protein B fractions. Truncates of *Ms. trichosporium* OB3b protein B were also observed. Nevertheless, the protein was identified as being of sufficient purity for subsequent analysis by mass spectrometry.

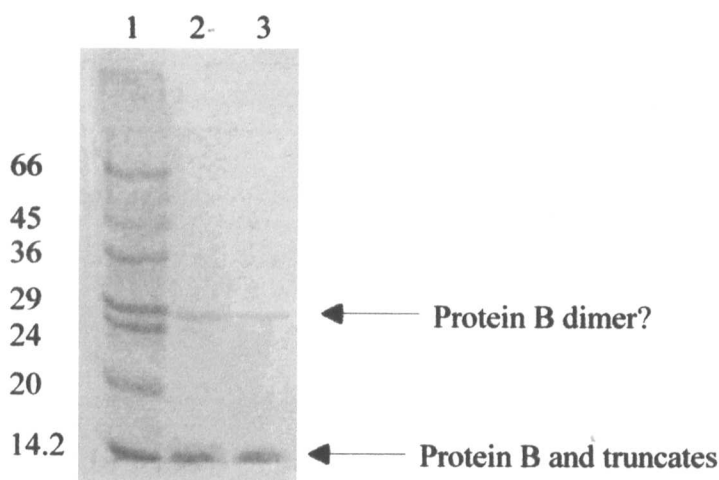
Figure 3.13: SDS-PAGE analysis of wild type *Ms. trichosporium* OB3b protein B at different stages of purification.

Lane 1: Molecular weight markers (bovine albumin, 66 kDa; egg albumin, 45 kDa; glyceraldehyde-3-P-dehydrogenase, 36 kDa; bovine carbonic anhydrase, 29 kDa; bovine pancreas trypsinogen, 24 kDa; soybean trypsin inhibitor, 20 kDa; bovine milk α -lactalbumin, 14.2 kDa).

Lane 2: Protein B after MONO Q step.

Lane 3: Protein B after S75 step.

Each lane contained ~ 5 μ g protein.



3.5.2 ESI-MS analysis of *Ms. trichosporium* OB3b protein B

Purification of wild-type *Ms. trichosporium* OB3b protein B, like that of *Mc. capsulatus* (Bath) protein B, resulted in a mixture of intact full length protein B as well as truncated forms. Therefore, it was necessary to confirm that the co-purifying proteins were indeed truncates and to elucidate whether the cleavage sites were the same as those observed for *Mc. capsulatus* (Bath) protein B. Determining the molecular mass of the intact protein was also essential in elucidating whether or not it agreed with the published sequence data for the protein.

Electrospray ionisation mass spectrometry (ESI-MS) was used to analyse desalted samples of *Ms. trichosporium* OB3b protein B, after the final purification step. The

mass spectrum obtained is shown in Figure 3.14 and the peak data detailing the corresponding cleavage sites are in Table 3.1.

Figure 3.14: ESI-MS of purified protein B from *Ms. trichosporium* OB3b.

The ESI-MS of the *Ms. trichosporium* OB3b protein B was recorded on a Quattro II tandem mass-spectrometer with an electrospray ion source and the data was processed using the MassLynx program (VG Biotech) (Chapter 2, Section 2.16.1).

Relative abundance

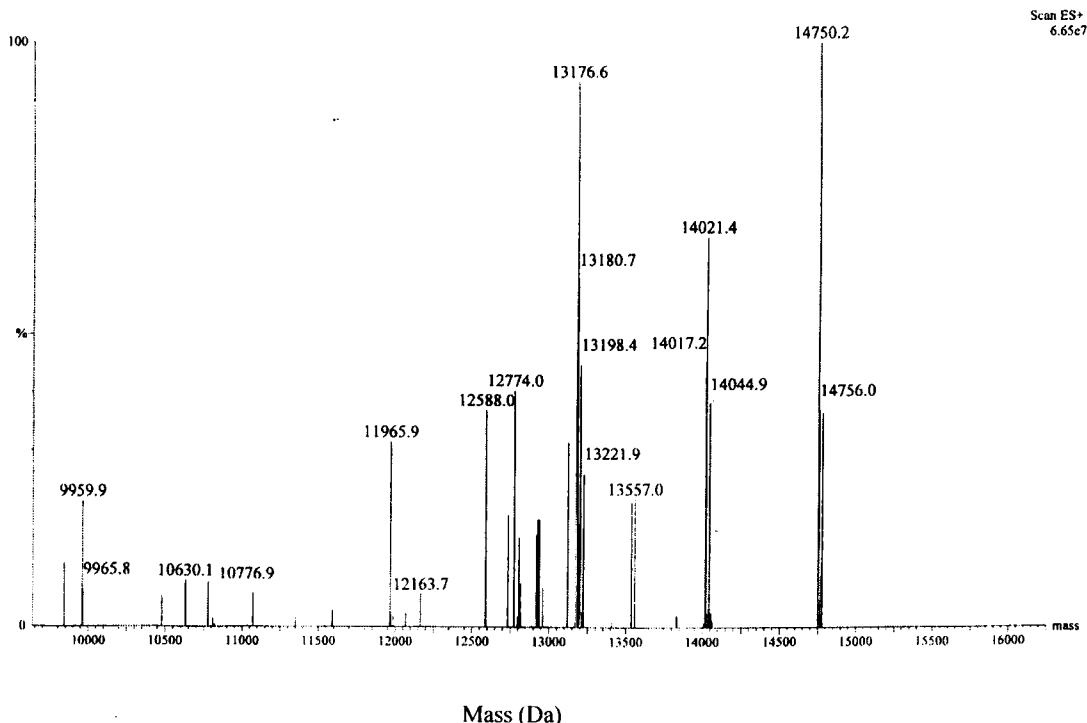


Table 3.1: ESI-MS data for purified protein B from *Ms. trichosporium* OB3b indicating the corresponding cleavage sites.

Cleavage sites were identified using the Proteins function of the BioLynx software, part of the MassLynx Program (VG Biotech) (Chapter 2, Section 2.16.1).

Observed molecular mass (Da)	Cleavage site, numbered with respect to the wild-type <i>Ms. trichosporium</i> OB3b protein B sequence
14750.2	OB3b protein B intact
14021.4	Y ⁷ -N ⁸
13176.6	T ¹⁵ -G ¹⁶
12774.0	F ¹⁹ -A ²⁰
11965.9	E ²⁶ -E ²⁷

ESI-MS of wild-type *Ms. trichosporium* OB3b protein B indicated that it contained a mixture of intact protein B and various N-terminally truncated forms of the protein. The molecular mass of the intact protein was determined to be 14750.2 Da, which is

approximately 133 Da lower than the value of 14882.9 Da predicted from the available sequence information (ProtParam Tool on the ExPASy Website; <http://www.expasy.ch/>). This is because the sequence data begin with the ATG start codon, and ATG also codes for methionine (131.2 Da). Methionine is often post translationally removed, which explains the discrepancy in molecular mass.

The N-terminally truncated proteins were not cleaved at the same positions as observed in *Mc. capsulatus* (Bath) protein B, a result considered and analysed further in Chapter 4.

3.6 Purification of recombinant *Ms. trichosporium* OB3b protein B

As a result of the truncates observed in purifying wild-type *Ms. trichosporium* OB3b protein B (Section 3.5), purification of the wild-type recombinant protein was undertaken. A construct, similar to those available for *Mc. capsulatus* (Bath) protein B, was available for *Ms. trichosporium* OB3b protein B for expression of the protein as a GST fusion (Lloyd, 1997). The plasmid [pGEX-MTB] (Chapter 2, Section 2.27.1) was used in the same way as [pGEX-WTB] and [pGEX-G13Q], as detailed in Section 3.4, to improve protein expression levels. The same purification protocol was used (Chapter 2, Section 2.4) and gave the same results as those identified for WTB and G13Q. This provided an efficient method of purifying highly pure, active, uncleaved recombinant *Ms. trichosporium* OB3b protein B for further studies.

3.7 Determination of the extinction-coefficients of the regulatory proteins

For protein structure studies, it was necessary to determine the concentration of the proteins accurately. Therefore, it was important to elucidate the extinction-coefficients of the proteins (Chapter 2, Section 2.10.2).

Fluorescence was used to monitor the time taken for guanidine hydrochloride to denature the protein. This involved monitoring the change in fluorescence over time for samples of recombinant *Ms. trichosporium* OB3b protein B, G13Q and protein B' incubated in the denaturant (Chapter 2, Section 2.17). As the proteins became denatured the expected shift in d_{\max} to ~ 350 nm after ~ 2.5 hours incubation was observed. Thus, the difference in absorbance at 280nm was determined for the native and denatured samples. This information, together with the theoretical extinction-coefficient values calculated using Equation 3.1, enabled the native extinction-coefficient values to be determined using Equation 3.2.

Equation 3.1:

$$\text{Theoretical } \epsilon_{\text{unfolded}} = (\chi_W \times \epsilon_W) + (\chi_Y \times \epsilon_Y) + (\chi_F \times \epsilon_F)$$

where χ =number of residues
 ϵ =extinction coefficient
W = tryptophan
Y = tryosine
F = phenylalanine

Equation 3.2:

$$\epsilon_{\text{native}} = (A_{\text{native}} \times \epsilon_{\text{unfolded}}) / A_{\text{unfolded}}$$

where A=Absorbance at 280nm

The extinction-coefficients calculated for recombinant *Ms. trichosporium* OB3b protein B, G13Q and protein B' (Table 3.2) were found to be fairly similar to the expected values determined by Equation 3.1.

Table 3.2: Extinction-coefficient data

Protein	Theoretical $\epsilon_{\text{unfolded}}$	Experimental ϵ_{native}
G13Q	17780	16839
Protein B'	16500	16032
Rec. <i>Ms. trichosporium</i> OB3b protein B	15220	16837

The experimental ϵ_{native} values were used for determining the protein concentrations for all the subsequent experiments conducted.

3.8 Separation of protein B and truncate(s) by chromatofocusing chromatography

Protein B from *Mc. capsulatus* (Bath) purified by the method of Pilkington *et al.* (1990) has been identified as consisting of a mixture of intact protein B and truncated protein B' (Section 3.2). Extended incubation of this purified protein B/B' leads to further truncate formation, notably that of B'' (Bhambra, 1996; Lloyd *et al.*, 1997). Truncation has also been observed to occur for *Mc. capsulatus* (Bath) protein B from recombinant sources as well as wild-type and recombinant *Ms. trichosporium* OB3b protein B. Therefore, it was considered necessary to develop a means of separating protein B and its truncate(s) from one another. Thus further studies involving pure, homogeneous protein B and/or truncate protein(s) would be possible.

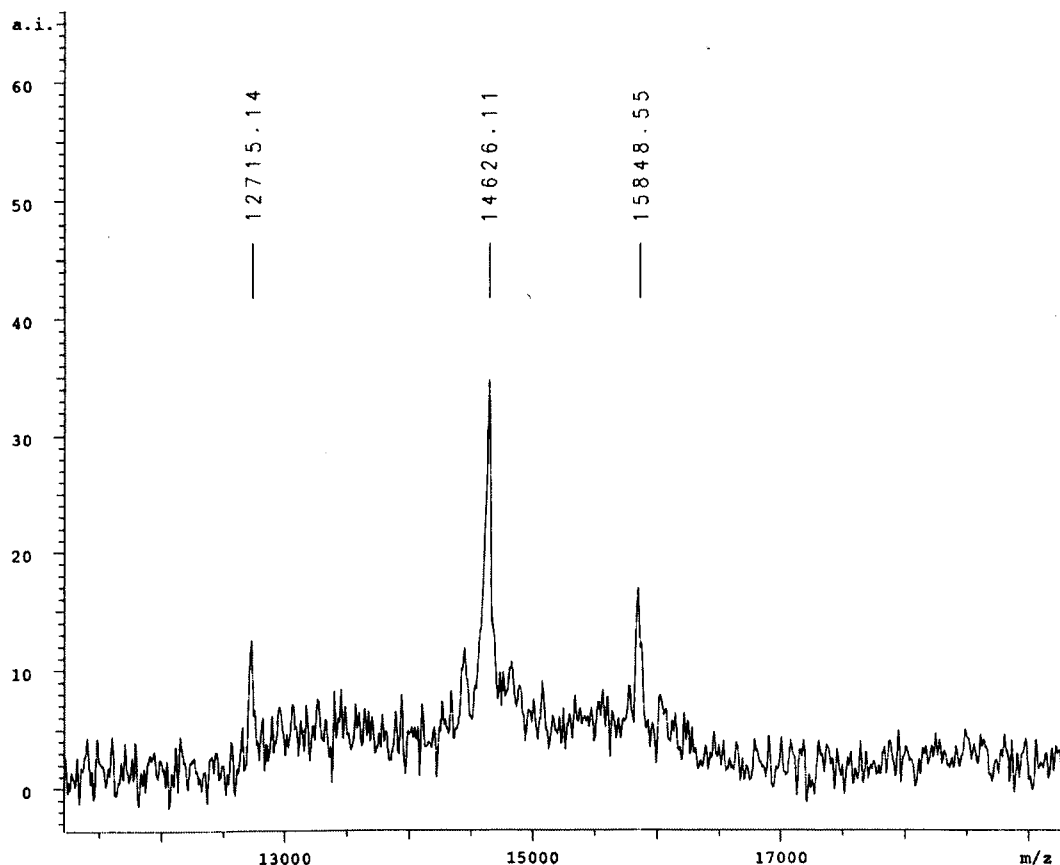
Chromatofocusing is an ion exchange chromatography technique that separates proteins on the basis of their isoelectric points. The technique takes advantage of the buffering action of the charged group of the MONO P ion exchanger. It achieves this by creating a pH gradient using two buffers of different pH values, the first (Buffer A) is used to adjust the pH of the chromatofocusing column and the second (Buffer B) is then run through the column, thereby creating a pH gradient along the column itself. This causes proteins to migrate along the column according to their pI values (Pharmacia LBK Biotechnology Division, Bucks, UK). For samples of wild-type *Mc. capsulatus* (Bath) protein B and its truncates, it was anticipated that their sequence of elution from the column would be B'' (pI= 4.64), B' (pI= 4.55) and finally intact protein B (pI = 4.49), since the protein with the highest pI value elutes first. The theoretical pI value of each of the proteins was determined by analysis of their amino acid sequences using the ProtParam tool on the ExPASy website (<http://www.expasy.ch/>). Chromatofocusing resolves proteins with pI units differing by as little as 0.02, making it ideal for separating the different forms of protein B.

Two samples of protein B purified from *Mc. capsulatus* (Bath) by the method of Pilkington *et al.* (1990) were subjected to chromatofocusing chromatography on a

MONO P FPLC column (Amersham Pharmacia Biotech, Bucks., UK) (Chapter 2, Section 2.8). Sample 1 had been incubated at 20 °C for ~ 4 hours to induce cleavage and exhibited an activity level of approximately 2000 nmol/min/mg, compared to that of Sample 2 which was fresh from purification and exhibited a higher level of activity of approximately 3500 nmol/min/mg. The activity levels of the samples correlate with the proportions of inactive proteins B' and B'' present, compared to active protein B. Mass spectrometry (Figure 3.15) and SDS-PAGE (Sample 1, Figure 3.18, Lane 2; Sample 2, Figure 3.16, Lane 2) analysis of the two samples more accurately confirmed the nature and relative proportions of the proteins within the two samples. It was, therefore, concluded that Sample 1 contained proteins B:B':B'' at an approximate ratio of 4:10:2.5, whereas Sample 2 contained the proteins at an approximate ratio of 10:6:1. This information was used in the assigning of the chromatofocusing peaks.

Figure 3.15: (i) MALDI-ToF MS of Sample 1 and (ii) ESI-MS of Sample 2.

(i) The MALDI-ToF MS of Sample 1 was recorded on a Proflex III mass spectrometer. Data were recorded by a 1 GHz Le Croy digitiser and analysed by Bruker Xtof 3.1.0 software (Chapter 2, Section 2.16.2). Data displayed as mass to charge ratio (m/z) against arbitrary intensity (a.i.). 12715 peak corresponds to protein B'', 14626 peak to protein B' and 15848 to protein B.



(ii) The ESI-MS of Sample 2 was recorded on a Quattro II tandem mass-spectrometer with an electrospray ion source and the data were processed using the MassLynx program (VG Biotech) (Chapter 2, Section 2.16.1). Peak 15852 corresponds to protein B, peak 14629 to protein B' and 12718 to protein B''.

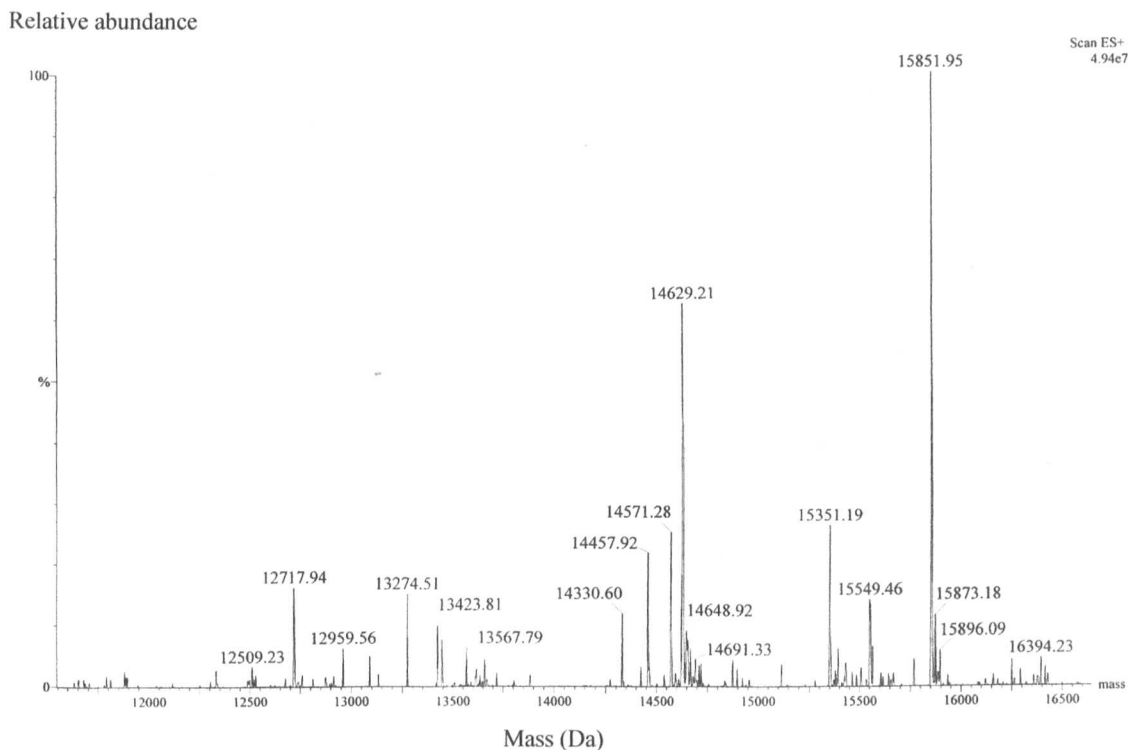
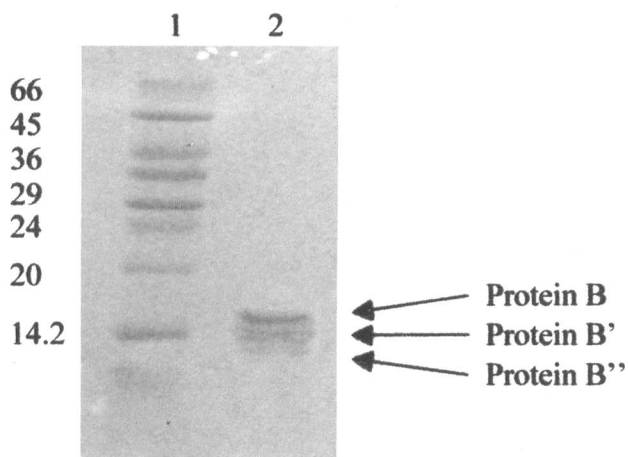


Figure 3.16: SDS-PAGE of Sample 2.

Lane 1: Molecular weight markers (bovine albumin, 66 kDa; egg albumin, 45 kDa; glyceraldehyde-3-P-dehydrogenase, 36 kDa; bovine carbonic anhydrase, 29 kDa; bovine pancreas trypsinogen, 24 kDa; soybean trypsin inhibitor, 20 kDa; bovine milk α -lactalbumin, 14.2 kDa).

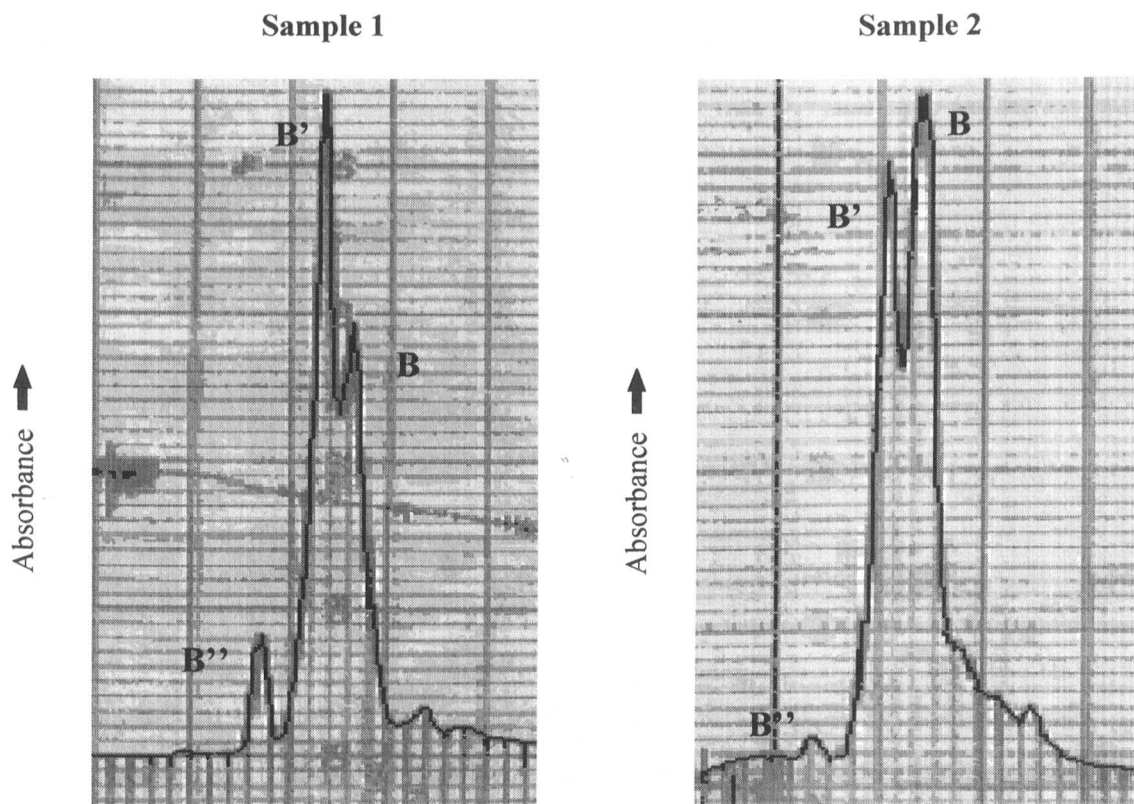
Lane 2: Sample 2 of proteins B, B' and B'' at an ~ ratio of 10:6:1.



The MONO P chromatofocusing column was equilibrated with Start Buffer A (25 mM methylpiperazine, pH 5.64). The protein samples for analysis were buffer exchanged into the Start Buffer A and then loaded onto the column. The B'', B' and B proteins eluted over a linear pH gradient created on the column by the application of Buffer B (1 in 10 dilution of Polybuffer 74™ (Amersham Pharmacia Biotech, Bucks., UK), pH 3.5 at 1 ml/min). The fractions corresponding to the different protein peaks were separately pooled for further analysis of the isolated protein forms. The elution profiles obtained for the two samples of wild-type protein B from *Mc. capsulatus* (Bath) are shown in Figure 3.17.

Figure 3.17: Chromatofocusing elution profiles for wild type protein B from *Mc. capsulatus* (Bath).

Start Buffer A, 25 mM methylpiperazine, pH 5.64; Buffer B 1 in 10 dilution Polybuffer 74™, pH 3.5 at 1 ml/min on a MONO P HR 5/20 chromatofocusing chromatography column. The separation of the proteins B, B' and B'' is identified on the traces.



The three major chromatofocusing peaks for sample 1 were in similar proportions to the concentrations of B, B' and B'' identified by the mass spectrometry and SDS-PAGE data. The peaks were, therefore, presumed to correspond to the three forms of

the protein, as indicated in Figure 3.17, Sample 1. The chromatofocusing elution profile for Sample 2, which had been identified as containing more of the active protein B, further supported the assignment of B, B' and B'' peaks to be as indicated in Figure 3.17.

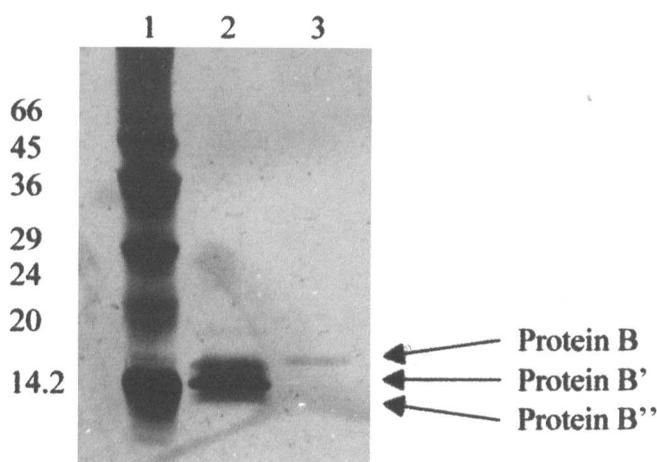
SDS-PAGE analysis of the protein B fraction obtained from chromatofocusing chromatography indicated the protein to be pure, as observed by the single band at 16 kDa and as compared to the impure starting material (Sample 1) of protein B from *Mc. capsulatus* (Bath) which contained proteins B, B' and B'' (Figure 3.18).

Figure 3.18: SDS-PAGE of the protein B fraction obtained from chromatofocusing chromatography.

Lane 1: Molecular weight markers (bovine albumin, 66 kDa; egg albumin, 45 kDa; glyceraldehyde-3-P-dehydrogenase, 36 kDa; bovine carbonic anhydrase, 29 kDa; bovine pancreas trypsinogen, 24 kDa; soybean trypsin inhibitor, 20 kDa; bovine milk α -lactalbumin, 14.2 kDa).

Lane 2: Sample 1 of proteins B, B' and B'' at an ~ ratio of 4:10:2, prior to chromatofocusing chromatography.

Lane 3: Protein B fraction from chromatofocusing chromatography.



Propylene oxidation activity assays (Chapter 2, Section 2.12.1) of the fractions assigned to B' gave no sMMO activity, whereas those for the putative B fractions showed the presence of active protein B. Assays were conducted containing 8 μ M of each protein hydroxylase and reductase in 25 mM MOPS buffer pH 7, and purified protein B in the Polybuffer 74TM in which it was eluted from the chromatofocusing column. It proved impossible to remove the Polybuffer 74TM from the protein B or highly concentrate the protein without further degradation of the protein occurring,

as extended time scales were involved in the concentration and dialysis processes. Control reactions of sMMO activity containing the hydroxylase, reductase and protein B in 25 mM MOPS buffer pH 7 were compared to the activity levels obtained upon addition of Polybuffer 74TM to the system, in the quantity in which it had to be added in the test study to give 8 μ M protein B. It was found that a decrease in specific activity of approximately 60 % resulted. Taking this into account, an estimated specific activity value of 6380 nm/min/mg was obtained for the protein B purified by chromatofocusing and verifies the protein to be active protein B in a highly pure form.

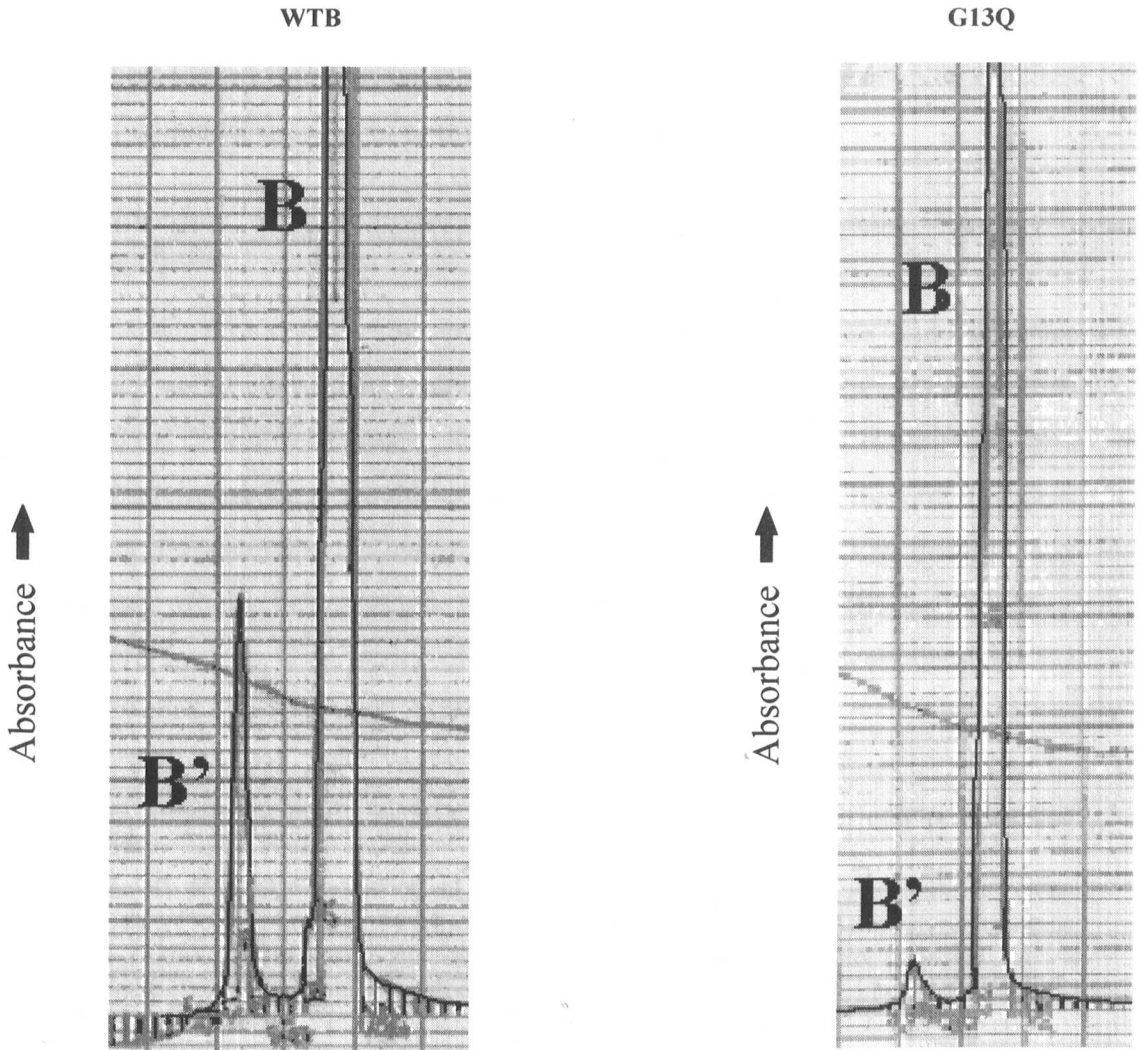
WTB and G13Q, produced from the pGEX-2T expression system (Section 3.4), were also subjected to chromatofocusing chromatography. Optimum separation of the intact protein from the truncated form was achieved using Start Buffer A, at pH 5.7, and Buffer B at pH 4, applied at a flow rate of 0.3 ml/min (Figure 3.19).

The traces in Figure 3.19 give further evidence that chromatofocusing is capable of separating proteins B and B'. Both the samples of recombinant protein had been cleaved from their precursor GST-fusion proteins with thrombin, directly before being applied to the column. Therefore, these results can be interpreted as comparing B' formation within the two samples, as the intact fusion protein does not undergo significant cleavage to give truncated proteins over such a short period of time (Lloyd *et al.*, 1997).

G13Q has been shown previously to be more stable than WTB, with B' formation occurring at a much reduced rate in the mutant form (Lloyd *et al.*, 1997). This is reflected in the chromatofocusing elution profiles (Figure 3.19) by the very small presumptive B' peak for G13Q compared to the larger B' peak for WTB.

Figure 3.19: Chromatofocusing elution profiles for WTB and G13Q.

Start Buffer A, 25 mM methylpiperazine, pH 5.7; Buffer B 1 in 10 dilution Polybuffer 74TM, pH 4 at 0.3 ml/min on a MONO P HR 5/20 chromatofocusing chromatography column. The separation of the proteins is as identified on the elution profiles.



Mass spectrometry analysis of the peaks from chromatofocusing chromatography proved unsuccessful as the Polybuffer 74TM in which the proteins were eluted appeared to distort the signal, and attempts at its removal proved problematic.

Thus, separation of protein B and B' was shown to be possible by the use of the purification procedure described. This proved vital in enabling studies into the mechanism of B to B' cleavage, detailed in Chapter 4.

3.9 Determination of the purity of hydroxylase and reductase, as purified by the current published protocols

Previous methods of purification of the hydroxylase and reductase (Pilkington and Dalton, 1990) were analysed to determine the levels of purity achieved. Optimisation of these methods was undertaken as it was deemed necessary to develop an efficient system for obtaining proteins of optimal purity.

3.9.1 Purification of the hydroxylase and reductase proteins from *Mc. capsulatus* (Bath)

The published protocol for the purification of the hydroxylase and reductase involved the use of ion exchange- and gel filtration- chromatography (Pilkington and Dalton, 1990). These techniques, which separate proteins by the exploitation of a different protein property, would be expected to clearly separate the proteins from one another. For example, the hydroxylase, reductase and protein B all differ greatly in size and would be expected to be easily separated by the gel filtration chromatography step. The purity of the proteins obtained by these methods was analysed by SDS-PAGE (Figure 3.20).

Figure 3.20: SDS-PAGE of the sMMO proteins purified by the method of Pilkington and Dalton, (1990).

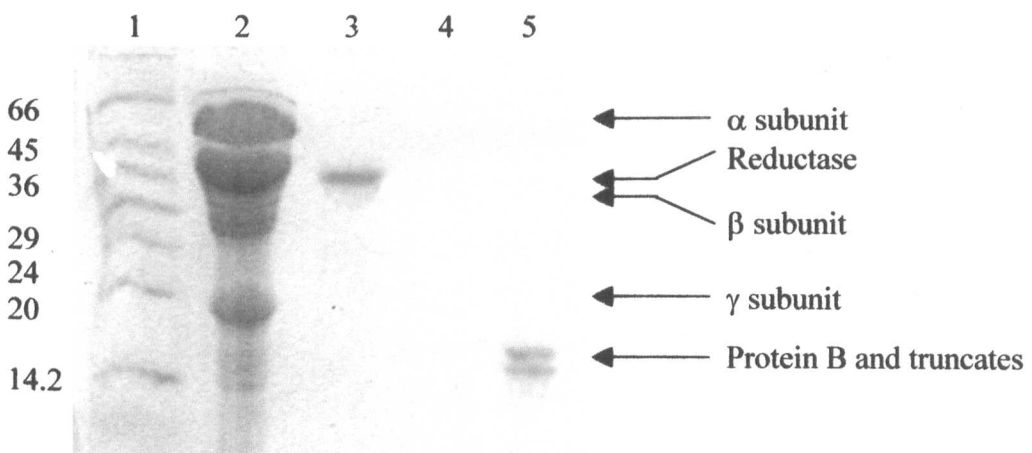
Lane 1: Molecular weight markers (bovine albumin, 66 kDa; egg albumin, 45 kDa; glyceraldehyde-3-P-dehydrogenase, 36 kDa; bovine carbonic anhydrase, 29 kDa; bovine pancreas trypsinogen, 24 kDa; soybean trypsin inhibitor, 20 kDa; bovine milk α -lactalbumin, 14.2 kDa).

Lane 2: Hydroxylase, consisting of α , β and γ subunits.

Lane 3: Reductase.

Lane 4: Blank.

Lane 5: Protein B and truncates.



SDS-PAGE analysis indicated the samples of hydroxylase and reductase to be approximately 75 % and 90 % pure, respectively (Figure 3.20). However, activity assays containing 8 μ M of each of the purified hydroxylase and reductase proteins, in the absence of any protein B, gave a low level of activity, indicating contamination to be present. Western blot analysis of the hydroxylase and reductase proteins, probing with antibodies to *Mc. capsulatus* (Bath) protein B/B', was performed to determine whether any protein B remained bound to either of the proteins (Figure 3.21).

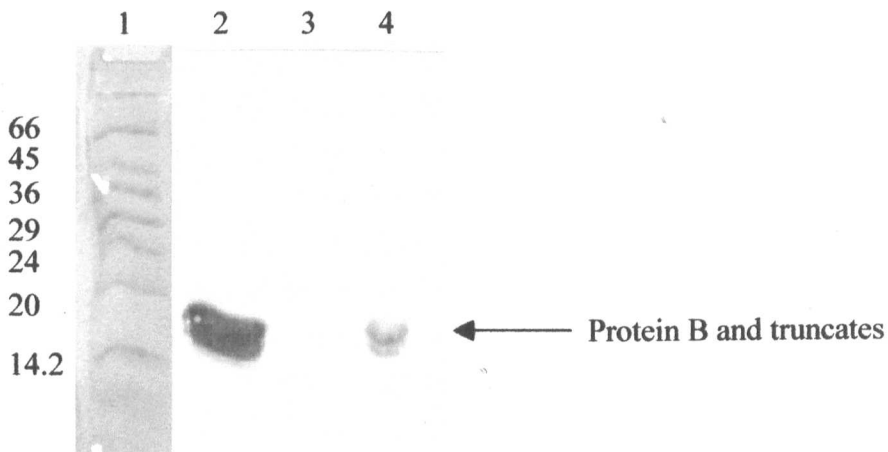
Figure 3.21: Western blot analysis of the sMMO proteins as purified by the method of Pilkington and Dalton, (1990), probing with antibodies to *Mc. capsulatus* (Bath) protein B/B'.

Lane 1: Molecular weight markers (bovine albumin, 66 kDa; egg albumin, 45 kDa; glyceraldehyde-3-P-dehydrogenase, 36 kDa; bovine carbonic anhydrase, 29 kDa; bovine pancreas trypsinogen, 24 kDa; soybean trypsin inhibitor, 20 kDa; bovine milk α -lactalbumin, 14.2 kDa).

Lane 2: Hydroxylase.

Lane 3: Reductase.

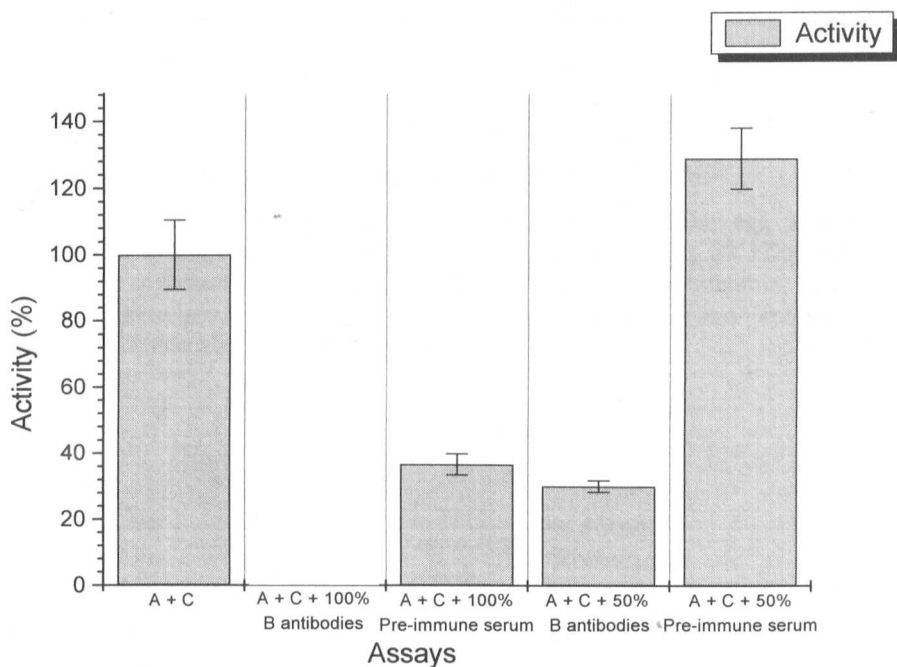
Lane 4: Protein B and truncates.



Western blot analysis identified protein B to have remained bound to the hydroxylase protein after purification (Figure 3.21). To confirm this result activity assays containing 8 μ M of each of the purified hydroxylase and reductase proteins were conducted in the presence of protein B antibodies, in order to determine whether activity would be lost. This would confirm if residual protein B, bound to the purified hydroxylase protein, was responsible for the minimal activity observed (Figure 3.22).

Figure 3.22: sMMO activity assays of the hydroxylase and reductase purified by the method of Pilkington and Dalton (1990) and the effect of adding *Mc. capsulatus* (Bath) protein B/B' antibodies.

sMMO propylene oxidation assays (Chapter 2, Section 2.12.1) were performed by mixing ~8 μ M aliquots of hydroxylase and reductase with various quantities of undiluted *Mc. capsulatus* (Bath) protein B/B' antibodies or pre-immune serum. 100% antibodies or pre-immune serum represents 400 μ l in a total assay volume of 500 μ l. Enzyme activity is shown as a percentage of the activity of hydroxylase and reductase alone. The hydroxylase is denoted by H and the reductase by R. The activities presented are the mean of 3-4 separate experiments. Standard error bars are shown.



The activity lost upon addition of protein B antibodies confirmed that the activity possessed by the hydroxylase and reductase alone was due to protein B contamination and proved that in the absence of protein B, hydroxylase and reductase are definitely inactive. This is unlike the sMMO of *Ms. trichosporium* OB3b where the hydroxylase and reductase retain minimal activity in the absence of protein B (Liu *et al.*, 1995). The serum itself appeared to interfere with the activity of the complex when added at 100 %, but at 50 % had no effect on the activity, unlike the protein B antibody-containing serum which inhibited the activity by ~ 70 %. The inhibition observed by the pre-immune serum was probably due to the high concentration of proteins contained within the serum interfering with the binding within the assay mix, therefore, preventing the small amounts of impure hydroxylase and reductase from complexing to give activity. However, at 50 % concentration this problem was overcome, indicating that the lack of protein B antibodies in this sample prevented activity from being inhibited.

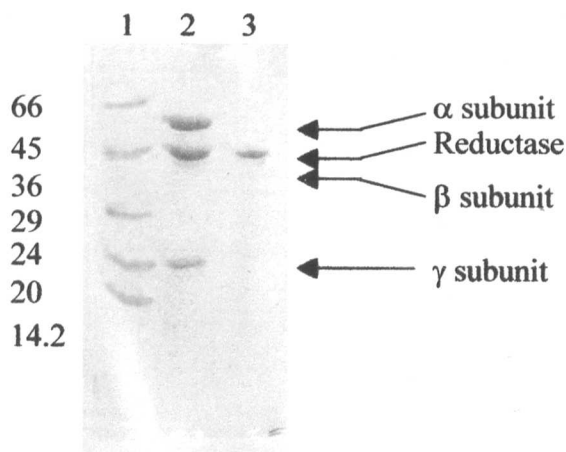
Further purification of the hydroxylase and reductase proteins was performed by the addition of an extra ion exchange chromatography procedure (Chapter 2, Section 2.3.3, Step 3; Section 2.3.4, Step 3). The hydroxylase and reductase protein purified by this method gave no residual activity when assayed in the absence of protein B, thus confirming them to be pure and free of contaminating protein(s). SDS-PAGE analysis indicated the proteins to be > 95 % pure (Figure 3.23). They were, therefore, used for subsequent structural studies.

Figure 3.23: SDS-PAGE of purified hydroxylase and reductase proteins

Lane 1: Molecular weight markers (bovine albumin, 66 kDa; egg albumin, 45 kDa; glyceraldehyde-3-P-dehydrogenase, 36 kDa; bovine carbonic anhydrase, 29 kDa; bovine pancreas trypsinogen, 24 kDa; soybean trypsin inhibitor, 20 kDa; bovine milk α -lactalbumin, 14.2 kDa).

Lane 2: Hydroxylase after final MONO Q step, consisting of α , β and γ subunits.

Lane 3: Reductase after final MONO Q step.



3.10 Conclusion

Optimisation of protocols for the purification of *Mc. capsulatus* (Bath) protein B', *Ms. trichosporium* OB3b protein B, WTB and G13Q were developed for the isolation of protein of > 95 % purity required for further characterisation studies. A separation procedure by chromatofocusing was also developed to separate protein B and its truncates from each other. The purification of the hydroxylase and reductase from *Mc. capsulatus* (Bath) were also optimised resulting in higher purity of these sMMO components. The studies using protein B antibodies to inhibit the residual

activity of the hydroxylase and reductase present in semi-pure preparations also confirmed that the hydroxylase and reductase alone are inactive and that protein B is essential for activity. This highlights the difference between the sMMO of *Mc. capsulatus* (Bath) and the homologous system from *Ms. trichosporium* OB3b, as, in the latter case, the sMMO enzyme appears to function in the absence of protein B (Liu *et al.*, 1995). The reason for this difference between the two systems remains unclear, as in most other respects they are similar. The fact that low levels of activity obtained from sMMO assays of the hydroxylase and reductase proteins from *Mc. capsulatus* (Bath) purified by the method of Pilkington *et al.* (1990) indicates the difficulty in obtaining highly pure, homogeneous hydroxylase protein and emphasises its strength of binding with protein B. This therefore suggests the possibility that the low level of activity observed for the hydroxylase and reductase proteins alone from *Ms. trichosporium* OB3b could be the result of a purity problem.

Protein B purified from *Mc. capsulatus* (Bath) and *Ms. trichosporium* OB3b were illustrated as undergoing cleavage to form N-terminally truncated versions of the proteins. Mass spectrometry indicated the cleavage sites of *Ms. trichosporium* OB3b protein B truncation to be different from those observed for protein B of *Mc. capsulatus* (Bath), a result further considered and expanded upon in Chapter 4.

The ability to separate proteins B and B', a process previously unachievable, by the use of chromatofocusing chromatography has also been vital in providing a means to study protein B to B' formation, as described in Chapter 4.

Chapter 4

The Cleavage of Protein B

4.1 Introduction

Protein cleavage usually occurs by chemical or enzymatic means. Many enzymes are activated by specific proteolytic cleavage reactions as a mechanism of activity regulation. For example, some enzymes, such as chymotrypsin which is involved in digestion, are synthesised as inactive precursors known as zymogens or proenzymes, and in the case of chymotrypsin, chymotrypsinogen. Activation is mediated by cleavage of the zymogen, such as chymotrypsinogen, due to the action of a specific enzyme, in this instance trypsin. Thus, the zymogen is kept in a form that can be readily activated, when needed, as the proteolytic reaction serves to give rise to an active species very rapidly, rather than waiting for an active form to be synthesised *de novo* (Stryer, 1988).

Within the last decade, proteins have also been identified that can undergo self-catalysed modification reactions, which do not require the intervention of other enzymes. These reactions include protein splicing and autoproteolysis. Protein splicing was first observed for the protein product of the *Saccharomyces cerevisiae* TFP1 gene (Hirata *et al.*, 1990; Kane *et al.*, 1990). The 69 kDa subunit of vacuolar ATPase of the yeast *Candida tropicalis* (Gu *et al.*, 1993) and the DNA polymerases of the extreme thermophilic archaebacterium *Thermococcus litoralis* (Hodges *et al.*, 1992) are further examples of proteins which undergo protein splicing (Shao and Kent, 1997). Similarly, autoproteolysis has been observed for glycosylasparaginases and pyruvoyl enzyme precursors. The initial formation of an ester bond by the acyl rearrangement of a peptide bond, are common features of these autoprocessing reactions. Although such acyl rearrangements are thermodynamically unfavourable, their coupling to diverse types of self-catalysed irreversible steps drives the protein rearrangements to completion (Perler *et al.*, 1997).

It has been proposed that the mechanism of cleavage of protein B to form inactive truncates could be autocatalytic. The suggestion was made in view of the fact that the addition of protease inhibitors and the expression of recombinant protein B in protease deficient strains of *E. coli*, failed in preventing the occurrence of the cleavage reaction (Bhambra, 1996; Lloyd *et al.*, 1997). However, in contrast to protein B being inactivated due to cleavage, the other proteins mentioned are activated by the process. Nevertheless, the ability to rapidly shut down sMMO activity, possibly in response to lack of substrate, has been proposed as a mechanism of preventing the wasteful oxidation of NADH, thus conserving the cell's energy (Green and Dalton, 1989; Kazlauskaite *et al.*, 1996). This effect could be mediated by cleavage of protein B to form inactive protein B' (Lloyd *et al.*, 1997). However, the possibility that the cleavage product, protein B', may have some as-yet undefined activatory role within a system other than that of sMMO, cannot be ruled out.

Conserved motifs, have been identified in proteins which undergo these autoprocessing reactions and they have been identified as being essential for the splicing reaction. Although protein B, by sequence analysis, has been shown not to contain any of these conserved sequence motifs (Section 4.4.1), it is possible that it may cleave by a similar chemical mechanism.

A combination of N-terminal sequencing and ESI-MS has been used to identify the cleavage site in wild type protein B from *Mc. capsulatus* (Bath) which results in the formation of the inactive truncate, protein B'' (Bhambra, 1996; Lloyd *et al.*, 1997). It was found that the protein was cleaved between Met¹²-Gly¹³, such that 12 amino acids were lost from the N-terminus. This processing of protein B was also observed for the recombinant protein expressed in *E. coli* (Bhambra, 1996; Lloyd *et al.*, 1997). Protein B from *Mc. capsulatus* (Bath) and *Ms. trichosporium* OB3b have a 89.4 % similarity between their protein sequences (Cardy *et al.*, 1991a) and yet protein B' formation had not been reported in *Ms. trichosporium* OB3b. However, this could be attributed to the lack of a Met¹²-Gly¹³ site within the protein. This observation provided the strategy for the work of Lloyd *et al.* (1997) in which a more stable protein B was produced by mutation of the Gly¹³ residue to a glutamine. However, the work did not specifically identify the level to which cleavage still occurred within the N-terminal region of the mutant G13Q, or whether the cleavage site

remained the same as that observed for the wild-type protein. Subsequent work to produce highly purified wild type *Ms. trichosporium* OB3b protein B (Chapter 3, Section 3.5) enabled analysis of its cleavage to be possible and identified that the Met¹²-Gln¹³ site was not the site of cleavage in this case (Chapter 3).

This Chapter details a comparison of the cleavage sites within the recombinant, wild-type and mutant protein B proteins in order to determine whether any trend was present which could identify whether the mechanism of cleavage is site specific. Studies into the mechanism of cleavage and the effect of losing certain amino acids from the N-terminus of protein B on its structure are also described. These studies were undertaken to further the understanding of the production of protein B' and to attempt to identify the reason for its occurrence and inactivity within the sMMO system.

4.2 Is the mechanism of cleavage of protein B autocatalytic?

Various approaches were undertaken in an attempt to elucidate the nature of cleavage of protein B and to identify whether its mechanism of occurrence was autocatalytic.

4.2.1 Studying the mechanism of cleavage

The technique of chromatofocusing was used to determine whether protein B, when separated from its truncated forms (Chapter 3, Section 3.8), could be detected as undergoing further cleavage to form truncates. Active wild-type protein B from *Mc. capsulatus* (Bath) was separated into its truncated forms by chromatofocusing (Chapter 3, Section 3.8, Figure 3.17, Sample 2). The pooled protein B fractions were then subjected to chromatofocusing (Chapter 2, Section 2.8) again after incubation at 20 °C for ~ 3 hours. Once the active protein B fractions had been separated, the fractions were pooled and subjected to a repetition of this procedure a further two times (Figure 4.1, Elutions 1-3).

The chromatofocusing elution profile (Figure 4.1, Elution 1) indicated the presence of presumptive protein B, B' and B'' peaks, suggesting that protein B cleaved with the formation of its truncates during the time it was incubated at 20 °C. Elution 2 indicates that protein B to protein B' cleavage occurred during the incubation stage. Elution 3 gives further evidence for the cleavage of protein B.

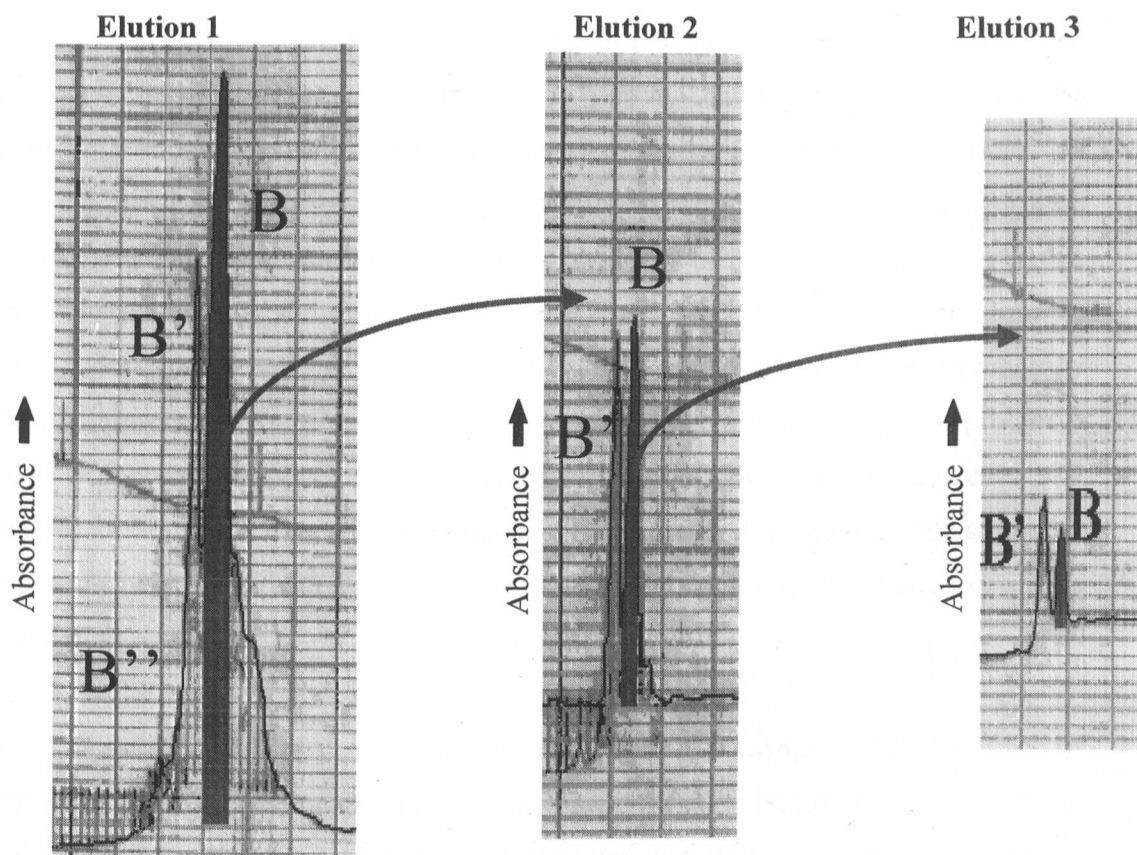
Figure 4.1: Chromatofocusing elution profiles monitoring for the presence of protein B and its truncates.

Conditions of MONO P run included Start buffer as 25 mM N-Methylpiperazine pH 5.7, Protein eluted from the column with 10 times diluted Polybuffer 74™ pH 3.5.

Elution 1) Sample of highly pure protein B after ~ 3 h incubation at 20 °C.

Elution 2) Sample of purified protein B from run 1 after a further ~ 3 h incubation at 20 °C.

Elution 3) Sample of purified protein B from run 2 after a further ~ 3 h incubation at 20 °C.



Thus, a highly purified sample of protein B from chromatofocusing was observed to partially degrade to protein B' over the ~ 3 hours incubation at 20 °C. The mixture formed could then be repeatedly resolved and repurified (Figure 4.1). Each sample of repurified protein B underwent cleavage to protein B', indicating that the truncates were likely to be generated autocatalytically. This proposal was supported by the fact

that prior to chromatofocusing chromatography, the protein had been extensively purified and identified by SDS-PAGE (Figure 3.16, Lane 2) and mass spectrometry analysis (Figure 3.15 (ii)) to be free of contaminating proteins, such as proteases. It is also supported by the work of Bhambra (1996) and Lloyd *et al.* (1997), where the addition of a wide variety of protease inhibitors and expression of recombinant *Mc. capsulatus* (Bath) protein B in protease deficient *E. coli* strains, both failed to prevent the protein B truncation reaction.

4.2.2 How does protein B cleave?

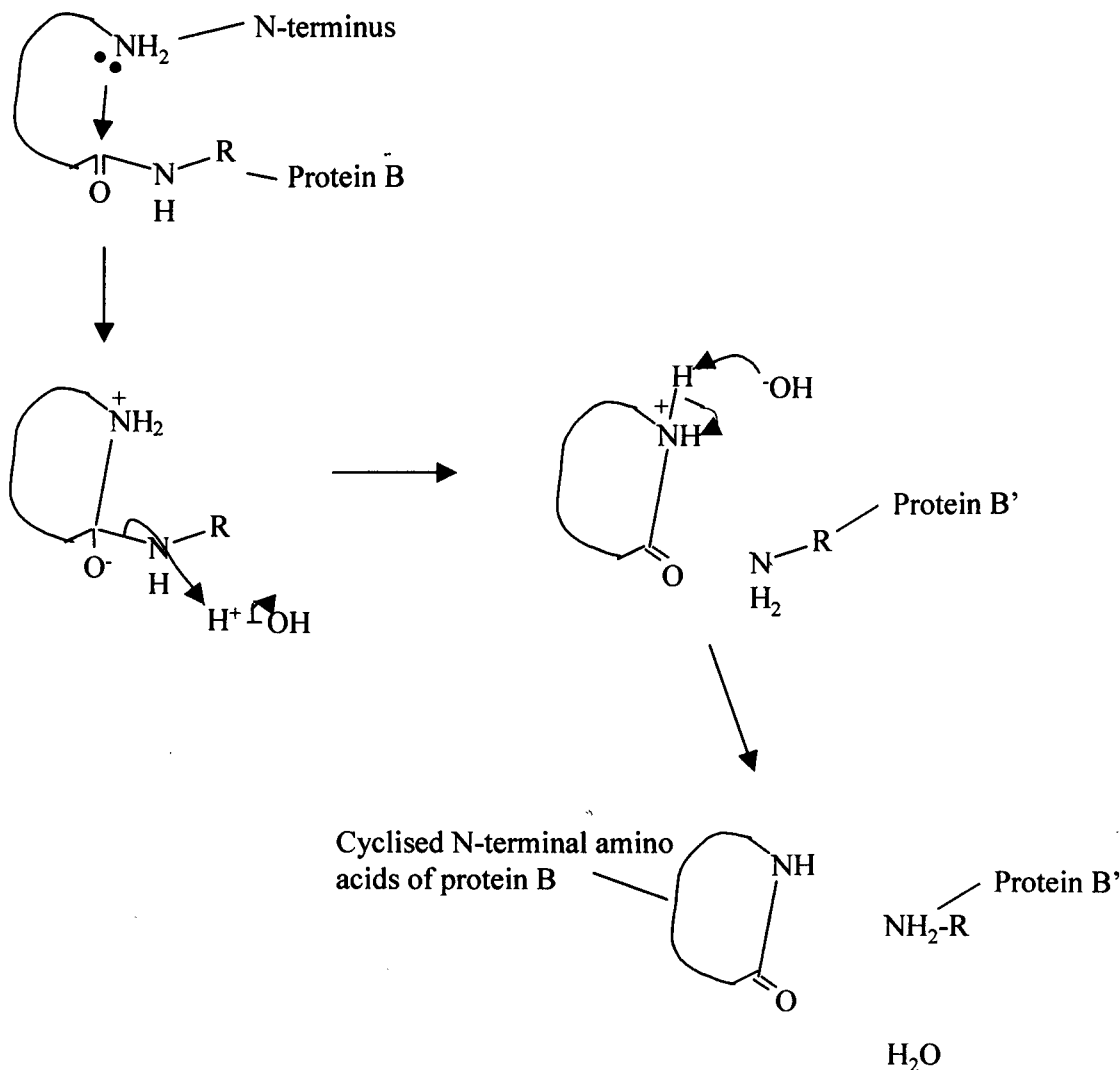
Recent research has identified that autoprocessing pathways rely on the formation and resolution of internal (thio) esters (Perler, 1998; Stoddard and Pietrokovski, 1998). It has been shown that the nucleophilic amino acids Cys, Ser and Thr can rearrange in proteins, replacing the amide peptide bond between itself and the preceding amino acid with a more reactive thioester or ester bond. Such bonds can then be broken by hydrolysis, to bring about the cleavage reaction. Aminohydrolase and aspartate decarboxylase processing are examples of proteins which undergo this type of reaction (Duggleby *et al.*, 1995; Lowe *et al.*, 1995; Guan *et al.*, 1996; Ramjee *et al.*, 1997). Sequence analysis of protein B failed to identify any level of homology with autoprocessing proteins. Nevertheless, it is possible that cleavage of protein B may occur via a similar chemical mechanism, involving attack by a specifically nucleophilic residue on a certain amino acid(s), as dictated by the protein's structure. Subsequent ester formation would allow rapid hydrolysis to occur leading to truncate formation.

One possible mechanism to explain autocatalytic cleavage could be that of intramolecular cyclisation via nucleophilic attack from the N-terminal serine residue of protein B on its other amino acids. It was believed that the N-terminal region of protein B must be flexible in order to undergo cleavage so readily, an idea which has been verified by the recent structural determination of the protein by NMR (Chang *et al.*, 1999; Walters *et al.*, 1999). The flexible N-terminal region of protein B could allow the N-terminal amino acid to attack amino acids within a certain region, as dictated by its structure. Upon the cyclisation reaction (Mechanism 4.1) water would be lost, such that the N-terminal region would be detected by mass spectrometry as

being the correct molecular weight, but lacking a mass of 18 Da attributable to the water molecule lost during the process. This strategy was adopted to investigate the possibility of this mechanism being responsible for protein B cleavage.

Mechanism 4.1: Cyclisation reaction mechanism resulting in the loss of the first 12 amino acids from the N-terminus of protein B.

The NH_2 group of the N-terminal amino acid attacks the carbonyl group of the amino acid residue at the site of cleavage to form a cyclic intermediate. N-protonation of the cyclic intermediate leads to protein B' formation and the loss of the first 12 amino acids of protein B as a cyclic peptide with the loss of a water molecule.

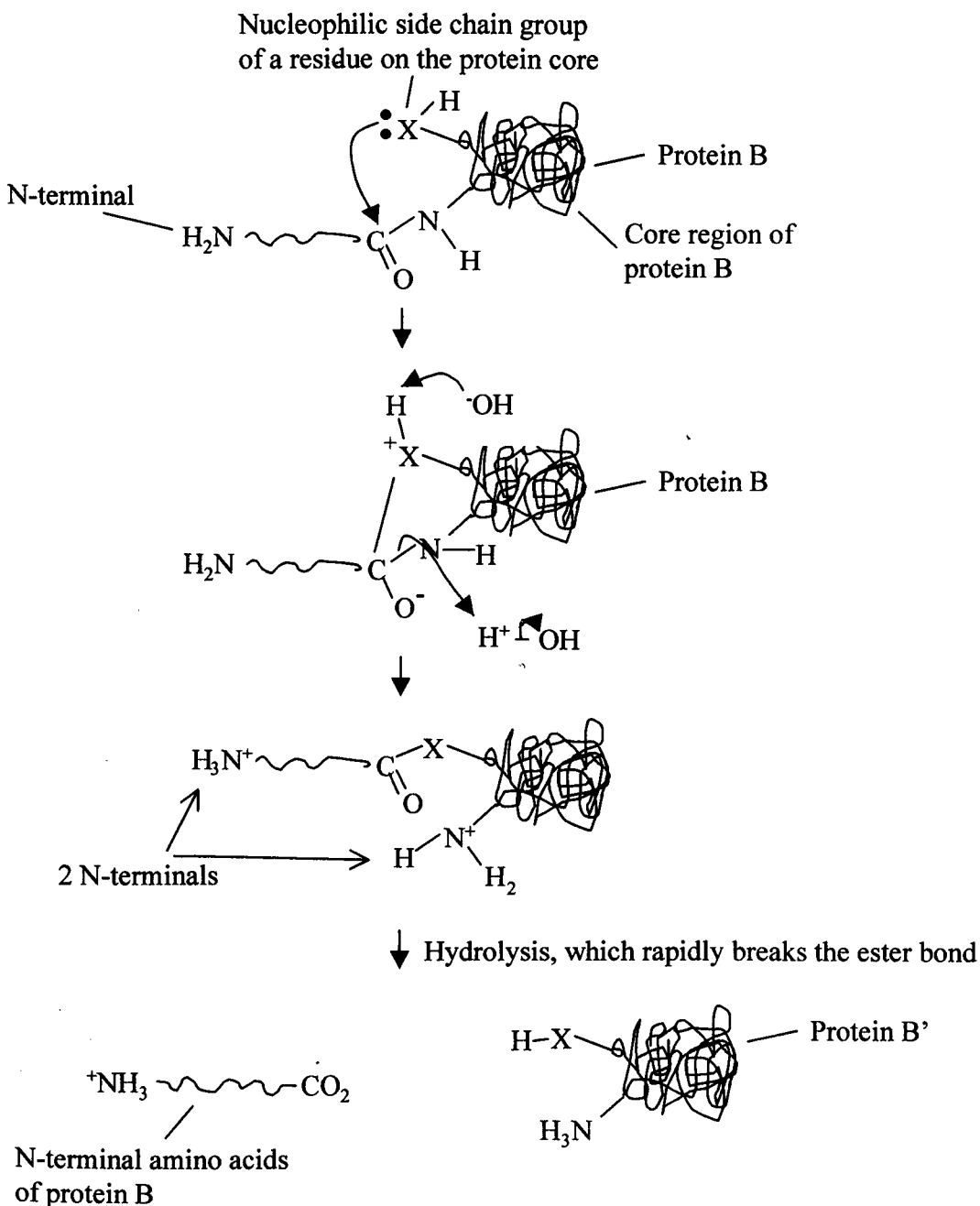


Mass spectrometry (Chapter 2, Section 2.16.1) was conducted on samples of WTB, which had been left to cleave at room temperature overnight. However, the technique was unable to identify the 12 amino acid fragment cleaved from the N-terminus of the protein. It was possible that this problem arose due to the fact that the first 12 amino acids contain no basic amino acid residues, and, therefore, the fragment would not attract protons efficiently to facilitate its identification by mass spectrometry.

A second possible mechanism to explain the observations was that a specifically nucleophilic side chain group, present on the surface of the core region of the protein B, could interact with the mobile N-terminal region, initiating the cleavage reaction (Mechanism 4.2).

Mechanism 4.2: Possible mechanism for the cleavage of the first 12 amino acids from the N-terminus of protein B.

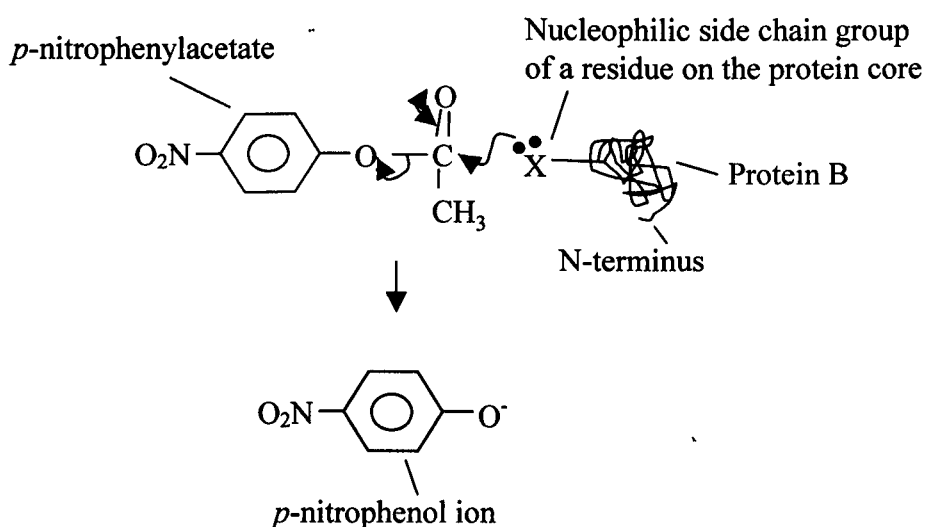
Nucleophilic side chain group of a residue on the core region of protein B, such as a side chain hydroxyl or thiol group of a serine, threonine or cystine, attacks the carbonyl group of the amino acid residue at the cleavage site to form a cyclic intermediate. N-protonation subsequently results in ester formation and an intermediate, which is identified as having two N-terminals. Hydrolysis rapidly breaks the ester bond forming the protein B' truncate and a peptide of first 12 N-terminal amino acids of protein B.



Identification of whether a specifically nucleophilic side chain group was present in an accessible region of protein B involved the use of *p*-nitrophenylacetate, which reacts with nucleophilic groups to form *p*-nitrophenol (Balls and Wood, 1956), as shown by Mechanism 4.3.

Mechanism 4.3: Reaction of *p*-nitrophenylacetate with a nucleophilic group to form *p*-nitrophenol.

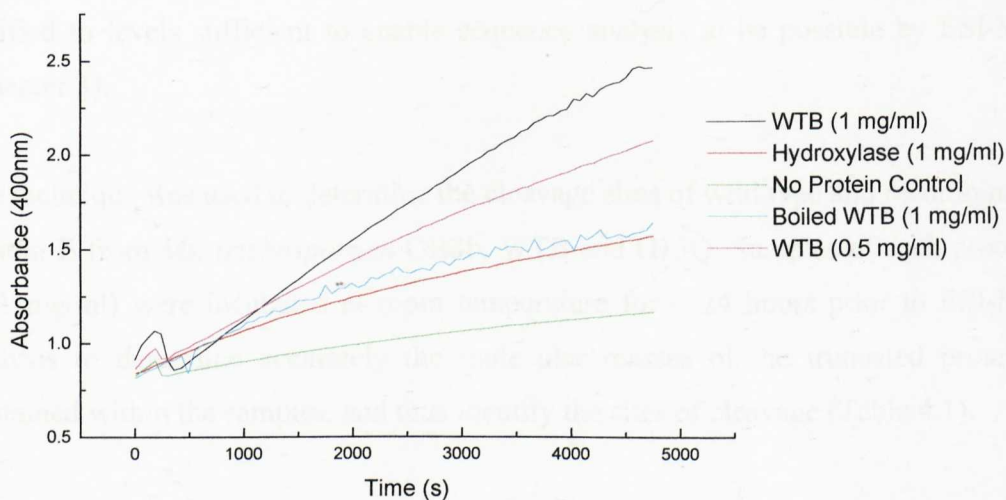
Nucleophilic side chain group of a residue on the core region of protein B, such as a side chain hydroxyl or thiol group of a serine, threonine or cysteine, attacks the carbonyl group of the acetate moiety of *p*-nitrophenylacetate. This results in the formation of the *p*-nitrophenol ion.



The formation of *p*-nitrophenol was monitored spectrophotometrically at 400nm over time in the presence of different concentrations of WTB (Chapter 2, Section 2.13). Controls included the background rate of *p*-nitrophenylacetate conversion to *p*-nitrophenol, as well as the rate of conversion of *p*-nitrophenylacetate to *p*-nitrophenol in the presence of a control protein known to be stable (hydroxylase) and boiled WTB, which also does not undergo cleavage. The results are displayed in Figure 4.2.

Figure 4.2: Monitoring the formation of *p*-nitrophenol.

The formation of *p*-nitrophenol from *p*-nitrophenylacetate was monitored at 400nm over time in the presence of different concentrations of WTB. Control reactions were conducted in the absence of protein, in the presence of hydroxylase protein and boiled WTB (Chapter 2, Section 2.13).



These data indicate that a specific nucleophilic amino acid side group is present to initiate the reaction of *p*-nitrophenylacetate to *p*-nitrophenol, as an increased reaction rate is observed for *p*-nitrophenylacetate in the presence of increasing concentrations of WTB. Also the reaction is slow, as is observed for the cleavage of protein B over time. The control reactions indicated that a background level of conversion was present and that minimal conversion was observed for the hydroxylase protein, which is known to be stable, and for the control sample of boiled protein B which does not undergo cleavage. This also suggests that the nucleophilicity of the specific side group is dependent upon the structure of the protein, as denatured protein loses its activity within the *p*-nitrophenylacetate assay. It is clear from this evidence that an autocatalytic mechanism of cleavage is most likely responsible for protein B truncate formation.

4.3 ESI-MS analysis of the cleavage of protein B from various sources

Wild-type recombinant *Ms. trichosporium* OB3b protein B, WTB and G13Q can be purified to levels sufficient to enable sequence analysis to be possible by ESI-MS (Chapter 3).

The technique was used to determine the cleavage sites of wild type and recombinant protein B from *Ms. trichosporium* OB3b, WTB and G13Q. Samples of each protein (~ 1 mg/ml) were incubated at room temperature for ~ 24 hours prior to ESI-MS analysis to determine accurately the molecular masses of the truncated proteins contained within the samples, and thus identify the sites of cleavage (Table 4.1).

Table 4.1: ESI-MS of the cleavage products of (i) wild type protein B from *Ms. trichosporium* OB3b, (ii) recombinant protein B from *Ms. trichosporium* OB3b, (iii) G13Q and (iv) WTB

The ESI-MS of the proteins was recorded on a Quattro II tandem mass-spectrometer equipped with an electrospray ion source. Data were processed using the MassLynx program (VG Biotech) (Chapter 2, Section 2.16.1).

(i) Wild-type *Ms. trichosporium* OB3b protein B

Observed molecular mass (Da)	Cleavage site, numbered with respect to the wild-type <i>Ms. trichosporium</i> OB3bB protein B sequence
14749.9	OB3b protein B intact
14017.2	Y ⁷ -N ⁸
13178.2	T ¹⁵ -G ¹⁶
13118.0	G ¹⁶ -K ¹⁷
12772.7	F ¹⁹ -A ²⁰
11965.1	E ²⁶ -E ²⁷

(ii) Recombinant *Ms. trichosporium* OB3b protein B

Observed molecular mass (Da)	Cleavage site numbered with respect to the wild-type <i>Ms. trichosporium</i> OB3bB protein B sequence
15027	Rec. OB3b protein B intact
13279	K ¹⁴ -T ¹⁵

(iii) G13Q

Observed molecular mass (Da)	Cleavage site numbered with respect to the wild-type <i>Mc. capsulatus</i> (Bath) protein B sequence
16300	G13Q intact
14700	M ¹² -Q ¹³

(iv) WTB

Observed molecular mass (Da)	Cleavage site numbered with respect to the wild-type <i>Mc. capsulatus</i> (Bath) protein B sequence
16230	WTB intact
14630	M ¹² -G ¹³

The cleavage sites identified for WTB and G13Q, M¹²-G¹³ and M¹²-Q¹³ respectively, are equivalent to the main cleavage site observed within the wild-type *Mc. capsulatus* (Bath) protein B, which results in protein B' formation (Bhambra, 1996). Therefore, it would appear that the extra N-terminal amino acids, resulting from the cloning system used for the expression of the recombinant proteins, do not affect the cleavage site, as they are observed to be the same.

The greater molecular mass of recombinant *Ms. trichosporium* OB3b protein B compared to that of the wild-type protein reflects the fact that the recombinant protein contains an extra two N-terminal amino acids, as a result of the cloning system used. This difference seems to have affected the cleavage sites, as they differ for the wild-type and recombinant proteins. Nevertheless, the cleavage occurs in roughly the same area of the N-terminal region of the proteins, as in the recombinant protein it occurs on the N-terminal side of the T¹⁵ residue, whereas in the native protein it occurs on the C-terminal side of the same amino acid. Therefore, it may be possible that steric effects are responsible for the cleavage as it occurs at approximately the same place, but is not amino acid specific. These data could suggest that the site could be a certain distance away from a particularly nucleophilic amino acid side chain group on the surface of the protein core. This could react with the flexible N-terminus of protein B specifically at this point, irrespective of the amino acids present at this position. Interestingly, the main cleavage site for recombinant *Ms. trichosporium* OB3b protein B (K¹⁴-T¹⁵) is two amino acid residues further from the N-terminal than the cleavage sites of WTB and G13Q. This could be

because the core regions of the two proteins differ slightly, so it is possible that a specifically reactive side chain group may be in a slightly different position in the two proteins. Alternatively, the flexibility of the N-terminal region of the two proteins may differ to some extent as a result of their slightly different amino acid compositions.

4.4 The role of protein B' within the sMMO system

It has been proposed that protein B' formation could occur as a general regulatory mechanism, possibly in response to certain conditions, such as those of copper excess, in order to control the amount of active protein B within the cell. Thus, the inactivation of the sMMO system by the formation of protein B' would allow the conservation of energy within the cell, as it would prevent the wasteful oxidation of NADH in the absence of, for example, substrate (Kazlauskaite *et al.*, 1996; Lloyd *et al.*, 1997). However, other proteins, which are known to undergo cleavage reactions either by autocatalytic mechanisms or specific proteolysis reactions, do so as a means of enzyme activation (Perler *et al.*, 1997). Thus it cannot be ruled out that the formation of protein B' may have an activatory role within an alternative system yet to be elucidated.

It has been shown that protein B' binds weakly to the hydroxylase of sMMO but has no effect on the redox potential value of the hydroxylase, unlike protein B which lowered the redox potential value, thus enabling oxygen activation to occur (Bhambra 1996; Kaslauskaite *et al.*, 1996). Therefore, it is seen to be important to identify any functions of protein B' to determine if it has any role within the sMMO system.

4.4.1 Sequence similarity searching

The approach was taken to elucidate if protein B' had any other function than that of inhibiting sMMO activity. Comparison of sequence similarity searches for protein B' to the results obtained for protein B was conducted. This was in order to elucidate whether the loss of the 12 amino acids from the N-terminus of protein B would

identify a protein with a more significant sequence similarity to protein B' than protein B, for which activity could then be determined.

The BLAST (Basic Local Alignment Search Tool) program available from the National Centre for Biotechnology Information (NCBI) was used (<http://www.ncbi.nlm.nih.gov/BLAST/>) to reveal sequence similarity for proteins B and protein B' from *Mc. capsulatus* (Bath) to other known protein sequences. This program was used to search for similarity between the query sequences and sequences in the peptide database (using BLASTP). The results obtained are shown in Figure 4.3.

Figure 4.3: Hit list from BLASTP report showing sequences producing significant alignments to (i) protein B' and (ii) protein B.

Sequences producing significant alignments are detailed with their accession numbers. Score and E values are indicated.

(i) *Mc. capsulatus* (Bath) protein B'

Sequences producing significant alignments:	Score (bits)	E Value
sp P18797 MMOB_METCA METHANE MONOOXYGENASE REGULATORY PROTE...	263	3e-70
pdb 1CKV Structure Of The Soluble Methane Monooxygenase...	263	3e-70
dbj BAA84753.1 (AB025021) soluble methane monooxygenase re...	182	1e-45
sp P27356 MMOB_METTR METHANE MONOOXYGENASE REGULATORY PROTE...	169	8e-42
gb AAC45291.1 (U81594) soluble methane monooxygenase prote...	169	1e-41
gb AAF01270.1 AF153282_3 (AF153282) MmoB [Methylocystis sp....	168	2e-41
gb AAB58743.1 (AF001356) TbhD [Burkholderia cepacia]	40	0.007
dbj BAA07113.1 (D37875) coupling protein [Nocardia corallina]	37	0.060
sp Q00459 TMOD_PSEME TOLUENE-4-MONOOXYGENASE SYSTEM PROTEIN...	37	0.078
gb AAB09621.1 (U04052) toluene-3-monooxygenase ferredoxin ...	32	2.0
pir S44305 phenol hydroxylase - Pseudomonas putida >gi 483...	32	2.6
sp P19731 DMPM_PSESP PHENOL HYDROXYLASE P2 PROTEIN (PHENOL ...	32	2.6
pir S47416 phenolhydroxylase chain C - Pseudomonas putida ...	31	4.5

(ii) *Mc. capsulatus* (Bath) protein B

Sequences producing significant alignments:	Score (bits)	E Value
sp P18797 MMOB_METCA METHANE MONOOXYGENASE REGULATORY PROTE...	289	5e-78
pdb 1CKV Structure Of The Soluble Methane Monooxygenase...	287	3e-77
dbj BAA84753.1 (AB025021) soluble methane monooxygenase re...	198	3e-50
sp P27356 MMOB_METTR METHANE MONOOXYGENASE REGULATORY PROTE...	182	2e-45
gb AAC45291.1 (U81594) soluble methane monooxygenase prote...	181	2e-45
gb AAF01270.1 AF153282_3 (AF153282) MmoB [Methylocystis sp....	179	8e-45
gb AAB58743.1 (AF001356) TbhD [Burkholderia cepacia]	40	0.008
dbj BAA07113.1 (D37875) coupling protein [Nocardia corallina]	37	0.069
sp Q00459 TMOD_PSEME TOLUENE-4-MONOOXYGENASE SYSTEM PROTEIN...	37	0.090
gb AAB09621.1 (U04052) toluene-3-monooxygenase ferredoxin ...	32	2.3
pir S44305 phenol hydroxylase - Pseudomonas putida >gi 483...	32	3.0
sp P19731 DMPM_PSESP PHENOL HYDROXYLASE P2 PROTEIN (PHENOL ...	32	3.0
pir S47416 phenolhydroxylase chain C - Pseudomonas putida ...	31	5.2

No differences were observed for the sequences identified as having similarity to proteins B and B'. However, the (Expect) E-values, which provide an estimate of the

statistical significance, indicated that protein B' was more similar to, for example, the regulatory proteins of toluene monooxygenase and phenol hydroxylase than protein B itself, as indicated by the lower E-values. sMMO has a wide substrate range, although previous work on protein B' has only shown it to be inactive when oxidising propylene (Bhambra, 1996). Therefore, it is possible that the formation of protein B' changes the substrate specificity of sMMO enabling it to oxidise only larger substrate molecules, such as toluene or benzene, as suggested by the increase in similarity to the regulatory proteins of these larger substrate molecule oxidising enzymes.

4.4.2 Can sMMO oxidise large substrate molecules when protein B' is used as the regulatory protein?

sMMO can oxidise benzene to phenol (Green and Dalton, 1989; Jiang, 1993). GC analysis (Chapter 2, Section 2.12) indicated that the product of benzene oxidation, phenol, had a retention time of ~2.24 minutes. Assays were conducted using 8 μ M of each hydroxylase, reductase and either protein B or protein B' and 10 mM benzene. Samples were incubated at 45 °C for 30 seconds before addition of 5 mM NADH. Samples were analysed by GC after 3 and 30 minutes incubation at 45 °C.

Phenol, produced from benzene oxidation, was observed by the peak at retention time ~ 2.24 minutes for the assay samples containing sMMO. However, no peak corresponding to phenol was observed for the sMMO assay samples containing protein B' in place of protein B. This suggested that protein B' was definitely inactive within the sMMO system and thus did not function in permitting the enzyme to oxidise only larger substrate molecules, for which benzene is typical.

4.4.3 Does protein B' bind to the hydroxylase?

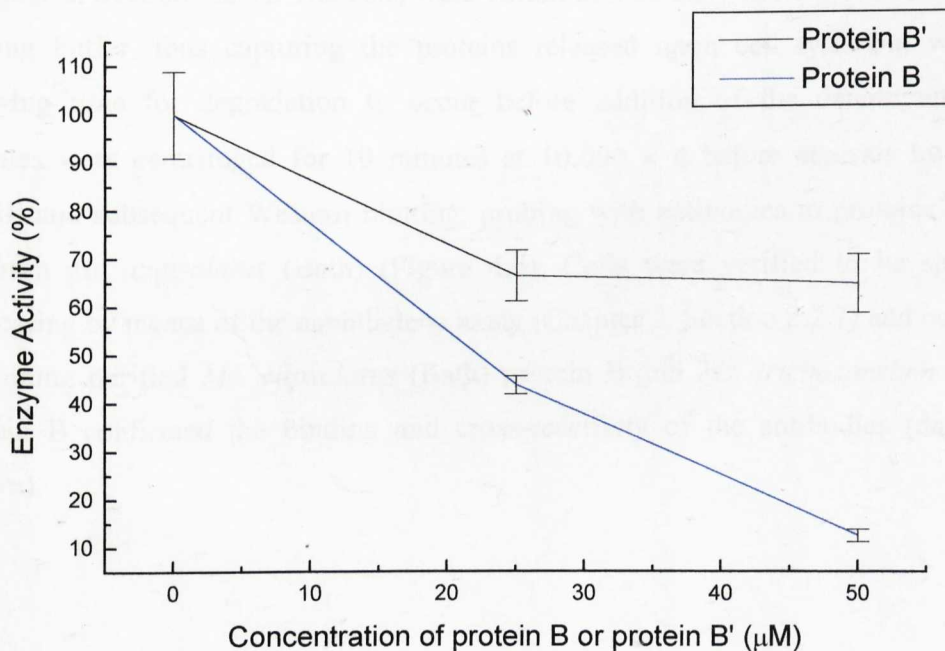
As protein B' is known to be inactive within the sMMO system, it was necessary to accurately confirm if protein B' bound to any significant degree to the hydroxylase. This would, therefore, identify whether the reason for the inactivity of protein B' was due to an inability to bind effectively to the hydroxylase or whether it related

more specifically to the actual absence of the first 12 N-terminal amino acids. Previous studies have used surface plasmon resonance to indicate that protein B' bound much more weakly than protein B to the hydroxylase (Bhambra 1996; Lloyd *et al.*, 1997). Similarly the binding of protein B' to the hydroxylase was also determined using direct electrochemistry (Kazlauskaitė *et al.*, 1996). Work by Jiang *et al.* (1993), indicated that protein B inhibited the hydroxylase when functioning via the peroxide shunt mechanism. Therefore, studies were undertaken to determine if protein B' could inhibit the hydroxylase when functioning via the peroxide shunt reaction, as this would indicate whether B' could bind effectively to the hydroxylase.

Assays of propylene oxidation by the H₂O₂-coupled reaction with hydroxylase were effected in the presence of proteins B and B'. Product formation was monitored by GC (Chapter 2, Section 2.12) after 10 minutes incubation (Figure 4.4).

Figure 4.4: The effect of proteins B and B' on the oxidation of propylene in the hydroxylase /H₂O₂ system.

H₂O₂-coupled propylene oxidation assays (Chapter 2, Section 2.12.3) contained 24 μM hydroxylase, 100 mM H₂O₂ and proteins B and B' at 0, 25, and 50 μM concentrations. Reactions were incubated for 10 min before injecting 500 μl of the gas phase of the reaction onto a calibrated Porapak Q GC column for product quantification. Enzyme activity is shown as a percentage of the activity of the hydroxylase activated via the peroxide shunt mechanism which represents 550.3 nmol propylene oxide produced (9.2 nmol/min/mg). The activities presented are the mean of 3-4 separate experiments. Standard error bars are shown.



A slight inhibition of activity was observed for the hydroxylase functioning via the H₂O₂ system in the presence of protein B' compared to the effect observed for protein B itself. This suggested that protein B' binds to the hydroxylase but not as strongly as protein B as it is insufficient to cause the dramatic effect observed by protein B. This is consistent with the conclusion of previous workers (Bhambra, 1996; Kazlauskaite *et al.*, 1996; Lloyd *et al.*, 1997).

4.5 Does protein B' exist within sMMO-expressing cells?

Protein B' has been purified from sMMO-expressing *Mc. capsulatus* (Bath) and *Ms. trichosporium* (OB3b) cells. Previous work by Lloyd *et al.* (1997) indicated that protein B' formation only occurred upon cell breakage, as analysis of whole cell lysates and soluble extracts of sMMO-expressing *Mc. capsulatus* (Bath) cells indicated only the latter to contain protein B'. However, the method of capturing the proteins contained within the sMMO-expressing methanotroph cells was modified to answer this question. Samples of the sMMO-expressing cells were removed from chemostat cultures in which they were growing under oxygen-limiting conditions (Chapter 2, Section 2.2.4). The cells were boiled immediately in SDS-PAGE sample loading buffer, thus capturing the proteins released upon cell lysis but without allowing time for degradation to occur before addition of the denaturant. The samples were centrifuged for 10 minutes at 10.000 × g before analysis by SDS-PAGE and subsequent Western blotting, probing with antibodies to proteins B and B' from *Mc. capsulatus* (Bath) (Figure 4.5). Cells were verified to be sMMO-expressing by means of the naphthalene assay (Chapter 2, Section 2.2.7) and controls containing purified *Mc. capsulatus* (Bath) protein B and *Ms. trichosporium* OB3b protein B confirmed the binding and cross-reactivity of the antibodies (data not shown).

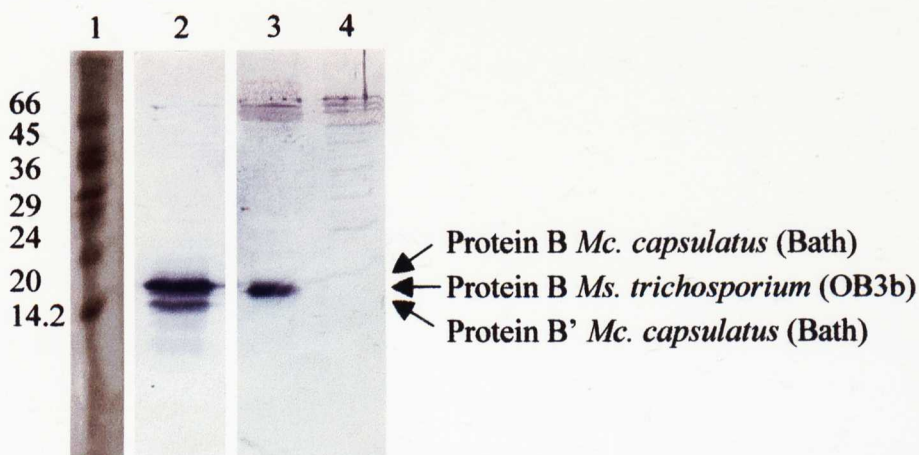
Figure 4.5: Western blot of proteins B and B' in sMMO-expressing *Mc. capsulatus* (Bath) and *Ms. trichosporium* OB3b whole cells.

Lane 1: Molecular weight markers (bovine albumin, 66 kDa; egg albumin, 45 kDa; glyceraldehyde-3-P-dehydrogenase, 36 kDa; bovine carbonic anhydrase, 29 kDa; bovine pancreas trypsinogen, 24 kDa; soybean trypsin inhibitor, 20 kDa; bovine milk α -lactalbumin, 14.2 kDa).

Lane 2: *Mc. capsulatus* (Bath) cells expressing sMMO.

Lane 3: *Ms. trichosporium* OB3b cells expressing sMMO.

Lane 4: *Mc. capsulatus* (Bath) cells expressing pMMO.



The Western blot (Figure 4.5) clearly identified protein B' as being present in sMMO-expressing cells of *Mc. capsulatus* (Bath) but not present in those of *Ms. trichosporium* OB3b. The control samples of pMMO-expressing *Mc. capsulatus* (Bath) cells confirmed the absence of sMMO within pMMO-expressing cells.

It is unclear why protein B' should be present in sMMO-expressing cells of one type of methanotroph and not the other. Experiments were conducted to determine whether the addition of copper to *Mc. capsulatus* (Bath) cells altered the level of protein B or protein B' during the conversion of the cells to pMMO expression. However, the levels of proteins B and B' remained constant throughout the time course until the cells expressed pMMO.

4.6 Structural analysis of proteins B and B'

Until very recently, when the NMR structures of protein B from both *Mc. capsulatus* (Bath) and *Ms. trichosporium* OB3b were published (Chang *et al.*, 1999; Walters *et al.*, 1999), no information was available on the structural characteristics of protein B. Studies were undertaken to determine the structural features of protein B and protein B' and hence by comparison of the two, it was hoped that information on the possible reason(s) for the inactivity of protein B' could be determined.

4.6.1 Secondary structure analysis of protein B and B'

Techniques sensitive to the secondary structure content of proteins, which could be interpreted to give information on the differences between proteins B and B', were pursued. The techniques of circular dichroism (CD), fluorescence, and Fourier Transform Infrared Spectroscopy (FTIR) were used.

4.6.1.1 Circular dichroism analysis

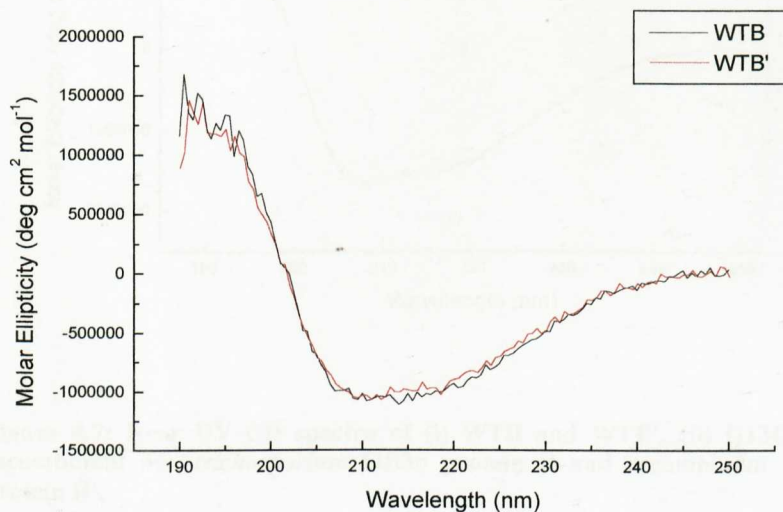
CD can be used to give secondary structure information. CD measurements made in the far UV region (170-250 nm) report on the backbone structure of the protein, as at these wavelengths contributions made to the spectra are dominated by the contributions of peptide bonds. CD bands in the near UV region (250-300 nm) originate from the aromatic amino acids and are very small in the absence of ordered structure and represent a highly sensitive criterion for the native state of a protein, and thus can be used as a fingerprint of the correctly folded conformation.

Near and far UV CD analyses were conducted on samples of WTB, G13Q and recombinant *Ms. trichosporium* OB3b protein B, and their equivalent protein B' proteins (WTB', G13Q protein B' and recombinant *Ms. trichosporium* OB3b protein B') produced after incubation of the intact protein samples at 20 °C for 24 hours. Figures 4.6 and 4.7 show the CD spectra obtained.

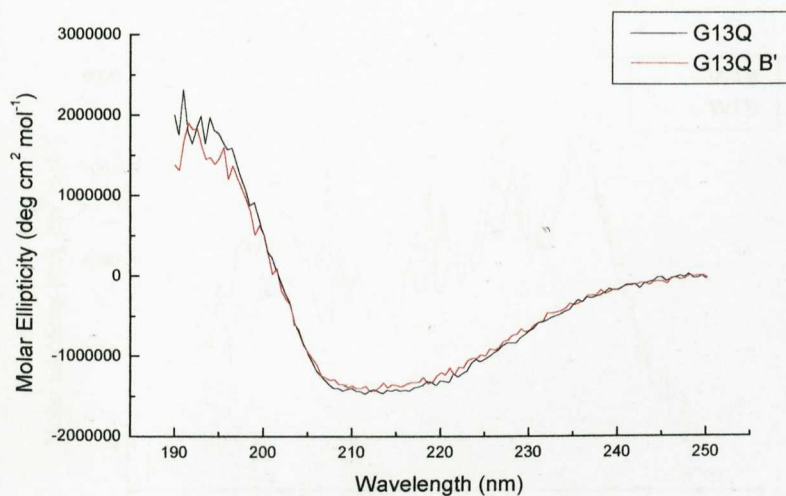
Figure 4.6: Far UV CD spectra of (i) WTB and WTB', (ii) G13Q and G13Q B' and (iii) recombinant *Ms. trichosporium* OB3b protein B and recombinant *Ms. trichosporium* OB3b protein B'.

The CD spectra were recorded on a Jasco J715 spectropolarimeter at room temperature (Chapter 2, Section 2.18). The spectra shown are averages of 10 scans of each protein (0.12 mg/ml in 50 mM phosphate buffer, pH 7) in a 1 mm pathlength quartz cuvette.

(i)



(ii)



(iii)

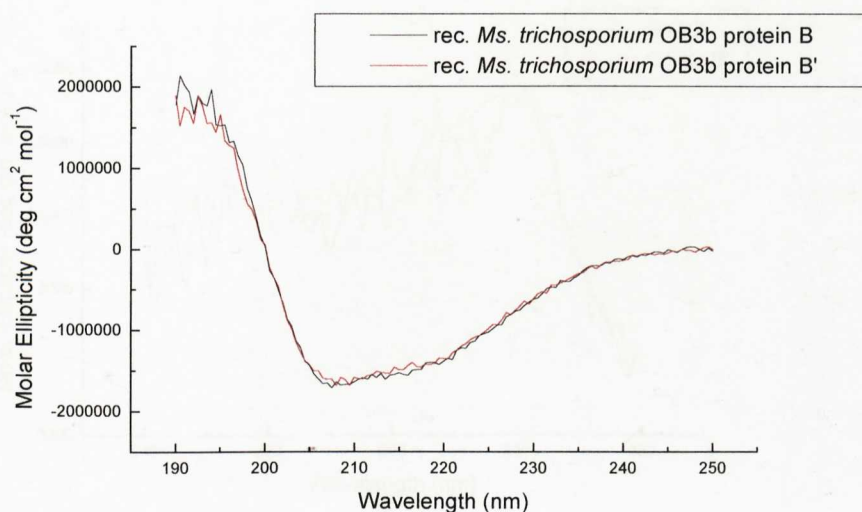
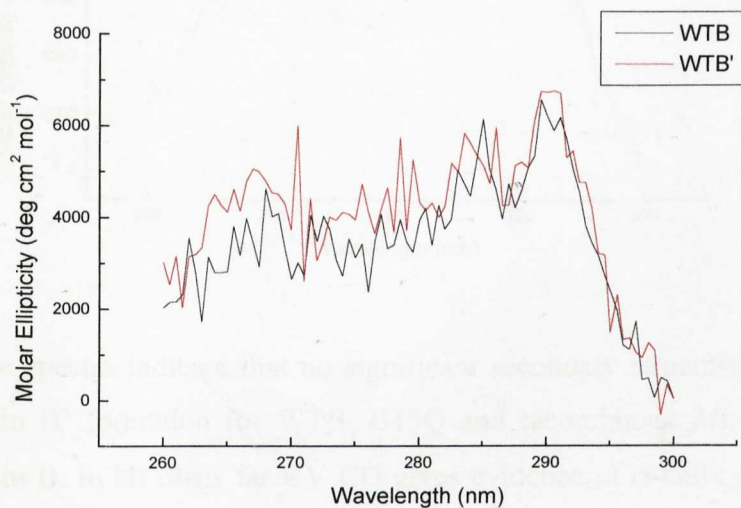


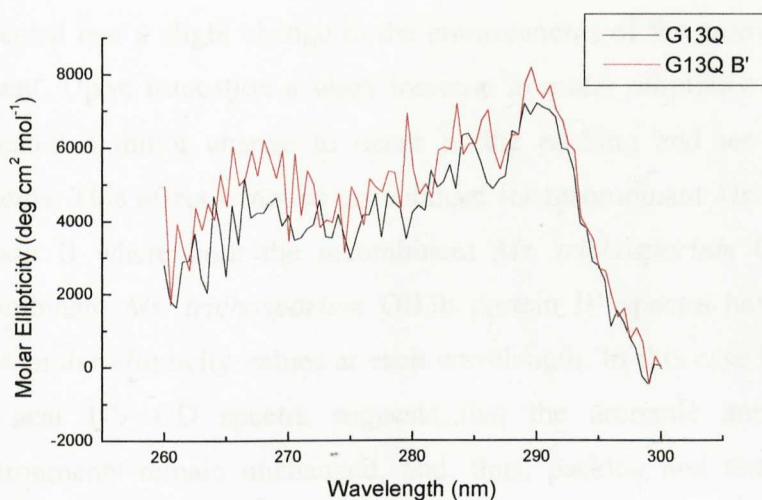
Figure 4.7: Near UV CD spectra of (i) WTB and WTB', (ii) G13Q and G13Q B' and (iii) recombinant *Ms. trichosporium* OB3b protein B and recombinant *Ms. trichosporium* OB3b protein B'.

The CD spectra were recorded on a Jasco J715 spectropolarimeter at room temperature (Chapter 2, Section 2.18). The spectra shown are averages of 10 scans of each protein (0.5 mg/ml in 50mM phosphate buffer, pH 7) in a 1 cm pathlength quartz cuvette.

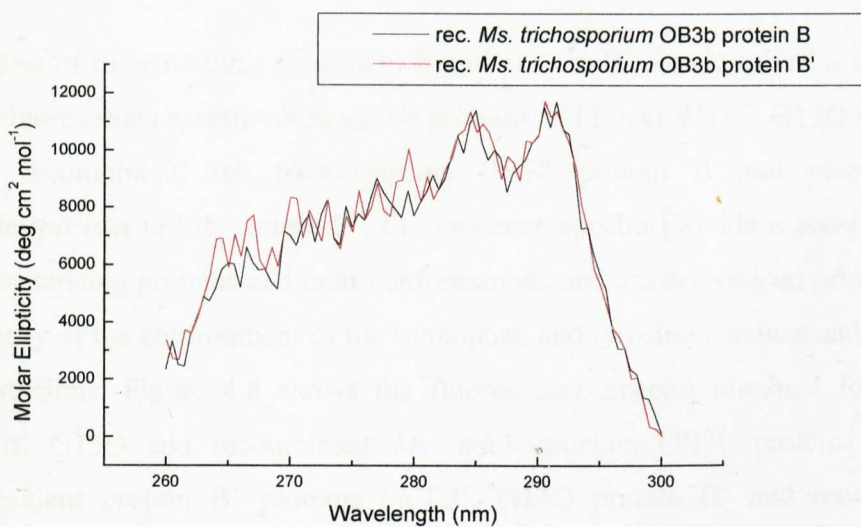
(i)



(ii)



(iii)



These spectra indicate that no significant secondary structure change accompanied protein B' formation for WTB, G13Q and recombinant *Ms. trichosporium* OB3b protein B. In all cases far UV CD gives evidence of α -helix and β -sheet character; the minima at 208 nm, 222 nm and maximum at 192 nm, indicate a moderate proportion of α -helical character and the minimum at 215 nm indicates β -sheet character to also be present. However, recombinant *Ms. trichosporium* OB3b protein B is seen to be more α -helical than WTB and G13Q, as it has a more pronounced minimum at 208 nm.

The near UV CD data for the intact and truncated proteins for WTB and G13Q indicated that a slight change in the environments of the aromatic amino acids was present. Upon truncation a weak increase in molar ellipticity was observed, which indicated a minor change to occur in the packing and tertiary structure of the proteins. This effect is not so pronounced for recombinant *Ms. trichosporium* OB3b protein B where both the recombinant *Ms. trichosporium* OB3b protein B and recombinant *Ms. trichosporium* OB3b protein B' spectra have approximately the same molar ellipticity values at each wavelength. In this case the lack of change in the near UV CD spectra suggests that the aromatic amino acids and their environments remain unchanged, and, thus, packing and tertiary structure of the protein remain the same upon truncation.

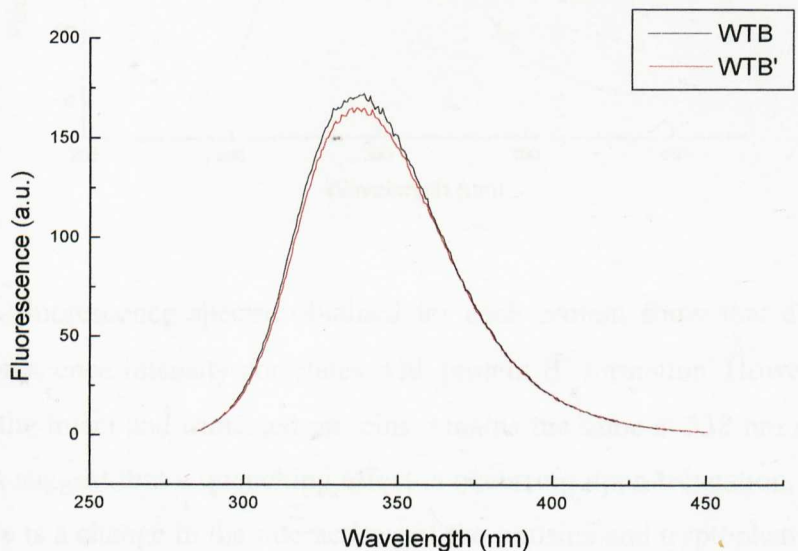
4.6.1.2 Fluorescence analysis

Studies of the structures of protein B and protein B' also involved a comparison of the fluorescence spectra obtained for proteins WTB and WTB', G13Q and G13Q B', and recombinant *Ms. trichosporium* OB3b protein B and recombinant *Ms. trichosporium* OB3b protein B'. Fluorescence spectra provide a sensitive means of characterising proteins and their conformations and are determined principally by the polarity of the environment of the tryptophan and tyrosine residues and their specific interactions. Figure 4.8 shows the fluorescence spectra obtained for samples of WTB, G13Q and recombinant *Ms. trichosporium* OB3b protein B, and their equivalent protein B' proteins (WTB', G13Q protein B' and recombinant *Ms. trichosporium* OB3b protein B') produced after incubation of the intact protein samples at 20 °C for 24 hours.

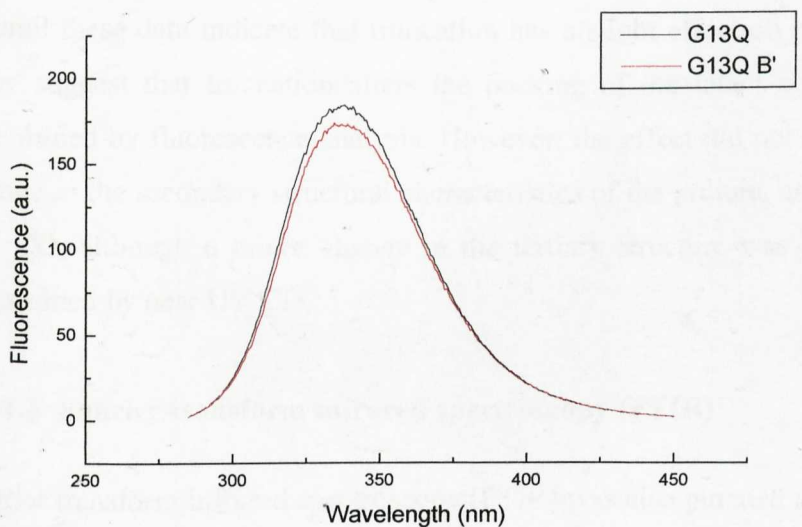
Figure 4.8: Fluorescence spectra of (i) WTB and WTB', (ii) G13Q and G13Q B' and (iii) recombinant *Ms. trichosporium* OB3b protein B and recombinant *Ms. trichosporium* OB3b protein B'.

The fluorescence spectra were recorded on a Perkin-Elmer LF-50 fluorimeter at room temperature with excitation at 280 nm (Chapter 2, Section 2.17). The spectra shown are sum of 8 scans of each protein (0.5 mg/ml in 50 mM phosphate buffer, pH 7) in a 3 ml quartz cuvette with a 10 mm pathlength.

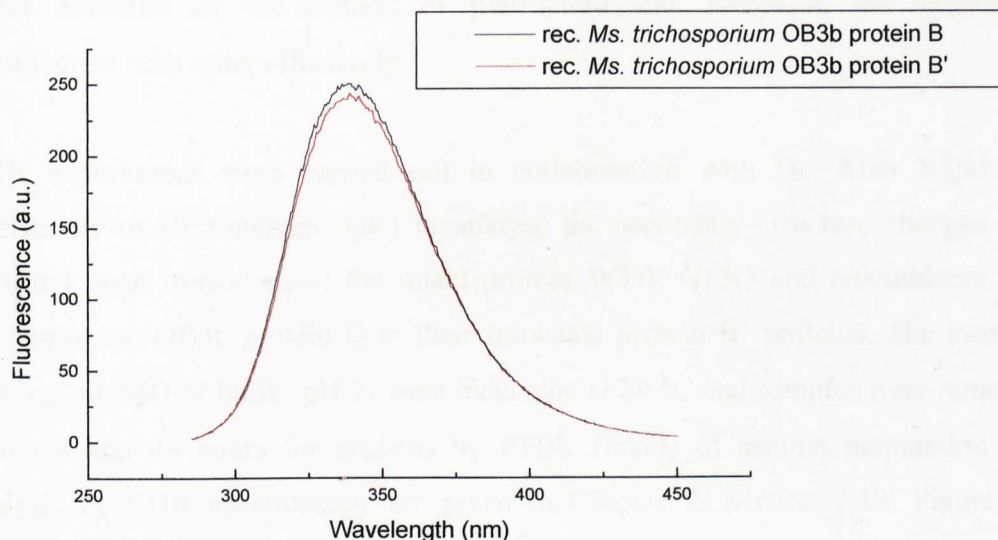
(i)



(ii)



(iii)



The fluorescence spectra obtained for each protein show that a slight decrease in fluorescence intensity correlates with protein B' formation. However, the λ_{max} value for the intact and truncated proteins remains the same at 338 nm in each case. These data suggest that a quenching effect is occurring upon truncation. This indicates that there is a change in the interactions of the tyrosine and tryptophan amino acids of the proteins with their neighbouring groups.

Overall these data indicate that truncation has a slight effect on protein B structure. They suggest that truncation alters the packing of the intact active protein B, as determined by fluorescence analysis. However, the effect did not cause a significant change in the secondary structural characteristics of the protein, as determined by far UV CD, although a minor change in the tertiary structure was also visualised, as determined by near UV CD.

4.6.1.3 Fourier transform infrared spectroscopy (FTIR)

Fourier transform infrared spectroscopy (FTIR) was also pursued to gain information on any secondary structural changes that occur to protein B upon truncation to protein B'. IR spectra give details on molecular vibrations, which can be interpreted to give molecular conformation information. Unlike CD, which, in general, can only

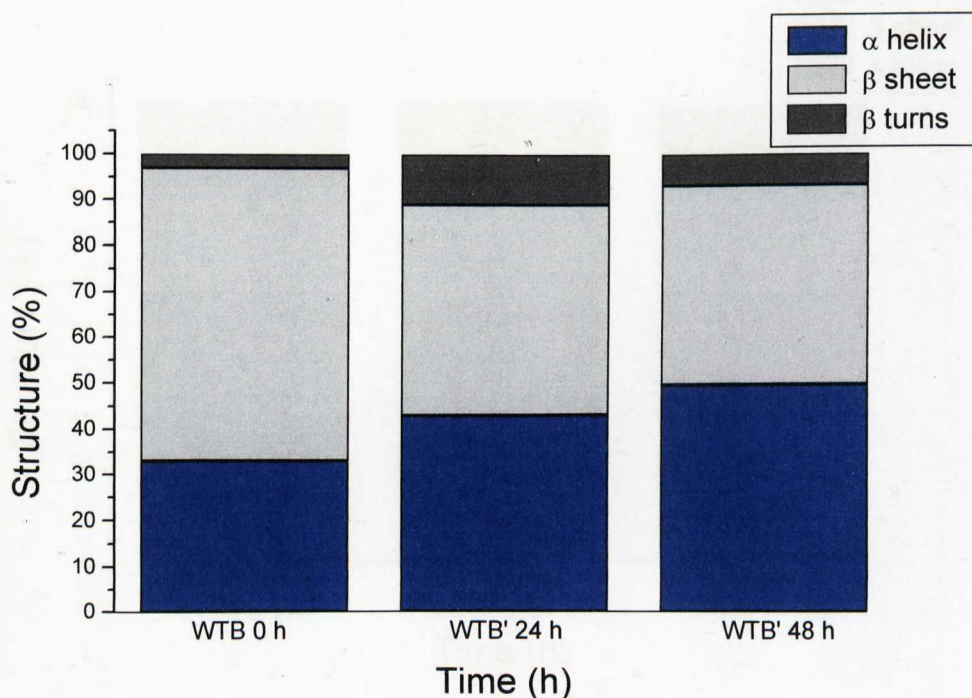
give details on the proportion of α -helix content of a protein reliably, FTIR provides better estimates of the content of β -structure and, therefore, the techniques complement each other effectively.

FTIR experiments were carried out in collaboration with Dr. Alan Wilkinson (University of Birmingham, UK) to analyse the secondary structure changes that occurred upon truncation of the intact protein WTB, G13Q and recombinant *Ms. trichosporium* OB3b protein B to their truncated protein B' proteins. The proteins (0.5 mg/ml, MOPS buffer pH 7) were incubated at 20 °C and samples were removed at 0, 24 and 48 hours for analysis by FTIR. Details of sample preparation and analysis by FTIR spectroscopy are given in Chapter 2, Section 2.19. Figure 4.9 illustrates the change in secondary structure observed for the various samples.

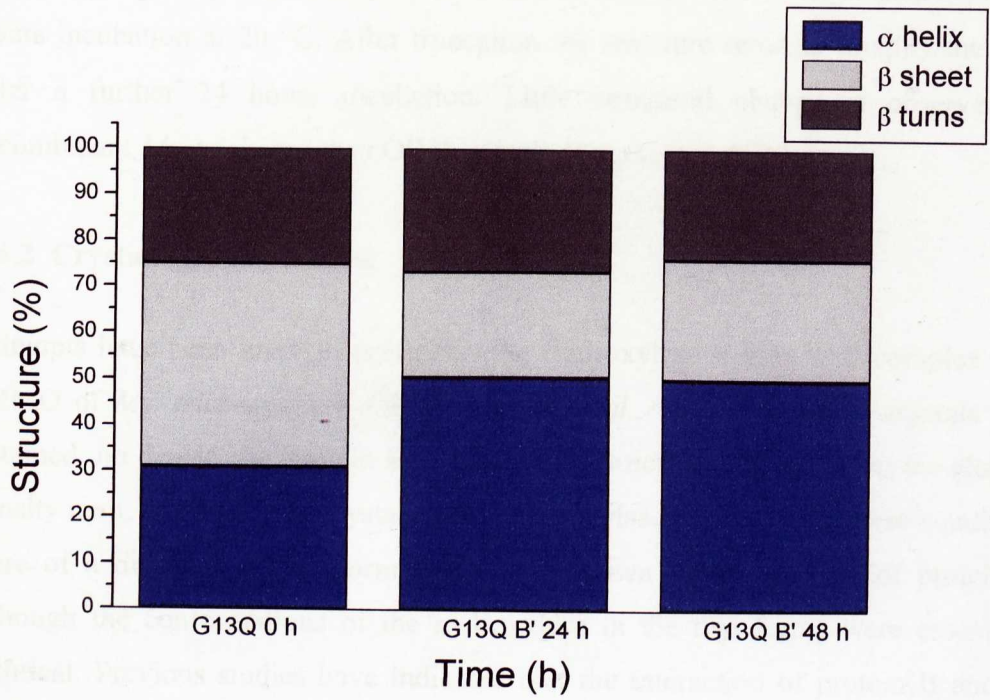
Figure 4.9: Amide I band fitting results for the FTIR spectroscopy data for (i) WTB, (ii) G13Q and (iii) recombinant *Ms. trichosporium* OB3b protein B giving the secondary structure content for each protein after incubation at 20 °C at 0 h, 24 h and 48 h.

FTIR spectra of each of the protein (8 mg/ml in 50 mM deuterated sodium phosphate buffer) were recorded at room temperature using a Bruker IFS 66 FTIR spectrometer equipped with an MCT detector. Single beam spectra were collected which consisted of 256 scans. Data was collected at 2 cm^{-1} wavenumber resolution (Chapter 2, Section 2.19).

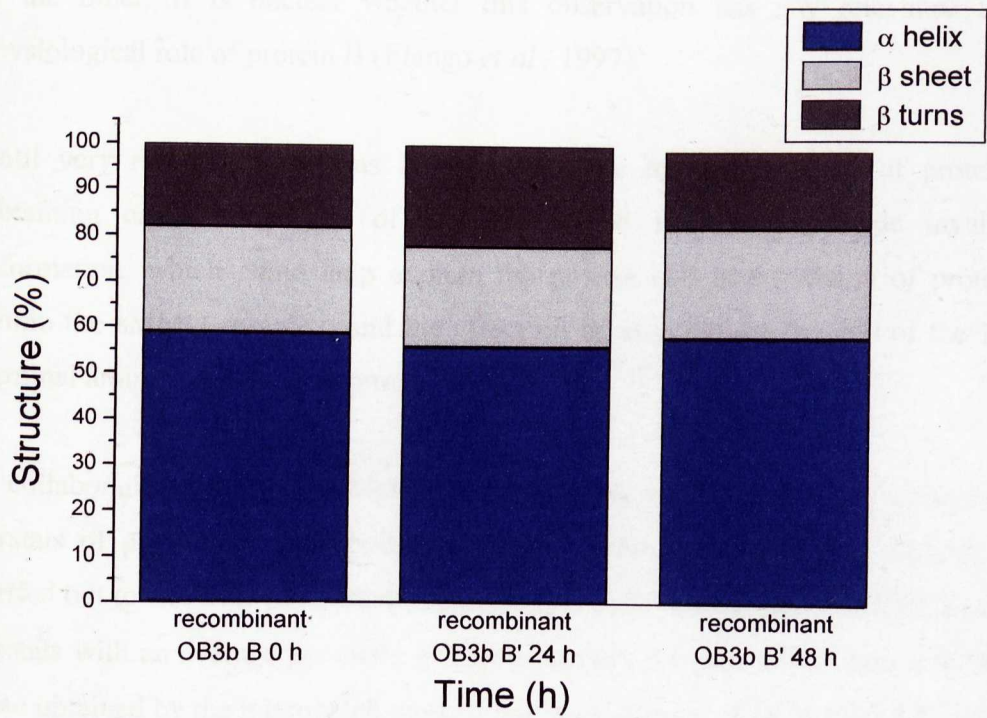
(i)



(ii)



(iii)



These FTIR data show there to be a decrease in β -character for both proteins WTB and G13Q as the proteins become truncated to their protein B' equivalents over 24 hours incubation at 20 °C. After truncation the structure remains roughly the same after a further 24 hours incubation. Little structural change is observed for recombinant *Ms. trichosporium* OB3b protein B upon truncation.

4.6.2 Crystallography studies

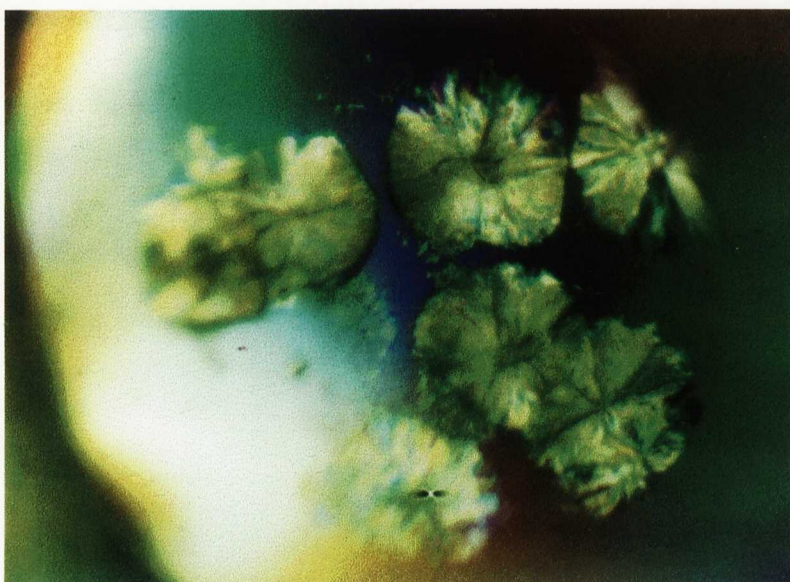
Attempts have been made to crystallise the Hydroxylase – Protein B complex from sMMO of *Ms. trichosporium* OB3b (Elango *et al.*, 1997). Although crystals were obtained, no density for protein B in the crystal structure was shown in the electron density map. However, the crystals of the hydroxylase grown under these conditions were of a different crystal form from those grown in the absence of protein B, although the conformations of the hydroxylase in the two forms were essentially identical. Previous studies have indicated that the interaction of protein B and the hydroxylase alters the structure of the hydroxylase and that these alterations reverse slowly upon protein B dissociation (Liu *et al.*, 1995). In the crystal structure of the hydroxylase grown in the presence of protein B, one dimer is rotated slightly relative to the other. It is unclear whether this observation has any relevance to the physiological role of protein B (Elango *et al.*, 1997).

Until very recently, little was known about the tertiary structure of protein B. Obtaining crystal structures of proteins B and B' would provide invaluable information, which could help explain the precise role and function of protein B within the sMMO complex, and the effect on its structure of the loss of the 12 N-terminal amino acids to form protein B'.

In collaboration with Dr. R. McKenna, (University of Warwick, UK) screening for crystals of protein B/B' by both the hanging drop and microbatch methods was carried out to test over 1200 conditions (Chapter 2, Section 2.22). Weakly diffracting crystals with an average geometry of approximately 0.1 mm × 0.25 mm × 0.25 mm were obtained by the microbatch method under conditions of 18 % PEG 8 K, 25 mM lithium sulphate, 25 mM Tris-HCl pH 7 (Figure 4.10).

Figure 4.10: Photograph showing the crystalline entities of protein B/B'.

Weakly diffracting 'quasi' crystals obtained by the microbatch method under conditions of 18 % PEG 8 K, 25 mM lithium sulphate, 25 mM Tris-HCl pH 7.



The crystallisation trial shown (Figure 4.10) contains needle-like structures radiating from a central nucleation point. Crystalline entities are visible towards the edges and can be seen by the light polarization effects. Seeding of these crystals failed to produce crystals of improved quality. Even though this work did not produce any well diffracting stable crystals for structural studies, the production of even the small 'quasi-crystals' is, nonetheless, a major step towards this goal.

4.6.3 Dimer studies of proteins B and B'

Protein B from *Methylocystis sp.* strain M has been shown to exist as a dimer (Shinohara *et al.*, 1998). Protein B from *Ms. trichosporium* OB3b has been observed as having a molecular weight of 31 kDa, suggesting that it too may be capable of existing as a dimer (Fox *et al.*, 1989; Chapter 3). Similar observations have also been made for *Mc. capsulatus* (Bath) protein B (Bhambra, 1996). Since the hydroxylase is a dimer it is logical that protein B may exist as a dimer, so that each hydroxylase monomer can interact with a protein B monomer for activity. Thus, the extra dimer interactions of protein B may serve to provide extra stabilisation of the Hydroxylase – Protein B complex. Therefore, it is important to determine accurately whether protein B exists, as a dimer as this can aid in furthering the understanding of the

component interactions of sMMO necessary for activity. Alternatively, it is possible that protein B' forms dimers and it is these that have been observed, mistakenly as protein B dimers. It is possible that it is this occurrence that results in the inactivity of protein B within the sMMO system. Therefore, various techniques have been used to determine whether proteins B or B' exist as dimers in solution.

4.6.3.1 PAGE analysis of protein B

Analysis of wild-type *Mc. capsulatus* (Bath) protein B', WTB and recombinant *Ms. trichosporium* OB3b protein B by SDS-PAGE indicated them to run at their expected molecular weight values, although a band at 30 kDa was often observed for the proteins run on SDS-PAGE. This band was indicated to be that of protein B/B' by Western blot analysis, probing with antibodies to protein B/B' (data not shown). Therefore, it appeared that the proteins could exist as 'dimers' even after denaturation for SDS-PAGE analysis, whilst some of the protein was observed as running in the correct position. Native-PAGE analysis proved difficult in actually assigning weights for the proteins, although they were observed as running at values higher than ~ 16 kDa, and often 2 bands were observed. This data suggested that the proteins were possibly capable of existing as dimers, but could exist as monomers at the same time.

To determine whether dimer formation was as a result of a disulphide bond between to monomers of the proteins, SDS-PAGE was carried out on samples treated with and without β -mercapto-ethanol, a reducing agent which breaks such bonds. SDS-PAGE analysis indicated the treated and untreated samples to be the same, both with a weak band at ~ 30 kDa. Native PAGE analysis gave the same results. Overall, PAGE analysis proved inconclusive in identifying accurately the presence of protein B or protein B' dimers, but did provide evidence of their transient existence.

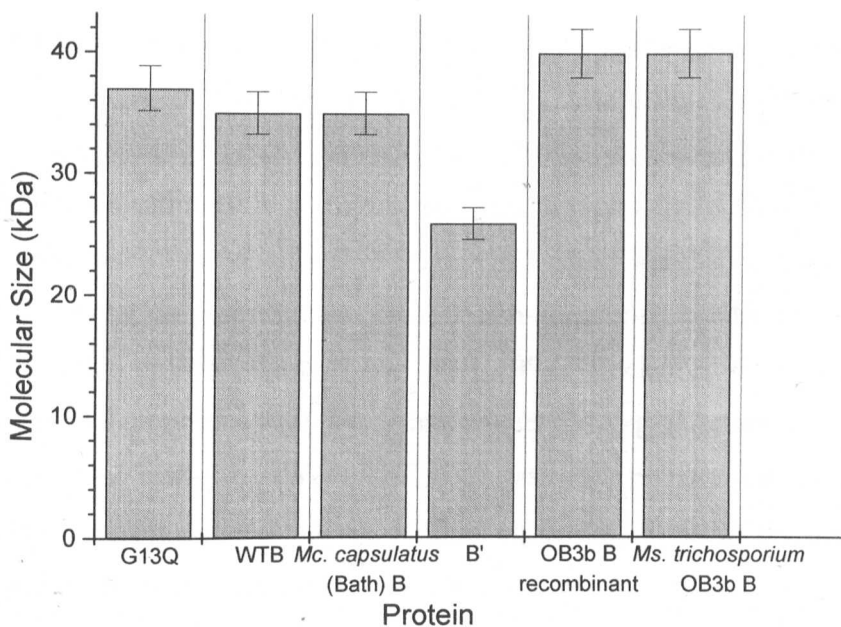
4.6.3.2 Molecular size determination

Size exclusion chromatography can be used to indicate the molecular size of proteins by a comparison of their relative mobilities on the column compared to that of the protein standards used in the calibration of the column. It would indicate whether the proteins existed as monomers or dimers, or a mixture of the two. It was noted that anomalous running of proteins on the column can also occur.

Samples of the proteins G13Q, WTB, wild-type *Mc. capsulatus* (Bath) protein B and B', recombinant and wild-type *Ms. trichosporium* protein B were subjected to size exclusion chromatography on a Superdex 75 FPLC column (Chapter 2, Section 2.9) and the elution volume for each was recorded and the molecular size inferred from the calibration curve. The results obtained for the molecular size of each of the proteins are shown in Figure 4.11.

Figure 4.11: Size exclusion chromatography of G13Q, WTB, wild-type *Mc. capsulatus* (Bath) protein B and B', recombinant and wild-type *Ms. trichosporium* OB3b protein B.

Data displayed are the means of 3 separate experiments. Error bars are displayed.



The molecular sizes inferred from the data show that the proteins do not elute at the expected molecular size of ~ 16 kDa. However, G13Q, WTB and wild-type *Mc. capsulatus* (Bath) protein B all eluted at approximately the same retention time, indicating them to be very similar or the same in shape and size, as would be expected. This was also the case for recombinant *Ms. trichosporium* OB3b protein B and wild-type *Ms. trichosporium* OB3b protein B. Protein B', known to be smaller than its intact predecessors, eluted to give a correspondingly smaller molecular size, but one which was still greater than that expected for its molecular weight. Also, the smaller wild-type and recombinant *Ms. trichosporium* OB3b proteins eluted to give higher molecular sizes than the recombinant *Mc. capsulatus* (Bath) based proteins, WTB and the single mutant G13Q. The values do not correspond to 'dimers' of the proteins, so this would imply that the proteins are eluting as a reflection of their different shapes, and do not infer their weights. Also, only one elution peak was observed for each protein, so the proteins are not identified as existing as mixtures of monomers and dimers under these conditions. This work is in agreement with recent work by Brandstetter *et al.* (1999), where it was also found that protein B from *Mc. capsulatus* (Bath) eluted at an anomalously high molecular size value.

4.6.3.3 MALDI-ToF MS analysis of protein B

The use of mass spectrometry in the analysis of native protein conformation has proved difficult, particularly because of the denaturing conditions required for ionising molecules for mass measurements. However, recently matrix assisted laser desorption ionisation time of flight mass spectrometry (MALDI-ToF MS) has been used in the determination of native protein molecular weights by modification of the sample preparation procedures to provide non-denaturing conditions required for the stability of the protein (Karas *et al.*, 1989, 1990; Glocker *et al.*, 1996). Thus in this study, in collaboration with Dr. Anne-Mette Hoberg (Department of Biological Sciences, University of Warwick, UK), sample preparation procedures were modified to create non-denaturing, 'softer' conditions to see if the protein could be observed in the dimer conformation.

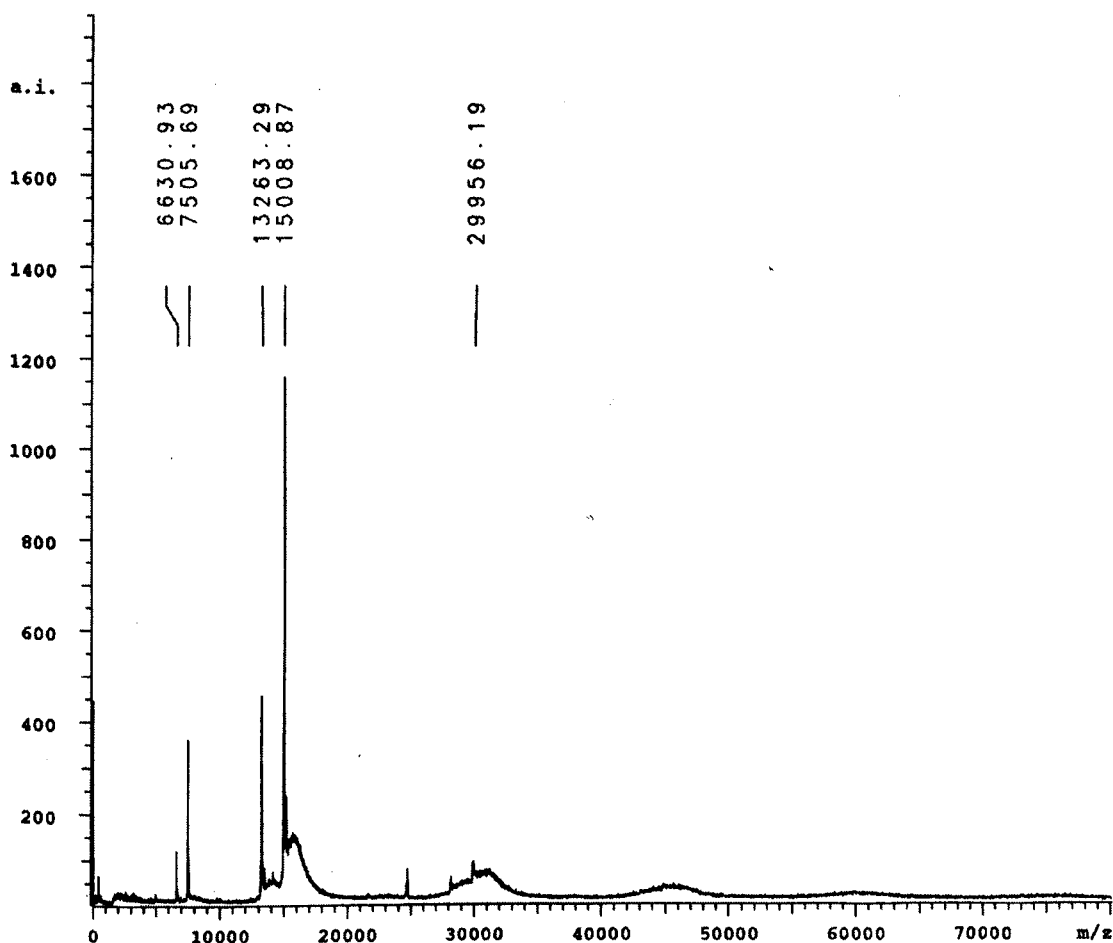
A Proflex III MALDI-ToF mass spectrometer was used for the analysis of recombinant *Ms. trichosporium* OB3b protein B (Chapter 2, Section 2.16.1). The

MALDI-ToF 'dried-droplet' sample preparation method resulted in a distinct peak at 15008.9 Da and a very low intensity peak at 29956.2 Da, possibly the dimer. Similarly, analysis of *Mc. capsulatus* (Bath) protein B' by the same method gave distinct peaks at 14635.4 Da (B') and 13277.6 Da (another cleavage product) and very low intensity peaks at 29214.9 Da and 25006.3 Da, which could correspond to the respective dimers (Figure 4.12).

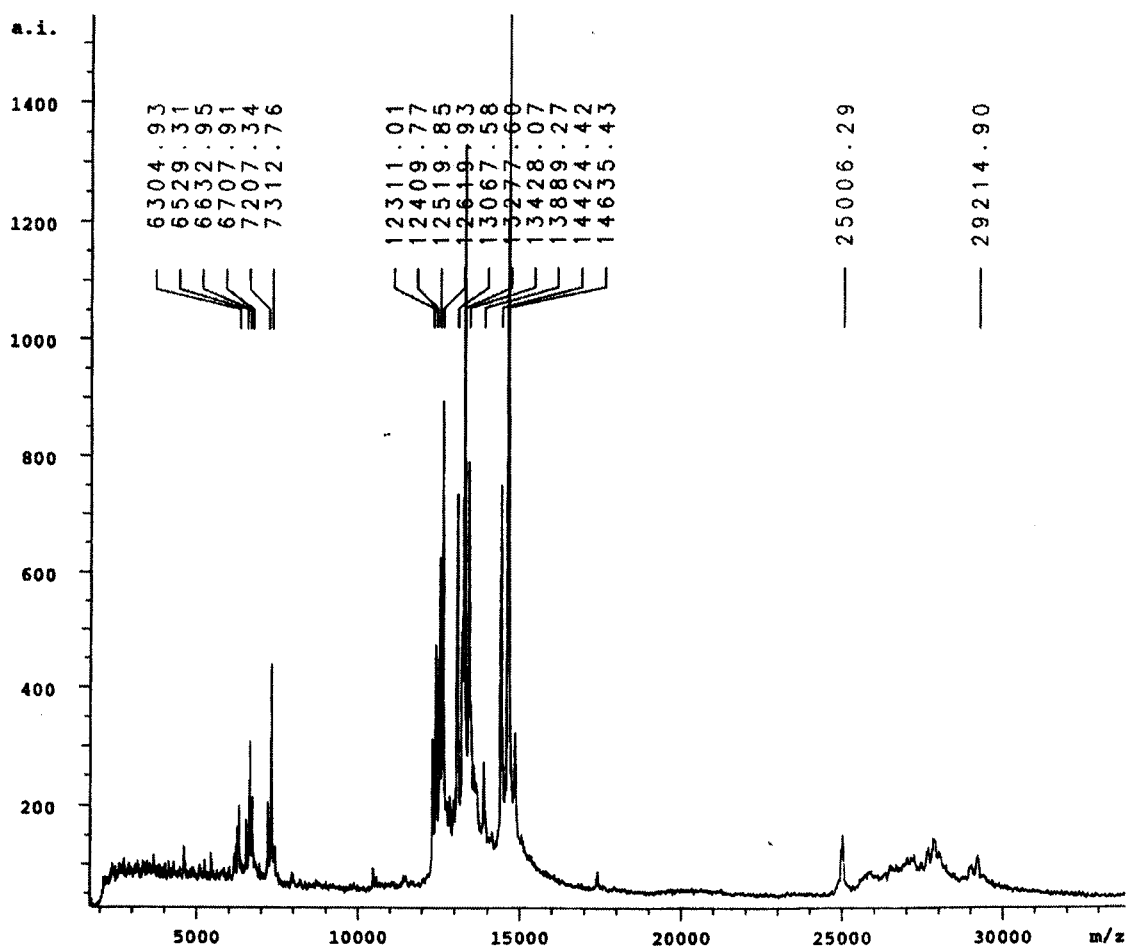
Figure 4.12: Analysis of (i) recombinant *Ms. trichosporium* OB3b protein B and (ii) wild-type *Mc. capsulatus* (Bath) protein B by MALDI-ToF mass spectrometry.

The MALDI-ToF MS of the proteins were recorded on a Bruker Proflex III MALDI-ToF mass spectrometer. Data were recorded by a 1GHz Le Croy digitiser and analysed by Bruker Xtof 3.1.0. software. Data displayed as mass to charge ratio (m/z) against arbitrary intensity (a.i.) (Chapter 2, Section 2.16.1).

(i)



(ii)



This study provided evidence for the protein existing predominantly in the monomer form but that dimer formation was identifiable under certain conditions.

4.6.3.4 Sedimentation equilibrium analysis

Analytical ultracentrifugation experiments on proteins WTB, protein B' and G13Q were conducted in collaboration with Dr. N. Errington (National Centre for Molecular Hydrodynamics, University of Leicester, UK) in order to determine whether the proteins existed as dimers in solution.

By means of sedimentation equilibrium experiments in the analytical ultracentrifuge, changes in molecular weight, when molecules associate to form more complex structures such as dimers, can be studied. The technique provides a method of

determining the molecular weight of the complex as it exists in solution, and estimating the binding constants of the interactions between the components.

Sedimentation equilibrium experiments were conducted on samples of WTB, protein B' and G13Q (Chapter 2, Section 2.21). The association of the proteins in solution is a function of their behaviour during sedimentation and can be distinguished from non-specific aggregation by analysis of residual plots after fitting the data to particular models of association. The data for WTB, G13Q and protein B' fitted poorly to the single ideal species model with WTB and G13Q indicating self-association behaviour. The deviation to the model encountered for protein B' (Figure 4.13) was proposed to be due to either protein degradation occurring, possibly by means of the truncation reaction, or due to the non-ideality phenomena, which has the effect of reducing the apparent molecular weight obtained by sedimentation equilibrium analysis. The data for WTB and G13Q were fitted to self-association models from which a K_d for each was deduced. Good data fits were obtained for the self-association models for WTB and G13Q based upon the residuals to the fit (Figures 4.14 and 4.15). Nevertheless, it was possible that non-ideality effects were present for WTB and G13Q due to their high level of similarity to protein B'. However, as non-ideality and self-association have opposing effects upon the molecular weight obtained, it was impossible to extricate one from the other. For this reason, the K_d and K_a values have to be quoted as estimates based on the data analysis conducted here, and in the light of the results obtained for protein B', cannot be stated as being precise values.

Figure 4.13: Sedimentation equilibrium profiles for protein B' at (i) 1 mg/ml and (ii) 2 mg/ml.

Graphs display the fit of the sedimentation equilibrium data (coloured circles) to the single ideal species model (black line) at the given speeds.

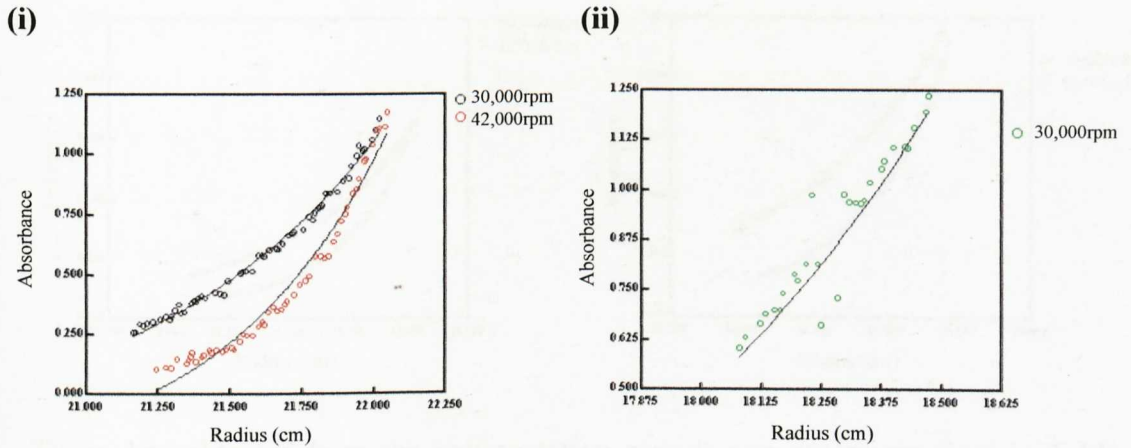


Figure 4.14: Sedimentation equilibrium profiles for WTB at (i) 1 mg/ml and (ii) 2 mg/ml.

Graphs display the fit of the sedimentation equilibrium data (coloured circles) to the monomer-dimer self-association model (black line) at the given speeds.

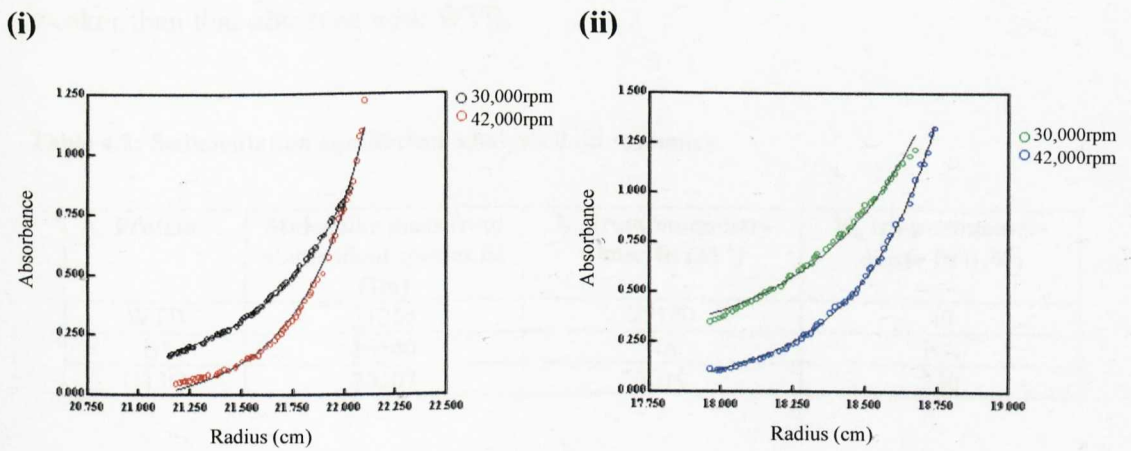
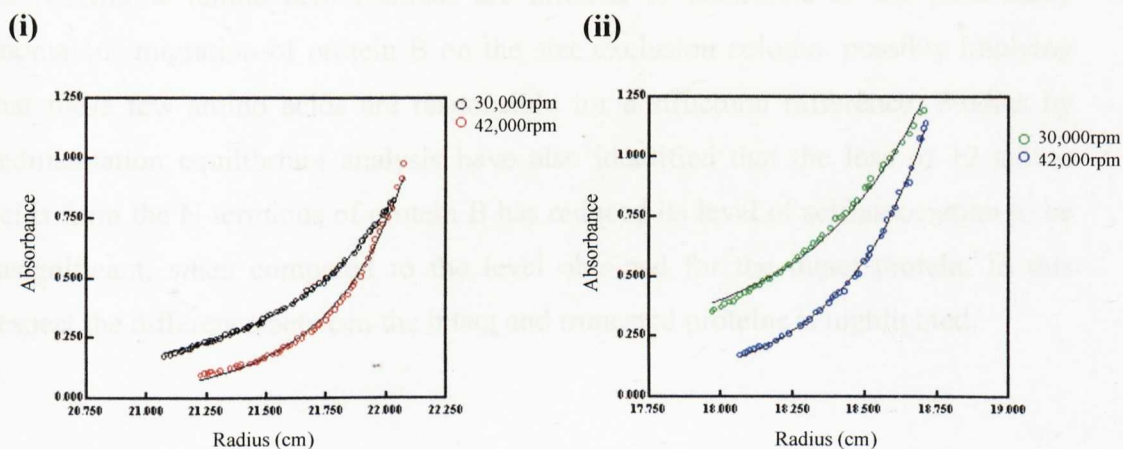


Figure 4.15 Sedimentation equilibrium profiles for G13Q at (i) 1 mg/ml and (ii) 2 mg/ml.

Graphs display the fit of the sedimentation equilibrium data (coloured circles) to the monomer-dimer self-association model (black line) at the given speeds.



These data obtained from the sedimentation experiments are summarised in Table 4.2 and are conclusive in the findings that protein B' does not self-associate to any significant degree, whereas WTb and the G13Q mutant show an equilibrium between monomeric and dimeric forms. From the dissociation constants it can be seen that the interaction between the G13Q peptides is approximately 10 times weaker than that observed with WTb.

Table 4.2: Sedimentation equilibrium analysis data summary.

Protein	Molecular mass from single ideal species fit (Da)	K_a from monomer-dimer fit (M^{-1})	K_d from monomer-dimer fit (μM)
WTb	21365	25100	40
B'	10540	NA	NA
G13Q	20307	3019	330

Although, the experiments failed in accurately identifying dimers of proteins B or B', they did provided evidence for their transient existence under certain non-specific conditions. Nevertheless, proteins B and B' have been identified as fairly similar in that they cause the proteins to give anomalously high values by size exclusion chromatography. However, the overall structures of wild-type *Mc*.

capsulatus (Bath) proteins B and B' are suggested to differ, as a difference of ~ 8 kDa is observed between their experimental molecular size values when the loss of the first 12 N-terminal amino acids corresponds to only 1.2 kDa. Therefore, the first 12 N-terminal amino acid residues are inferred to contribute to the particularly anomalous migration of protein B on the size exclusion column, possibly implying that these few amino acids are responsible for a structural difference. Studies by sedimentation equilibrium analysis have also identified that the loss of 12 amino acids from the N-terminus of protein B has reduced its level of self-association to be insignificant, when compared to the level obtained for the intact protein. In this respect the difference between the intact and truncated proteins is highlighted.

4.6.4 Biophysical characterisation of proteins B and B'

The techniques of small angle X-ray scattering (SAXS) and atomic force microscopy (AFM) were used to further compare the structures of proteins B and B'. SAXS can be used to determine the solution structure of proteins at relatively low resolution and can, therefore, provide valuable information on the overall shape of a protein molecule. Similarly, AFM was used to probe for differences in the conformation of the two proteins.

4.6.4.1 Small angle X-ray scattering (SAXS)

SAXS studies were carried out in collaboration with Drs. Jill Trewhella and Steve Gallagher (Los Alamos National Laboratory, USA) (Chapter 2, Section 2.25). The solution scattering profiles for each were measured (Figure 4.16). Scattering data were collected for proteins G13Q and protein B' over a range of concentrations from 2-15 mg/ml, in 25 mM MOPS, pH 7, 13 °C. For each component there was no concentration dependence of scattering data, indicating that interparticle interference effects were negligible and hence no correction was required. The vector length distribution functions for each component, calculated as the inverse Fourier transform of the scattering profiles, are shown in Figure 4.17. A significant increase in d_{\max} was observed for protein B' compared to G13Q. The best-fit ellipsoid models for G13Q and protein B' have approximate dimensions 50, 34, 30 Å and 66, 28, 27

Å respectively. These models give reduced χ^2 values of 1.01 and 1.02 respectively, indicating a near perfect fit (which would have $\chi^2 = 1.0$) to the scattering data. As a measure of the discrimination between these fits to the data, the scattering data for G13Q can be compared to the best fit ellipsoid determined for protein B' which gives an $\chi^2 = 12.5$. *Vice versa*, the experimental data for protein B' compared to the best fit model for G13Q gives $\chi^2 = 13.0$. The measure of the I_0 values and molecular volumes show that both protein G13Q and protein B' are monodisperse in solution, indicating that the observed changes in structural parameters cannot be attributed to aggregation (Table 4.3). Thus, protein B' is identified as being structurally longer and thinner than protein G13Q.

Figure 4.16: Solution scattering profiles ($I(Q)$ versus Q data) for G13Q (■) and protein B' (□). The solid lines represent the model $I(Q)$ profiles calculated using uniform ellipsoids for G13Q and B'. The error bars are based on counting statistics only.

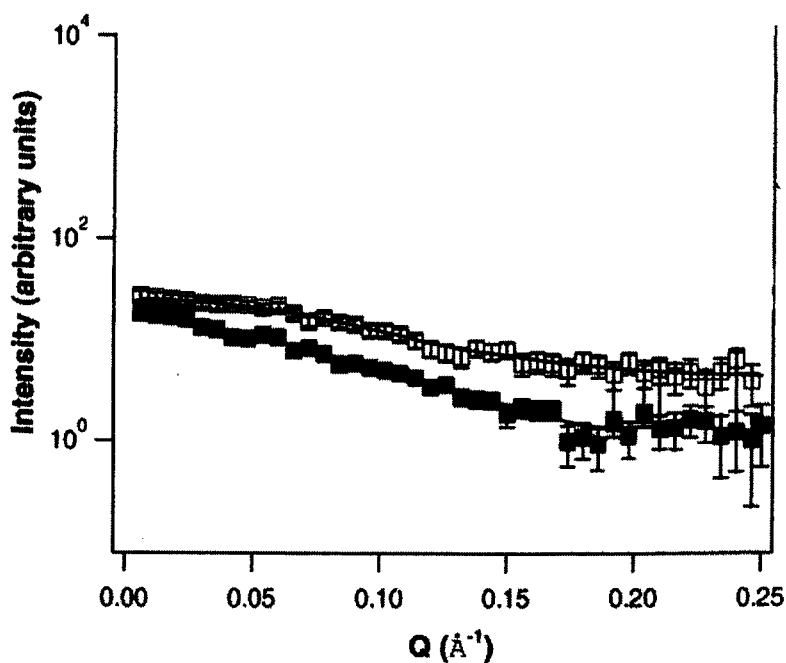


Figure 4.17: Vector length distribution functions ($P(r)$ functions) for G13Q (■) and protein B' (□).

The experimentally derived values are indicated by (■) G13Q and (□) B'. The solid lines are the $P(r)$ functions calculated for the models indicated in Figure 4.16.

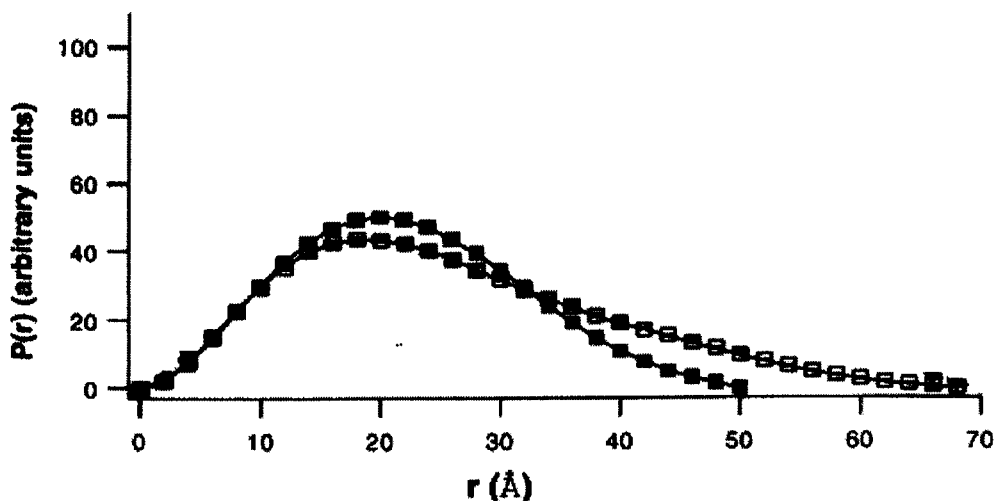


Table 4.3: R_g , d_{max} , and molecular volumes for proteins G13Q and protein B'.

Protein	R_g (Å)	d_{max} (Å)	Measured I_0 (arbitrary units)	Measured volume (Å ³)	Expected volume (Å ³)
G13Q	17.5±0.9	50	3950±150	19200±3100	19400
B'	19.8±0.9	70	3650±160	20300±1700	17900

The observed extension of the structure upon removal of the N-terminal segment of protein B, therefore, must be due to a partial unfolding or to some sort of opening of the structure triggered by the loss of interactions with the N-terminal residues.

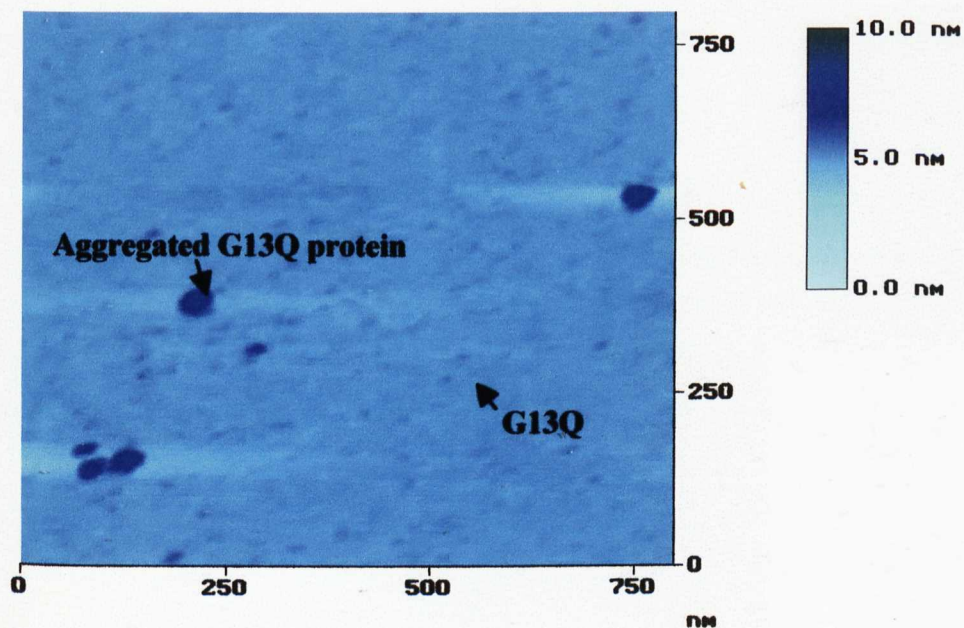
4.6.4.2 Atomic force microscopy (AFM)

Atomic force microscopy, otherwise known as scanning force microscopy, was invented in 1986 (Binnig *et al.*, 1986). It is a powerful tool for the investigation of biological structures, yielding a three dimensional image at low resolution. The technique is based on the movement of a sharp tip at the free end of a soft cantilever which scans over a samples keeping the tip at almost touching distance from the sample surface. The tip and cantilever movement is coupled to an optical readout system for monitoring the bending of the cantilever induced by the surface topography, and digitally reproduces the topography of the sample surface.

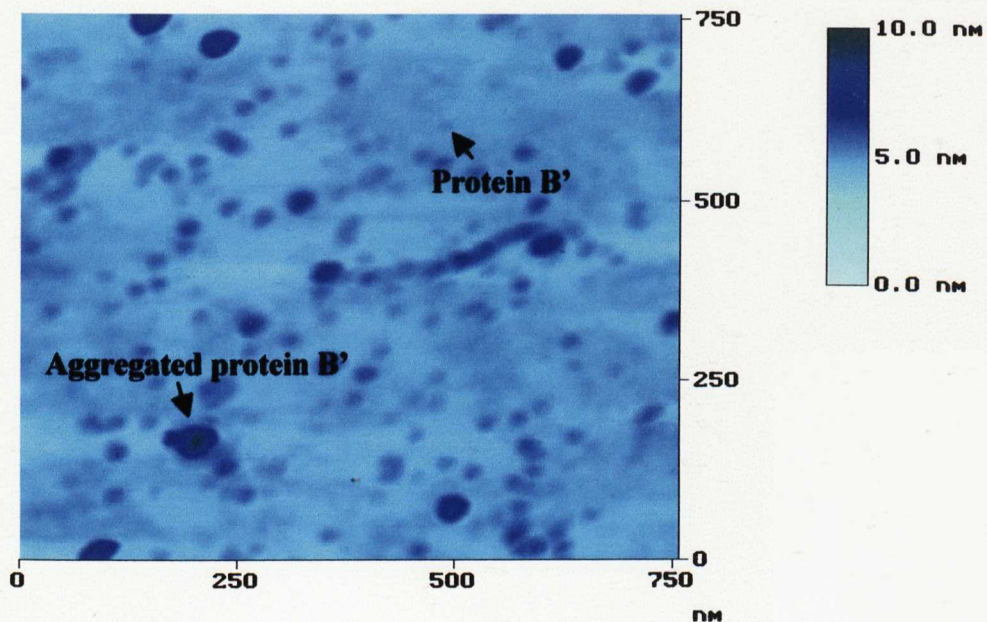
In collaboration with Mr. Bernie Sattin (Department of Chemistry, University of Toronto, Canada) samples of proteins G13Q and protein B' were immobilised on mica and air dried. The samples were imaged by tapping mode AFM in air, using a TESP (diving board cantilever) oscillated at its resonance frequency to a free amplitude of approximately 30 nm. Once the AFM was engaged in imaging, parameters were controlled to achieve a high resolution image with minimal tip-samples interaction (Chapter 2, Section 2.26). The images obtained for proteins G13Q and protein B' are shown in Figure 4.18.

Figure 4.18: Tapping mode AFM images of (i) G13Q and (ii) protein B'.
Labelled are samples of each protein and their aggregates.

(i)



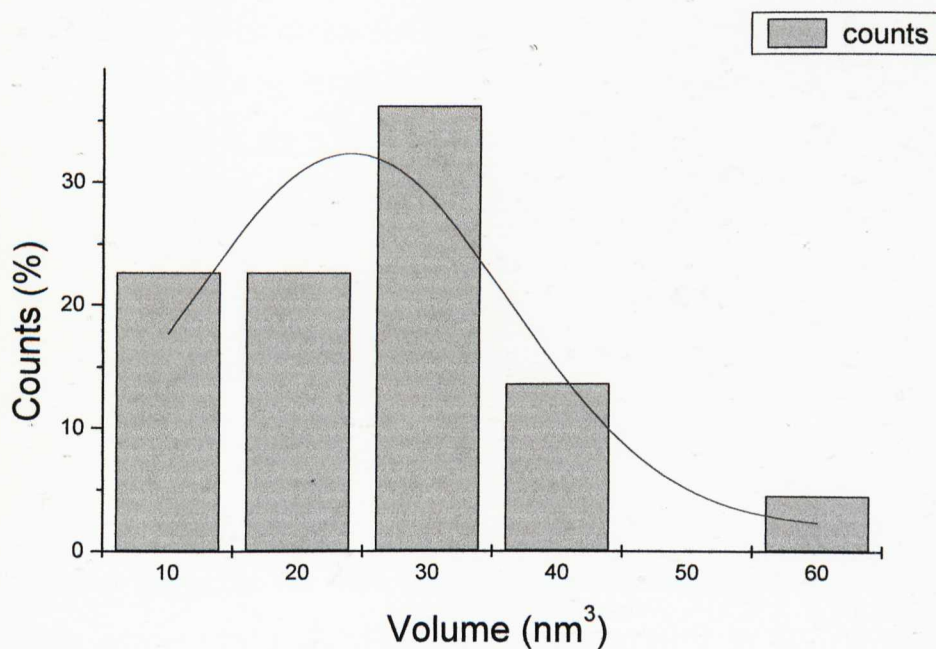
(ii)



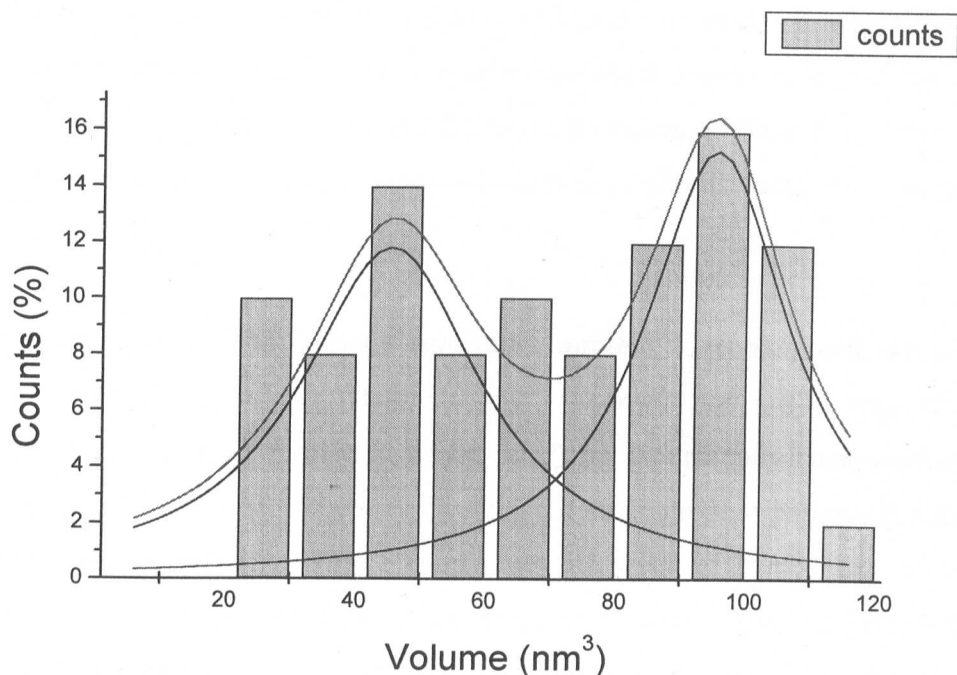
The images indicate that under the conditions of the experiment protein B' tended to aggregate more than protein G13Q. The volumes corresponding to the immobilised protein molecules were calculated for each protein to determine the observed volumes for each, as displayed in Figure 4.19.

Figure 4.19: Distribution of the observed volumes of (i) protein G13Q and (ii) protein B'. Observed volumes data analysed using Origin™ 4.10 software (Microcal Software Inc., USA).

(i)



(ii)



The data distribution was identified as being bimodal for protein B', whereas this was not the case for G13Q, confirming the observations that protein B' was aggregating under the conditions of the experiment. The first peak was considered to be that of protein B' alone and the second peak, the aggregates formed. G13Q was shown to have a volume of $\sim 30 \text{ nm}^3$, whereas protein B' was observed to have a volume of $\sim 40 \text{ nm}^3$. This is in agreement with the SAXS data which indicated protein B' to be larger than G13Q, although due to the differences in the two techniques (SAXS which studies the protein in solution whereas AFM analysis was conducted on dried protein samples), the volumes obtained in each case could not be compared. Nevertheless, the AFM results similarly support the idea of an opening of the protein B molecule upon protein B' formation due to the fact that a larger volume is observed for protein B'.

4.7 Conclusion

The ability to separate proteins B and protein B' by chromatofocusing lead to analysis which suggested that autocatalysis was the most likely cause of the cleavage of *Mc. capsulatus* (Bath) protein B. This was supported by the evidence for a

nucleophilic amino acid side chain group being present as a means of mediating the cleavage reaction. These results, together with previous studies in which the addition of protease inhibitors and expression of recombinant protein B in protease-deficient strains of *E. coli* failed to prevent the cleavage reaction (Bhambra, 1996; Lloyd *et al.*, 1997), further support the autocatalysis mechanism as being responsible for the cleavages observed.

The identification of the various truncates of protein B, recombinant and wild-type, from both *Mc. capsulatus* (Bath) and *Ms. trichosporium* OB3b suggests the N-terminal region of the protein to be flexible. This has recently been verified by the elucidation of the NMR structures of the two methanotrophic proteins (Chang *et al.*, 1999; Walters *et al.*, 1999). Studies into the possible mechanism of cleavage identified a hydrolytic mechanism as being involved and that the initiation of the reaction could occur via a nucleophilic side chain group coming into contact with the flexible N-terminal region. Thus, the slight differences in the structures of these two proteins could be responsible for the slight differences in the sites of cleavage observed. These would suggest steric effects, caused by the different amino acid sequences giving the proteins slightly different structures, to be involved in determining the site(s) of cleavage. Nevertheless, the proteins both become N-terminally truncated, presumably by the same mechanism, and in this respect remain similar.

Protein B' has not been identified as having a functional role within the sMMO system, although binding studies suggest it to bind weakly to the hydroxylase. The presence of protein B' within the sMMO-expressing *Mc capsulatus* (Bath) cells, would suggest it has a function, although it is possible that this may not relate to the sMMO system.

Structurally proteins B and B' are similar. Evidence from CD, fluorescence, SAXS, and AFM suggests an 'unpacking' occurs upon truncation, which changes the shape of the protein, but does not alter the secondary structure content significantly. This 'unpacking' could be the reason for protein B' binding less strongly, if at all, under certain conditions to the hydroxylase. The data also do not give information on the structure of the N-terminal region of protein B, as upon its loss no significant change

in secondary structure is observed. Therefore, the N-terminal region can be identified as being relatively unstructured.

The techniques of PAGE, size exclusion chromatography, MALDI-ToF mass spectrometry and sedimentation equilibrium analysis all provided weak evidence for dimer formation for wild-type *Mc. capsulatus* (Bath), wild-type and recombinant *Ms. trichosporium* OB3b protein B, G13Q, WTB and protein B', suggesting that self-association was possible. SAXS, however, provided no evidence for this. Nevertheless, the extent of dimer formation, as monitored by the different techniques, varies, and all suggested the monomer form to be the dominant species. Therefore, association of monomers to form dimers appeared to be possible under certain conditions, but was not necessarily the native form of the protein. These data were in agreement with the work of Chang *et al.* (1999) and Fox *et al.* (1991), where limited dimer formation was observed for *Ms. trichosporium* OB3b protein B in solution under various conditions. The studies however, failed to identify dimer formation as a major difference between the intact and truncated forms of protein B and it, therefore, does not represent the means by which protein B' is inactive within the sMMO system.

Very recently the structures of protein B from *Mc. capsulatus* (Bath) and *Ms. trichosporium* OB3b have been determined by NMR analysis (Chang *et al.*, 1999; Walters *et al.*, 1999). Nevertheless, the progress achieved with regard to the crystallisation of *Mc. capsulatus* (Bath) protein B/B' is important as the NMR structures failed to give definitive structure to the whole of the N-terminal region of the protein. The resolution of a crystal structure of intact protein B is still vital in elucidating the nature of the important N-terminal region and its orientation with respect to the core of the protein. Even the production of the small quasi-crystals identified here is a major step towards achieving this aim. The crystallisation trials may, however, have been hindered by the low level of stability of the protein, possibly due to the 'flexible' N-terminal region of the protein enabling cleavage reactions to occur. Thus, the need to stabilise the protein against such cleavage reactions is highlighted, not only for improving the possibility of obtaining larger, stable, well diffracting crystals, but also for other experiments on protein B to be

conducted without interference from the cleavage reaction. This issue is considered in Chapter 5.

Chapter 5

Stabilisation of Protein B by Biochemical Methods

5.1 Introduction

The stabilisation of protein B against irreversible inactivation via truncation to protein B' is of major importance, if further studies of the protein are to be possible. The truncation process constantly poses immense difficulties when conducting biochemical and structural analyses, as the protein readily degrades. The problem has partly been overcome for *Mc. capsulatus* (Bath) protein B by the mutation of the Gly¹³ residue to a glutamine (Lloyd *et al.*, 1997), which has reduced the rate of the cleavage reaction enabling analysis of the protein to be possible. However, the G13Q mutant still degrades to form its protein B' equivalent, known as G13QB', at the Met¹²-Gln¹³ site (numbered with respect to the wild-type protein B sequence), which corresponds to the site of cleavage within the wild-type protein (Chapter 4). Therefore, minimising inactivation is crucial for the successful study of the protein itself and with respect to the sMMO system.

Since the first observations of the truncation of *Mc. capsulatus* (Bath) protein B (Pilkington *et al.*, 1990), various attempts have been made to stabilise the protein against this occurrence. The addition of protease inhibitors during the purification procedure of native wild-type protein B failed to prevent truncation occurring (Lloyd *et al.*, 1997), as did purification under methane saturating conditions, anaerobic conditions and in the absence of freeze-thaw cycles (Bhambra, 1996). Such conditions have been shown in the past to prevent the inactivation of other enzymes.

Surveying a range of conditions under which the stability of the enzyme may be improved was, therefore, considered worthwhile. The aim of the work presented in this Chapter was to determine whether any conditions could be found that would suppress protein B' formation.

5.2 Effect of protein concentration and temperature on stability

Increasing protein concentration can affect the stability of a protein, as it makes the environment around the protein similar to that of the cell. Within cells, proteins are subject to the influence of high concentrations of various macromolecules, often amounting to concentrations of hundreds of mg/ml. Thus, although biochemical experiments try to reproduce quasi physiological conditions of temperature, pH and salt concentrations, rarely are proteins observed experiencing the effects of the typically high concentrations of various macromolecular species found in physiological media. Such physiological media are referred to as 'crowded'. Crowding favours the formation of compact structures and macromolecular complexes and decreases the diffusional mobility of macromolecules (Ralston, 1990; Minton, 1997). In some circumstances these factors can aid in increasing protein stability. Therefore, optimising levels of protein concentration can be important. A decrease in protein concentration, although lowering the possible rate and degree of aggregation, increases the exposure of the protein to the solvent environment, which may ultimately promote the autocatalytic degradation observed. A delicate balance of non-covalent forces including, hydrophobic, ionic and van der Waals interactions as well as hydrogen bonds, holds the native catalytic form of protein B together. Upon exposure to adverse environmental conditions, such as low protein concentrations, these forces can be weakened or broken, resulting in partial or total unfolding of the protein (Creighton, 1989). This in turn may enhance the possibility of the cleavage reaction occurring, leading to inactivation.

Similarly, inactivation can occur due to heat, as thermal unfolding of the enzyme can take place. This exposes reactive groups and hydrophobic areas that can subsequently react, possibly causing the cleavage reaction observed for protein B. Although sMMO is most active at 45 °C, at this temperature the protein interactions of the components may be stabilising one another, particularly when present within the cell environment where more protective agents may be present. However, the purified protein alone within only a buffer environment, would be expected to experience the destabilising effects previously described (Creighton, 1989).

5.2.1 Analysis by SDS-PAGE

The technique of SDS-PAGE is useful in clearly identifying the presence of intact and truncated versions of protein B within a given sample. Studies into the effect of temperature on samples of G13Q and recombinant *Ms. trichosporium* OB3b protein B were monitored over a 6 hour time period at 20, 45 and 60 °C (Figure 5.1).

Figure 5.1: SDS-PAGE analysis of G13Q and recombinant *Ms. trichosporium* OB3b protein B after incubation at (i) 20 °C, (ii) 45 °C and (iii) 60 °C for 0 h, 2 h, 4 h and 6 h.

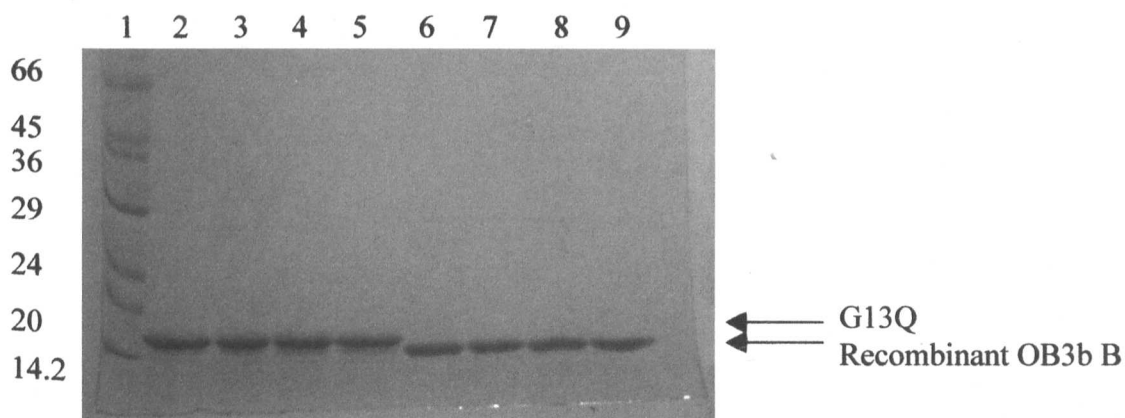
Lane 1: Molecular weight markers (bovine albumin, 66 kDa; egg albumin, 45 kDa; glyceraldehyde-3-P-dehydrogenase, 36 kDa; bovine carbonic anhydrase, 29 kDa; bovine pancreas trypsinogen, 24 kDa; soybean trypsin inhibitor, 20 kDa; bovine milk α -lactalbumin, 14.2 kDa).

Lanes 2-5: G13Q (~1.5 mg/ml) at 0 h, 2 h, 4 h, 6 h respectively after incubation.

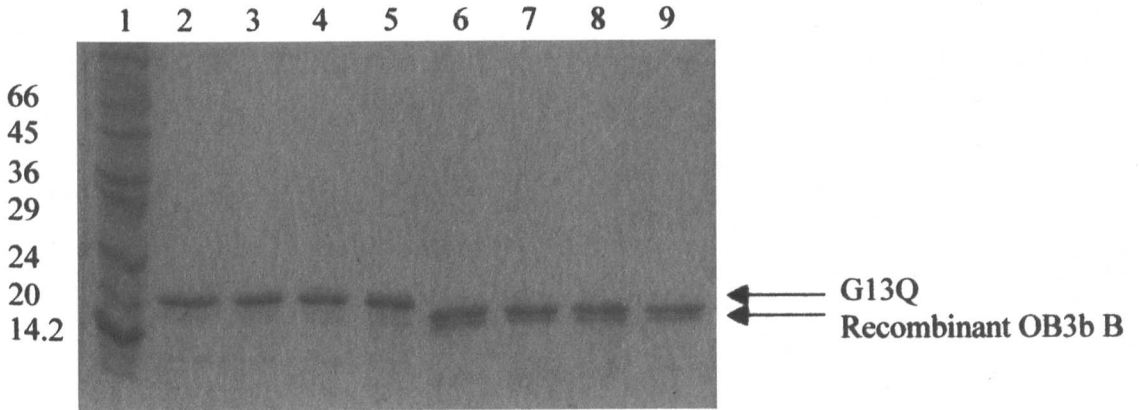
Lanes 6-9: recombinant *Ms. trichosporium* OB3b protein B (~1.5 mg/ml) at 0 h, 2 h, 4 h, 6 h respectively after incubation.

Each lane contained ~ 5 μ g protein.

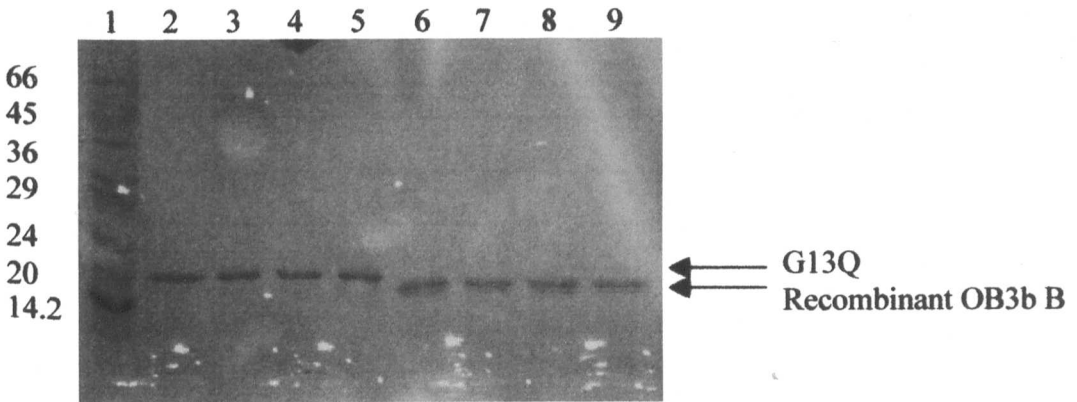
(i)



(ii)



(iii)



SDS-PAGE analysis indicated that temperature does not affect the cleavage rate of G13Q or recombinant *Ms. trichosporium* OB3b protein B, as the level of truncation remained approximately the same over time in each case (Figure 5.1).

Similarly, SDS-PAGE was used to monitor the effect of concentration on the stability of proteins G13Q, recombinant *Ms. trichosporium* OB3b protein B, and WTB over time at 6 mg/ml and 0.25 mg/ml for 24 hours at 20 °C (Figure 5.2).

Figure 5.2: SDS-PAGE analysis of (i) G13Q and recombinant *Ms. trichosporium* OB3b protein B and (ii) WTB after incubation at 6 mg/ml and 0.25 mg/ml for 24 h at 20 °C.

(i) Lane 1: Molecular weight markers (bovine albumin, 66 kDa; egg albumin, 45 kDa; glyceraldehyde-3-P-dehydrogenase, 36 kDa; bovine carbonic anhydrase, 29 kDa; bovine pancreas trypsinogen, 24 kDa; soybean trypsin inhibitor, 20 kDa; bovine milk α -lactalbumin, 14.2 kDa).

Lane 2: G13Q 6 mg/ml, 0 h incubation at 20 °C.

Lane 3: G13Q 6 mg/ml, 24 h incubation at 20 °C.

Lane 4: G13Q 0.25 mg/ml, 0 h incubation at 20 °C.

Lane 5: G13Q 0.25 mg/ml, 24 h incubation at 20 °C.

Lane 6: Recombinant *Ms. trichosporium* OB3b protein B 6 mg/ml, 0 h incubation at 20 °C.

Lane 7: Recombinant *Ms. trichosporium* OB3b protein B 6 mg/ml, 24 h incubation at 20 °C.

Lane 8: Recombinant *Ms. trichosporium* OB3b protein B 0.25 mg/ml 0 h incubation at 20 °C

Lane 9: Recombinant *Ms. trichosporium* OB3b protein B 0.25 mg/ml 24h incubation at 20°C

(ii) Lane 1: Molecular weight markers (bovine albumin, 66 kDa; egg albumin, 45 kDa; glyceraldehyde-3-P-dehydrogenase, 36 kDa; bovine carbonic anhydrase, 29 kDa; bovine pancreas trypsinogen, 24 kDa; soybean trypsin inhibitor, 20 kDa; bovine milk α -lactalbumin, 14.2 kDa).

Lane 2: WTB 6 mg/ml, 0 h incubation at 20 °C.

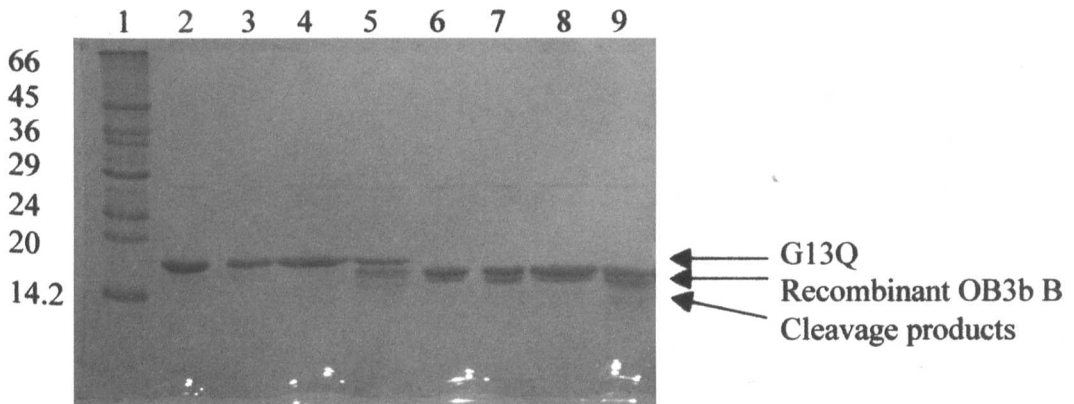
Lane 3: WTB 6 mg/ml, 24 h incubation at 20 °C.

Lane 4: WTB 0.25 mg/ml, 0 h incubation at 20 °C.

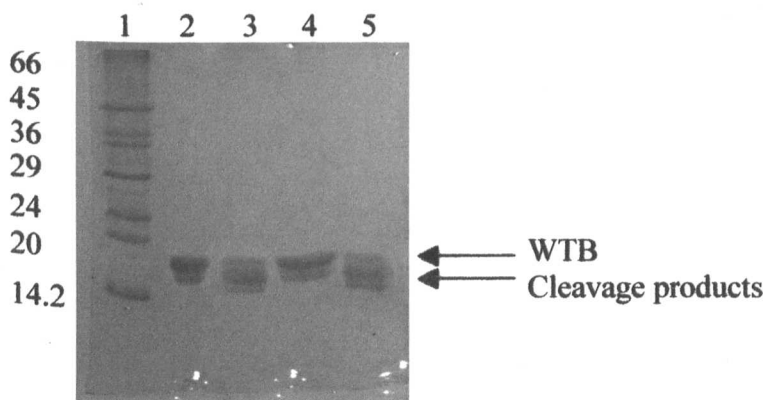
Lane 5: WTB 0.25 mg/ml, 24 h incubation at 20 °C.

Each lane contained ~ 5 μ g protein.

(i)



(ii)



Analysis for the presence of truncation of the proteins indicated that G13Q was more stable to cleavage at higher concentrations. The single G13Q band on the gel (Figure 5.2 (i), Lane 3) indicated that intact protein was present in the 24 hours, 6 mg/ml sample, when compared with the same protein at higher dilution after 24 hours where many bands were visible (Figure 5.2 (i), Lane 5), indicating protein truncation to have occurred. Less of a difference in stability was observed for WTB and recombinant *Ms. trichosporium* OB3b protein B incubated for the same length of time at the 2 levels of concentration. For WTB and recombinant *Ms. trichosporium* OB3b protein B, about the same degree of truncation was identified as occurring in both samples (Figure 5.2 (ii) and Figure 5.2 (i), Lanes 6-9).

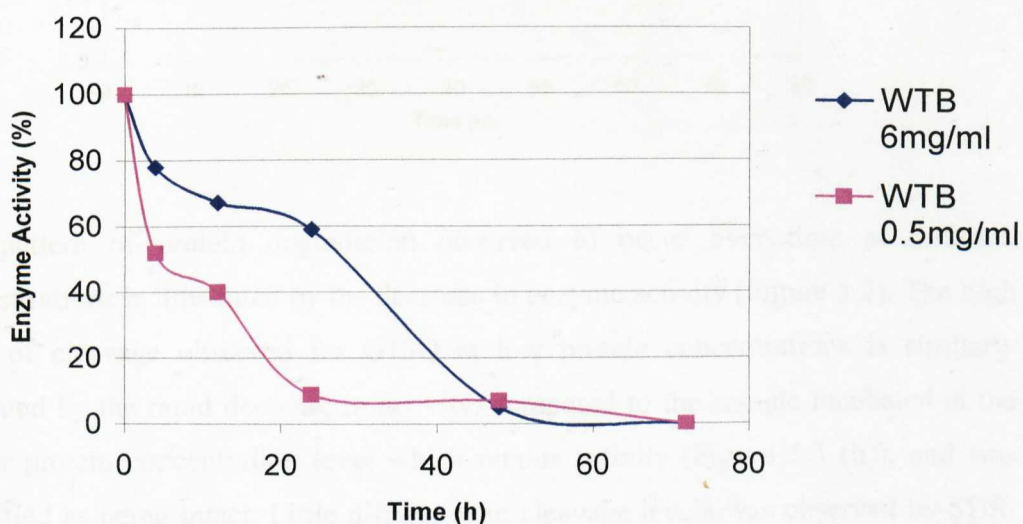
5.2.2 Analysis of protein B' formation by activity measurement

The truncation observed for the samples WTB and G13Q resulted in the production of their protein B' equivalents, amongst other truncates. As protein B' is inactive, its inactivity can be used to monitor the differences in the amount of protein B' formation in each of the samples at the different concentrations over time (Figure 5.3). However, it was unknown whether the cleavage of *Ms. trichosporium* OB3b protein B resulted in inactivity within the sMMO system. Analysis of this protein, using the same strategy as that for WTB and G13Q, was undertaken to elucidate this.

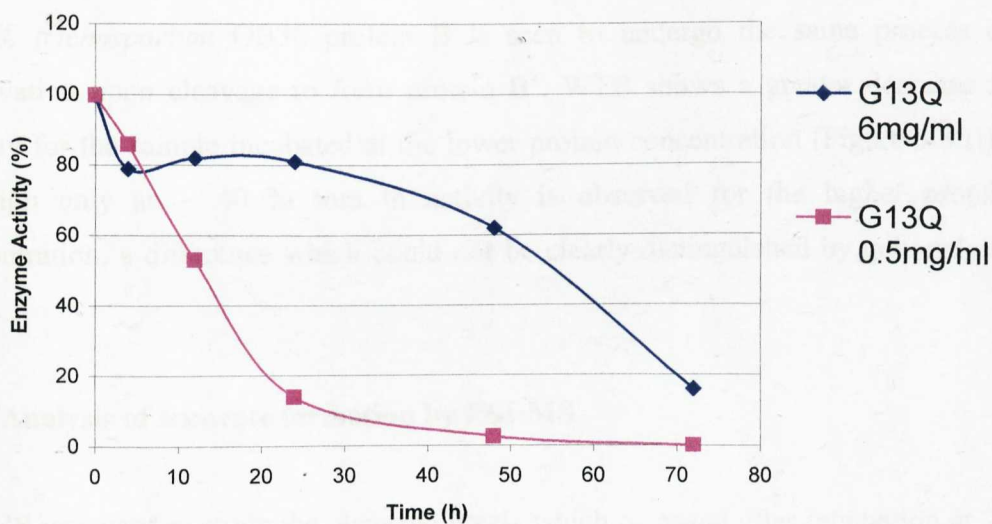
Figure 5.3: sMMO propylene oxidation assays of (i) WTB, (ii) G13Q and (iii) recombinant *Ms. trichosporium* OB3b protein B after incubation at 20 °C at concentrations of 0.5 mg/ml and 6 mg/ml.

sMMO propylene oxidation assays (Chapter 2, Section 2.12.1) were performed by adding 8 μM aliquots of hydroxylase and reductase to 8 μM of protein B. Enzyme activity is shown as a percentage of the activity remaining after incubation compared to the activity at 0 h. 100% activity represents; 1956 nmol/min/mg G13Q, 1896 nmol/min/mg WTB and 1267 nmol/min/mg recombinant *Ms. trichosporium* OB3b protein B. The activities presented are the mean of 3-4 separate experiments. Standard error was $\sim 10\%$.

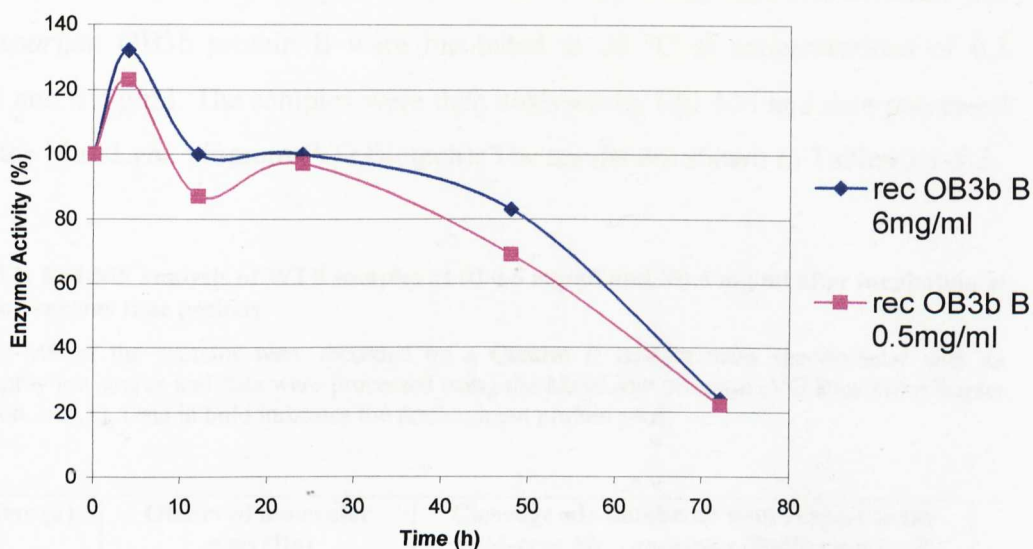
(i)



(ii)



(iii)



The pattern of protein degradation observed to occur over time at different concentrations is illustrated by the decrease in enzyme activity (Figure 5.3). The high level of cleavage observed for G13Q at low protein concentrations is similarly indicated by the rapid decrease in activity, compared to the sample incubated at the higher protein concentration level which retains activity (Figure 5.3 (ii)), and was identified as being intact. Little difference in cleavage levels was observed by SDS-PAGE for the two samples of recombinant *Ms. trichosporium* OB3b protein B and correspondingly, there is no real difference in the decrease in activity over time for them (Figure 5.3 (iii)). Nevertheless, the loss of activity is correlated with truncation, so *Ms. trichosporium* OB3b protein B is seen to undergo the same process of inactivation upon cleavage to form protein B'. WTB shows a greater decrease in activity for the sample incubated at the lower protein concentration (Figure 5.3 (i)), although only an ~ 40 % loss in activity is observed for the higher protein concentration, a difference which could not be clearly distinguished by gel analysis alone.

5.2.3 Analysis of truncate formation by ESI-MS

ESI-MS was used to study the cleavage levels which occurred after incubation at 20 °C at the different concentrations of 6 mg/ml and 0.5 mg/ml. This technique enabled the assignment of the number and type of cleavage products within the different

samples of each protein. Samples of proteins WTB, G13Q and recombinant *Ms. trichosporium* OB3b protein B were incubated at 20 °C at concentrations of 0.5 mg/ml and 6 mg/ml. The samples were then analysed by ESI-MS and data processed using the MassLynx program (VG Biotech). The results are shown in Tables 5.1-5.3.

Table 5.1: ESI-MS analysis of WTB samples at (i) 0.5 mg/ml and (ii) 6 mg/ml after incubation at 20 °C for various time periods.

The ESI-MS of the proteins were recorded on a Quattro II tandem mass spectrometer with an electrospray ion source and data were processed using the MassLynx program (VG Biotech) (Chapter 2, Section 2.16.1). Data in bold indicates the predominant protein peak.

(i)

Time (h)	Observed molecular mass (Da)	Cleavage site numbered with respect to the wild-type <i>Mc. capsulatus</i> (Bath) protein B sequence
0	16230.0	Intact
24	16230.0 14752.0 14630.0 13740.0 13620.0 13570.0	Intact S ¹ -V ² and D ¹³² -R ¹³³ M¹²-G¹³ A ²⁰ -D ²¹ and H ¹³⁹ -A ¹⁴⁰ G ¹¹⁹ -N ¹²⁰ Q ²² -F ²³

(ii)

Time (h)	Observed molecular mass (Da)	Cleavage site numbered with respect to the wild-type <i>Mc. capsulatus</i> (Bath) protein B sequence
0	16230.0	Intact
24	16230.0 14630.0	Intact M¹²-G¹³
36	16230.0 14630.0 13620.0	Intact M¹²-G¹³ G ¹¹⁹ -N ¹²⁰
48	14630.0 13740.0 13620.0	M¹²-G¹³ A ²⁰ -D ²¹ and H ¹³⁹ -A ¹⁴⁰ G ¹¹⁹ -N ¹²⁰

Table 5.2: ESI-MS analysis of G13Q samples at (i) 0.5 mg/ml and (ii) 6 mg/ml after incubation at 20°C for various time periods.

The ESI-MS of the proteins were recorded on a Quattro II tandem mass spectrometer with an electrospray ion source and data were processed using the MassLynx program (VG Biotech) (Chapter 2, Section 2.16.1). Data in bold indicates the predominant protein peak.

(i)

Time (h)	Observed molecular mass (Da)	Cleavage site numbered with respect to the wild-type <i>Mc. capsulatus</i> (Bath) protein B sequence
0	16300.0	Intact
24	16300.0 14273.6 13420.5 13261.0	Intact G¹⁶-K¹⁷ F ²³ -F ²⁴ G ¹¹⁹ -N ¹²⁰

(ii)

Time (h)	Observed molecular mass (Da)	Cleavage site numbered with respect to the wild-type <i>Mc. capsulatus</i> (Bath) protein B sequence
0	16300.0	Intact
24	16300.0	Intact
48	16300.0 14700.0	Intact M ¹² -Q ¹³
72	16300.0 14700.0	Intact M ¹² -Q ¹³

Table 5.3: ESI-MS analysis of recombinant *Ms. trichosporium* OB3b protein B samples at (i) 0.5 mg/ml and (ii) 6 mg/ml after incubation at 20 °C for various time periods.

The ESI-MS of the proteins were recorded on a Quattro II tandem mass spectrometer with an electrospray ion source and data were processed using the MassLynx program (VG Biotech) (Chapter 2, Section 2.16.1). Data in bold indicates the predominant protein peak.

(i)

Time (h)	Observed molecular mass (Da)	Cleavage site numbered with respect to the wild-type <i>Ms. trichosporium</i> OB3b protein B sequence
0	15026.8	Intact
24	15027.0 13280.0 11590.0	Intact K ¹⁴ -T ¹⁵ Q ²⁹ -V ³⁰

(ii)

Time (h)	Observed molecular mass (Da)	Cleavage site numbered with respect to the wild-type <i>Ms. trichosporium</i> OB3b protein B sequence
0	15026.8	Intact
24	15028.6 13280.0	Intact K ¹⁴ -T ¹⁵
48	15028.6 13280.0	Intact K ¹⁴ -T ¹⁵
72	15029.0 13280.0	Intact K ¹⁴ -T ¹⁵

For both WTB and G13Q at 0.5 mg/ml (Figures 5.1 (i) and 5.2 (i)) many cleavages were identified by ESI-MS, correlating with the decrease in activity observed for the same protein in the sMMO assay. Also correlating with the assay results were the data for the concentrated samples of WTB and G13Q (Figures 5.1 (ii) and 5.2 (ii)) for which fewer cleavages were seen, and the dominant protein present in each case was the intact protein. However, for low protein concentrations of recombinant *Ms. trichosporium* OB3b protein B, an extra cleavage product was observed (Figure 5.3 (i)) equivalent to the B'' cleavage site observed in wild-type *Mc. capsulatus* (Bath) protein B (Bhambra, 1996), and the cleavage site identified in *Methylocystis* sp. Strain M (Shinohara *et al.*, 1998). However, the amounts of the cleavages present in

the recombinant *Ms. trichosporium* OB3b protein B sample were very low, correlating with the similar activity observed at time 0 hours and 24 hours for both samples. For the WTB and G13Q protein samples at the higher protein concentration, after 24 hours incubation, the main cleavages occurring were N-terminal in nature, whereas for the low protein concentration samples, N- and C-terminal cleavages were observed. This indicates that cleavage at the higher protein concentration was more N-terminally orientated than that at lower concentration. This observation was in agreement with the identification that at higher protein concentrations the protein was more stable and presumably less unfolded than at low dilutions, where upon increased exposure to the solvent environment appears to promote degradation at the C-terminus.

5.3 Effect of additives on the stability of protein B

Salts can exert effects on proteins that are dependent on both the concentration and nature of the salt. NaCl and MgCl₂ can reduce the solubility of hydrophobic groups on the protein molecule by increasing the ionic strength of the solution. These salts can also enhance water clusters around the protein, resulting in a loss in the total free energy of the system, as the entropy of water decreases. These two effects together can stabilise proteins by causing the process of the 'salting-out' of hydrophobic residues leading to the molecule becoming more compact (Creighton, 1989). In the case of protein B this may reduce the flexibility of the N-terminal region of the protein, so limiting the cleavage reaction.

Glycerol has long been known to be capable of stabilising enzymes in solution (Gekko and Timasheff, 1981). The molecule has a high content of hydroxyl groups and is, therefore, capable of forming multiple hydrogen bonds and can act like water. Thus glycerol can cause 'preferential hydration', a thermodynamic phenomenon (Schachmann and Lauffer, 1949) which causes a microscopic phase separation between the protein and the solvent, resulting in a stabilising effect.

Enzymes have been known to be inactivated by reaction with heavy metals, such as mercury and lead. However, in this case the transition metal, copper, was considered

as possibly exerting an effect on protein B, as it is vitally important in *Mc. capsulatus* (Bath) and *Ms. trichosporium* OB3b cells in determining whether sMMO or pMMO is expressed (Stanley *et al.*, 1993). Therefore, in an attempt to re-create the cellular environment with the intention of enhancing the stability of protein B, studies into whether copper would have a stabilising effect on protein B were conducted.

To monitor the effect of different reagents on the truncation of protein B, SDS-PAGE was used. The single mutant of protein B, G13Q, was studied as this protein has already been shown to be more stable than wild type protein B (Lloyd *et al.*, 1997; Chapter 3) and, therefore, it was considered useful to investigate the possibility of enhancing its stability further. Also, since the G13Q protein behaves the same as the wild-type protein B, as far as cleavage is concerned, any conclusions drawn about this mutant would apply to the wild-type protein. Thus, samples of G13Q (~ 1 mg/ml) were incubated with either 10 mM NaCl, 10 mM MgCl₂, 15 % glycerol or 80 μM CuSO₄ for 24 hours and samples taken at time 0 and 24 hours were compared (Figure 5.4). The control samples contained no reagent.

Figure 5.4: SDS-PAGE of G13Q incubated for 24 h in different test solutions.

Lane 1: Molecular weight markers (bovine albumin, 66 kDa; egg albumin, 45 kDa; glyceraldehyde-3-P-dehydrogenase, 36 kDa; bovine carbonic anhydrase, 29 kDa; bovine pancreas trypsinogen, 24 kDa; soybean trypsin inhibitor, 20 kDa; bovine milk α-lactalbumin, 14.2 kDa).

Lane 2: G13Q 1 mg/ml, 0 h incubation at 20 °C.

Lane 3: G13Q 1 mg/ml, 24 h incubation at 20 °C.

Lane 4: G13Q 1 mg/ml, 0 h incubation at 20 °C with NaCl (10 mM).

Lane 5: G13Q 1 mg/ml, 24 h incubation at 20 °C with NaCl (10 mM).

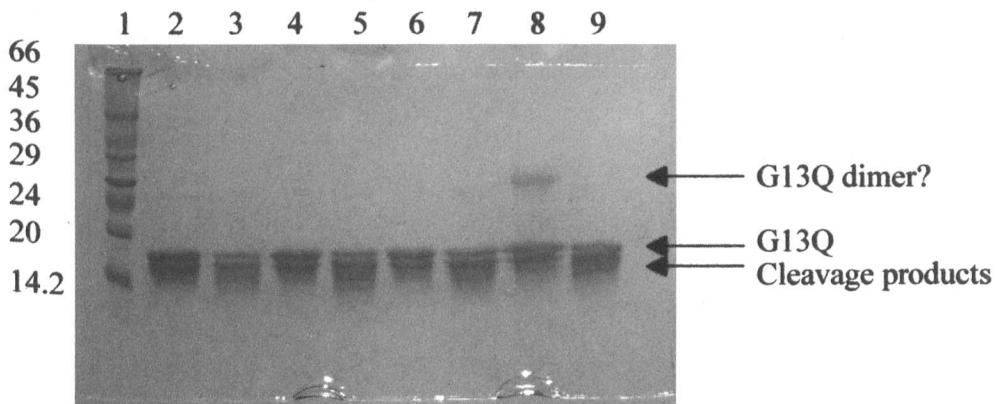
Lane 6: G13Q 1 mg/ml, 0 h incubation at 20 °C with MgCl₂ (10 mM).

Lane 7: G13Q 1 mg/ml, 24 h incubation at 20 °C with MgCl₂ (10 mM).

Lane 8: G13Q 1 mg/ml, 24 h incubation at 20 °C with CuSO₄ solution (80 μM).

Lane 9: G13Q 1 mg/ml, 24 h incubation at 20 °C with glycerol (15 %).

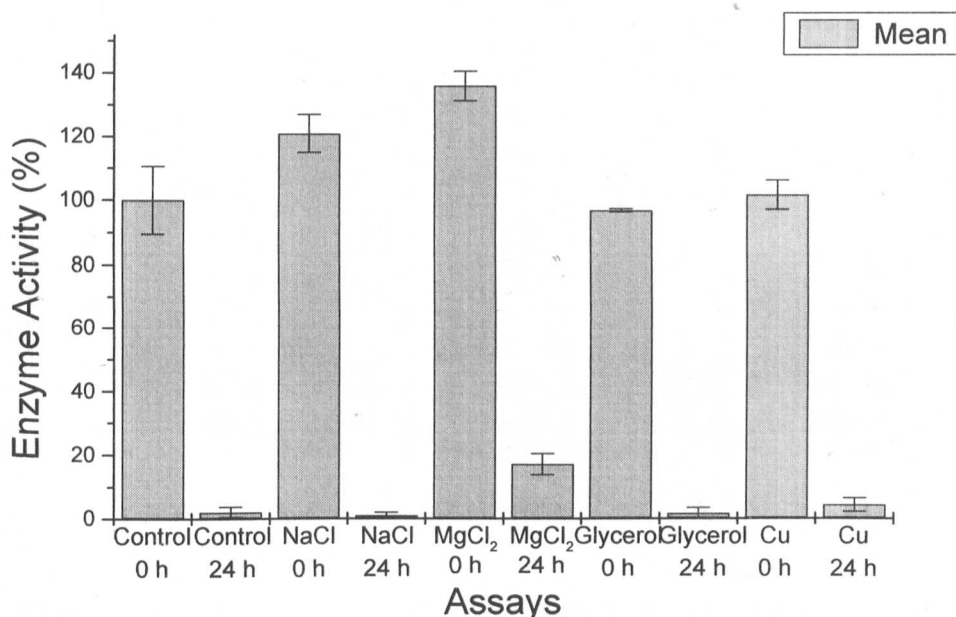
Each lane contained ~ 5 μg protein.



In all cases cleavage to form the truncates of G13Q occurred. On closer examination it appeared that possibly slightly more intact G13Q was retained when the protein was incubated with $MgCl_2$ (Figure 5.4, Lane 6) compared to the control samples and other test solutions. However, the use of visual inspection was too subjective to be a reliable measure of stabilisation. Therefore, sMMO activity was used to elucidate which solutions stabilised G13Q against truncation. Propylene oxidation assays were carried out for 1 mg/ml protein samples in the test solutions containing either 10 mM NaCl, 10 mM $MgCl_2$, 80 μM $CuSO_4$ or 15 % glycerol after 0 and 24 hours incubation at 20 °C (Figure 5.5).

Figure 5.5: sMMO propylene oxidation assays of G13Q after incubation in different test solutions for 0 h and 24 h at 20 °C.

sMMO propylene oxidation assays (Chapter 2, Section 2.12.2) were performed by adding 8 μM amounts of hydroxylase and reductase to 8 μM of protein G13Q contained within the different test solutions. Enzyme activity is shown as a percentage of the activity remaining after incubation compared to the activity at 0 h for G13Q with no additives. 100 % activity represents; 1956 nmol/min/mg G13Q. The activities presented are the mean of 3-4 separate experiments. Standard error bars are shown.

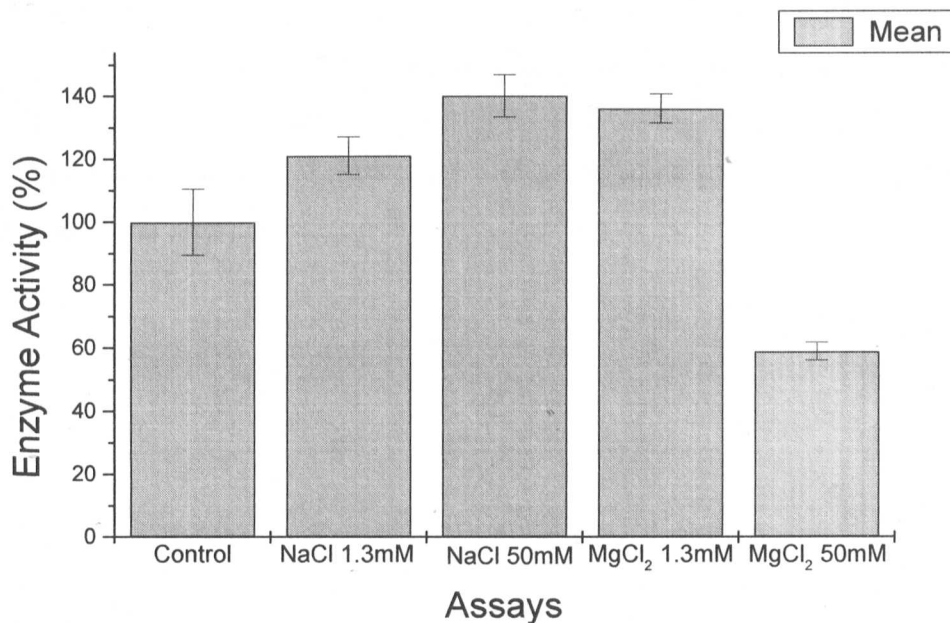


The sMMO assays (Figure 5.5) indicated that $MgCl_2$ had a stabilising effect on G13Q as it retained ~ 15 % more activity than the other solutions tested and the

control sample, which were all virtually inactive after the 24 hour incubation period. Also the assays indicated that the activity of the sMMO complex itself could be improved by the addition of NaCl and MgCl₂ to the system at a concentration of 1.3 mM (equivalent to the addition of 8 μM G13Q from 1 mg/ml in 10 mM salt), as seen by the improved activities for the time 0 hour incubations for these two test solutions. Further assays were, therefore, conducted to determine whether activity could be improved by the addition of higher concentrations of the two salts to the sMMO assay system. Propylene oxidation assays were conducted in the presence of various concentrations of NaCl and MgCl₂ (Figure 5.6).

Figure 5.6: sMMO propylene oxidation assays conducted in the presence of NaCl and MgCl₂ at various concentrations.

sMMO propylene oxidation assays (Chapter 2, Section 2.12.12) were performed by adding 8 μM amounts of hydroxylase and reductase to 8 μM of protein G13Q and various concentrations of salts. Enzyme activity is shown as a percentage of the activity compared to the activity for G13Q containing no additives. 100 % activity represents; 1956 nmol/min/mg G13Q. The activities presented are the mean of 3-4 separate experiments. Standard error bars are shown.



The assays indicated that NaCl and MgCl₂ added at certain levels increased the activity of the sMMO complex (Figure 5.6) and so suggest that the salts were improving the interactions of the components and thus enhancing activity.

5.3.1 Effect of metals on protein B

It was noted, from SDS-PAGE analysis (Figure 5.4), that incubating G13Q in the presence of copper had the effect of causing the formation of a protein band at 30 kDa. It was proposed that this could correspond to dimer formation, although it was unusual that the dimer should not have been broken into its constituent monomers when boiled in the presence of reducing agents and denaturants (β -mercaptoethanol and SDS). It was proposed that copper-induced dimer formation may provide a means of stabilising protein B, as reduced truncate formation was identified for the samples incubated in copper, compared to the copper-free control sample (Figure 5.4). Although incubation for 24 hours with copper resulted in the proteins inactivation within the sMMO assay, it was important to elucidate the effect copper was having on G13Q to prevent truncate formation and cause dimerisation. Therefore, studies proceeded to determine the effect of copper on G13Q as well as WTB and protein B', and to compare it to the effect observed of other metals on the proteins. Thus, the effect of copper, cadmium, magnesium and zinc on G13Q, WTB and protein B' were tested by native-PAGE analysis. Protein (0.12 mg/ml) was incubated with solutions of each of the metals (20 μ M - 80 μ M copper and 20 μ M of the other metal salts) at 20 °C for ~ 4 hours (Figure 5.7).

Figure 5.7: Native-PAGE analysis of (i) G13Q, (ii) WTB and (iii) protein B' in the presence of different metals

(i) Lane 1: Molecular weight markers (jack bean urease, 272 kDa (trimer) and 545 kDa (hexamer); bovine albumin, 66 kDa (monomer) and 132 kDa (dimer); egg albumin, 45 kDa; bovine carbonic anhydrase, 29 kDa; bovine milk α -lactalbumin, 14.2 kDa).

Lane 2: G13Q.

Lane 3: G13Q + 20 μ M Cu.

Lane 4: G13Q + 25 μ M Cu.

Lane 5: G13Q + 30 μ M Cu.

Lane 6: G13Q + 40 μ M Cu.

Lane 7: G13Q + 80 μ M Cu.

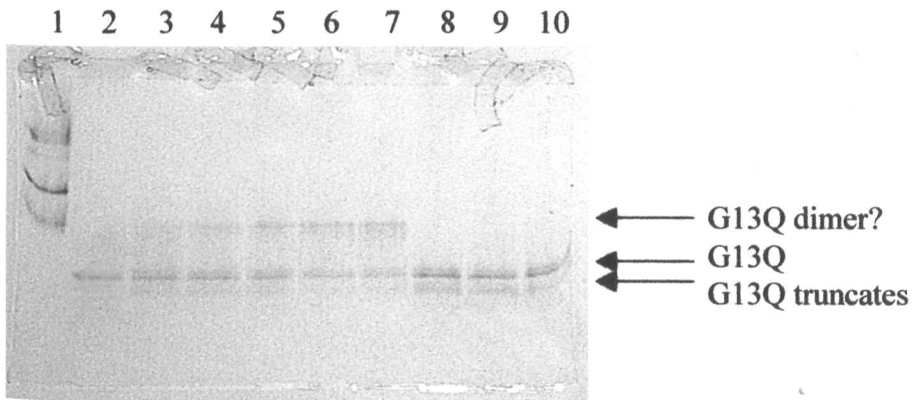
Lane 8: G13Q + 20 μ M Cd.

Lane 9: G13Q + 20 μ M Zn.

Lane 10: G13Q + 20 μ M Mg.

Each lane contained $\sim 5 \mu$ g protein.

(i)



(ii-iii) Lane 1: Molecular weight markers (jack bean urease, 272 kDa (trimer) and 545 kDa (hexamer); bovine albumin, 66 kDa (monomer) and 132 kDa (dimer); egg albumin, 45 kDa; bovine carbonic anhydrase, 29 kDa; bovine milk α -lactalbumin, 14.2 kDa).

Lane 2: WTB/B'

Lane 3: WTB/B' + 20 μ M Cu

Lane 4: WTB/B' + 25 μ M Cu

Lane 5: WTB/B' + 40 μ M Cu

Lane 6: WTB/B' + 80 μ M Cu

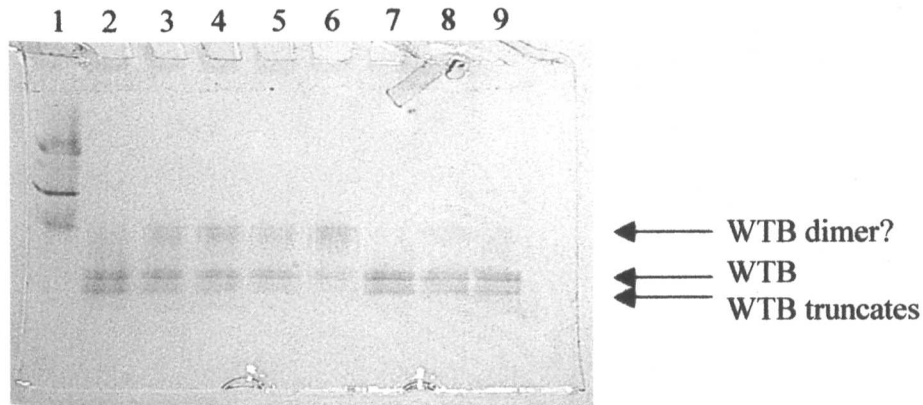
Lane 7: WTB/B' + 20 μ M Cd

Lane 8: WTB/B' + 20 μ M Zn

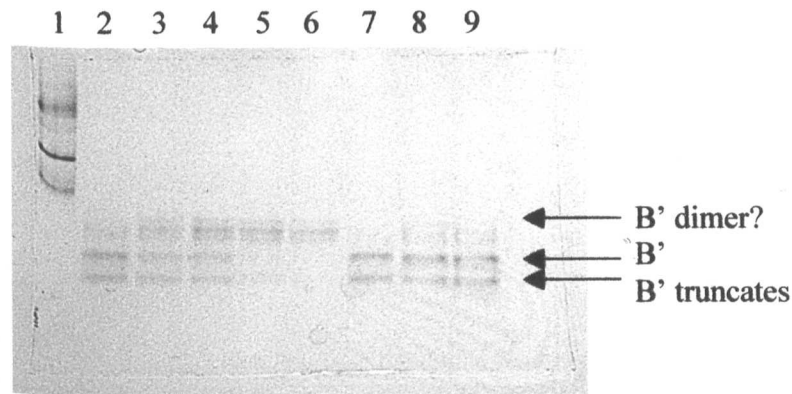
Lane 9: WTB/B' + 20 μ M Mg

Each lane contained \sim 5 μ g protein.

(ii)



(iii)



Native-PAGE analysis demonstrated that copper had an effect on the proteins unlike that of any of the other metals tested (Figure 5.7). The proteins incubated in solutions of increasing copper concentrations were observed to run differently, and could indicate dimer formation. Alternatively, it could be a charge effect causing the proteins to run at a value indicative of a higher molecular weight than the values expected. Also with increased copper concentration a reduction in truncate formation

was identified. This was observed by the reduction in or the lack of bands on the gels corresponding to truncates for the protein samples incubated with copper, compared to the control samples and samples incubated with cadmium, zinc and magnesium. In an attempt to further understand the 'copper effect' it was important to determine whether the proteins were capable of binding copper.

5.3.2 Does protein B bind copper?

Although initial analysis of the protein sequence did not reveal any obvious copper-binding site, in the absence of any structural data for the protein at the time of this work, the coordination of copper binding residues was unknown and so the possibility could not automatically be ruled out. After all, for some reason the presumptive dimers were formed and lack of truncation observed for protein B in the presence of copper, and there must be a reason to explain the sudden change in the character of the protein. G13Q was used for further analysis to determine if copper bound, as the protein had been shown to be more stable than WTB (Lloyd *et al.*, 1997).

5.3.2.1 Copper affinity column studies

The approach was taken to determine whether G13Q would bind to copper by using a HiTrap® affinity column (Amersham Pharmacia Biotech, Bucks., UK). The chelating sepharose media within the column was charged with copper. Therefore, the column would retain selectively only proteins that exposed complex forming amino acids, such as histidine, on their surface.

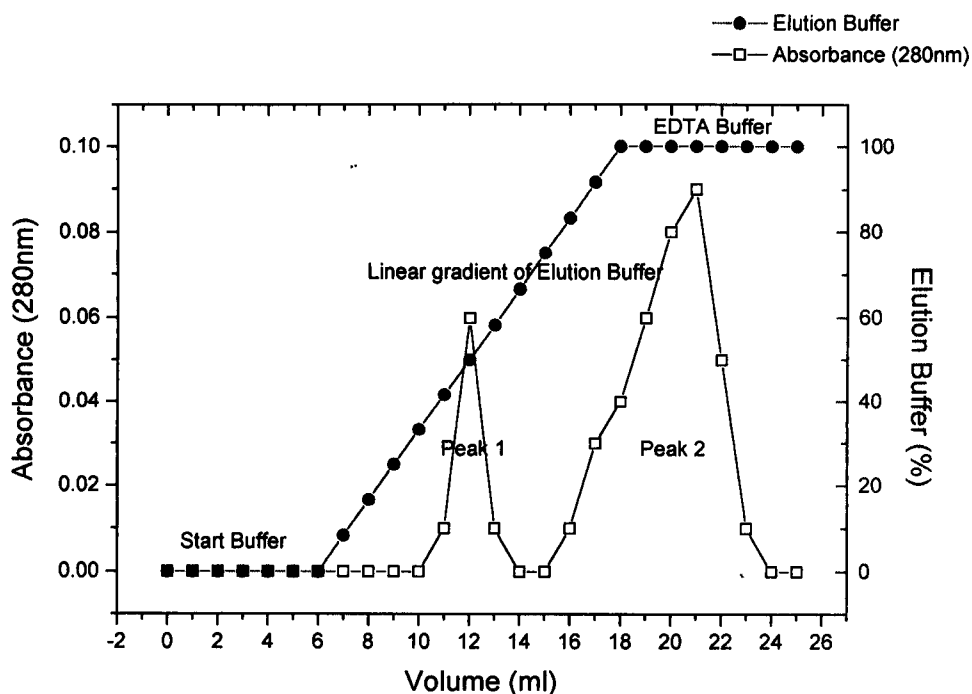
A salt gradient of ammonium chloride was used to elute the bound protein from the column. Thus, a linear gradient of the salt was used to determine the strength of binding of the protein to the column. The addition of the metal chelating agent, EDTA, to the column removed the bound copper for column regeneration.

G13Q in start buffer containing 0.02 M Na₂HPO₄, 1M NaCl, pH 7.2 was loaded onto the copper charged HiTrap® column and washed with 1 column volume of the same buffer. A linear gradient from 0-100 % elution buffer containing 0.02 M Na₂HPO₄, 1

M NH₄Cl, pH 7.2 was applied over 3 column volumes. Copper elution from the column was achieved by washing the column with 1-2 column volumes of 0.02 M Na₂HPO₄, 1 M NaCl, 0.05M EDTA, pH 7.2 (Chapter 2, Section 2.7). The elution profile is illustrated in Figure 5.8.

Figure 5.8: Elution profile of G13Q run on a HiTrap® copper affinity column.

The protein elution profile (□) is displayed together with the corresponding elution buffer gradient (●).



The elution profile (Figure 5.8) indicates that G13Q bound efficiently to the affinity column. A small amount of the protein eluted at ~ 50 % ammonium chloride elution buffer (peak 1), but the rest of the protein remained bound to the column and was only eluted when the copper itself was stripped from the column using the EDTA wash buffer (peak 2). SDS and native-PAGE analysis of the fractions indicated both peaks contained protein G13Q (Figure 5.9). It is important to note that copper absorbed at 280 nm also and so contributed towards the absorbance of the second peak.

Figure 5.9: (i) SDS and (ii) Native-PAGE analysis of copper affinity column elution fractions

Lane 1: Molecular weight markers (SDS: bovine albumin, 66 kDa; egg albumin, 45 kDa; glyceraldehyde-3-P-dehydrogenase, 36 kDa; bovine carbonic anhydrase, 29 kDa; bovine pancreas trypsinogen, 24 kDa; soybean trypsin inhibitor, 20 kDa; bovine milk α -lactalbumin, 14.2 kDa. Native: jack bean urease, 272 kDa (trimer) and 545 kDa (hexamer); bovine albumin, 66 kDa (monomer) and 132 kDa (dimer); egg albumin, 45 kDa; bovine carbonic anhydrase, 29 kDa; bovine milk α -lactalbumin, 14.2 kDa).

Lane 2: G13Q sample used for analysis.

Lane 3: G13Q after buffer exchange into start buffer.

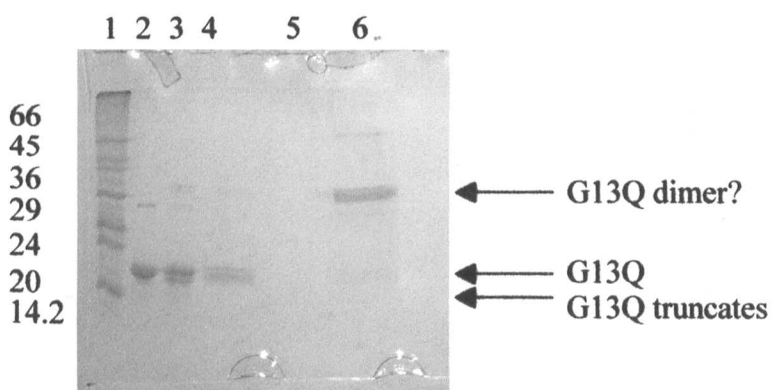
Lane 4: G13Q First elution peak 1 in 50 % elution buffer.

Lane 5: G13Q Blank track.

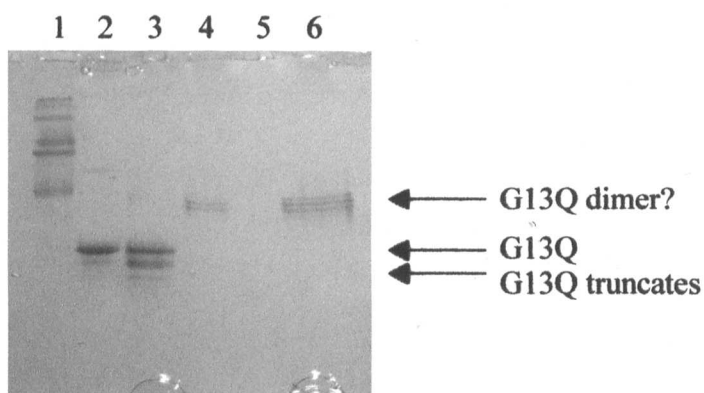
Lane 6: G13Q Second elution peak 2 in EDTA buffer solution.

Each lane contained ~ 5 μ g protein.

(i)



(ii)



The G13Q protein, which eluted with the copper stripped from the column during the EDTA wash, remained as a dimer after SDS and native-PAGE analysis (Figure 5.9 (i) and (ii), Lane 6). The fraction eluted from the column by ~ 50 % ammonium chloride elution buffer (peak 1), and thus presumably more weakly bound to the column, was only observed as a dimer by native-PAGE analysis, and was visualised

as the constituent monomers by SDS-PAGE analysis (Figure 5.9 (i) and (ii), Lane 4). These data suggest that some of the copper could have remained bound to protein B causing dimerisation in the case of the EDTA eluted fractions, thus retaining dimer structure when analysed under denaturing conditions by gel electrophoresis.

It was considered that protein B' may behave differently to G13Q with regard to copper binding, and that copper binding may be different between the two proteins, possibly implicating a reason for the existence of protein B'. However, analysis of protein B' by the same method of copper affinity chromatography on the HiTrap® column gave the same results as those obtained for G13Q. This supported the notion that the two proteins were indeed very similar, as they reacted in the same way when treated with copper.

5.3.2.2 Fluorescence quenching studies

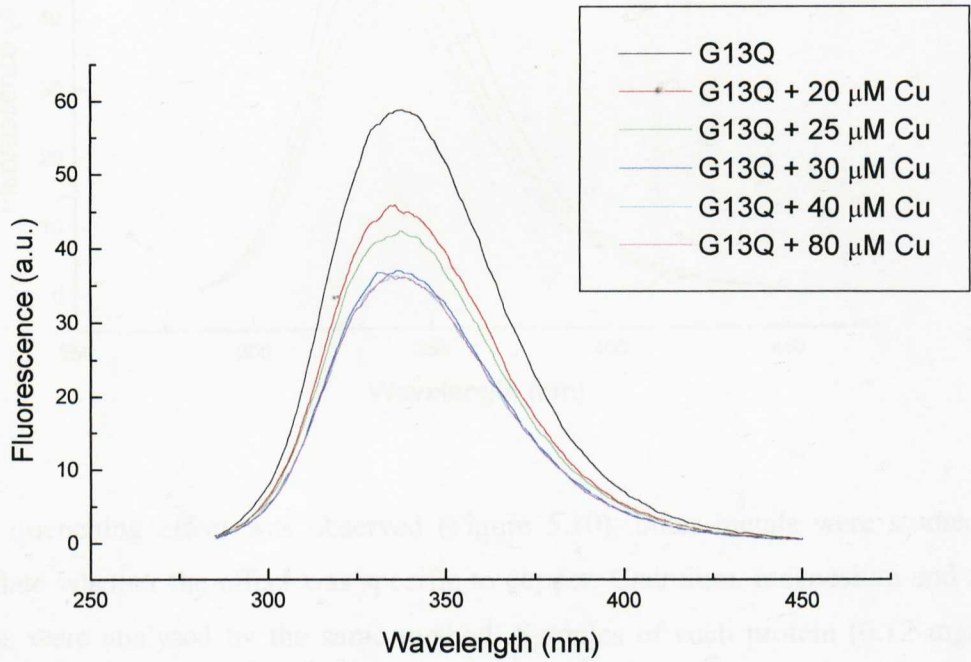
Fluorescence spectroscopy provides a sensitive means of characterising protein conformation. The polarity of the environment of the tryptophan and tyrosine residues of a protein and their specific interactions chiefly determines the nature of the fluorescence spectrum obtained. The change in fluorescence intensity by the addition of certain reagents provides a means to measure the accessibility of these amino acids in the protein structure.

Fluorescence quenching provides a method of probing the accessibility of tryptophan residues to small molecules. This technique was used to analyse the effect of copper on proteins G13Q, WTB and protein B'. Samples of each protein (0.12 mg/ml) were incubated with increasing concentrations of copper between 20 - 80 μ M. Fluorescence data for each were recorded (Figure 5.10).

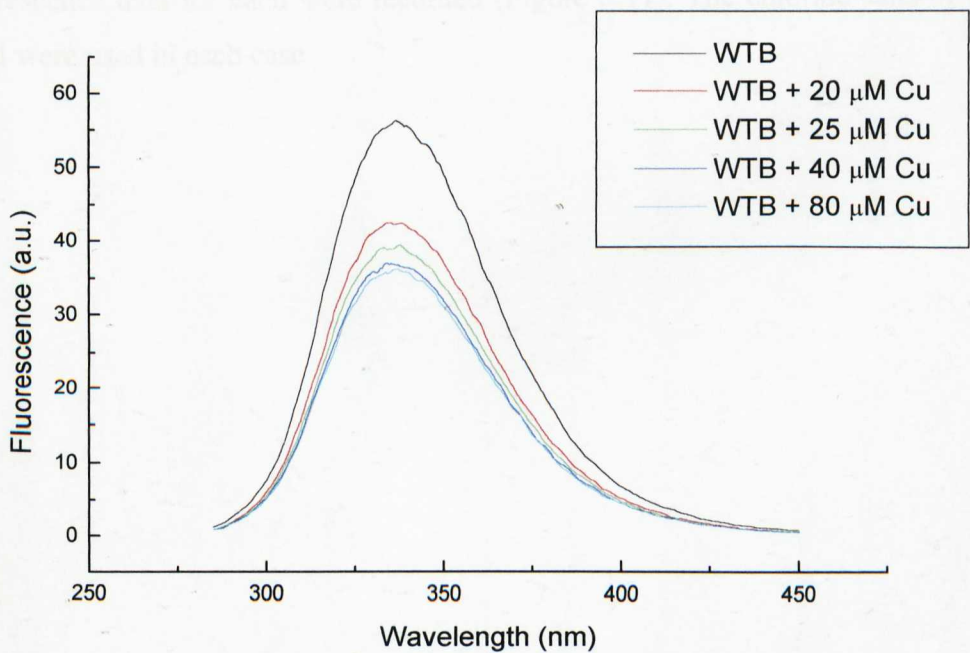
Figure 5.10: The effect of copper on the fluorescence spectra of (i) G13Q, (ii) WTB and (iii) protein B'.

Protein (0.12 mg/ml) was incubated with copper at various concentrations for ~10min at 20 °C. The solutions were placed in a 3ml quartz cuvette with a 10 mM pathlength for fluorescence analysis. The emission spectra were recorded at room temperature with excitation at 280nm on a Perkin-Elmer LS-50 fluorimeter (Chapter 2, Section 2.17).

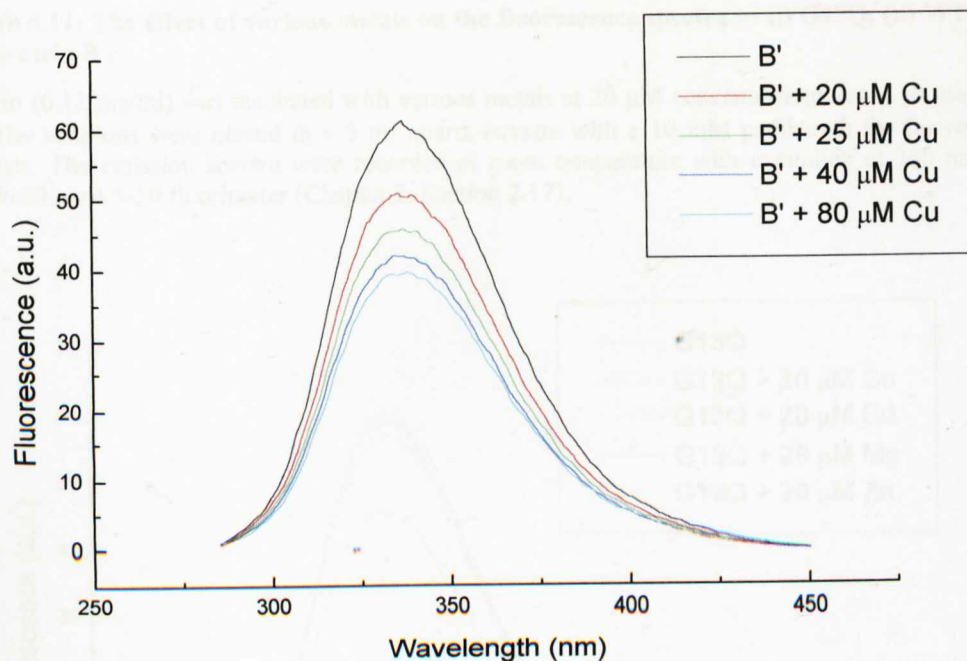
(i)



(ii)



(iii)

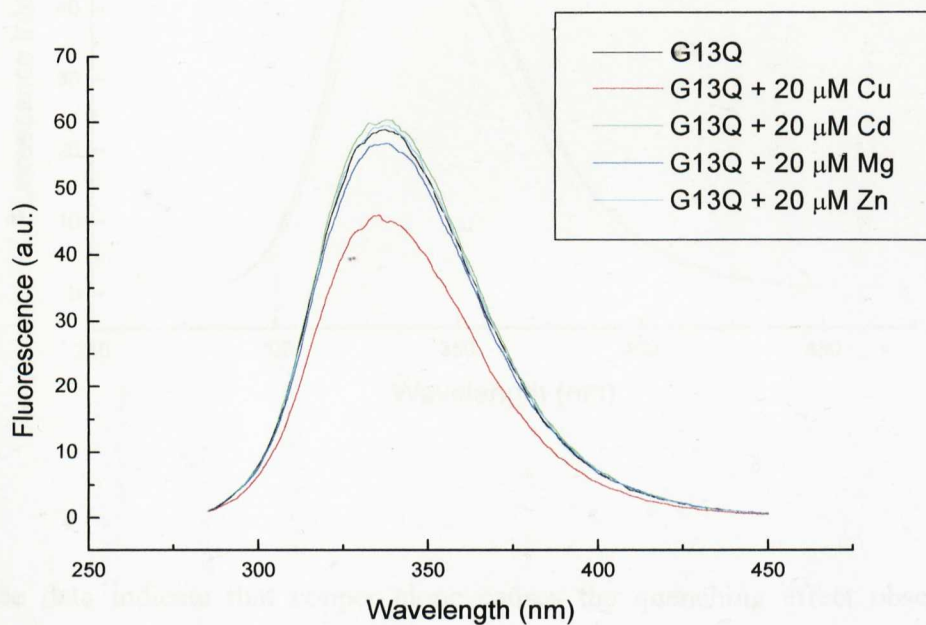


As a quenching effect was observed (Figure 5.10), other metals were studied to elucidate whether the effect was specific to copper. Cadmium, magnesium and zinc metals were analysed by the same method. Samples of each protein (0.12 mg/ml) were incubated with 20 μM concentrations of cadmium, magnesium and zinc. Fluorescence data for each were recorded (Figure 5.11). The chloride salts of each metal were used in each case.

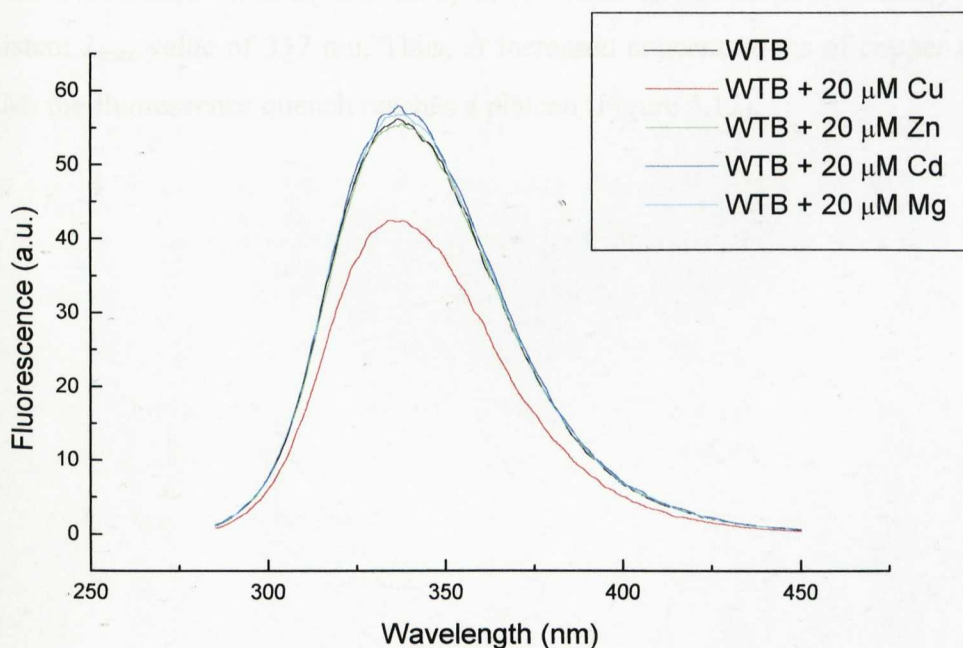
Figure 5.11: The effect of various metals on the fluorescence spectra of (i) G13Q, (ii) WTB and (iii) protein B'.

Protein (0.12 mg/ml) was incubated with various metals at 20 μM concentrations for ~ 10 min at 20 $^{\circ}\text{C}$. The solutions were placed in a 3 ml quartz cuvette with a 10 mM pathlength for fluorescence analysis. The emission spectra were recorded at room temperature with excitation at 280 nm on a Perkin-Elmer LS-50 fluorimeter (Chapter 2, Section 2.17).

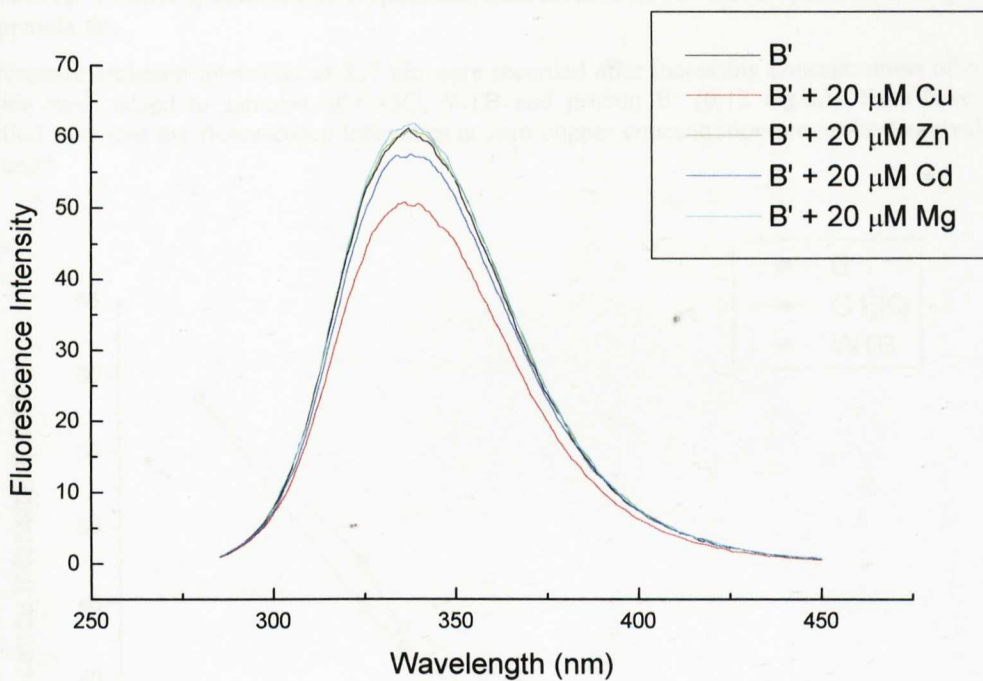
(i)



(ii)



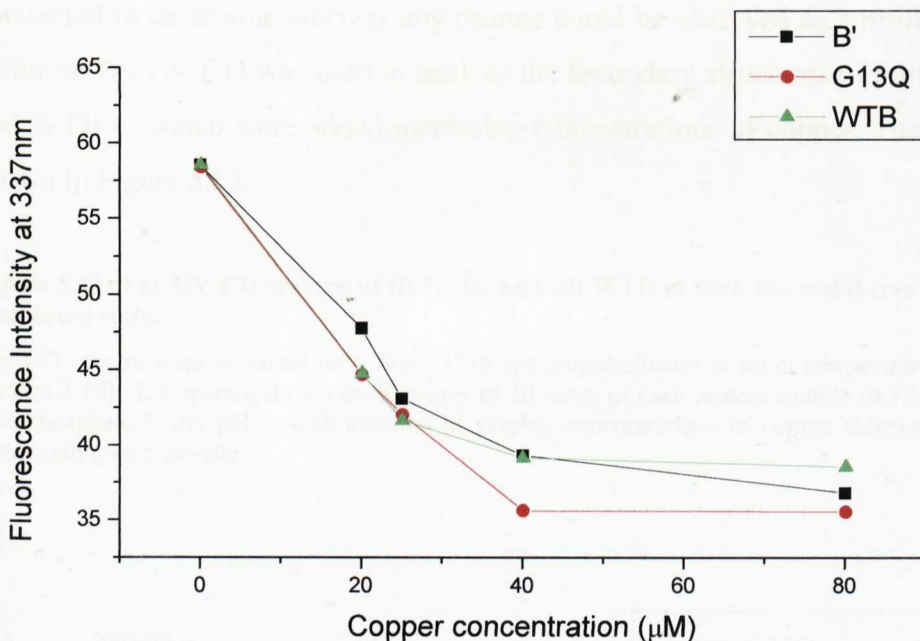
(iii)



These data indicate that copper alone causes the quenching effect observed for proteins G13Q, WTB and protein B' (Figure 5.11). Also the copper quenching effect appears to be saturable, as monitored by the decrease in fluorescence intensity at the consistent λ_{\max} value of 337 nm. Thus, at increased concentrations of copper above 40 μM , the fluorescence quench reaches a plateau (Figure 5.12).

Figure 5.12: Copper quenching of tryptophan fluorescence at 337nm for proteins G13Q, WTB and protein B'.

Fluorescence emission intensities at 337 nm were recorded after increasing concentrations of copper chloride were added to samples of G13Q, WTB and protein B' (0.12 mg/ml). Data have been modified such that the fluorescence intensities at zero copper concentration are at the same value in each case.



Overall, copper was shown to bind to G13Q, WTB and protein B' and there was seen to be little difference in the ability of each of the proteins tested to bind to the copper. The quenching effect observed indicates that the binding of copper either causes a conformational change or that tryptophan residues are very near to the copper-binding site. There is no apparent change in the λ_{\max} values upon copper quenching. This shows that water has not been excluded upon complex formation between the protein and copper, as any decrease in polarity would be observed as causing a shift to shorter wavelengths.

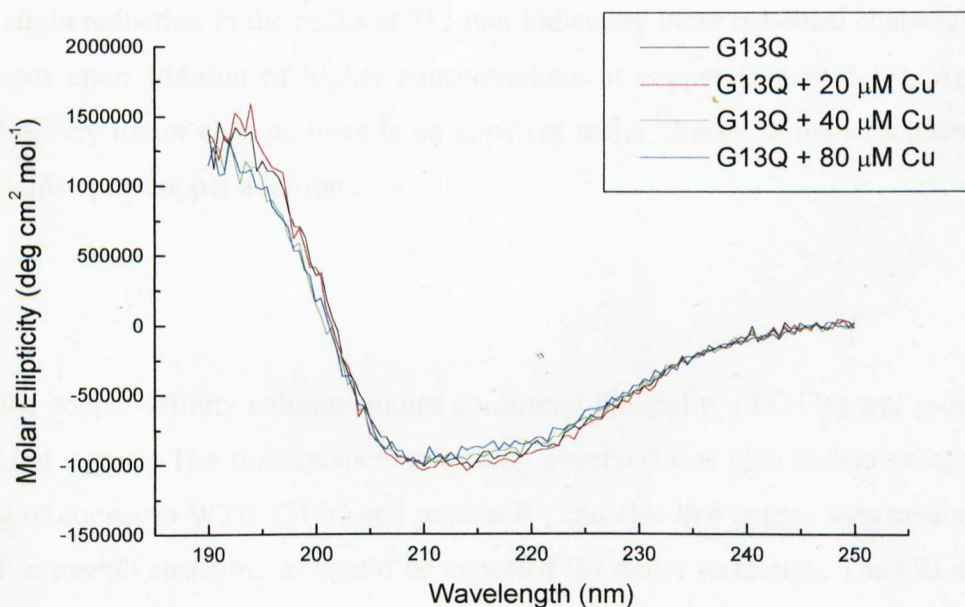
5.3.2.3 Is the secondary structure of protein B affected by copper binding?

Since quenching of fluorescence had been observed upon addition of copper to G13Q, WTB and protein B', it was possible that there may be a conformational change taking place upon the binding of copper. Secondary structural analysis was conducted to determine whether any change could be observed as a result of copper addition. Far UV CD was used to analyse the secondary structures of proteins G13Q and WTB to which were added increasing concentrations of copper. The results are shown in Figure 5.13.

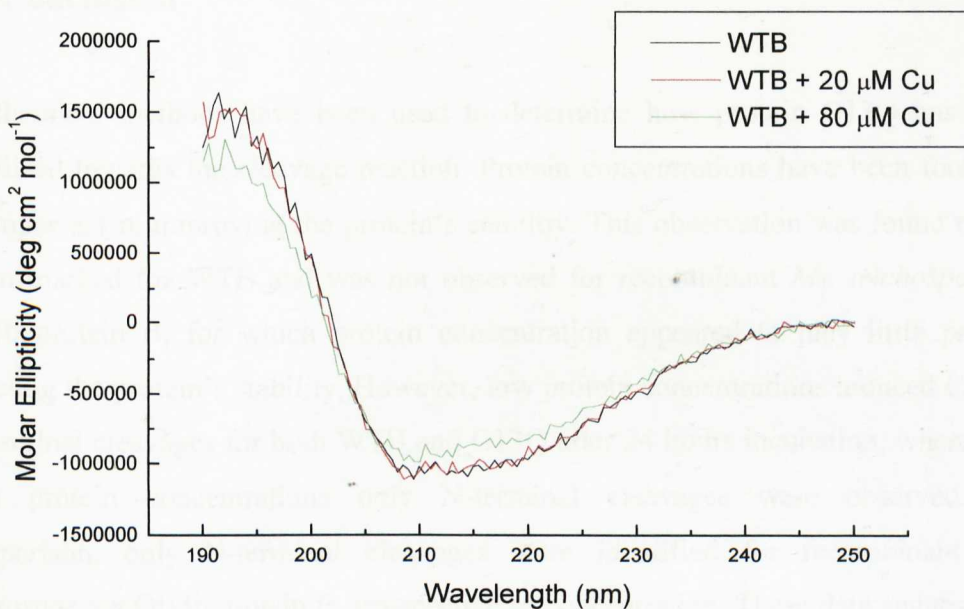
Figure 5.13: Far UV CD spectra of (i) G13Q and (ii) WTB in both the metal-free and copper-complexed state.

The CD spectra were recorded on a Jasco J715 spectropolarimeter at room temperature (Chapter 2, Section 2.18). The spectra shown are averages of 10 scans of each protein sample (0.12 mg/ml) in 50 mM phosphate buffer pH 7, with addition of varying concentrations of copper chloride, in a 1 mm pathlength quartz cuvette.

(i)



(ii)



The spectra for G13Q and WTB suggest a very slight loss of β character, as observed by the slight reduction in the peaks at 215 nm, indicating more α -helical character to be present upon addition of higher concentrations of copper (Figure 5.13). Apart from this very minor change, there is no apparent major change in the structures of the proteins upon copper addition.

Thus, the copper-affinity column studies confirmed the ability of G13Q and protein B' to bind copper. The fluorescence quenching observed was also indicative of the binding of copper to WTB, G13Q and protein B', and also that copper was causing a change in overall structure, as would be expected for dimer formation. The CD data suggested only a slight change in secondary structure to occur upon copper binding. Therefore, the constituent monomers of the copper induced dimers must not be significantly changed in secondary structure terms by the dimerisation event. Reduced truncate formation was also identified for increased copper levels, as the dimers of WTB, G13Q and protein B' were formed, suggesting that in some way the dimer form stabilised the proteins against N-terminal cleavage.

5.4 Conclusion

Biochemical methods have been used to determine how protein G13Q has been stabilised towards the cleavage reaction. Protein concentrations have been found to be important in improving the protein's stability. This observation was found not to be so marked for WTB and was not observed for recombinant *Ms. trichosporium* OB3b protein B, for which protein concentration appeared to play little part in affecting the protein's stability. However, low protein concentrations induced C- and N-terminal cleavages for both WTB and G13Q after 24 hours incubation, whereas at high protein concentrations only N-terminal cleavages were observed. By comparison, only N-terminal cleavages were identified for recombinant *Ms. trichosporium* OB3b protein B, irrespective of concentration. These data suggest that protein concentration is affecting the proteins in different ways indicating that the structures of each are slightly different, which makes them respond in slightly different ways to the environmental effects experienced.

The addition of $MgCl_2$ has also been shown to stabilise G13Q by maintaining the activity of the protein at low concentration after extended incubation time. This result further supports the proposal that the protein *per se*, may be involved in autocatalytic cleavage (Chapter 4). The Mg^{2+} ion is large with a positive charge and so would be attracted to the protein's nucleophilic residue(s), thus preventing or reducing the cleavage reaction. The additions of salts (NaCl or $MgCl_2$) to the sMMO assay were shown to significantly increase the activity observed. This suggests that the presence of salts in the assay mix could have improved the component interactions thus leading to greater levels of activity. This result is in agreement with the recent findings of Brandstetter *et al.* (1999), where it was identified that hydroxylase binding to protein B was increased with the increasing ionic strength of the solution, and suggests that the sMMO component interactions are dominated by hydrophobic contacts.

Although unable to provide a stabilising effect, copper was clearly shown to bind to G13Q, WTB and protein B' and resulted in dimer formation. Also, it was evident that the copper did not destabilise the protein, as it did not cause a rapid truncation effect upon its addition to the proteins. No major secondary structural change accompanied copper binding, so it is possible that the quenching of fluorescence, observed for the proteins upon addition of copper, was due to copper binding close to tryptophan residues, or to the induction of a tertiary structural change in the protein, possibly one of dimer formation. Copper inactivated protein B within the sMMO system. Furthermore, copper has already been shown to effect the sMMO assay system by inhibition of the reductase (Green *et al.*, 1985). In the present case, copper was identified as a progressive inhibitor showing its effect only after 24 hours incubation. Therefore, it was concluded that the copper level, being ~ 12.5 % of the concentration used in the Green *et al.* (1985) studies, was insufficient to bring about reductase inhibition within the sMMO assay. In this study copper inactivated protein B, possibly as a result of binding to the protein and causing it to form dimers. This could be of importance within the cell, when, upon the presence of increased copper levels resulting in pMMO expression, the inactivation of protein B by binding copper rapidly shuts down sMMO activity to prevent the wasteful oxidation of NADH. Recently the stimulatory protein DmpM of phenol hydroxylase, which shows strong sequence similarity to protein B, has been shown to exist in an active monomer form as well as an inactive dimer form (Cadieux and Poulowski, 1999). The inactive dimer form has been proposed to exist for the same reason of preventing unnecessary oxidation of NADH under certain conditions. In an attempt to monitor for dimer formation within sMMO-expressing *Mc. capsulatus* (Bath) cells undergoing the copper switch in response to increased copper levels, native-PAGE and Western blot analysis, probing with antibodies to *Mc. capsulatus* (Bath) protein B/B', were used. Unfortunately the studies failed to accurately determine whether an identifiable copper induced protein B dimer was present. These preliminary studies, nevertheless, provide a rational framework within which further studies can be planned and implemented.

Overall, these studies, although primarily attempting to stabilise protein B, have given insights into the structure and characteristics of the protein. Also, a strategy for improving the stability of G13Q has been developed involving the addition of MgCl₂

and maintaining the protein at high protein concentration levels. This is of vital importance for future studies using protein G13Q, in preference to WTB, as the protein has already been made more resistant to cleavage by the G¹³ to glutamine mutation. Thus, improving the stability of this protein further, by the modifications proposed here, provides a protein which is suitable for use in place of wild-type protein B for most experiments, particularly those which occur over extended time periods, such as crystallography. The fact the MgCl₂ not only stabilises protein G13Q but also improves the activity of the sMMO complex, possibly by improving component interactions, also provides a starting point for attempting to crystallise the whole sMMO complex.

It would also be of interest to determine if implementation of these modifications to the purification procedures of native, wild-type protein B would improve the yield of intact protein. Only then would it become clear whether or not the inactivation of the protein could be truly overcome by biochemical means.

Chapter 6

Effect of M12A:G13Q Double Mutation on the Stability and Structure of *Mc. capsulatus* (Bath) Protein B

6.1 Introduction

The *Mc. capsulatus* (Bath) single mutant of protein B, G13Q, degrades to form a truncate protein B' equivalent known as G13Q B'. The site of cleavage has been identified as Met¹²-Gln¹³, numbered with respect to the wild-type *Mc. capsulatus* (Bath) protein B sequence and equivalent to the cleavage site of the wild-type protein (Chapter 4). It was important, therefore, to try and prevent cleavage at this site by mutating the residues at the amino acid 12-13 position. This would also give further information on the effect of any changes in the structure of protein B, caused by the double mutation, with respect to its level of stability.

Alanine is a small, unreactive amino acid and for this reason was chosen to replace the Met¹² residue at the cleavage site. The glutamine residue at position 13 of the G13Q mutant protein B was retained, as this had already been shown to be beneficial in reducing the rate of protein B' formation (Lloyd *et al.*, 1997). The intention was to establish whether this double mutation could overcome protein B' formation. The work in this chapter details the production and characterisation of the M12A;G13Q protein B double mutant .

6.2 Construction of the double mutant M12A:G13Q of protein B from *Mc. capsulatus* (Bath)

To allow the direct comparison of the double mutant M12A:G13Q to the single mutant G13Q and recombinant wild-type protein B itself (WTB), the same system was used for its cloning and expression. G13Q and WTB were both available as GST-fusion proteins by expression of the vectors pGEX-G13Q and pGEX-WTB respectively (Lloyd *et al.*, 1997; Lloyd 1997). Thus, attempts were made to introduce

the M12A:G13Q mutation into pGEX-WTB using the Unique Site Elimination Kit (Amersham Pharmacia Biotech, Bucks., UK). Unfortunately this system failed to produce the mutations. Therefore, the strategy of introducing the mutations by PCR was adopted.

6.2.1 PCR amplification and construction of vectors

The vector used for the construction of the double mutant protein with a GST tag was pGEX-2T, which contains a 26 kDa GST gene (Sj26) of *Shistosoma japonicum* under the control of an IPTG inducible *tac* promoter (Amersham Pharmacia Biotech, Bucks., UK). Figure 6.1 details the construction of the GST-fused M12A:G13Q vector and Table 6.1 shows the primers used. The fragment of DNA, from PCR amplification, which encoded the M12A:G13Q protein B double mutant, was ligated into the pGEX vector and introduced into *E. coli* Inv α F' by transformation. Transformants were isolated and sequenced to reveal those which contained the double mutant clones. Once identified the pGEX-M12A:G13Q vector was transformed into protease deficient *E. coli* AD202 cells (Nakano *et al.*, 1994) for expression to be conducted.

Figure 6.1: Construction of *Mc. capsulatus* (Bath) protein B double mutant vector.

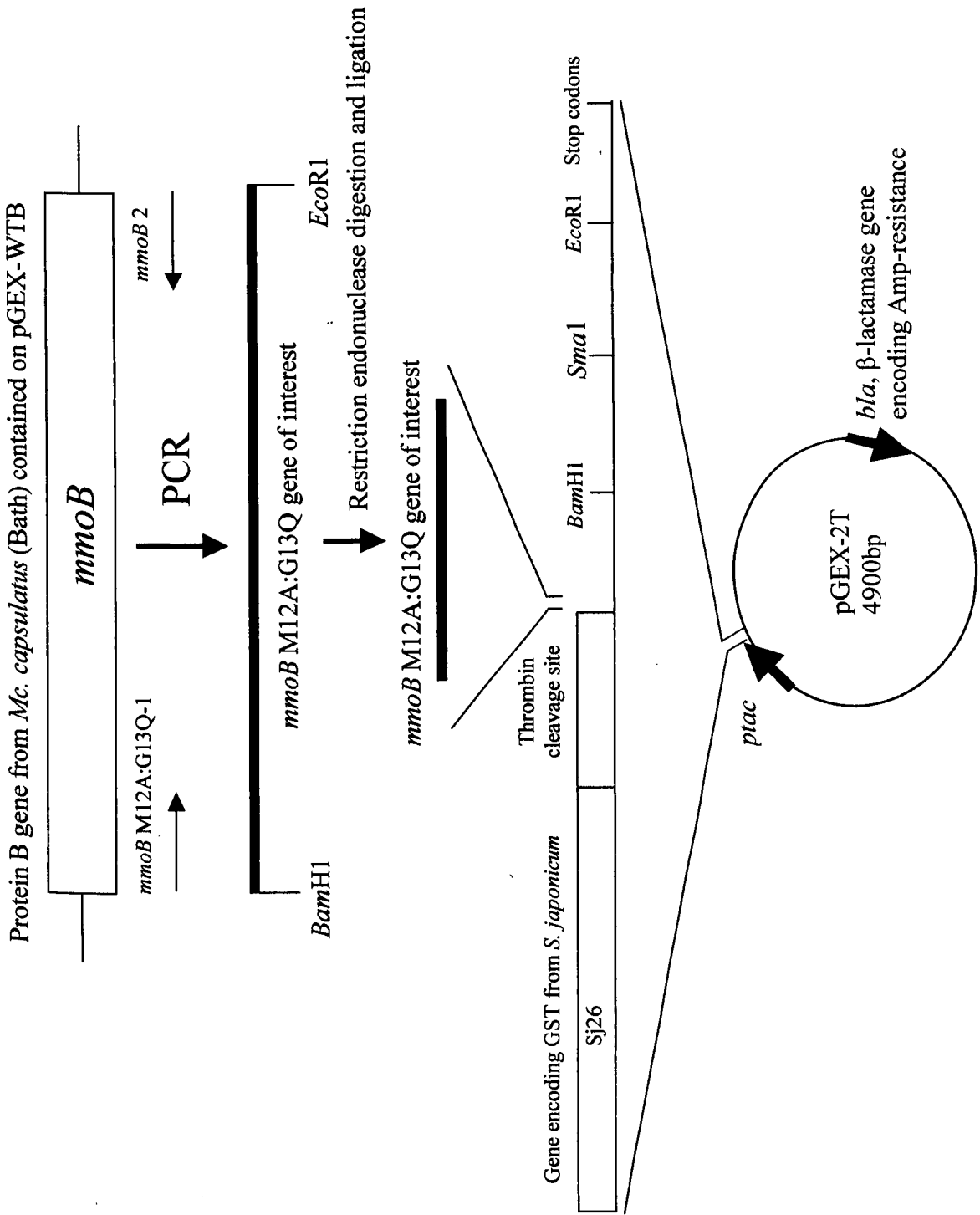


Table 6.1: PCR amplification of *mmoB* *Mc. capsulatus* (Bath) M12A:G13Q gene for the construction of the GST fusion protein.

Amplified gene	Primers used ¹	Restriction sites	Vector name
<i>mmoBM12A:G13Q</i>	<i>mmoBM12A:G13Q-1</i> : 5' CGC <u>GGA TCC ACG</u> ATG AGC GTA AAC AGC AAC GCA TAC GAC GCC GGC ATC GCG CAG CTG AAA GGC AAG 3'	<i>Bam</i> H1	pGEX-M12A:G13Q
	<i>mmoB-2</i> : 5' GGC <u>GAA TTC</u> TAA GCG TGA TAG TCT TCG AG 3'	<i>Eco</i> R1	

¹Restriction enzyme sites are underlined

Sites encoding the double mutation are in **bold**

Start codons are in *italics*

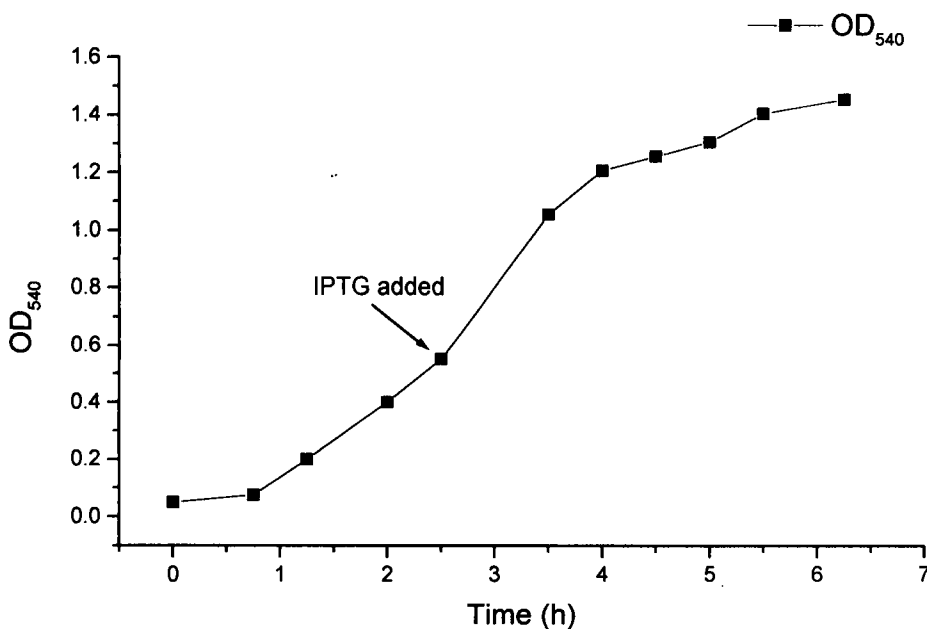
pGEX-2T inserts were DNA sequenced in two separate reactions using:

- 1) the pGEX 5' universal sequencing primer: 5' CCA TCC TCC AAA ATC GGA TCT GGT 3'
- 2) the pGEX 3' sequencing primer: 5' CCG GGA GCT GCA TGT GTC AGA GG 3'

6.2.2 Expression of pGEX-M12A:G13Q

Protein expression was achieved by induction of the transformed *E. coli* AD202 cells at an OD₅₄₀ of 0.5 by addition of 1mM IPTG at 37 °C (Figure 6.2).

Figure 6.2: Growth curve of *E. coli* AD202 expressing M12A:G13Q mutant protein B from *Mc. capsulatus* (Bath).

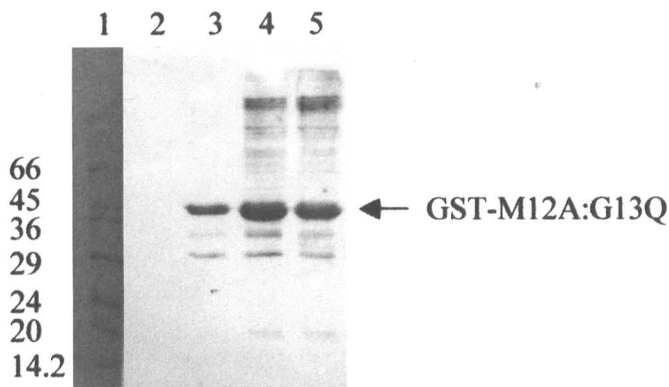


After addition of the IPTG, the cells continued to grow exponentially. Western blots of whole cell lysates, probing with anti-serum to *Mc. capsulatus* (Bath) protein B/B' were undertaken on samples at 0, 2, 4 and 6 hours after IPTG induction. Proteins with an approximate molecular mass of 42 kDa were identified which cross-reacted with the *Mc. capsulatus* (Bath) protein B/B' antibody, thus confirming that this protein probably represented GST-M12A:G13Q, consisting of the GST protein tag of ~ 26 kDa attached to the protein B double mutant of ~ 16 kDa, giving the observed molecular mass. Figure 6.3 indicates the accumulation of this protein.

Figure 6.3: Western blotting of whole cell lysates of *E. coli* AD202 transformed with pGEX-M12A:G13Q.

Lane 1: Molecular weight markers (bovine albumin, 66 kDa; egg albumin, 45 kDa; glyceraldehyde-3-P-dehydrogenase, 36 kDa; bovine carbonic anhydrase, 29 kDa; bovine pancreas trypsinogen, 24 kDa; soybean trypsin inhibitor, 20 kDa; bovine milk α -lactalbumin, 14.2 kDa).

Lanes 2-5: Whole cell lysates of *E. coli* AD202[pGEX-M12A:G13Q] 0 h, 2 h, 4 h and 6 h respectively after IPTG induction blotted with antisera to *Mc. capsulatus* (Bath) protein B/B'.



To determine whether GST-M12A:G13Q was expressed as a soluble protein, soluble extract was prepared and analysed by SDS-PAGE, which indicated over expression of the protein by a large band at ~ 42 kDa. Also, propylene oxidation assays were conducted (Chapter 2, Section 2.12.2) and confirmed that protein B activity was present in the soluble fraction upon reconstitution of the sMMO system by addition of $8 \mu\text{M}$ aliquots of hydroxylase and reductase. Thus, further optimisation of induction conditions was unnecessary, and the double mutant was identified as being active.

6.2.3 Purification of M12A:G13Q

The GST tag of the M12A:G13Q protein enabled rapid affinity purification to be possible. Purification was conducted using the procedure optimised for the purification of GST- *Ms. trichosporium* OB3b protein B, GST-WTB and GST-G13Q, as detailed in Chapter 3, Section 3.4 and Chapter 2, Section 2.4. Using this method, the M12A:G13Q protein was obtained at a purity of $\sim 95\%$. Figure 6.4 illustrates the final purification step of M12A:G13Q from *E. coli* AD202 [pGEX-M12A:G13Q].

Figure 6.4: SDS-PAGE of the purification of M12A:G13Q protein B from *E. coli* AD202 [pGEX-M12A:G13Q].

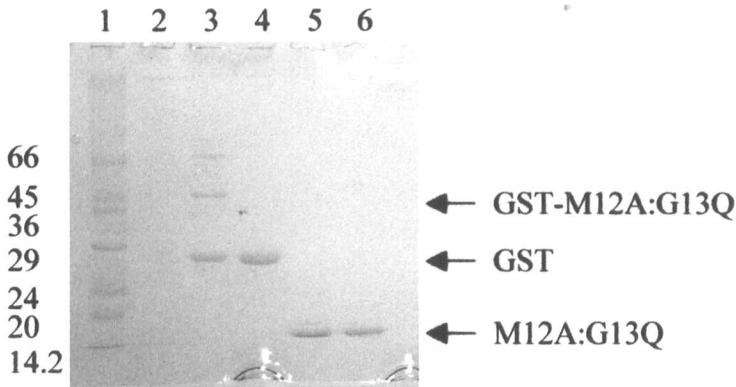
Lane 1: Molecular weight markers (bovine albumin, 66 kDa; egg albumin, 45 kDa; glyceraldehyde-3-P-dehydrogenase, 36 kDa; bovine carbonic anhydrase, 29 kDa; bovine pancreas trypsinogen, 24 kDa; soybean trypsin inhibitor, 20 kDa; bovine milk α -lactalbumin, 14.2 kDa).

Lane 2: Blank.

Lanes 3-5: Samples of peaks from S75 purification step.

Lane 6: Purified M12A:G13Q after concentration.

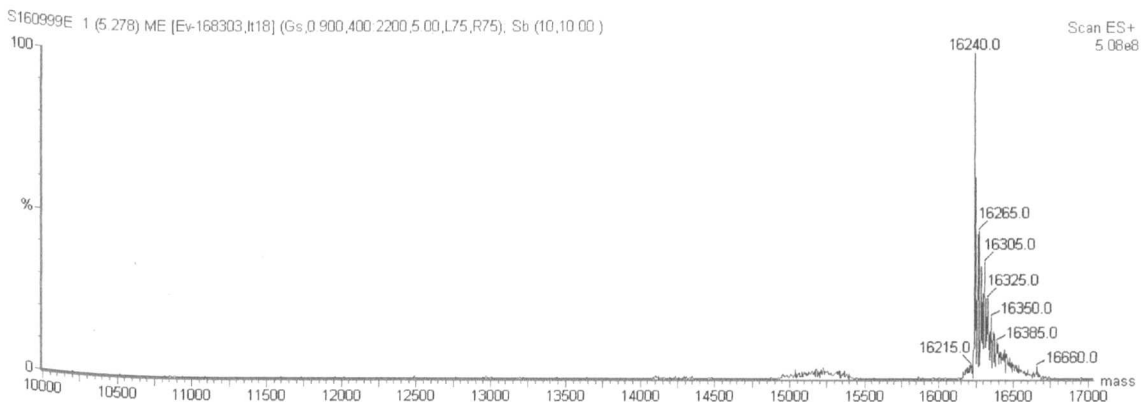
Each lane contained ~ 5 μ g protein



ESI-MS analysis confirmed the M12A:G13Q protein to be pure and the sequence to be correct, as a molecular mass of 16,240.0 Da was determined compared to the expected molecular mass of 16240.14 Da. The mass spectrometry data also indicated that no degradation had occurred during purification (Figure 6.5). These results indicated that the protein was of sufficient purity for further analysis to be undertaken.

Figure 6.5: ESI-MS of pure M12A:G13Q.

The ESI-MS of the sample was recorded on a Quattro II tandem mass-spectrometer with an electrospray ion source and the data was processed using the MassLynx program (VG Biotech) (Chapter 2, Section 2.16.1).



Work by Lloyd *et al.* (1997) had shown that the activity of the G13Q mutant was comparable to the activity of WTB. Therefore, propylene oxidation assays (Chapter 2, Section 2.12.2) were conducted and determined the activity of M12A:G13Q to be 1995 ± 215 nmol/min/mg, compared to the activity of G13Q which was 1956 ± 117 nmol/min/mg

The activity of M12A:G13Q was, therefore, comparable to that of the G13Q mutant. The mutation of M¹² to alanine had not affected the activity of protein B. The double mutant was also assayed for activity prior to the removal of the GST moiety. The GST-M12A:G13Q protein was also found to be active, which was in agreement with the work of Lloyd *et al.* (1997), which had indicated GST-WTB and GST-G13Q to also be active.

6.3 Characterisation of M12A:G13Q

Since the activity of the double mutant was identified as being comparable to that of G13Q, it was necessary to determine the effect of the specific mutations incorporated into protein B, on its stability, affinity for the hydroxylase and secondary structure.

6.3.1 Effect of mutation M12A:G13Q on the stability of protein B

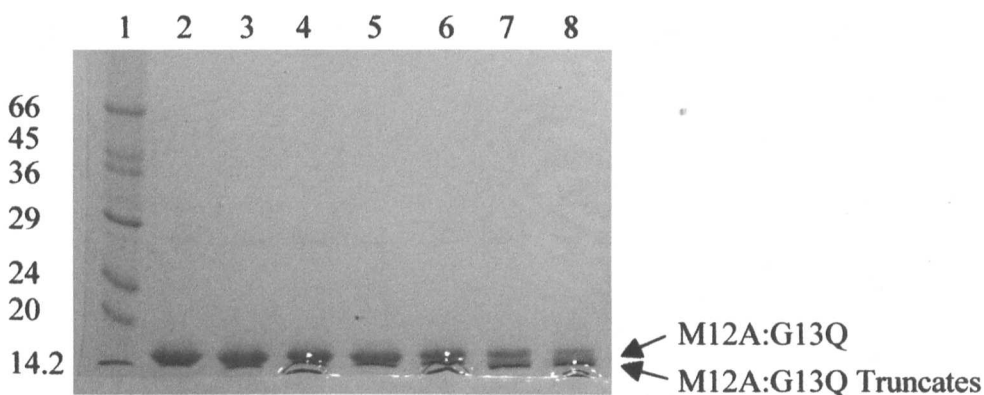
It was important to determine if the double mutation would prevent protein B truncation from occurring. SDS-PAGE analysis of samples of M12A:G13Q at 1 mg/ml, incubated at 20 °C for 0 - 48 hours identified that the double mutant protein underwent cleavage to form truncates (Figure 6.6).

Figure 6.6: SDS-PAGE of M12A:G13Q incubated at 20 °C for 48 h.

Lane 1: Molecular weight markers (bovine albumin, 66 kDa; egg albumin, 45 kDa; glyceraldehyde-3-P-dehydrogenase, 36 kDa; bovine carbonic anhydrase, 29 kDa; bovine pancreas trypsinogen, 24 kDa; soybean trypsin inhibitor, 20 kDa; bovine milk α -lactalbumin, 14.2 kDa).

Lanes 2-8: M12A:G13Q 0 h, 4 h, 8 h, 12 h, 24 h, 36 h, and 48 h respectively after incubation at 20 °C.

Each lane contained ~ 5 μ g protein



The stability of protein G13Q was shown to be affected by protein concentration, an effect which was not so prominent in the WTB sample (Chapter 5). Therefore, it was necessary to identify whether the double mutant would be similar to G13Q or WTB in its observed truncation at different concentrations. SDS-PAGE analysis was conducted on two samples of M12A:G13Q, one at 0.5 mg/ml and the other at 6 mg/ml after incubation at 20 °C for 0 and 24 hours. The results clearly indicated that in both samples truncation had occurred (Figure 6.7).

Protein B becomes inactivated by truncation to protein B' (Bhambra 1996). Therefore, inactivation within the sMMO assay was also monitored to determine the stability of the protein, as any decrease in activity could be attributed to protein B' formation. The stability of the protein following incubation at 20 °C was monitored. Also, as protein concentration was shown to have an effect on protein stability in the case of G13Q (Chapter 5), the stability of M12A:G13Q at two different concentrations, one high and one low, was studied to elucidate whether this protein was affected by concentration in a similar manner to that observed for G13Q. The activity assay method was therefore used to compare the stability of protein M12A:G13Q at the two different concentrations and to proteins WTB and G13Q under the same conditions (Figures 6.8 and 6.9).

Figure 6.7: SDS-PAGE of two samples of M12A:G13Q at different concentrations incubated at 20 °C for 24 h.

Lane 1: Molecular weight markers (bovine albumin, 66 kDa; egg albumin, 45 kDa; glyceraldehyde-3-P-dehydrogenase, 36 kDa; bovine carbonic anhydrase, 29 kDa; bovine pancreas trypsinogen, 24 kDa; soybean trypsin inhibitor, 20 kDa; bovine milk α -lactalbumin, 14.2 kDa).

Lanes 2 and 3: M12A:G13Q (6 mg/ml) at 0 h and 24 h respectively after incubation at 20 °C.

Lanes 4 and 5: M12A:G13Q (0.5 mg/ml) at 0h and 24h respectively after incubation at 20°C.

Each lane contained ~ 5 μ g protein

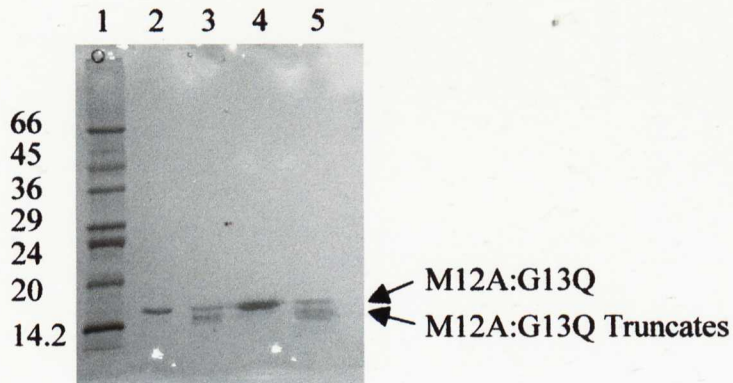


Figure 6.8: sMMO propylene oxide stability assays of M12A:G13Q at two different concentrations of 0.5 mg/ml and 6 mg/ml, incubated at 20 °C.

sMMO propylene oxidation assays (Chapter 2, Section 2.12.2) were performed by adding 8 μ M aliquots of hydroxylase and reductase to 8 μ M of the protein B double mutant M12A:G13Q. Enzyme activity is shown as a percentage of the activity remaining after incubation compared to the activity at 0 h. 100 % activity represents 2015 nmol/min/mg. The activities presented are the mean of 3-4 separate experiments. Standard error was ~10 %.

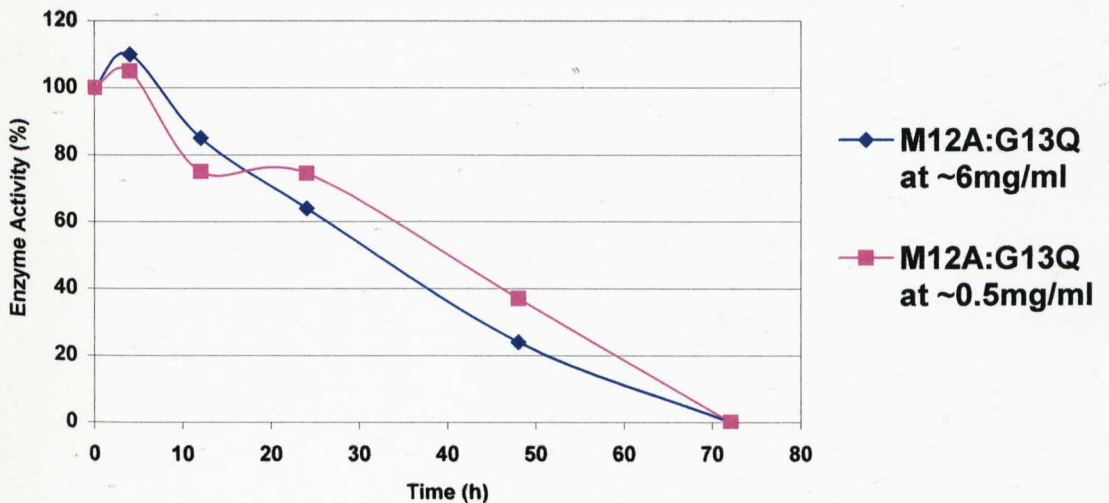
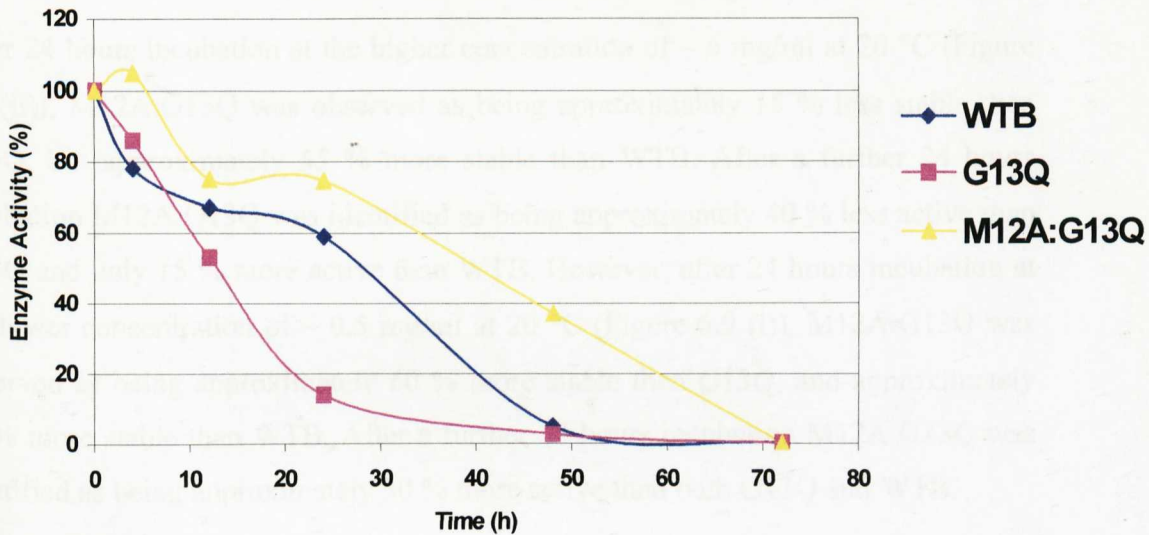


Figure 6.9: Comparison of sMMO propylene oxide stability assays of (i) proteins WTB, G13Q and M12A:G13Q at ~0.5 mg/ml and (ii) proteins WTB, G13Q and M12A:G13Q at ~6 mg/ml incubated at 20 °C.

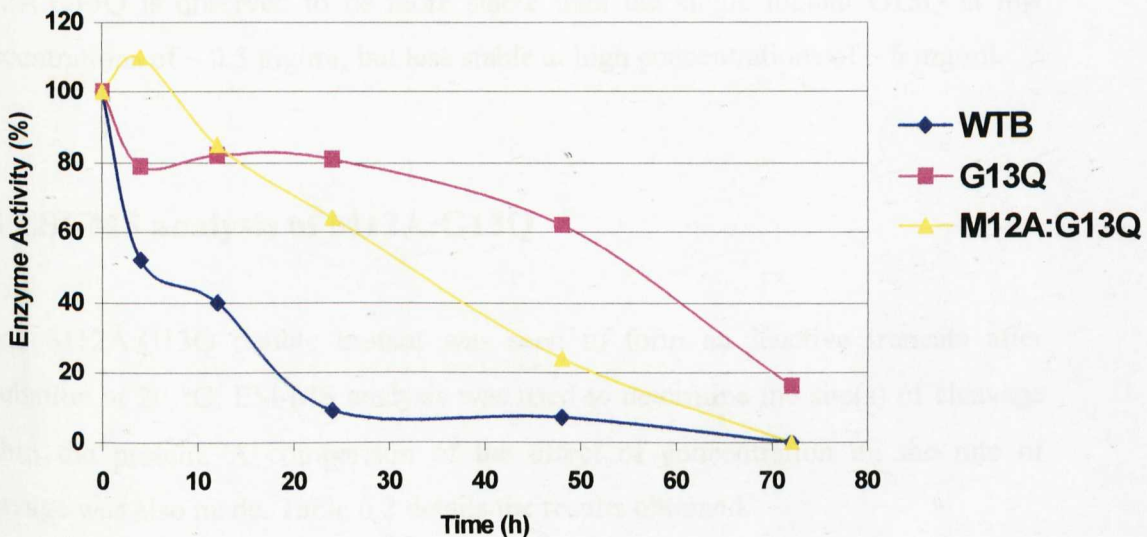
sMMO propylene oxidation assays (Chapter 2, Section 2.12.2) were performed by adding 8 μ M aliquots of hydroxylase and reductase to 8 μ M of protein B. Enzyme activity is shown as a percentage of the activity remaining after incubation compared to the activity at 0 h. 100 % activity represents; 1956 nmol/min/mg G13Q, 1896 nmol/min/mg WTB and 2015 nmol/min/mg M12A:G13Q. The data shown are the mean of 3-4 sMMO assays for each reaction. Standard error was ~10 %.

Data for WTB and G13Q have been previously shown in Chapter 5 and have been incorporated here for comparative purposes only.

(i)



(ii)



The activity of the double mutant of protein B from *Mc. capsulatus* (Bath) was seen to decrease over time, as observed for both WTB and the single mutant G13Q (Figures 6.8 and 6.9). However, more in keeping with the results obtained for WTB and recombinant *Ms. trichosporium* OB3b protein B, M12A:G13Q did not differ greatly in the loss of activity or truncation over time, when comparing samples incubated at high and low protein concentrations. Thus, the stabilising effect of higher protein concentrations, observed for G13Q, was not apparent in the samples of M12A:G13Q.

After 24 hours incubation at the higher concentration of ~ 6 mg/ml at 20 °C (Figure 6.9 (ii)), M12A:G13Q was observed as being approximately 15 % less stable than G13Q, but approximately 55 % more stable than WTB. After a further 24 hours incubation M12A:G13Q was identified as being approximately 40 % less active than G13Q and only 15 % more active than WTB. However, after 24 hours incubation at the lower concentration of ~ 0.5 mg/ml at 20 °C (Figure 6.9 (i)), M12A:G13Q was observed as being approximately 60 % more stable than G13Q, and approximately 15 % more stable than WTB. After a further 24 hours incubation M12A:G13Q was identified as being approximately 30 % more active than both G13Q and WTB.

Although not greatly affected in stability terms by protein concentration, M12A:G13Q is observed to be more stable than the single mutant G13Q at low concentrations of ~ 0.5 mg/ml, but less stable at high concentrations of ~ 6 mg/ml.

6.4 ESI-MS analysis of M12A:G13Q

Since M12A:G13Q double mutant was seen to form an inactive truncate after incubation at 20 °C, ESI-MS analysis was used to determine the site(s) of cleavage within the protein. A comparison of the effect of concentration on the rate of cleavage was also made. Table 6.2 details the results obtained.

Table 6.2: ESI-MS analysis of M12A:G13Q samples at (i) 0.5 mg/ml, and (ii) 6 mg/ml after incubation at 20 °C for various time periods

The ESI-MS of the proteins was recorded on a Quattro II tandem mass-spectrometer equipped with an electrospray ion source. Data were processed using the MassLynx program (VG Biotech) (Chapter 2, Section 2.16.1). Data in bold indicates dominant protein peak in each sample.

(i)

Time (h)	Observed molecular mass (Da)	Cleavage site numbered with respect to the wild-type <i>Mc. capsulatus</i> (Bath) protein B sequence
0	16240	Intact
24	16240	Intact
	15560	N ³ -S ⁴
	15360	N ⁵ -A ⁶
	15133	Y ⁷ -D ⁸
36	16240	Intact
	15361	N ⁵ -A ⁶
	15129	Y ⁷ -D ⁸
	14572	Q ¹³ -L ¹⁴
48	16240	Intact
	15563	N ³ -S ⁴
	14701	A ¹² -Q ¹³
	14572	Q¹³-L¹⁴
	13275	F ²⁴ -A ²⁵

(ii)

Time (h)	Observed molecular mass (Da)	Cleavage site numbered with respect to the wild-type <i>Mc. capsulatus</i> (Bath) protein B sequence
0	16240	Intact
2	16240	Intact
6	16240	Intact
12	16240	Intact
24	16240	Intact
	15560	N ³ -S ⁴
	15130	Y ⁷ -D ⁸
36	16240	Intact
	15560	N ³ -S ⁴
	15130	Y ⁷ -D ⁸
48	16240	Intact
	15560	N³-S⁴
	15360	N ⁵ -A ⁶
	15130	Y ⁷ -D ⁸
	14700	A ¹² -Q ¹³
	14570	Q ¹³ -L ¹⁴
	13270	F ²⁴ -A ²⁵
72	14700	A¹²-Q¹³
	13400	A ¹² -Q ¹³ + C-terminal cleavage
	13272	F ²⁴ -A ²⁵

The cleavage patterns are similar for the cleavage sites identified after incubation at 20 °C at the different concentrations (Table 6.2). At both the low protein

concentration of ~ 0.5 mg/ml and the higher protein concentration of ~ 6 mg/ml cleavage was not observed within the first 36 hours at the A¹²-Q¹³ site, equivalent to the M¹²-G¹³ cleavage site of wild type *Mc. capsulatus* (Bath) protein B, the M¹²-G¹³ cleavage site of WTB and the M¹²-Q¹³ cleavage site of G13Q (Chapter 5). Nevertheless, cleavage at A¹²-Q¹³ is observed in both cases after extended incubation at 20 °C for 48 hours. Interestingly, in both cases the activity decrease observed after ~ 24 hours incubation only corresponded to truncation of the N-terminus from S¹ up to and including Y⁷. Overall, the patterns of degradation are similar for both the concentrations studied, in agreement with the activity and SDS-PAGE results obtained, which also suggest that M12A:G13Q does not differ significantly in activity loss or truncation over time at the two different concentrations.

6.5 Affinity of M12A:G13Q for the hydroxylase

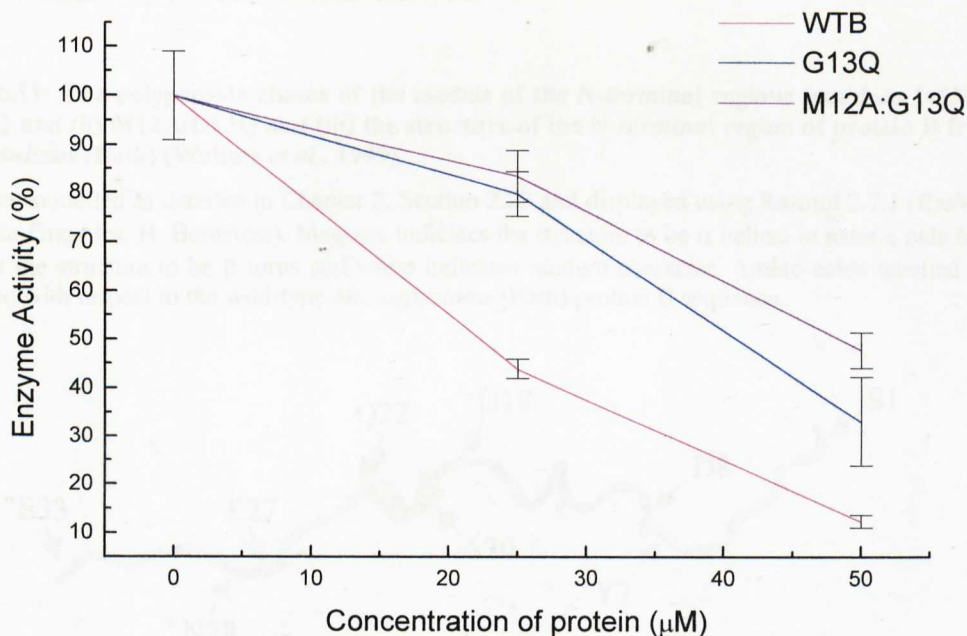
Surface plasmon resonance techniques have also been used to show that *Mc. capsulatus* (Bath) protein B binds to the hydroxylase and that protein B' binds to a much lesser extent (Bhambra, 1996; Kazlauskaite *et al.*, 1996). Protein B inhibits the activity of the hydroxylase, when functioning via the peroxide shunt system, indicating that the protein interacts significantly with the hydroxylase (Jiang *et al.*, 1993). Therefore, the inhibition of the peroxide shunt reaction was used as an indicator of protein B binding to the hydroxylase, the greater the inhibition, the greater the binding.

M12A:G13Q, WTB and G13Q were compared with regard to inhibition levels of the peroxide shunt reaction, when added at concentrations of 25 µM and 50 µM (Figure 6.10).

Figure 6.10: The effect of the double and single mutants of *Mc. capsulatus* (Bath) protein B and WTB on the oxidation of propylene in the hydroxylase/H₂O₂ system.

The hydroxylase was at a concentration of 24 μ M and H₂O₂ at 100 mM. Reactions were incubated for 10 min before injecting 500 μ l of the gas phase of the reaction onto a calibrated Porapak Q GC column for product quantification (Chapter 2, 2.12.3). Enzyme activity is shown as a percentage of the activity of the hydroxylase activated via the peroxide shunt reaction, which represents 550.3 nmol propylene oxide produced (9.2nmol/min/mg). The values presented are the mean of 3-4 separate experiments. Standard error bars are shown.

The data for WTB has been previously displayed in Chapter 4 and has been incorporated here for comparative purposes.



WTB inhibits the peroxide shunt reaction most strongly, whereas, G13Q and M12A:G13Q showed weaker inhibition levels, which were very similar (Figure 6.10).

6.6 Theoretical modelling of the N-terminal region of M12A:G13Q, as compared to G13Q and wild-type *Mc. capsulatus* (Bath) protein B

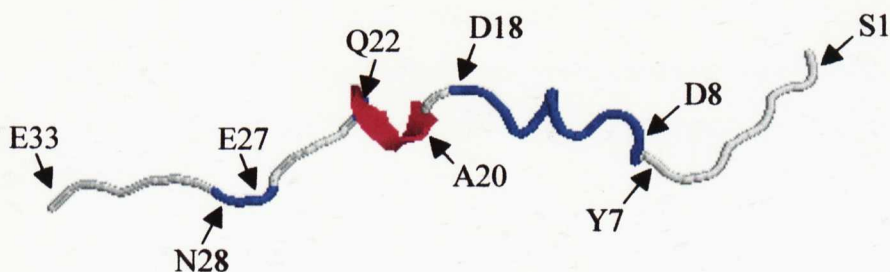
The recent availability of the NMR structure of protein B from *Mc. capsulatus* (Bath) (Walters *et al.*, 1999) permitted homology modelling to be initiated as a means of studying the effect of the mutations on the structure of the protein. It was hoped that this would give an insight into the functional differences observed between the proteins. The first 33 amino acids of the N-terminal region of the G13Q and M12A:G13Q mutants were identified as having 97 % and 94 % identity with the

equivalent amino acid residues of protein B from *Mc. capsulatus* (Bath). The orientation of the N-terminal of protein B with respect to the protein core is unknown and, as a result, the N-terminal regions were modelled alone. Models were produced using the Swissmodel programme available on the ExPASy server (Peitsch, 1995). Figure 6.11 shows models obtained for the polypeptide chains of G13Q and M12A:G13Q, compared to the structure of the equivalent region of wild type protein B as determined by NMR structural analysis.

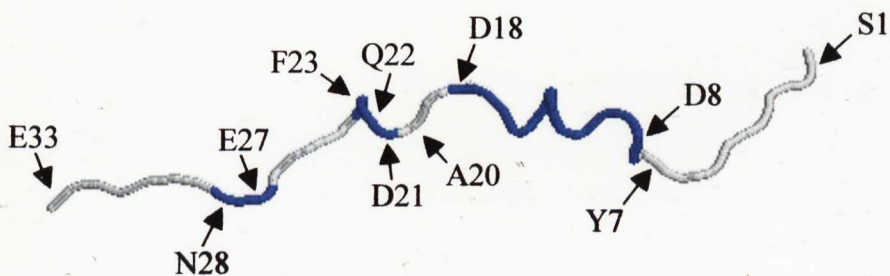
Figure 6.11: The polypeptide chains of the models of the N-terminal regions (residues 1-33) of (i) G13Q and (ii) M12A:G13Q and (iii) the structure of the N-terminal region of protein B from *Mc. capsulatus* (Bath) (Walters *et al.*, 1999).

Structures modelled as detailed in Chapter 2, Section 2.23 and displayed using Rasmol 2.7.1 (RasWin Molecular Graphics, H. Bernstein). Magenta indicates the structure to be α helical in nature, pale blue indicates the structure to be β turns and white indicates random character. Amino acids labelled are numbered with respect to the wild-type *Mc. capsulatus* (Bath) protein B sequence.

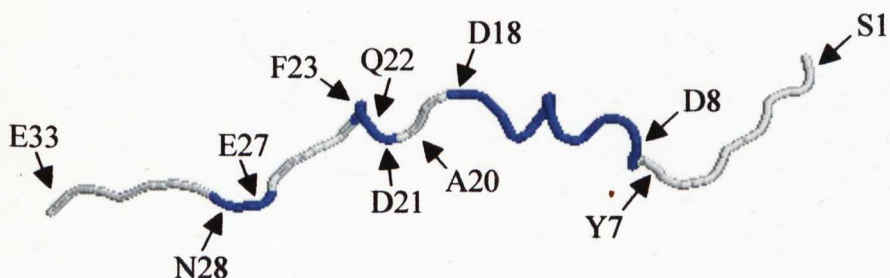
(i)



(ii)



(iii)



The models (Figure 6.11) indicated that there was a change in secondary structure at the Y⁷-D⁸ site. Residues S¹ to Y⁷ were random in character and D⁸ to D¹⁸ exhibited β -turn structure. Similarly, in each case, β -turn character was present for residues E27 and N28, whilst the neighbouring structure was random in nature. G13Q differed from wild-type protein B and M12A:G13Q in that its N-terminal region indicated α -helical character between residues A²⁰ and Q²². This was lacking for the other two proteins which exhibited instead a mixture of random character (A²⁰) and β -turn structure (D²¹ to F²³). Therefore, the double mutation of G¹³ to glutamine and M¹² to alanine did not apparently affect the secondary structure of the N-terminal region of the protein when compared to that for wild-type *Mc. capsulatus* (Bath) protein B, whereas, the single mutation of G¹³ to glutamine was predicted to cause a slight change in the secondary structure of the region. Interestingly, G13Q has been identified as the more stable protein under certain conditions, so the α -helical character identified may orientate the protein such that at high protein concentrations, protein interactions are enabled which cause stabilisation. In order to assess the validity of these models, work proceeded to gain experimental secondary structural information on the proteins.

6.7 Determination of the secondary structure of M12A:G13Q

In order to determine whether the M¹² to alanine and G¹³ to glutamine mutations incorporated into protein B from *Mc. capsulatus* (Bath) had an effect on the structure of the protein, secondary structure determination techniques, including near UV and far UV CD and fluorescence were conducted on the purified protein. Comparisons were made with the single protein B mutant, G13Q, and WTB itself.

Circular dichroism spectroscopy is very sensitive to the secondary structure of proteins, and far UV CD can be interpreted to give information on the secondary structural types present within a sample, whereas near UV CD spectroscopy provides evidence of the tertiary structure and dynamics of proteins.

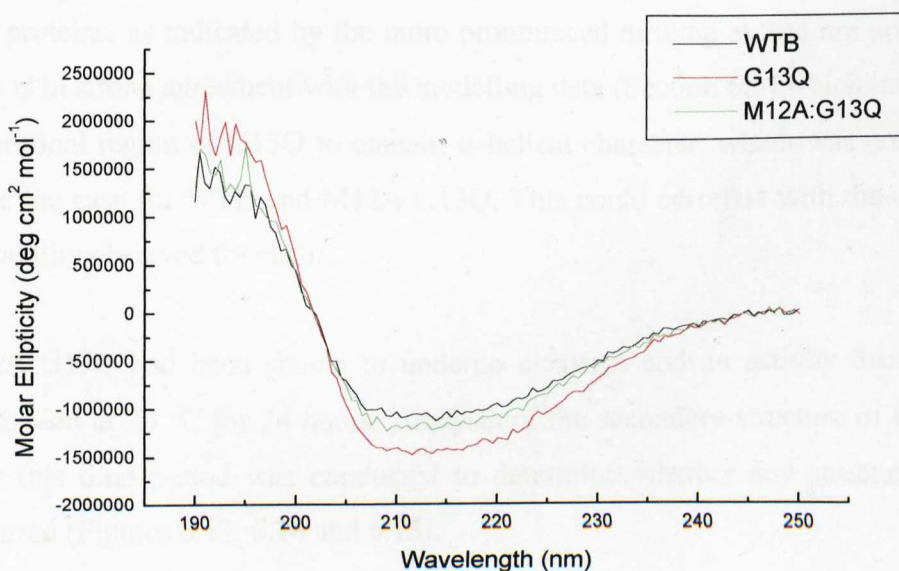
Fluorescence spectroscopy similarly provides a sensitive means of characterising proteins and their conformation. The tryptophan, tyrosine and phenylalanine residues, which are the same sequentially in each of the proteins studied here, determine the spectra obtained. The polarity of the environments of these residues can then be identified and thus the proteins can be analysed to elucidate whether this is the same or different in each case. Since the proteins only differ with regard to the amino acids mutated within the N-terminal region, and the core regions are the same, any change in fluorescence or secondary structure can only be interpreted as being a result of the mutations and the orientation of the N-terminal region relative to the core of the protein.

Figure 6.12 illustrates the far and near UV CD spectra for each of the proteins WTB, G13Q and M12A:G13Q.

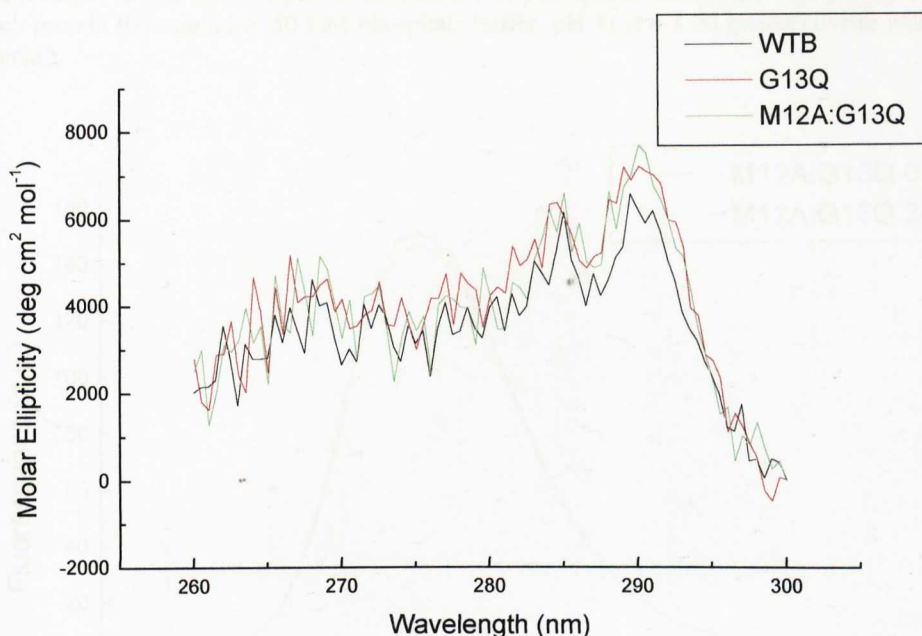
Figure 6.12: (i) Far UV CD and (ii) Near UV CD spectra of M12A:G13Q compared with those for WTB and G13Q.

The CD spectra were recorded on a Jasco J715 spectropolarimeter at room temperature (Chapter 2, Section 2.18). The spectra shown are averages of 10 scans of each protein (i) at 0.12 mg/ml and (ii) at 0.4 mg/ml in 50 mM phosphate buffer, pH 7, in a (i) 1 mm and (ii) 10 mm pathlength quartz cuvette. The data for WTB and G13Q has been displayed previously in Chapter 4 and is incorporated here for comparative purposes.

(i)



(ii)



The near UV CD data for WTB, G13Q and M12A:G13Q (Figure 6.12 (ii)) appear much the same, indicating there to be little difference in the packing and dynamics of the three proteins. However, the far UV CD data (Figure 6.12 (i)) indicate WTB and M12A:G13Q to be very similar in their secondary structural characteristics, whereas the data for of G13Q suggests there to be more α -helix content compared to the other two proteins, as indicated by the more pronounced minima at 208 nm and 222 nm. This is in strong agreement with the modelling data (Section 6.6) which indicated the N-terminal region of G13Q to contain α -helical character, which was not proposed to be the case for WTB and M12A:G13Q. This could correlate with the differences in stability observed for each.

M12A:G13Q had been shown to undergo cleavage and an activity decrease after incubation at 20 °C for 24 hours. Analysis of the secondary structure of the protein over this time period was conducted to determine whether any structural change occurred (Figures 6.13, 6.14 and 6.15).

Figure 6.13: Fluorescence spectra of M12A:G13Q after incubation at 20 °C for 0 h and 24 h.

The fluorescence spectra were recorded on a Perkin-Elmer LF-50 fluorimeter at room temperature with excitation at 280 nm (Chapter 2, Section 2.17). The spectra shown are sum/averages of 8 scans of each protein (0.5 mg/ml in 50 mM phosphate buffer, pH 7) in a 3 ml quartz cuvette with a 10 mm pathlength.

(i)

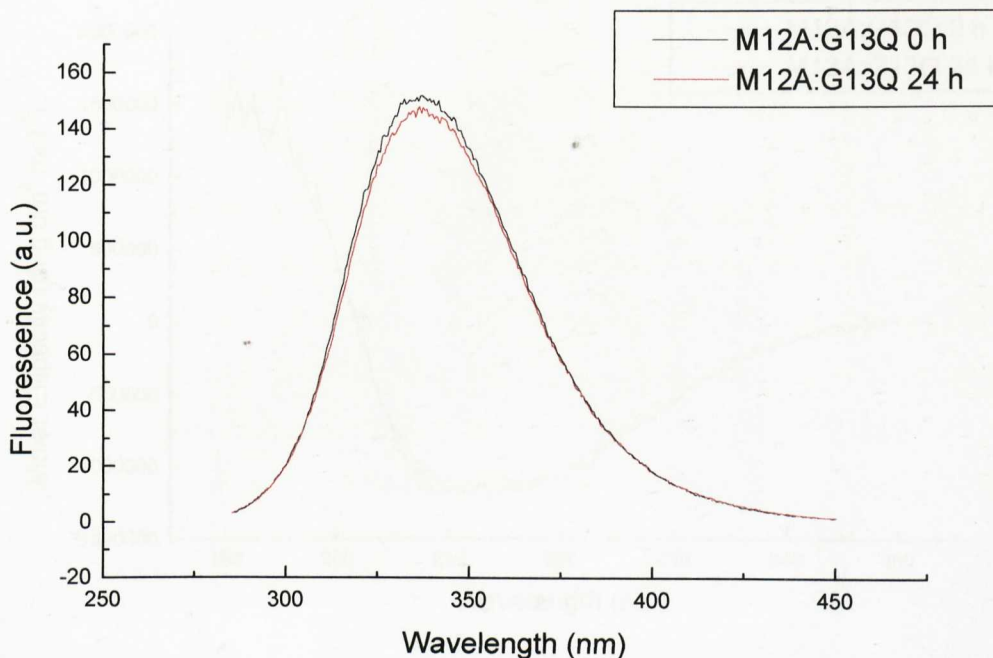


Figure 6.14: Far UV CD spectra of M12A:G13Q after incubation at 20 °C for 0 h and 24 h.

The CD spectra were recorded on a Jasco J715 spectropolarimeter at room temperature (Chapter 2, Section 2.18). The spectra shown are averages of 10 scans of each protein (0.4 mg/ml in 50 mM phosphate buffer, pH 7) in a 1 cm pathlength quartz cuvette.

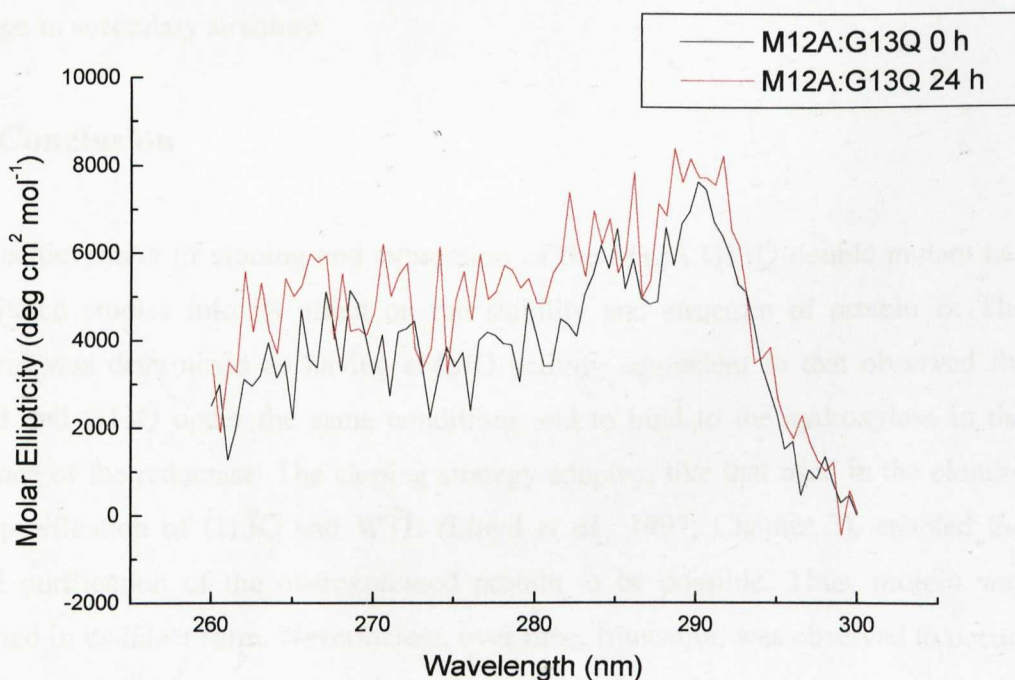
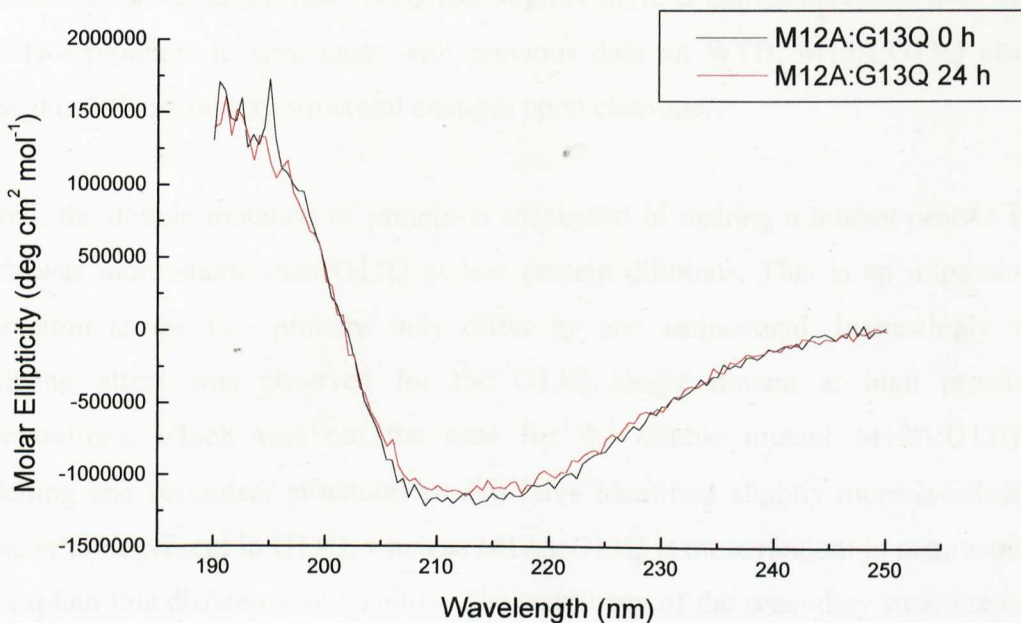


Figure 6.15: Near UV CD spectra of M12A:G13Q after incubation at 20°C for 0 h and 24 h.

The CD spectra were recorded on a Jasco J715 spectropolarimeter at room temperature (Chapter 2, Section 2.18). The spectra shown are averages of 10 scans of each protein (0.12 mg/ml in 50 mM phosphate buffer, pH 7) in a 1 mm pathlength quartz cuvette.



In each instance the secondary structure remains approximately the same, as no difference is observed for the CD and fluorescence data (Figures 6.13, 6.14 and 6.15). Therefore, the loss in activity observed after 24 hours cannot be attributed to a change in secondary structure.

6.8 Conclusion

The achievement of cloning and expression of the M12A:G13Q double mutant has facilitated studies into its effect on the stability and structure of protein B. The protein was determined as having sMMO activity equivalent to that observed for WTB and G13Q under the same conditions and to bind to the hydroxylase in the absence of the reductase. The cloning strategy adopted, like that used in the cloning and purification of G13Q and WTB (Lloyd *et al.*, 1997; Chapter 3), enabled the rapid purification of the overexpressed protein to be possible. Thus, protein was purified in its intact form. Nevertheless, over time, truncation was observed to occur, firstly at the N³-S⁴ position and then progressively from this region towards the C-

terminus, including the A¹²-Q¹³ site, equivalent to the site cleaved in the native *Mc. capsulatus* (Bath) protein B, WTB and G13Q.

Modelling studies suggested M12A:G13Q to be similar to WTB. CD supported these theoretical data indicating that G13Q had slightly more α -helical character than the other two proteins. In agreement with previous data on WTB, M12A:G13Q also undergoes little secondary structural changes upon cleavage.

Overall, the double mutation of protein B succeeded in making a mutant protein B which was more stable than G13Q at low protein dilutions. This is an important observation as the two proteins only differ by one amino acid. Interestingly, a stabilising effect was observed for the G13Q single mutant at high protein concentrations, which was not the case for the double mutant M12A:G13Q. Modelling and secondary structural studies have identified slightly more α -helical character to be present in G13Q, whereas M12A:G13Q is more random in nature and may explain this difference in stability. The stabilising of the secondary structure of G13Q may be positively influenced by increased protein concentrations decreasing exposure of the protein to the solvent environment. Reducing the protein concentration would, therefore, have a negative effect on structural forces and interactions resulting in the loss of secondary structure, possibly exposing the protein to cleavage and inactivation. By contrast, the less ordered nature of M12A:G13Q is less affected by protein concentration in terms of stability. Initially G13Q and M12A:G13Q exhibited the same level of specific activity, yet differed greatly in their activities after incubation over time at the two different concentrations. It is possible that this can be explained in terms of the inactivatory cleavage mechanism occurring by means of attack by a specifically nucleophilic amino side chain acid group on the exposed N-terminal region (Chapter 4). This proposal is supported by the fact that at high protein concentrations the α -helical nature of the N-terminus of G13Q is stabilised. This means that the region susceptible to attack is not exposed to the specifically reactive nucleophilic side chain group on the core of the protein. However, upon dilution, the α -helical character of the N-terminal region may become weakened or partially unfolded due to exposure to the adverse environmental conditions, which weaken or break the forces of interaction involved.

Thus, at low protein concentrations, the N-terminal region could become susceptible to nucleophilic attack leading to cleavage. However, for M12A:G13Q the random nature of the N-terminal region could mean it is exposed and, therefore, susceptible to the cleavage reaction at both high and low protein concentrations, as illustrated by the similar activities and cleavages of the protein over time at the two protein concentrations.

The mutations studied here have given insights into the character of *Mc. capsulatus* (Bath) protein B, enabling structure to be related to stability. It is interesting that cleavage at the Y⁷-D⁸ site of M12A:G13Q resulted in an activity decrease, which was identified by the presence of low activity truncates of M12A:G13Q lacking N-terminal amino acids S¹ to Y⁷. This highlights the importance of these first few N-terminal amino acids in relation to activity. It also poses the question of how many of them are actually essential for protein B activity within the sMMO complex. This is addressed in Chapter 7.

Chapter 7

Expression, purification and characterisation of truncates of recombinant protein B from *Mc. capsulatus* (Bath)

7.1 Introduction

In addition to work by Bhambra (1996) and Lloyd *et al.* (1997) which identified an inactive form of *Mc. capsulatus* (Bath) protein B lacking in the first 12 amino acids from the N-terminus, a truncation mutant of protein B deficient in the first 25 amino acids from the N-terminus was also shown to lack catalytic activity within the sMMO assay (Brandstetter *et al.*, 1999).

Recent studies favour the formation of the inactive protein B' truncate via an autocatalytic mechanism of cleavage (Chapter 4; Lloyd *et al.*, 1997; Bhambra, 1996). However, most proteins which undergo an autocatalytic cleavage reaction produce proteins with an activatory function. Examples of self-catalysed protein modifications, including protein splicing, autoprocessing and autocleavage reactions, have been discovered in all three kingdoms of life, eukaryotes, prokaryotes and archaea and represent exceptions to the idea that the final protein product is always co-linear with the nucleotide sequence of the gene (Shao and Kent, 1997; Perler *et al.*, 1997). Therefore, it must not be ruled out that the cleavage of protein B to protein B', although inactivating the sMMO complex, may have some other activatory role yet to be elucidated.

Nevertheless, it is interesting that the activity of the sMMO complex should be lost upon the loss of only 12 amino acids from the N-terminus of protein B. It is, therefore, necessary to determine exactly how many of these 12 amino acids are essential for sMMO activity, and whether these amino acids *per se* are responsible for the degradation of protein B. In order to address these issues, N-terminally truncated proteins of *Mc. capsulatus* (Bath) protein B were constructed, expressed, purified and analysed.

Truncates were constructed with the G13Q mutation and a C-terminal affinity tag to facilitate ease of purification and resistance to cleavage. Since the G13Q protein behaves the same as the wild-type protein B as far as cleavage is concerned, any conclusions on this mutant would apply to the wild-type protein.

The truncates were numbered with reference to their first amino acid and its position within the wild-type *Mc. capsulatus* (Bath) protein B sequence. Figure 7.1 below illustrates the numbering of the first few N-terminal amino acids of G13Q protein B.

Figure 7.1: Schematic illustration of the numbering of the N-terminal of *Mc. capsulatus* (Bath) protein B single mutant G13Q.

1	2	3	4	5	6	7	8	9	10	11	12	13	14	15	..	C-terminal
S	V	N	S	N	A	Y	D	A	G	I	M	Q	L	K		

Truncates were produced at the S⁴, N⁵, A⁶, Y⁷, D⁸, A⁹, G¹⁰, and Q¹³ positions as well as the intact G13Q protein with the same C-terminal tag. Figure 7.2 schematically represents the truncate proteins produced.

Figure 7.2: Schematic representation of the *Mc. capsulatus* (Bath) G13Q protein B truncates produced.

Truncate Protein	Schematic representation of truncate protein sequence
G13Q-tag	S ¹ V ² N ³ S ⁴ N ⁵ A ⁶ Y ⁷ D ⁸ A ⁹ G ¹⁰ I ¹¹ M ¹² Q ¹³ L ¹⁴ K ¹⁵C-terminal-tag
S4-tag	S ⁴ N ⁵ A ⁶ Y ⁷ D ⁸ A ⁹ G ¹⁰ I ¹¹ M ¹² Q ¹³ L ¹⁴ K ¹⁵C-terminal-tag
N5-tag	N ⁵ A ⁶ Y ⁷ D ⁸ A ⁹ G ¹⁰ I ¹¹ M ¹² Q ¹³ L ¹⁴ K ¹⁵C-terminal-tag
A6-tag	A ⁶ Y ⁷ D ⁸ A ⁹ G ¹⁰ I ¹¹ M ¹² Q ¹³ L ¹⁴ K ¹⁵C-terminal-tag
Y7-tag	Y ⁷ D ⁸ A ⁹ G ¹⁰ I ¹¹ M ¹² Q ¹³ L ¹⁴ K ¹⁵C-terminal-tag
D8-tag	D ⁸ A ⁹ G ¹⁰ I ¹¹ M ¹² Q ¹³ L ¹⁴ K ¹⁵C-terminal-tag
A9-tag	A ⁹ G ¹⁰ I ¹¹ M ¹² Q ¹³ L ¹⁴ K ¹⁵C-terminal-tag
G10-tag	G ¹⁰ I ¹¹ M ¹² Q ¹³ L ¹⁴ K ¹⁵C-terminal-tag
Q13B'-tag	Q ¹³ L ¹⁴ K ¹⁵C-terminal-tag

7.2 PCR amplification and construction of vectors

Protein B from *Mc. capsulatus* (Bath) has been expressed in an active form in *E. coli* cells transformed with a pT7-5B plasmid containing the gene encoding protein B, under the control of a T7-RNA polymerase promoter expression system (West *et al.*,

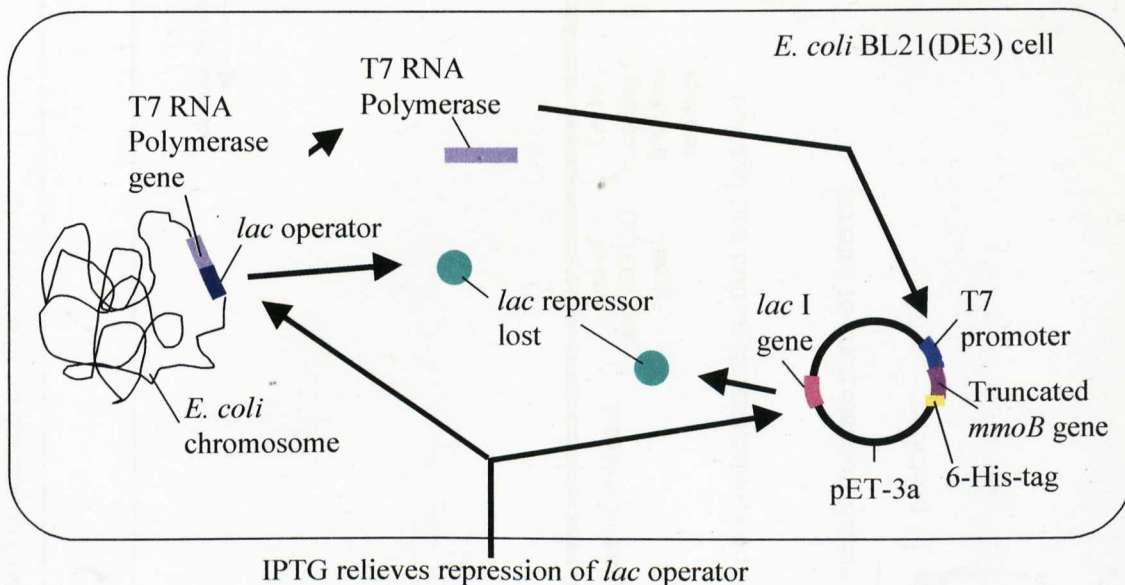
1992). Similarly, the wild-type and G13Q mutant proteins have been expressed as GST fusion proteins under the control of an IPTG inducible *tac* promoter (Lloyd *et al.*, 1997).

It was necessary to construct the protein B truncates with no extra amino acids at the N-terminus, which could result from the cloning strategy adopted, in order that the presence of certain amino acids at this position of the protein could be deduced. Thus, the method used was that of the Impact ITM (Intein Mediated Purification with an Affinity Chitin-binding Tag) system by New England Biolabs®. This system produces proteins with no extra amino acids present at the N-terminus, and thus was the method of choice when compared to producing the truncates with N-terminal affinity tags, as is the case with the GST fusion system (Amersham Pharmacia Biotech, Bucks., UK).

Unfortunately the Impact ITM system failed to produce clones so another, more reliable, cloning method was necessary to produce the truncates. The pET system (Novagen Inc., Madison, WI, USA) was chosen. For protein expression to be achieved the vectors have to be in *E. coli* cells which contain the T7 RNA polymerase gene under the control of the *lac* promoter, such as BL21(DE3). Therefore, when cells are induced with IPTG, the repression of the *lac* operator by the *lac* repressor of the host cell's genome is relieved, enabling T7 RNA polymerase production. Also the binding of the *lac* repressor to the *lacI* gene of the pET vector is relieved by induction. The T7 RNA polymerase can, therefore, bind to the T7 promoter of the pET vector and transcription of the insert can occur (Figure 7.3).

Figure 7.3: Schematic representation of the control elements of the pET system (adapted from Novagen pET manual).

Details are given in the text.



The primers for PCR amplification of the inserts were designed such that a six histidine tag (6-His-tag) was encoded at the C-terminus of the protein to allow purification of the protein on a nickel chelating column. A schematic representation of the cloning procedure is detailed in Figure 7.4.

PCR reactions were performed using the pGEX-G13Q plasmid (Lloyd *et al.*, 1997; Chapter 2, Section 2.27.1) as the template to amplify *mmoBG13Q* truncated genes. Details of the primers used can be found in Table 7.1 and the annealing temperature used in each case was 50 °C. The truncate genes were digested with *Bam*H1 and *Nde*1 restriction enzymes and then ligated with pET-3a that had been digested with the same restriction enzymes. After ligation and transformation into *E. coli* DH5 α , colonies were screened by restriction analysis and the inserts were DNA sequenced to confirm the identity of the PCR insert. Plasmids containing the desired truncate genes were transformed into *E. coli* BL21(DE3) cells for protein expression.

Figure 7.4: Construction of vectors for the expression of *Mc. capsulatus* (Bath) protein B truncates.

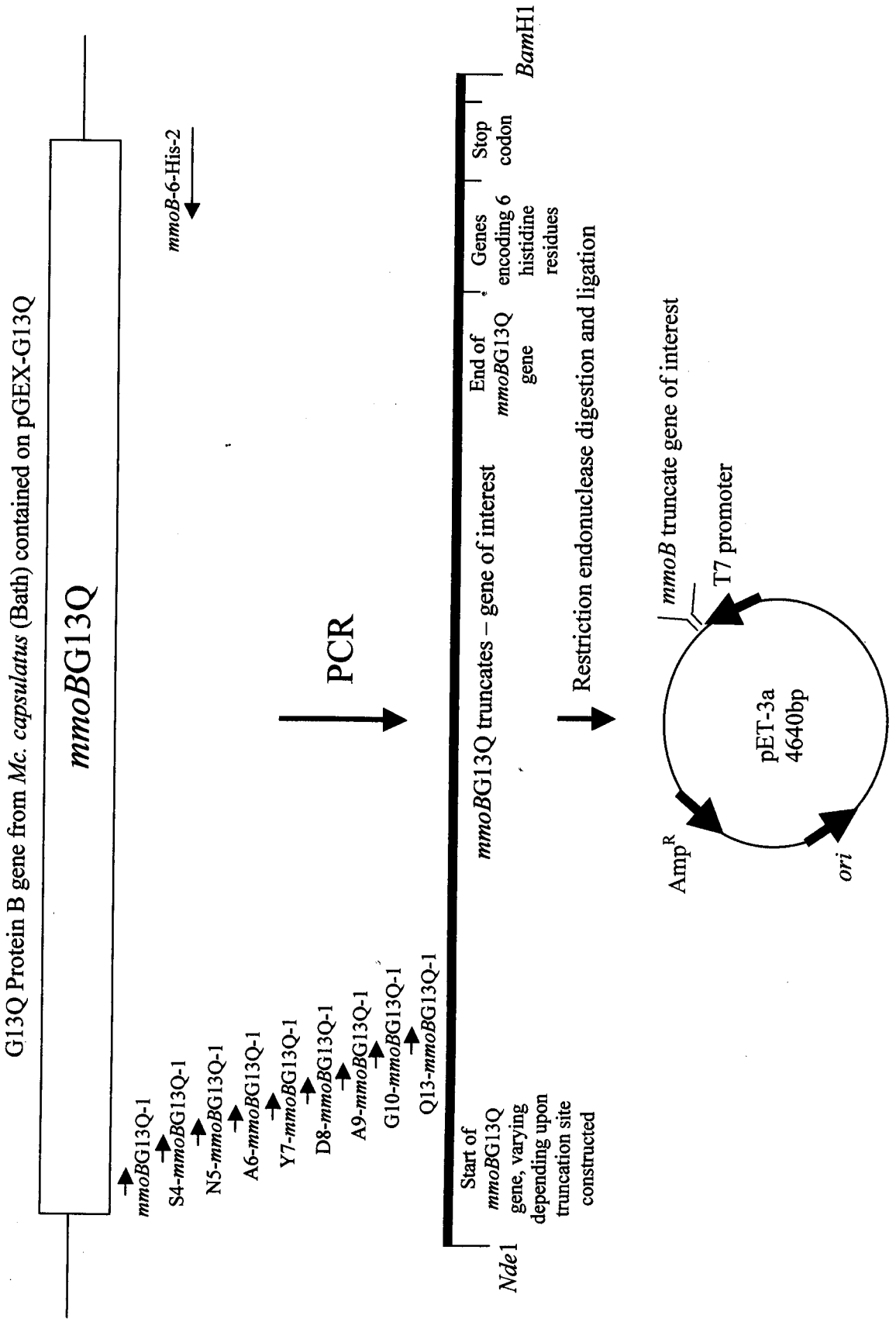


Table 7.1: PCR amplification of *mmoB* *Mc. capsulatus* (Bath) truncate genes for the construction of C-terminal 6-His-tag fusion proteins.

Amplified gene	Primers used ¹	Restricti on sites	Vector name
<i>mmo</i> BG13Q-6-His	<i>mmo</i> BG13Q-1 5' GG GAA TTC CAT <u>ATG</u> AGC GTA AAC AGC AAC GCA TAC 3'	<i>Bam</i> HI	pET-3a-
	<i>mmo</i> B-6His-2 5' TGT ATA GGA TCC <u>TCA</u> GTG ATG GTG ATG AGC GTG ATA GTC TTC GAG 3'	<i>Nde</i> I	G13Q-His-tag
S4- <i>mmo</i> BG13Q-6-His	S4- <i>mmo</i> BG13Q-1 5' GG GAA TTC CAT <u>ATG</u> AGC AAC GCA TAC GAC GCC GGC ATC 3'	<i>Bam</i> HI	pET-3a-S4-
	<i>mmo</i> B-6His-2 5' TGT ATA GGA TCC <u>TCA</u> GTG ATG GTG ATG AGC GTG ATA GTC TTC GAG 3'	<i>Nde</i> I	His-tag
N5- <i>mmo</i> BG13Q-6-His	N5- <i>mmo</i> BG13Q-1 5' GG GAA TTC <u>CAT</u> ATG AAC GCA TAC GAC GCC GGC ATC ATG CAG CTG AAA 3'	<i>Bam</i> HI	pET-3a-N5-
	<i>mmo</i> B-6His-2 5' TGT ATA GGA TCC <u>TCA</u> GTG ATG GTG ATG AGC GTG ATA GTC TTC GAG 3'	<i>Nde</i> I	His-tag
A6- <i>mmo</i> BG13Q-6-His	A6- <i>mmo</i> BG13Q-1 5' GG GAA TTC <u>CAT</u> ATG GCA TAC GAC GCC GGC ATC ATG CAG CTG AAA 3'	<i>Bam</i> HI	pET-3a-A6-
	<i>mmo</i> B-6His-2 5' TGT ATA GGA TCC <u>TCA</u> GTG ATG GTG ATG AGC GTG ATA GTC TTC GAG 3'	<i>Nde</i> I	His-tag
Y7- <i>mmo</i> BG13Q-6-His	Y7- <i>mmo</i> BG13Q-1 5' GG GAA TTC <u>CAT</u> ATG TAC GAC GCC GGC ATC ATG CAG CTG AAA 3'	<i>Bam</i> HI	pET-3a-Y7-
	<i>mmo</i> B-6His-2 5' TGT ATA GGA TCC <u>TCA</u> GTG ATG GTG ATG AGC GTG ATA GTC TTC GAG 3'	<i>Nde</i> I	His-tag
D8- <i>mmo</i> BG13Q-6-His	D8- <i>mmo</i> BG13Q-1 5' GG GAA TTC <u>CAT</u> ATG GAC GCC GGC ATC ATG CAG CTG AAA 3'	<i>Bam</i> HI	pET-3a-D8-
	<i>mmo</i> B-6His-2 5' TGT ATA GGA TCC <u>TCA</u> GTG ATG GTG ATG AGC GTG ATA GTC TTC GAG 3'	<i>Nde</i> I	His-tag
A9- <i>mmo</i> BG13Q-6-His	A9- <i>mmo</i> BG13Q-1 5' GG GAA TTC <u>CAT</u> ATG GCC GGC ATC ATG CAG CTG AAA GGC AAG 3'	<i>Bam</i> HI	pET-3a-A9-
	<i>mmo</i> B-6His-2 5' TGT ATA GGA TCC <u>TCA</u> GTG ATG GTG ATG AGC GTG ATA GTC TTC GAG 3'	<i>Nde</i> I	His-tag
G10- <i>mmo</i> BG13Q-6-His	G10- <i>mmo</i> BG13Q-1 5' GG GAA TTC <u>CAT</u> ATG GGC ATC ATG CAG CTG AAA GGC AAG 3'	<i>Bam</i> HI	pET-3a-G10-
	<i>mmo</i> B-6His-2 5' TGT ATA GGA TCC <u>TCA</u> GTG ATG GTG ATG AGC GTG ATA GTC TTC GAG 3'	<i>Nde</i> I	His-tag
Q13- <i>mmo</i> BG13Q-6-His	Q13- <i>mmo</i> BG13Q-1 5' GG GAA TTC <u>CAT</u> ATG CAG CTG AAA GGC AAG GAC TTC 3'	<i>Bam</i> HI	pET-3a-Q13-
	<i>mmo</i> B-6His-2 5' TGT ATA GGA TCC <u>TCA</u> GTG ATG GTG ATG AGC GTG ATA GTC TTC GAG 3'	<i>Nde</i> I	His-tag

¹Restriction enzyme sites are underlined

Genes encoding the 6-His-tag are in **bold**

Start and stop codons are in *italics*

pET-3a inserts were DNA sequenced in two separate reactions using:

1) the forward primer, T7 primer: 5' TAA TAC GAC TCA CTA TAG GG 3'

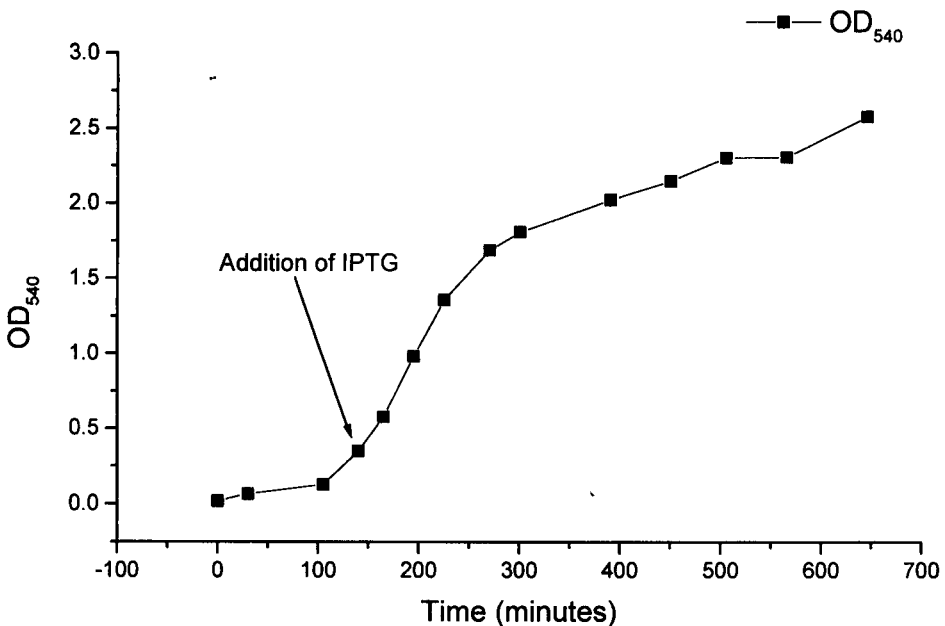
2) the reverse primer, T7 terminator primer: 5' GCT AGT TAT TGC TCA GCG 3'

7.3 Expression of truncated proteins

Protein expression was achieved by induction of the transformed *E. coli* BL21(DE3) cells at an OD₅₄₀ of 0.5 by addition of 1 mM IPTG at 37 °C (Figure 7.5).

Figure 7.5: Growth curve of *E. coli* BL21(DE3) expressing the Q13-His-tag truncate of protein B from *Mc. capsulatus* (Bath).

The growth curve is typical of that obtained for each of the 6-His-tagged protein B truncates.



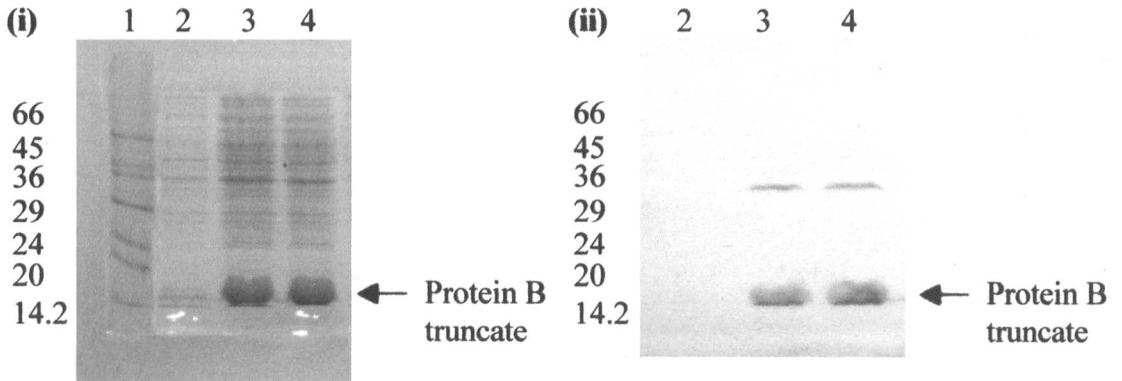
Whole cell lysates were taken at 0, 3 and 5 hours after IPTG induction and analysed using SDS-PAGE and Western blotting by probing with antisera to protein B. Proteins, each with an approximate molecular mass of 16,000 Da, were identified which cross-reacted with the *Mc. capsulatus* (Bath) protein B/B' antibodies. This confirmed that the proteins probably represented the 6-His-tagged truncated proteins in each case. Figure 7.6 indicates the accumulation of the Q13 protein B truncate, which was typical of the results obtained for the other truncated proteins.

Figure 7.6: (i) SDS-PAGE and (ii) Western blotting of truncated protein B expression in *E. coli* BL21(DE3).

(i) Lane 1: Molecular weight markers (bovine albumin, 66 kDa; egg albumin, 45 kDa; glyceraldehyde-3-P-dehydrogenase, 36 kDa; bovine carbonic anhydrase, 29 kDa; bovine pancreas trypsinogen, 24 kDa; soybean trypsin inhibitor, 20 kDa; bovine milk α -lactalbumin, 14.2 kDa).

Lanes 2-4: whole cell lysates of *E. coli* BL21(DE3) [pET-3a-Q13-His-tag] 0, 3 and 5 h respectively after IPTG induction.

(ii) Lanes 5-7: Western blot of lanes 2-4, probed with antiserum against protein B/B' from *Mc. capsulatus* (Bath).



SDS-PAGE analysis of soluble extracts for each of the truncate protein clones indicated that each of the soluble fractions contained the truncate protein. In order to determine if G13Q protein B with a C-terminal 6-His-tag was active, and to determine at which truncation point the activity of protein B was lost, propylene oxidation assays of the soluble extracts of each of the protein B truncates were performed in the presence of 8 μ M of each of the hydroxylase and reductase. As a control, the soluble extract of untransformed BL21(DE3) cells was also assayed. Results are shown in Table 7.2.

Table 7.2: Soluble extract assays of the truncated proteins of protein B

Assays containing 8 μ M aliquots of pure hydroxylase and reductase from *Mc. capsulatus* (Bath) and 5 mg soluble extract in MOPS buffer, pH 7 (Chapter 2, Section 2.12.2). The results are the conclusions of three separate experiments for each reaction. Activity is represented by \checkmark and inactivity by \times .

Soluble Extract	Activity
G13Q-His-tag	\checkmark
S4-His-tag	\checkmark
N5-His-tag	\checkmark
A6-His-tag	\checkmark
Y7-His-tag	\checkmark
D8-His-tag	\times
A9-His-tag	\times
G10-His-tag	\times
Q13-His-tag	\times
BL21(DE3) cells	\times

From the results of the soluble extract assays, the loss of activity occurs between residues Y⁷ and D⁸. It was also confirmed that G13Q protein B with a C-terminal 6-His-tag did not inhibit sMMO activity. The Q13 truncate, equivalent to protein B', was seen to be inactive, as expected. However, it was necessary to purify the proteins to obtain specific activity values for each of the individual truncated proteins and for further analysis.

7.4 Purification of the truncated proteins

Purification was achieved using the HisTrapTM kit (Amersham Pharmacia Biotech, Bucks., UK), which involved affinity chromatography using nickel chelating columns (Chapter 2, Section 2.6).

The proteins were eluted from the Ni-chelating columns using 500 mM imidazole. It was noted that imidazole inactivated sMMO itself, but it did not damage protein B, since sMMO activity was restored upon removal of the imidazole. Nevertheless, it was not possible to assay the activities of the truncated proteins in their semi-purified state. Also, imidazole was observed to cause precipitation of the truncated proteins when subjected to a freeze-thaw cycle. Thus, imidazole was removed immediately after the truncated proteins were eluted from the nickel-chelating columns by gel

filtration purification on a Superdex 75 column. This not only desalted the protein from the imidazole but also purified it from some contaminating higher molecular mass proteins. The purification procedure outlined above gave protein estimated to be ~ 95 % pure by SDS-PAGE analysis (Figure 7.7). Figure 7.8 shows each of the truncate proteins after the final purification step, indicating them all to be pure, and that little or no degradation had occurred during the purification procedure. These results were confirmed by ESI-MS analysis of the proteins which indicated them all to be pure, with very little or no degradation products. The ATG start codon, which codes for a methionine, is often post translationally removed, as was the case for wild-type protein B from *Mc. capsulatus* (Bath) and the truncate proteins G13Q-His-tag, S4-His-tag, A6-His-tag, A9-His-tag, and G10-His-tag . However, for N5-His-tag, Y7-His-tag, D8-His-tag and Q13-His-tag, the first methionine amino acid was retained, as detailed in Table 7.3. Overall, the indications were that these proteins were of sufficient purity for further analysis.

Figure 7.7: SDS-PAGE of the purification of Q13 protein B truncate from *E. coli* BL21(DE3) [pET-3a-Q13-His-tag].

The results are typical of those obtained for the purification of each of the truncate proteins.

Lane 1: Molecular weight markers (bovine albumin, 66 kDa; egg albumin, 45 kDa; glyceraldehyde-3-P-dehydrogenase, 36 kDa; bovine carbonic anhydrase, 29 kDa; bovine pancreas trypsinogen, 24 kDa; soybean trypsin inhibitor, 20 kDa; bovine milk α -lactalbumin, 14.2 kDa).

Lane 2: Soluble Extract of from *E. coli* BL21(DE3) [pET-3a-Q13-His-tag], ~ 50 μ g.

Lane 3: Flow through fraction from Ni chelating column, ~ 25 μ g.

Lane 4: Wash fraction from Ni chelating column, ~ 15 μ g.

Lane 5: Elution fraction from Ni chelating column, ~ 25 μ g.

Lane 6: S75 fraction of truncated protein B protein, ~ 15 μ g.

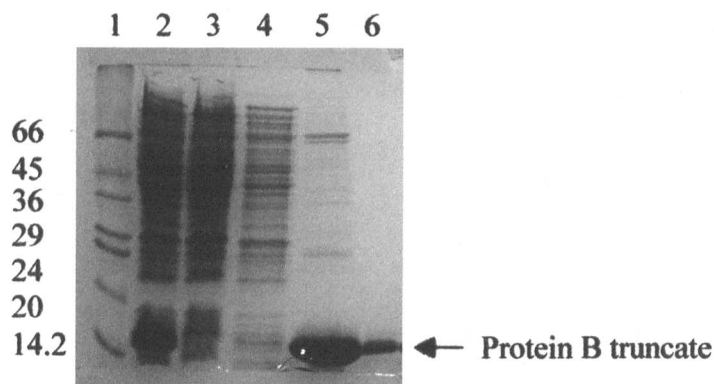


Figure 7.8: SDS-PAGE of purified 6-His-tagged protein B truncates from the various protein B truncate clones.

Lane 1: Molecular weight markers (bovine albumin, 66 kDa; egg albumin, 45 kDa; glyceraldehyde-3-P-dehydrogenase, 36 kDa; bovine carbonic anhydrase, 29 kDa; bovine pancreas trypsinogen, 24 kDa; soybean trypsin inhibitor, 20 kDa; bovine milk α -lactalbumin, 14.2 kDa).

Lane 2: G13Q-His-tag from *E. coli* BL21(DE3) [pET-3a-G13Q-His-tag].

Lane 3: S4-His-tag from *E. coli* BL21(DE3) [pET-3a-S4-His-tag].

Lane 4: N5-His-tag from *E. coli* BL21(DE3) [pET-3a-N5-His-tag].

Lane 5: A6-His-tag from *E. coli* BL21(DE3) [pET-3a-A6-His-tag].

Lane 6: Y7-His-tag from *E. coli* BL21(DE3) [pET-3a-Y7-His-tag].

Lane 7: D8-His-tag from *E. coli* BL21(DE3) [pET-3a-D8-His-tag].

Lane 8: A9-His-tag from *E. coli* BL21(DE3) [pET-3a-A9-His-tag].

Lane 9: G10-His-tag from *E. coli* BL21(DE3) [pET-3a-G10-His-tag].

Lane 10: Q13-His-tag from *E. coli* BL21(DE3) [pET-3a-Q13-His-tag].

Each lane contained ~ 5 μ g purified protein

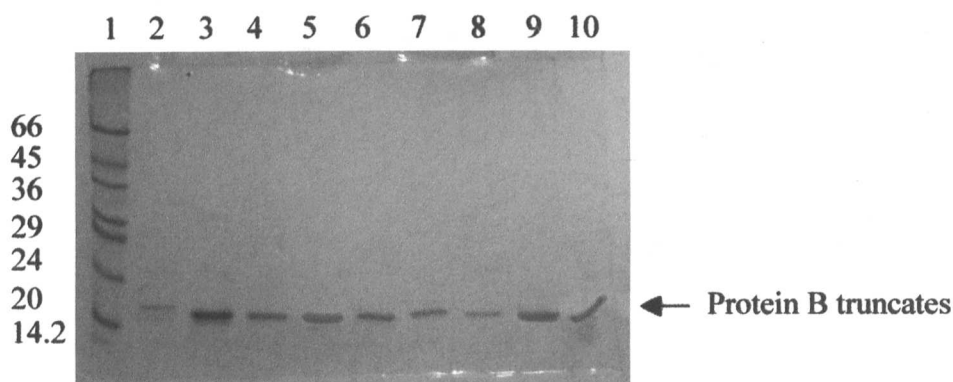


Table 7.3: ESI-MS analysis of the purified *Mc. capsulatus* (Bath) protein B truncates.

The ESI-MS of the samples were recorded on a Quattro II tandem mass-spectrometer with an electrospray ion source and the data was processed using the MassLynx program (VG Biotech) (Chapter 2, Section 2.16.1).

Protein	Calculated molecular mass (Da)	Observed molecular mass (Da)	Difference between calculated and observed masses (Da)	Reason for mass differences observed
G13Q-His-tag	16877.87	16745.0	132.87	Lacking N-terminal Methionine
S4-His-tag	16577.56	16445.0	132.56	Lacking N-terminal Methionine
N5-His-tag	16490.48	16490.0	-	Containing N-terminal Methionine
A6-His-tag	16376.38	16245.0	131.38	Lacking N-terminal Methionine
Y7-His-tag	16305.30	16305.0	-	Containing N-terminal Methionine
D8-His-tag	16142.12	16140.0	-	Containing N-terminal Methionine
A9-His-tag	16027.03	15895.0 -	132.0	Lacking N-terminal Methionine
G10-His-tag	15955.95	15825.0 -	130.95	Lacking N-terminal Methionine
Q13-His-tag	15654.54	15654.2	-	Containing N-terminal Methionine

7.5 Characterisation of the truncated proteins

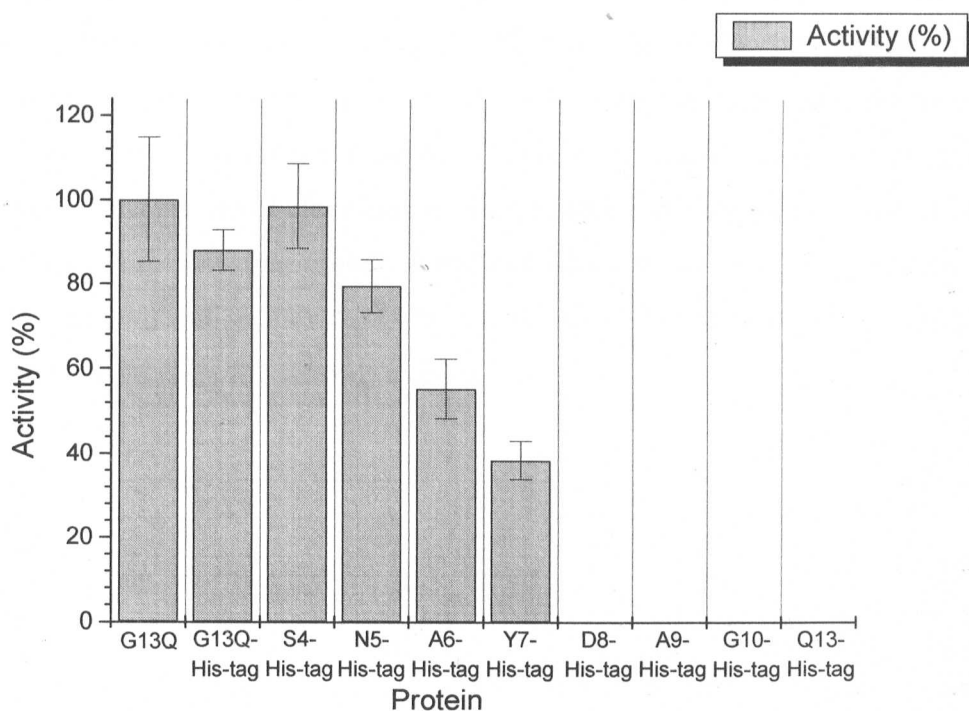
The specific activities of the protein B truncates were determined so that they could be compared directly to the wild-type protein B, and G13Q (Lloyd *et al.*, 1997). It was also important to compare the structural features of the truncated proteins to determine whether any insight into the mechanism of cleavage of protein B could be gained.

7.5.1 Activities of the protein B truncates

The activities of the protein B truncates were determined using the propylene oxidation assay. The results are presented in Figure 7.9.

Figure 7.9: Activities of the protein B truncates.

sMMO propylene oxidation assays (Chapter 2, Section 2.12.2) were performed by adding 8 μM aliquots of hydroxylase and reductase to 8 μM of the protein B truncate. Enzyme activity is shown as a percentage of the activity of G13Q which represents 1956 nm/min/mg protein. The activities presented are the mean of 3-4 separate experiments Standard error bars are shown.



The assay data for the pure protein B truncates confirmed the results obtained for the soluble extract assays of the protein B truncates (Table 7.2). The loss of the first 7 amino acids from the N-terminus of protein B leads to inactivation. As was expected, the C-terminal 6-His-tag had no effect on the activity of G13Q-His-tag, as its activity was approximately the same as that observed for the original G13Q mutant. Also, activity was retained at this level up to amino-acid S4, after which inactivation of protein B is seen to be gradual, as the activity level significantly decreased with the removal of each subsequent amino acid from the N-terminus.

7.5.2 Comparison of the cleavage sites that occur within the truncated proteins

It was unknown what effect truncating protein B would have on its ability to undergo the cleavage reaction, which possibly occurs via an autocatalytic mechanism (Chapter 4). In order to determine whether the protein B truncates cleaved, and if so, identify the cleavage site(s), ESI-MS was used.

The cleavage pattern of G13Q at high concentrations (~ 6 mg/ml) has been determined using ESI-MS for samples incubated at 20 °C for varying time lengths (Chapter 5). This approach was used here to identify the cleavage(s) that occurred within the various protein B truncates (Table 7.4). Therefore, it was possible to determine if the pattern of cleavage proteins produced was the same as that identified for G13Q and if truncating protein B had any effect on the rate of degradation. This in turn would identify important aspects of the N-terminal region of protein B relating to reasons for the cleavages observed.

Table 7.4: ESI-MS of the cleavage products of the protein B truncate proteins.

Truncated proteins (~ 6 mg/ml) were incubated at 20 °C and sampled and analysed by ESI-MS at time 0 h, 24 h, 3 days, and 6 days. A Quattro II tandem mass-spectrometer was used with an electrospray ion source and data were processed using the MassLynx program (VG Biotech) (Chapter 2, Section 2.16.1) Cleavages highlighted in bold represent the major peak(s) within the sample.

G13Q-His-tag

Incubation time at 20° C	Observed molecular mass (Da)	Cleavage site numbered with respect to the wild-type <i>Mc. capsulatus</i> (Bath) protein B sequence
0 h	16745.0	Intact
24 h	16743.02 15521.6 15279.5 14097.7 others	Intact M¹²-Q¹³ L¹⁴-K¹⁵ F²⁴-A²⁵ C-terminal
3 days	16744.76 others	Intact C-terminal
6 days	others	C-terminal

S4-His-tag

Incubation time at 20° C	Observed molecular mass (Da)	Cleavage site numbered with respect to the wild-type <i>Mc. capsulatus</i> (Bath) protein B sequence
0 h	16445.0	Intact
24 h	16444.2 15520.5 15279.5 14851 14025.0	Intact M¹²-Q¹³ L¹⁴-K¹⁵ D¹⁸-F¹⁹ A²⁵-D²⁶
3 days	15523.3 15281.86 14635.05	M¹²-Q¹³ L¹⁴-K¹⁵ A²⁰-D²¹
6 days	15281.77 14634.56 14026.32 others	L¹⁴-K¹⁵ A²⁰-D²¹ A²⁵-D²⁶ C-terminal

N5-His-tag

Incubation time at 20 °C	Observed molecular mass (Da)	Cleavage site numbered with respect to the wild-type <i>Mc. capsulatus</i> (Bath) protein B sequence
0 h	16490.0	Intact
24 h	16487.0 15519.3	Intact M ¹² -Q ¹³
3 days	16489.87 15522.5 15393	Intact M ¹² -Q ¹³ Q ¹³ -L ¹⁴
6 days	16489.3 15523.0 15393.6 14633.79 others	Intact M ¹² -Q ¹³ Q ¹³ -L ¹⁴ A ²⁰ -D ²¹ C-terminal

A6-His-tag

Incubation time at 20 °C	Observed molecular mass (Da)	Cleavage site numbered with respect to the wild-type <i>Mc. capsulatus</i> (Bath) protein B sequence
0 h	16245.0	Intact
24 h	16245.3 15521.59 15395.6	Intact M ¹² -Q ¹³ Q ¹³ -L ¹⁴
3 days	16244.79 15523.05 15394.9 15153.65	Intact M ¹² -Q ¹³ Q ¹³ -L ¹⁴ K ¹⁵ -G ¹⁶
6 days	16244.6 15523.05 15394.9 15153.65	Intact M ¹² -Q ¹³ Q ¹³ -L ¹⁴ K ¹⁵ -G ¹⁶

Y7-His-tag

Incubation time at 20 °C	Observed molecular mass (Da)	Cleavage site numbered with respect to the wild-type <i>Mc. capsulatus</i> (Bath) protein B sequence
0 h	16305.0	Intact
24 h	16304.4 15522.2	Intact M ¹² -Q ¹³
3 days	16306.42 15524.05 15154.51	Intact M ¹² -G ¹³ K ¹⁷ -D ¹⁸
6 days	16305.6 15524.0 15153.79 14706.57	Intact M ¹² -Q ¹³ K ¹⁷ -D ¹⁸ F ¹⁹ -A ²⁰

D8-His-tag

Incubation time at 20 °C	Observed molecular mass (Da)	Cleavage site numbered with respect to the wild-type <i>Mc. capsulatus</i> (Bath) protein B sequence
0 h	16140.0	Intact
24 h	16140.3 15649.7 15522.7 15280 15152.9 14246.1 others	Intact I ¹¹ -M ¹² M ¹² -Q ¹³ L ¹⁴ -K ¹⁵ K ¹⁵ -G ¹⁶ F ²⁴ -F ²⁵ C-terminal
3 days	15524 15154.96 others	M ¹² -Q ¹³ K ¹⁵ -G ¹⁶ C-terminal
6 days	15525.0 others	M ¹² -Q ¹³ C-terminal

A9-His-tag

Incubation time at 20 °C	Observed molecular mass (Da)	Cleavage site numbered with respect to the wild-type <i>Mc. capsulatus</i> (Bath) protein B sequence
0 h	15895.0	Intact
24 h	15824 15523.3 15395	Intact M ¹² -Q ¹³ Q ¹³ -L ¹⁴
3 days	15520.2 14965 others	M ¹² -Q ¹³ K ¹⁷ -D ¹⁸ C-terminal
6 days	15522.8 others	M ¹² -Q ¹³ C-terminal

G10-His-tag

Incubation time at 20 °C	Observed molecular mass (Da)	Cleavage site numbered with respect to the wild-type <i>Mc. capsulatus</i> (Bath) protein B sequence
0 h	15825	Intact
24 h	15825 15395	Intact Q ¹³ -L ¹⁴
3 days	15825 15523.54 15395.3	Intact M ¹² -Q ¹³ Q ¹³ -L ¹⁴
6 days	15825 15523.99 15153.68 others	Intact M ¹² -Q ¹³ K ¹⁵ -G ¹⁶ C-terminal

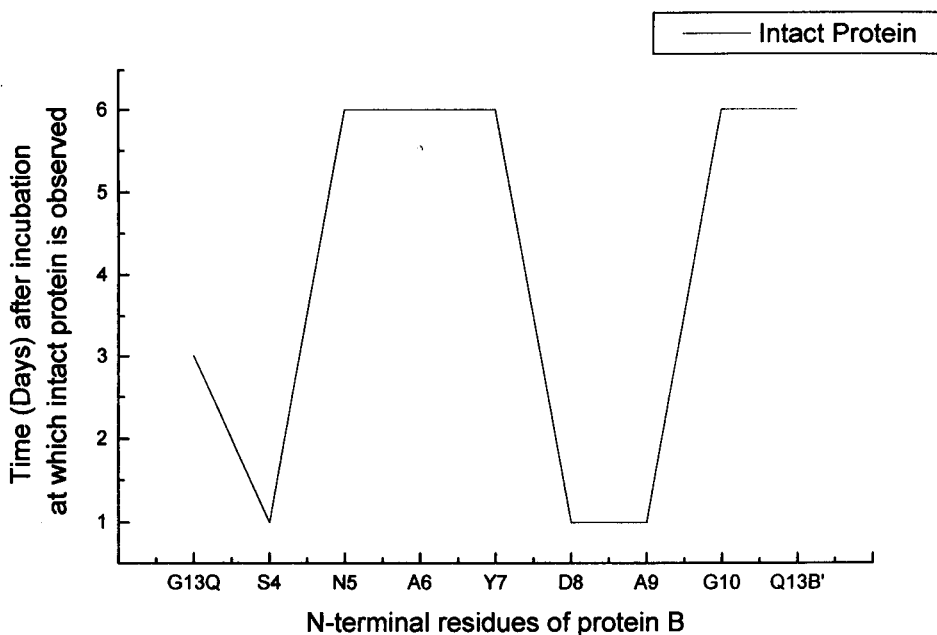
G13QB'-His-tag

Incubation time at 20 °C	Observed molecular mass (Da)	Cleavage site numbered with respect to the wild-type <i>Mc. capsulatus</i> (Bath) protein B sequence
0 h	15654.2	Intact
24 h	15654.2 14968.8	Intact K ¹⁷ -D ¹⁸
3 days	15654.54 14968.64	Intact K ¹⁷ -D ¹⁸
6 days	15654.67 14968.26	Intact K ¹⁷ -D ¹⁸

The data indicate that an increase in stability is observed as the level of truncation increases from the intact protein to truncate Y7, so over the range of the first 7 N-terminal amino acids a decrease is observed in the number and amount of cleavage proteins. However, the stability decreases sharply upon loss of the Y⁷ amino acid to give truncate D8. Stability then increases again for the truncated proteins from residues A⁹ to Q¹³. These observations are schematically represented in Figure 7.10, which graphically displays the level of intact protein remaining over time for each of the truncates with respect to their level of truncation.

Figure 7.10: Graphical representation of the change in the stability of protein B which occurs upon N-terminal truncation of the protein.

Schematic representation of the data from mass spectrometry analysis of truncate protein samples (~ 6 mg/ml) incubated at 20 °C over time. The graph illustrates the relationship between the level of protein B truncation and the point in time, after incubation, at which intact protein was observed.



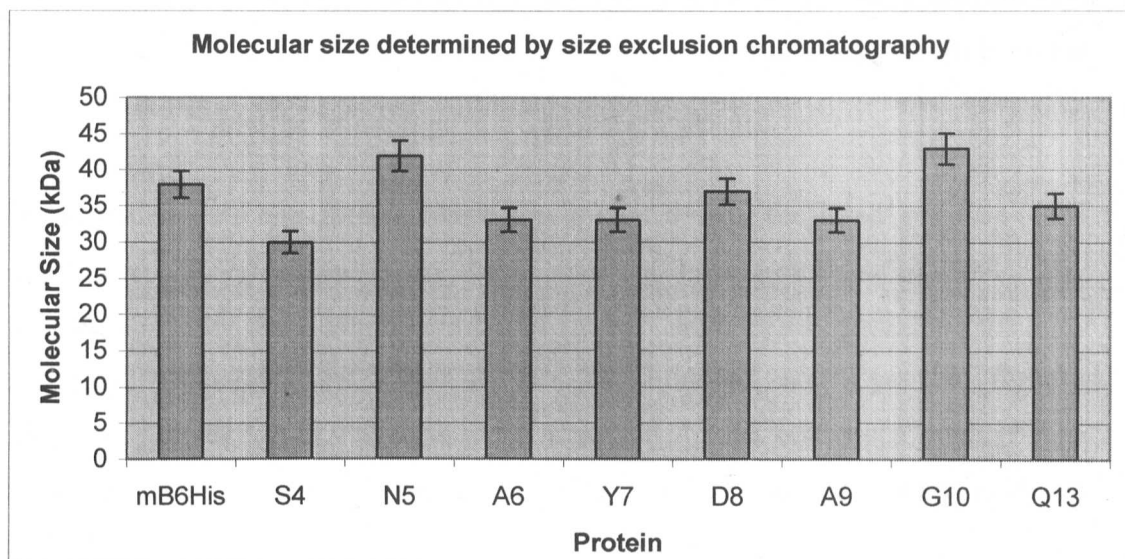
A dramatic change in the level of stability of the protein B truncates was observed between truncates Y7 and D8, the site at which activity within the sMMO complex assay was also lost. Therefore, this could imply that the factor responsible for increasing the stability of the Y7 truncate is lost upon removal of this amino acid, and it could be the loss of this factor which is responsible for the inactivity of the D8 truncate. Analysis of the structure of the proteins was, therefore, undertaken in an attempt to determine whether the significant factor observed could be related to the structure of protein B.

7.5.3 Comparison of the molecular dimensions of the truncated proteins by size exclusion chromatography

As previously mentioned (Section 7.4), SDS-PAGE analysis had indicated the molecular masses of the truncated proteins to be correct, a result which was confirmed by ESI-MS analysis. Therefore, a comparison of the molecular dimensions of the protein B truncates was undertaken using size exclusion chromatography. It is due to the fact that proteins vary considerably in shape from, for example, spherical to ellipsoidal, that gel filtration gives information on the molecular size but not generally molecular mass. As the molecular masses of the truncated proteins were known accurately, any deviation from these values could be seen as reflecting a difference in molecular shape between the proteins. It had previously been shown that the activity of protein B had been lost within the sMMO assay by the loss of the first 7 amino acids from the N-terminus of the protein. It was, therefore, considered important to determine whether any change in the molecular dimensions of the protein could be observed. The truncated proteins were, thus, subjected to size exclusion chromatography on the Superdex 75 FPLC column (Amersham Pharmacia Biotech, Burks., UK) and the elution volume for each was recorded and the molecular size inferred from the calibration curve (Figure 7.11) (Chapter 2, Section 2.9).

Figure 7.11: Size exclusion chromatography of protein B truncates.

Molecular size values displayed were inferred from the calibration curve. 5 % error bars are displayed.



The molecular sizes inferred from the data suggest the truncated proteins to range from 30-43 kDa (Figure 7.11). These data are in agreement with the size obtained for wild-type *Mc. capsulatus* (Bath) protein B (Chapter 4) of 35 kDa. The range of sizes observed indicates that the truncation of protein B causes slight changes in the molecular dimensions, such that the proteins elute slightly differently from the intact, wild-type protein B, but not significantly, as they are all roughly within the 5 % error range. Recent work by Brandstetter *et al.* (1999) suggested that the N-terminus of protein B was responsible for its anomalous migration in size exclusion chromatography. The truncation mutant they studied, which lacked the first 25 amino acids from the N-terminus, was shown to run as expected for its molecular mass on a gel filtration column, whereas the wild-type protein eluted at a higher retention volume. Here it has been shown that the truncation of the N-terminus of protein B up to residue 13 does not have a great enough effect on the N-terminus to enable elution at a retention volume closer to that expected for the molecular mass of protein B itself. Thus, the first 13 N-terminal amino acids are effecting the migration of the truncate proteins to give a molecular size equivalent to that of the wild-type protein.

7.5.4 Theoretical secondary structure determination of the N-terminus region of the protein B truncates

It was possible that a change in secondary structure of the N-terminal region of protein B was responsible for the change in stability at the Y⁷-D⁸ site. Consequently, a theoretical approach was used to elucidate the effect of truncating protein B on the secondary structure of the protein within this region.

The secondary structure of the proteins was predicted using the Jpred² program (Cuff and Barton 1999), available on the internet at <http://jura.ebi.ac.uk:8888/>. The program works by combining a number of modern, high quality prediction methods including PHD, DSC, PREDATOR, NNSSP, Mulpred, and Zpred to form a consensus (Jpred). A 72.9% accuracy is expected for the consensus method. The consensus secondary structure predictions for each of the truncate proteins is shown in Figure 7.12.

Figure 7.12: Secondary structure predictions of each of the truncated proteins of protein B from *Mc. capsulatus* (Bath) using the Jpred² program.

The first 34 N-terminal amino acids are shown with their corresponding secondary structure predictions. H indicates α -helix nature and E, extended conformation.

```

YourSeq      : MSVNSNAYDAGIMQLKGFADQFFADENQVVHE : YourSeq
cons         : -----HHHHHHHHHHHHHHHHHHHHHHHHHHHH----- : cons G13Q-His-tag
cons         : ---HHHHHHHHHHHHHHHHHHHHHHHHHHHHHHHHHHHH--- : cons S4-His-tag
cons         : ---HHHHHHHHHHHHHHHHHHHHHHHHHHHHHHHHHHHH--- : cons N5-His-tag
cons         : ---HHHHHHHHHHHHHHHHHHHHHHHHHHHHHHHHHHHH--- : cons A6-His-tag
cons         : -----HHHHHHHHHHHHHHHHHHHHHHHHHHHHHHHHHHHH--- : cons Y7-His-tag
cons         : -----HHHHHHHHHHHHHHHHHHHHHHHHHHHHHHHHHHHH--- : cons D8-His-tag
cons         : ---EE-----HHHHHHHHHHHHHHHHHHHHHHHHHHHHHHHHHH--- : cons A9-His-tag
cons         : --EEEE-----HHHHHHHHHHHHHHHHHHHHHHHHHHHHHHHHHH--- : cons G10-His-tag
cons         : -----HHHHHHHHHHHHHHHHHHHHHHHHHHHHHHHHHHHH--- : cons Q13B'

```

The NMR structure of protein B from *Mc. capsulatus* (Bath) was published very recently, after this work had been conducted. Nevertheless, the secondary structure data determined provided a possible insight into the effect of truncating protein B on the secondary structural features of the N-terminal region of the protein.

The secondary structure data predicts a sudden decrease in the content of α -helix for truncates Y7 and D8 compared to truncates A6, N5, S4 and the intact protein, with extended conformations being predicted for truncates A9 and G10. These factors may be involved in the reason for the inactivity of the truncated proteins upon truncation from residue D⁸ onwards. However, truncates Y7 and D8 were predicted

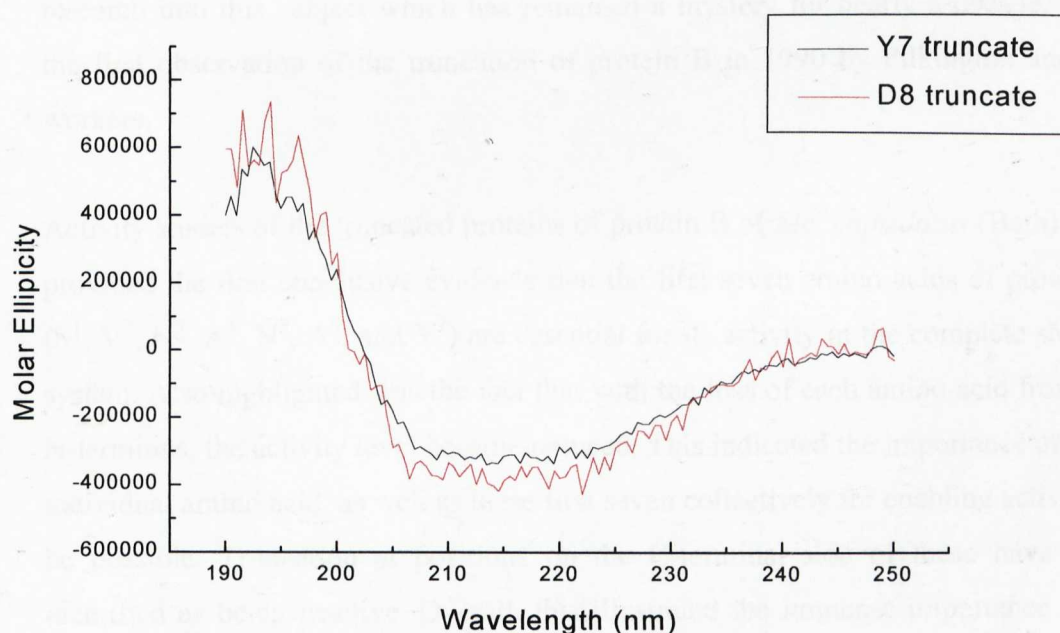
to have the same secondary structure within the N-terminal region and, therefore, the reason for the sudden loss in activity upon removal of the Y⁷ amino acid is not due to a secondary structure change being induced. Even if the secondary structure predictions are not as accurate as expected, they still provide a means to compare the effect of truncation upon the possible structure of the proteins computationally. Experimental secondary structure determination was undertaken to gain further insights into the reason for the loss of activity upon truncation of the protein.

7.5.5 Secondary structure determination of the truncated proteins

It was an important observation that the site at which activity was lost was the same as that at which the level of stability of the protein truncates decreased. Similarly, a decrease in the proportion of alpha helix content of the N-terminal region of the protein occurred within this region. CD studies of truncates Y7 and D8 were carried out to determine whether a difference in secondary structure could be observed (Figure 7.13).

Figure 7.13: Far UV CD spectra of the Y7 and D8 truncated proteins of protein B from *Mc. capsulatus* (Bath).

The CD spectra were recorded on a Jasco J715 spectropolarimeter at room temperature (Chapter 2, Section 2.18). The spectra shown are averages of 10 scans of each truncate protein (0.25 mg/ml) in 50 mM phosphate buffer, pH 7, in a 1 mm pathlength quartz cuvette.



The spectra both have minima at 208 nm and 222 nm and a maximum at 192 nm, indicative of a moderate proportion of alpha helix present in both proteins. The spectra are similar to those obtained for protein B itself and suggest that there is not a great structural difference between the two truncated proteins. They also indicate the truncates to have the same secondary structure as protein B itself, so the loss in activity at the Y⁷-D⁸ site cannot be accounted for by a loss of secondary structure of the inactive D8 truncate protein.

7.6 Conclusion

The development of a system for the expression of the protein B truncates, incorporating a C-terminal 6-His-tag, and for their rapid and simple affinity purification, has proved to be a most efficient method for obtaining highly pure samples of the proteins. The cloning method had the added advantage of incorporating no extra amino acids at the N-terminus, thus allowing the accurate study of reactions occurring within this region of the protein. Therefore, the availability of pure samples of the protein B truncates proved vital in facilitating the study of protein B to B' formation. The use of this system for the expression and purification of protein B truncates is, therefore, of importance for the continuation of research into this subject which has remained a mystery for nearly a decade, since the first observation of the truncation of protein B in 1990 by Pilkington and co-workers.

Activity studies of the truncated proteins of protein B of *Mc. capsulatus* (Bath) have provided the first conclusive evidence that the first seven amino acids of protein B (S¹, V², N³, A⁴, N⁵, A⁶, and Y⁷) are essential for its activity in the complete sMMO system. Also highlighted was the fact that with the loss of each amino acid from the N-terminus, the activity level became reduced. This indicated the importance of each individual amino acid, as well as these first seven collectively for enabling activity to be possible. Truncation at positions on the C-terminal side of these have been identified as being inactive. Overall, this illustrated the immense importance of so few amino acids with respect to involvement in conveying protein B activity.

Upon the loss of the Y⁷ amino acid to form the inactive D8 truncate protein, the stability of the protein was observed to decrease dramatically. It had been presumed possible that with increasing levels of truncation of protein B, stability to cleavage would improve, as the proposed mobility of the N-terminal region would be reduced as it became shorter. The observation of the sudden change in stability at the site at which activity was lost also suggested that the Y⁷ amino acid was vital for the stability and activity of protein B. Nevertheless, no significant change in overall or secondary structure was observed between the significant truncates, Y7 and D8.

The crucially important seventh amino acid, tyrosine, contains an –OH group as part of its side chain moiety. It is possible that the hydroxyl group forms an intermolecular hydrogen-bond with an amino acid side chain group on the surface of the core region of the protein, maintaining the N-terminal region in a specific orientation, essential for activity. Upon the loss of Y⁷, this essential conformation would be lost, preventing protein B from being active within the sMMO complex. It would also increase its instability, as it would result in the exposure of the remaining N-terminal region, thus allowing it to contact other groups which could bring about autocatalytic degradation (possibly via the autocatalytic mechanism proposed in Chapter 4). The weakening and resultant loss of this proposed important hydrogen bond might well occur routinely upon purification of protein B and so enable the cleavage reactions observed to be possible.

This work also opens up a number of further possibilities to be tested. These would include determining the binding affinities of each of the truncates to the other sMMO components and identifying in what respect the inactive truncates prevent sMMO activity from occurring. For example, it could be elucidated if any change in the redox potentials of the hydroxylase occurs upon the addition of the truncates. Overall, the development of this system for the expression and purification of the protein B truncates will prove invaluable in enabling further studies into the roles of protein B and its truncates within the sMMO system, and possibly within *Mc. capsulatus* (Bath) cells, to be finally understood.

Chapter 8

Component Interactions of sMMO

8.1 Introduction

In recent years there has been much progress towards understanding the mode of action of sMMO. In particular the crystallisation of the hydroxylase component (Rosenzweig *et al.*, 1993) allowed detailed examination of the residues involved in substrate binding and oxygen activation. Insights into local conformational changes and perturbations, that occur upon di-iron centre reduction or protein B binding, have been investigated, using techniques such as electron paramagnetic resonance (EPR), electrochemistry, circular dichroism (CD), magnetic circular dichroism (MCD), extended X-ray absorption fine structure (EXAFS) and fluorescence spectroscopy (Woodland *et al.*, 1986; Fox *et al.*, 1991; Froland *et al.*, 1992; Paulsen *et al.*, 1994; Rosenzweig and Lippard, 1994; Kazlauskaitė *et al.*, 1996; Coates-Pulver *et al.*, 1997; Davydov *et al.*, 1997). Knowledge of the physical interactions of the individual sMMO components, however, is limited, as the lack of a crystal structure of the sMMO complex means that it remains uncertain as to the precise stoichiometry and arrangements of the components within the complex. The crystal structure of the hydroxylase identified it as a dimer consisting of two trimers of the α , β , and γ subunits. From this data it was proposed that two equivalents of each of the reductase and protein B would be required to bind to each trimer of the hydroxylase dimer (Rosenzweig *et al.*, 1993). Evidence, such as surface plasmon resonance measurements, also indicated that the components bound in a 1:2:2 hydroxylase:protein B:reductase molar ratio (Lloyd *et al.*, 1997). Tentative assignments as to the binding sites of protein B and the reductase on the hydroxylase have been provided by cross-linking studies of sMMO from *Ms. trichosporium* OB3b (Fox *et al.*, 1991). Thus, as no studies have been conducted which give direct information on the relative disposition of the components within the complex or global conformational changes that may occur, this aspect of investigation has been undertaken in this study.

The techniques of single particle analysis by electron microscopy (SPA), atomic force microscopy (AFM) and small angle X-ray scattering (SAXS) have been used as powerful techniques for probing conformational changes and gaining information on the relative disposition of the components within the complex. This Chapter details the findings of this work.

8.2 Single particle analysis by electron microscopy

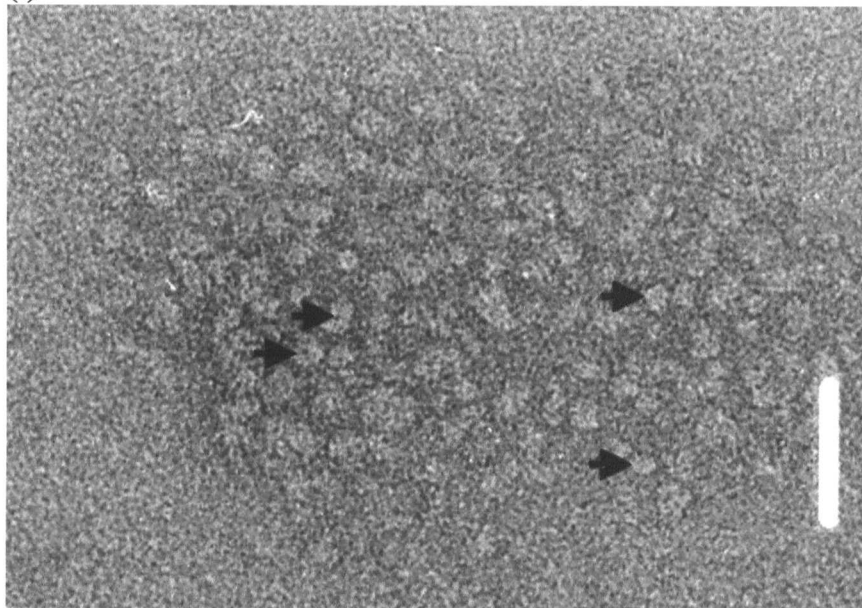
Electron microscopy (EM) is used to visualise how subunits interact in high-order, functional complexes, and image conformational changes which occur to control the assembly and activation of many protein complexes. The resolution of electron micrographs is limited when contrasted with that for X-ray crystallography. Proteins tend to give noisy images, even when micrographs are recorded using the most advanced instruments. However, the use of digital image processing largely overcomes this drawback.

Analysis of sMMO using this technique was undertaken in collaboration with Drs Bob Ford and Mark Rosenberg (Department of Biomolecular Sciences, UMIST, UK). Electron micrographs of (i) the hydroxylase, and (ii) the sMMO complex were recorded using a Philips CM100 electron microscope (Chapter 2, Section 2.20), so that comparisons could be made between the conformation of the hydroxylase alone and when in complex with the other sMMO components. Typical micrographs for the hydroxylase and sMMO complex are shown in Figure 8.1.

Figure 8.1: Typical electron micrographs of negatively stained (i) hydroxylase and (ii) sMMO complex.

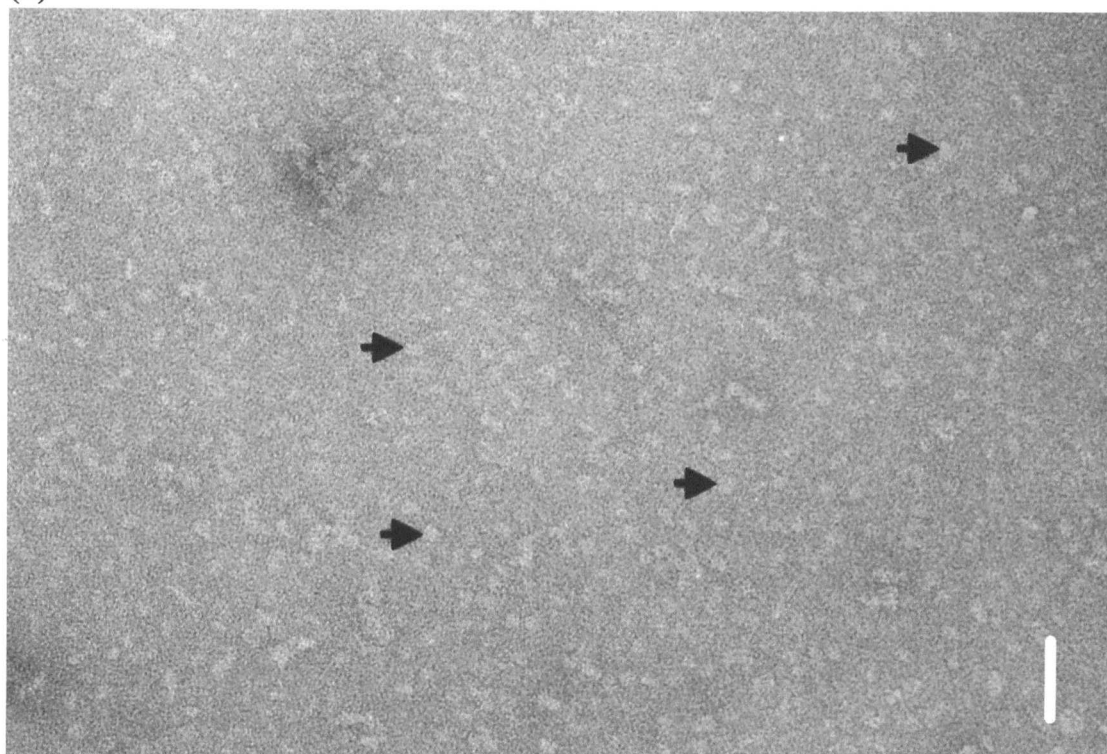
The proteins (i) hydroxylase (0.05 mg/ml) and (ii) sMMO complex (1:2:2) ratio of hydroxylase:protein B:reductase (0.1 mg/ml) were immobilised on carbon-coated EM grids and negatively stained with 4 % uranyl acetate. Electron micrographs were recorded at $\times 83$ -104 k magnification and scanned at a resolution of 5.4 Å/pixel. Arrows point to particles of the hydroxylase protein in (i) and the sMMO complex in (ii).

(i)



Bar = 40 nm/400 Å

(ii)



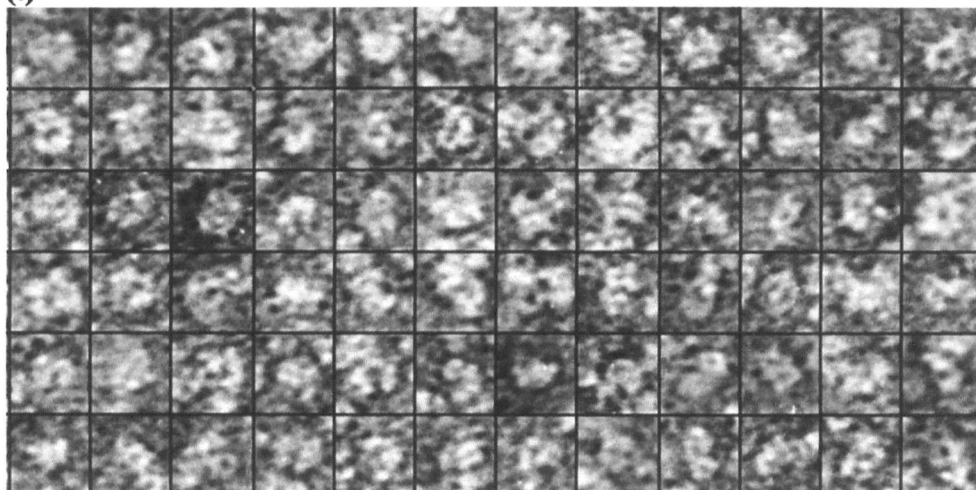
Bar = 60 nm/600 Å

Single particle analysis was carried out on the micrographs using SPIDER (Frank *et al.*, 1996). Particles were selected using Ximdisp (Chapter 2, Section 2.20), examples of which are shown for the hydroxylase and the sMMO complex in Figure 8.2.

Figure 8.2: Samples of the particles selected for SPA work from (i) the micrograph of the hydroxylase and (ii) the micrograph of the sMMO complex.

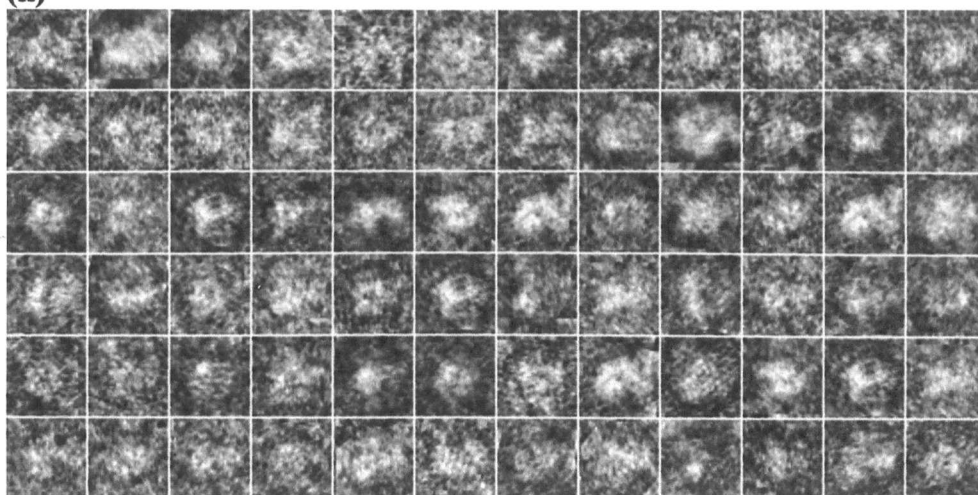
The sizes of the particles are indicated.

(i)



—
130 Å

(ii)



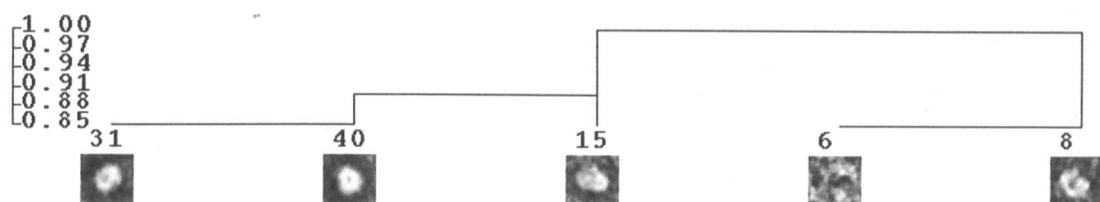
—
160 Å

Particles were subjected to an alignment procedure involving the use of an iterative process of cross-correction and auto-correction to rotationally align the molecules in their characteristic orientations. These were finally classified into groups, in order to produce average, refined images, as illustrated by the dendograms in Figure 8.3.

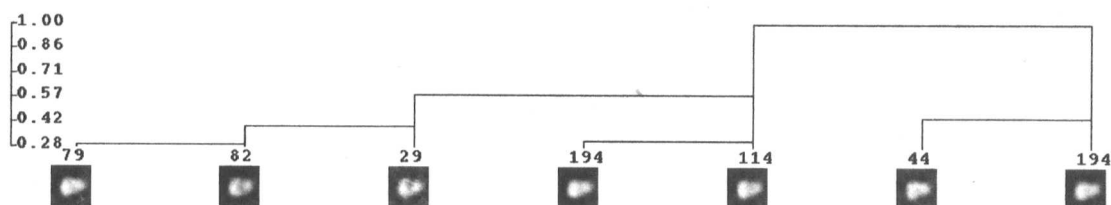
Figure 8.3: Dendogram representation of groups of particle averages of (i) the hydroxylase protein and (ii) the sMMO complex.

Selected particles (100 of the hydroxylase and 736 of the complex) were subjected to reference free translation and rotational alignment. Aligned particles were clustered into groups, based on a hierarchical method, so that averages of similar particles could be calculated (Chapter 2, Section 2.20). Groups of particle averages are visually displayed with their numerical value.

(i)



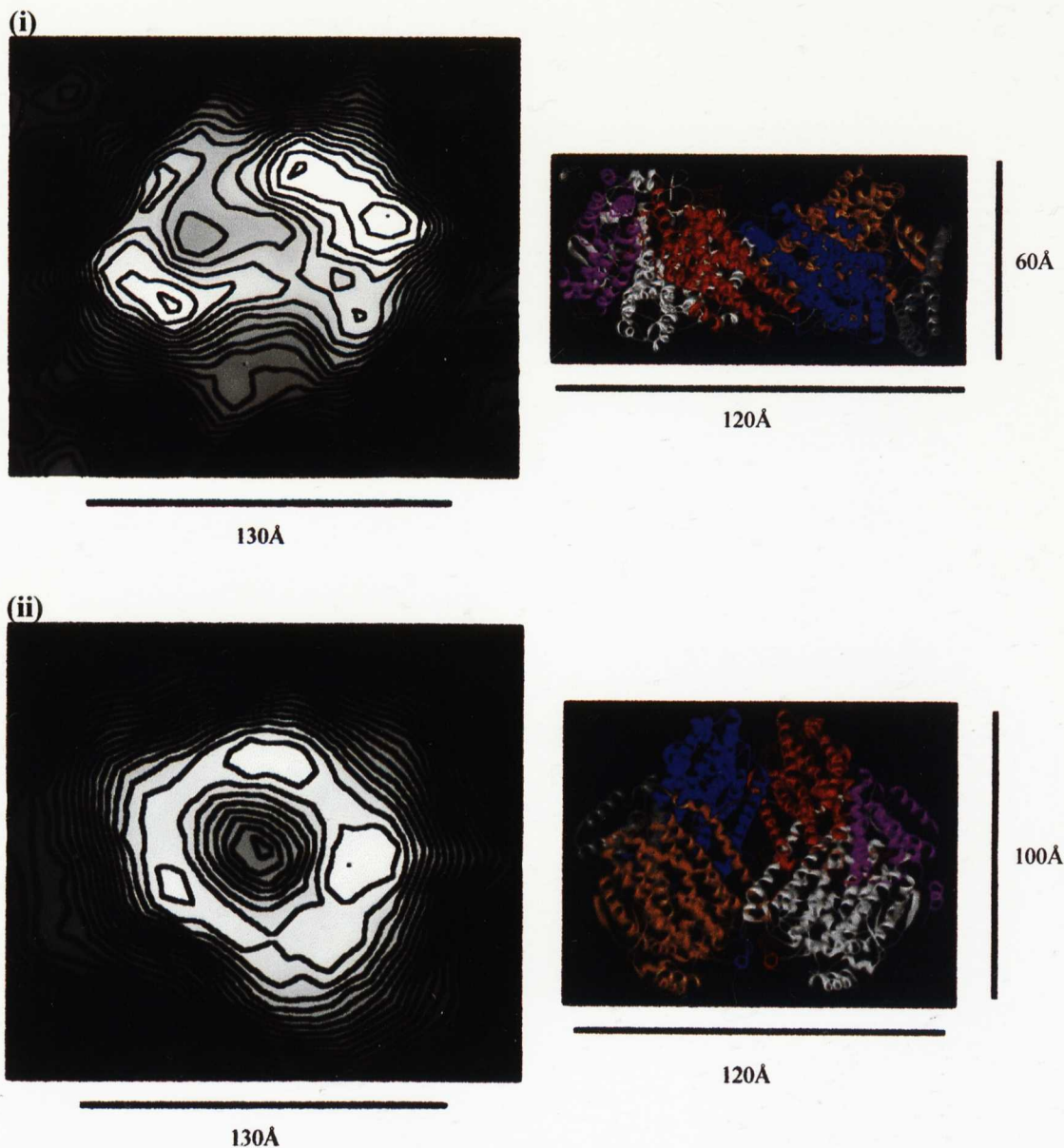
(ii)



The particle analysis studies identified two distinct species present within the hydroxylase sample, corresponding to particle averages 31 and 40 in Figure 8.3(i). These were identified as corresponding to the protein in two different orientations by analysis of their dimensions and indications of their structures. The two orientations are illustrated in Figure 8.4 where they are displayed next to the crystal structure in the same orientation.

Figure 8.4: Electron contour maps of the hydroxylase particle averages (i) 31 (Side View) and (ii) 40 (Front View) with the crystal structure (Rosenzweig *et al.*, 1993) in the same orientation.

Size values are indicated.

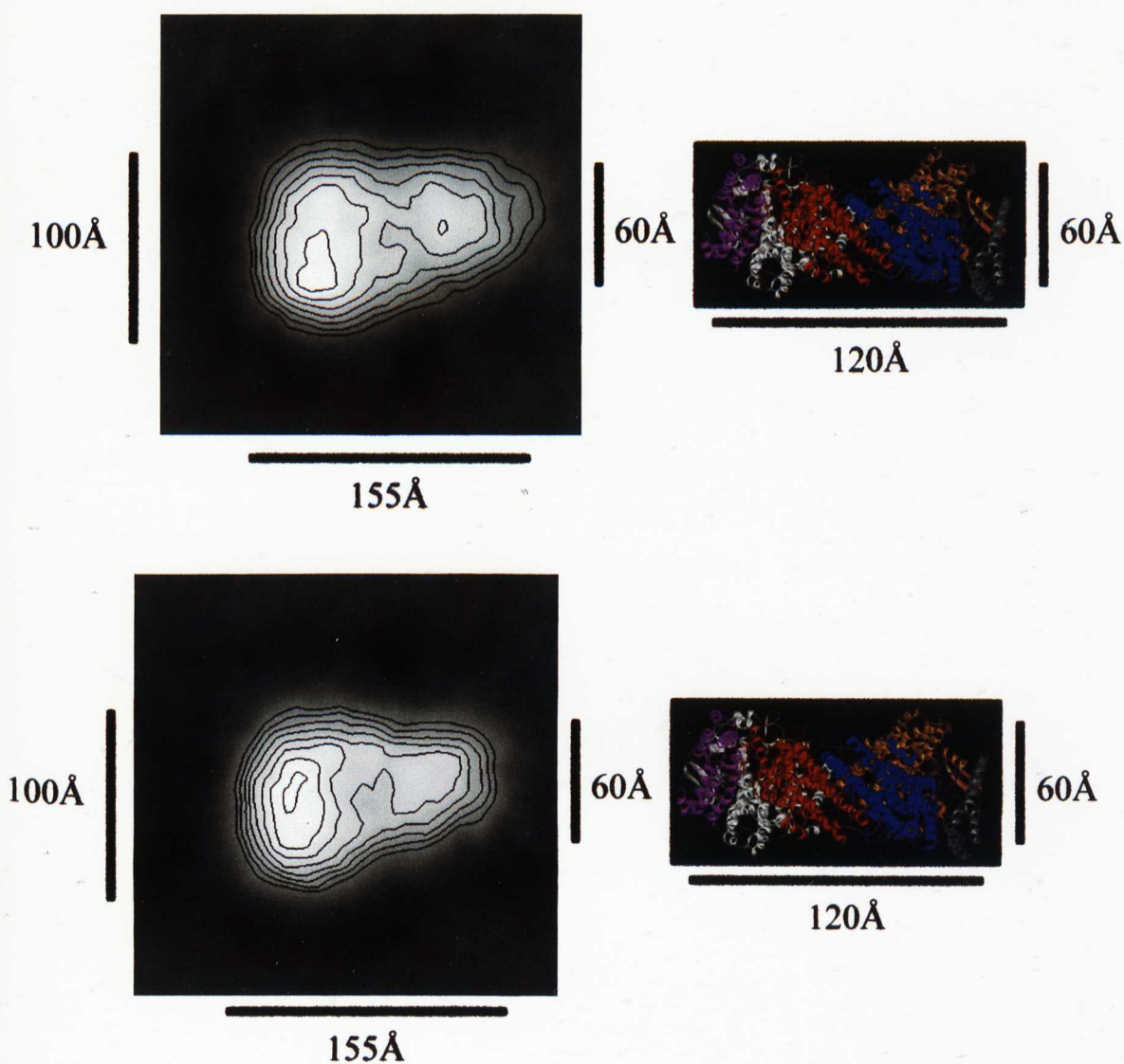


The hydroxylase was visualised as having approximately the same dimensions as those determined for the crystal structure of the protein (Rosenzweig *et al.*, 1993). It was, therefore, observed as retaining its bi-lobed dimer form at the low concentrations used here. The resolution of the SPA data is approximately 30 Å compared to the atomic resolution of 2.2 Å for the crystal structure data.

The particle analysis studies for the complex identified various groups of particles, differing from one another in orientation and resolution (Figure 8.3 (ii)). However, in each case the particles were identified as being of increased length (155 Å), compared to the particles of hydroxylase alone (Figure 8.4), and enlarged at one end to form an approximate 'pear' shape. The two largest particle average groups, both corresponding to particle averages of 194 (Figure 8.3 (ii)), were of increased resolution compared to the other groups and clearly illustrated this point (Figure 8.5).

Figure 8.5: Electron contour maps of the sMMO complex displayed with the crystal structure of the hydroxylase (Rosenzweig *et al.*, 1993) in the orientation in which it is thought to be present within the complex.

Particle averages of the two largest particle average groups are displayed. Size values are indicated.



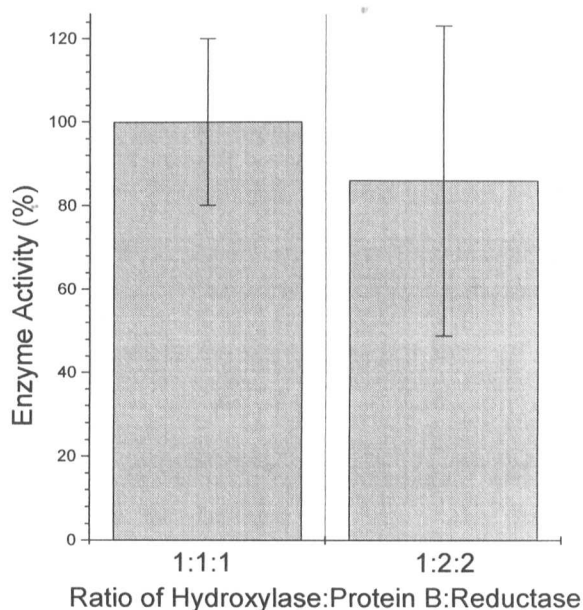
In both cases analysis of the complex dimensions and indications of structure suggest that the hydroxylase is present in the side view orientation (Figure 8.5). The images indicate there to be an increase in size only for one trimer of the hydroxylase dimer and consequently the 2-fold symmetry is not preserved. This would imply that only one trimer of the hydroxylase molecule is involved in binding to protein B and/or the reductase under the conditions of the experiment, whilst the second trimer remains unchanged. Resolution assessment of the complex data indicated it to be ~ 50 Å.

Formation of the sMMO complex by addition of the hydroxylase, reductase and protein B at molar ratios of 1:5:5 was undertaken in an attempt to improve complex formation and determine whether or not the 1:2:2 complex could be observed. This study, however, failed in producing large quantities of complexed protein, as ascertained by viewing the EM grid. Large amounts of smaller proteins, probably protein B and the reductase, were observed supporting the idea that complex formation had not been complete.

The data acquired therefore indicate that the complex does not exist in a 1:2:2 ratio of hydroxylase:reductase:protein B, as predicted for the binding of one molecule of each of protein B and the reductase to each trimer of the hydroxylase dimer (Rosenzweig *et al.*, 1993). Propylene oxidation activity assays were conducted to determine whether any increase in activity was observed for the complex formed at the 1:2:2 ratio, compared to that observed for the complex formed at a 1:1:1 ratio of hydroxylase:reductase:protein B. The results are shown in Figure 8.6.

Figure 8.6: Activity assays for the sMMO complex formed at different ratios of hydroxylase:protein B:reductase.

sMMO propylene oxidation assays (Chapter 2, Section 2.12.1) were performed for the 1:1:1 ratio of hydroxylase:protein B:reductase by mixing 8 μ M aliquots of the hydroxylase, protein B and reductase. For the 1:2:2 ratio of hydroxylase:protein B:reductase, 16 μ M aliquots of protein B and the reductase were added to 8 μ M of the hydroxylase. Enzyme activity is shown as a percentage of the activity of the 1:1:1 reaction which represents 1956 nmol/min/mg. The data shown are the mean of 3-4 sMMO assays for each reaction. Standard error bars are shown.



No significant difference was observed for the activity of the complex assayed under the two different conditions. This indicated that the reductase and protein B were not rate limiting when the complex was assayed at the 1:1:1 molar ratio of hydroxylase:protein B:reductase, since an increase in the ratio of these proteins gave no increase in activity. This evidence supported the SPA observations that only one half of the hydroxylase dimer was participating in binding (as activity was observed at its optimum level under these conditions). However, in the absence of studies to identify the level of iron present or the presence of damaged sites in the hydroxylase protein used in these experiments, it is unclear whether these observations are as a consequence of iron depleted or damaged hydroxylase lowering its activity and level of binding to the other sMMO components.

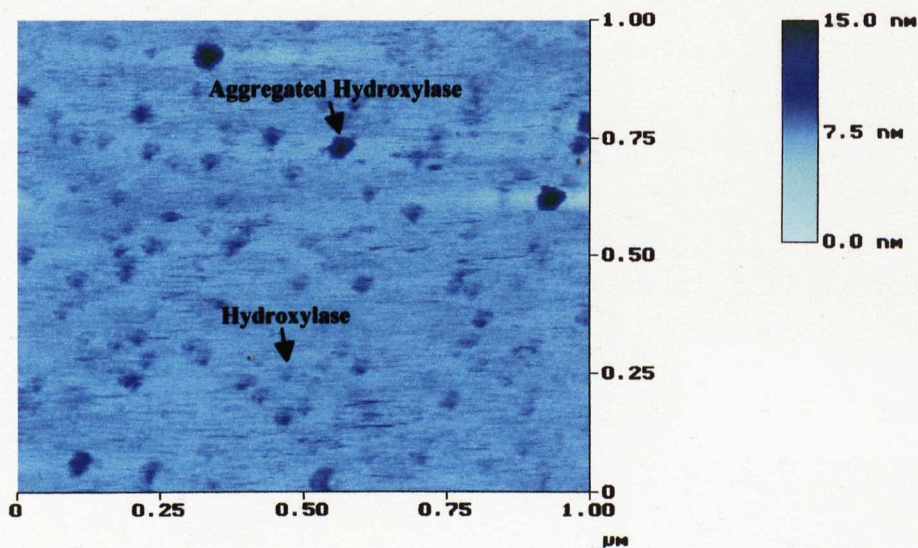
8.3 Atomic force microscopy

Atomic force microscopy or scanning force microscopy, as it is often referred to, is a powerful tool for the investigation of biological structures. Invented in 1986, it yields three-dimensional low-resolution structural information (Binnig *et al.*, 1986). As mentioned in Chapter 4, the technique is based on the movement of a sharp tip at the free end of a soft cantilever which scans over a sample keeping the tip at almost touching distance from the sample surface. The tip and cantilever movement is coupled to an optical readout system for monitoring the bending of the cantilever induced by the surface topography and thus digitally reproduces the topography of the sample surface (Schaper and Jovin, 1996). The technique was used to compare the structures of the hydroxylase protein alone, to that of the sMMO complex to determine whether any conformational change in the hydroxylase could be observed upon addition of the other components, protein B and the reductase. Fluid AFM analysis was conducted in an attempt to retain the proteins in their native conformations.

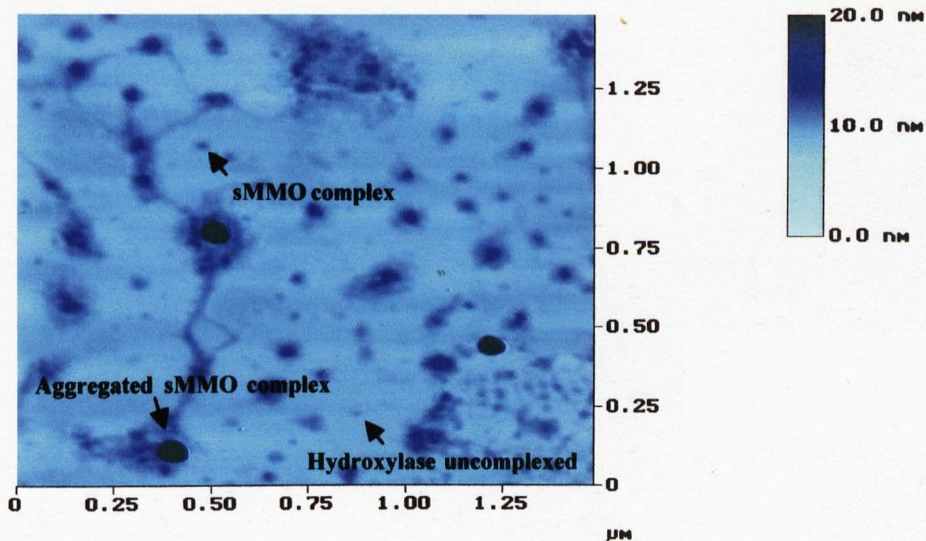
In collaboration with Mr. Bernie Sattin (Department of Chemistry, University of Toronto, Canada), samples of hydroxylase and the sMMO complex, prepared in a 1:2:2 ratio of proteins hydroxylase:protein B:redutase were analysed using this technique (Chapter 2, Section 2.26). The fluid AFM images obtained for the hydroxylase and the sMMO complex are shown in Figure 8.7.

Figure 8.7: Tapping mode AFM images of (i) the hydroxylase and (ii) the sMMO complex. Labeled are samples of the hydroxylase, sMMO complex and aggregates of the proteins.

(i)



(ii)



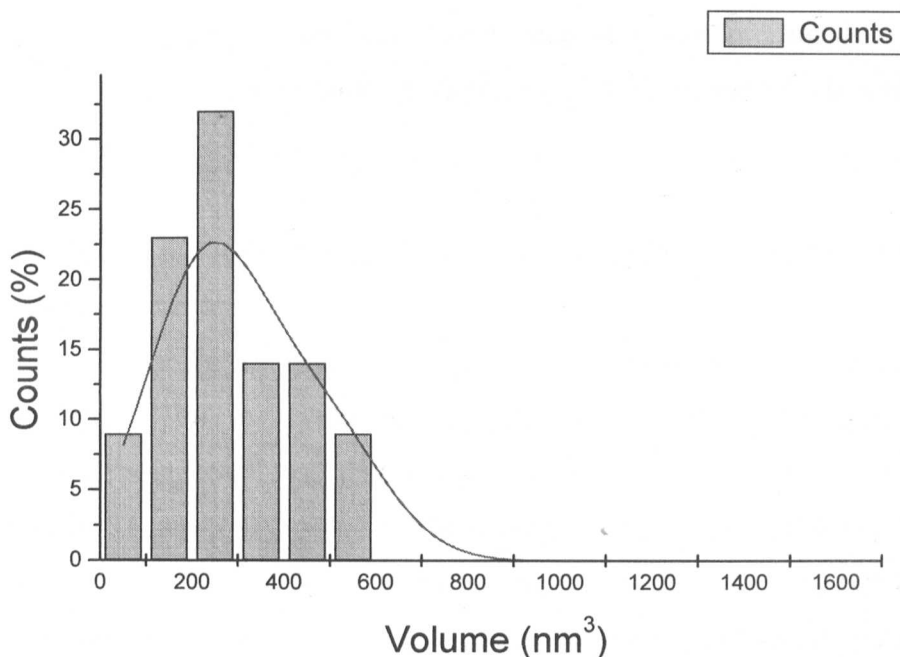
The images indicate that under the conditions of the experiments, the sMMO proteins had a tendency to aggregate (Figure 8.7). However, this did not significantly interfere with the process of data collection for the various particles observed. Analysis showed the hydroxylase sample to be fairly homogeneous and the proteins

to have immobilised in almost the same orientation on the mica surface in each case, as seen by the uniformity of the sample surface (Figure 8.7 (i)). In the case of the sMMO complex sample, some hydroxylase was seen to be unbound, whilst other particles appeared larger in size, correlating with complex formation (8.7(ii)). The volumes of the particles imaged in both cases were determined and the distribution of the observed volumes for the samples are shown in Figure 8.8.

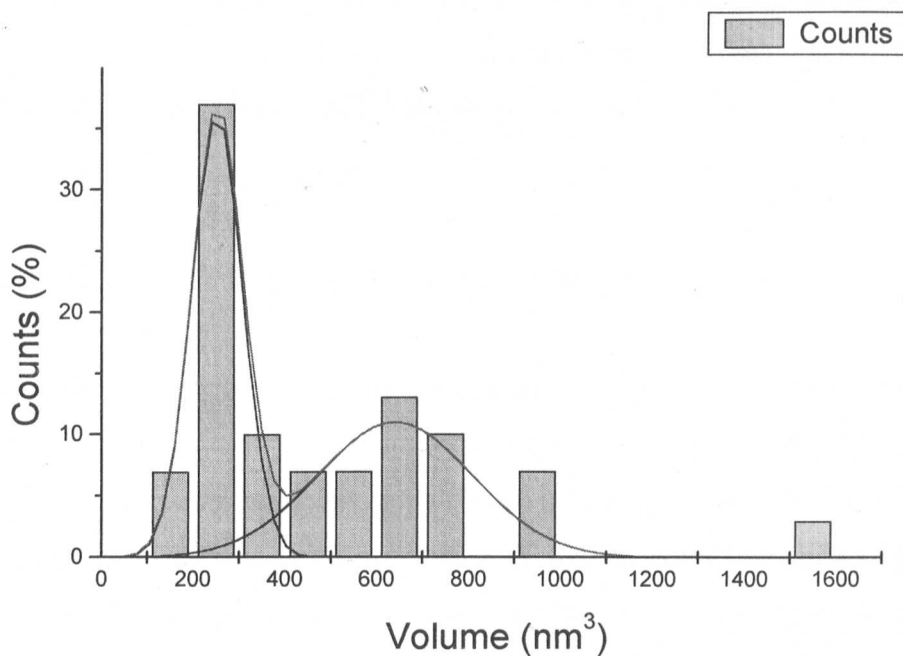
Figure 8.8: Distribution of the observed volumes of (i) hydroxylase and (ii) sMMO samples.

Observed volumes data analysed using Origin™ 4.10 software (Microcal Software Inc., USA).

(i)



(ii)



The graphs indicate that the hydroxylase has been observed by this technique as having a volume of $\sim 250 \text{ nm}^3$ (Figure 8.8 (i)). This particle size constitutes the largest proportion of particles in the sMMO complex sample (Figure 8.8 (ii)), further verifying that complex formation was incomplete, and much uncomplexed hydroxylase remained in solution. The second peak observed for the sMMO sample (Figure 8.8 (ii)) at a volume of $\sim 650 \text{ nm}^3$ is presumed to correspond to aggregates of the hydroxylase and the other proteins, as it would be too large to be the complex itself, being over double the size of the constituent hydroxylase protein. The varying particle volumes, in between and larger than this, are presumed to similarly correspond to aggregates of varying quantities of the proteins which constitute the complex itself.

The imaging of the reductase and protein B separately, in order to determine the sizes of the molecules under the conditions of fluid AFM analysis were also conducted, so that the composition of the complex could be identified, had it been formed clearly. However, it was only possible to conduct AFM imaging after the samples had been dried, and thus the various volumes obtained for the particles observed could not be compared to those obtained under fluid imaging. Similarly, difficulties were encountered when attempting to visualise the hydroxylase:protein B':reductase complex under fluid, which would have been an interesting comparison to the active sMMO complex, and determined whether indeed the complex did form. Overall, the technique proved to be problematic, as much protein aggregation meant that difficulties were encountered throughout.

8.4 Small angle X-ray scattering (SAXS)

The technique of SAXS, as mentioned in Chapter 4, is a valuable tool for studying the structural basis for biomolecular function, revealing details of functionally important conformational flexibility and interactions by the study of the conformations of biomolecules in solution as well as within functional complexes. SAXS is applicable to molecules and molecular assemblies ranging in sizes from 10-

1,000 Å (Trehella *et al.*, 1998). SAXS is thus ideally suited to the analysis of the sMMO proteins individually and in complex.

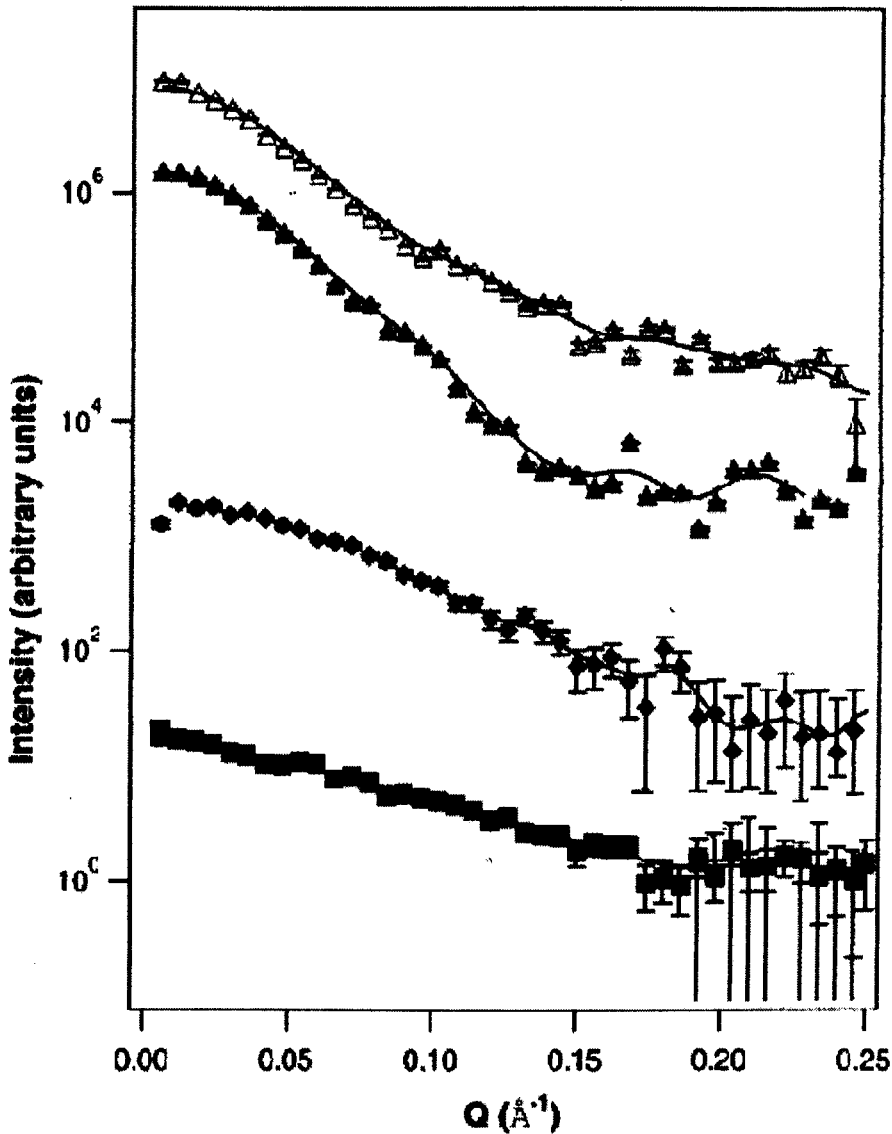
X-rays can be produced with wavelengths ranging from ~ 0.1 -100 Å and can therefore probe the most important dimensions of biomolecular structures (1-1000s Å). Upon encountering a particle in solution a small proportion of the X-rays will be deflected or 'scattered'. The structure of the particle dictates the angular dependence of the scattering. Solution scattering is therefore referred to as 'small-angle' scattering. The scattering data from a particle details structural information on the overall size and shape of the molecule. Scattering data is dependent on geometric shape and is therefore very highly sensitive to domain orientations, and thus conformational changes and/or flexibility, as well as molecular associations in solution (Trehella *et al.*, 1998).

The technique was used to study the stoichiometry and arrangements of the sMMO components within the complex in solution, and determine whether any shape changes occurred upon complex formation. SAXS studies were carried out in collaboration with Drs J. Trehella and S. Gallagher (Los Alamos National Laboratory, New Mexico, USA) (Chapter 2, Section-2.25).

Solution scattering profiles of the sMMO complex and the isolated components were measured and are shown in Figure 8.9 together with the model $I(Q)$ profiles calculated using uniform ellipsoids for the reductase and protein B, and the crystal structure coordinates for the hydroxylase (Rosenzweig *et al.*, 1993). For the sMMO complex itself, the model profile was calculated using the model shown in Figure 8.15.

Figure 8.9: $I(Q)$ versus Q data for sMMO and its individual components.

Experimental data are depicted by the symbols; protein B (■), reductase (◆), hydroxylase (▲), sMMO (1:10:10 mixture = 1:2:2 complex) (△). The scattering profiles are offset by multiplication factor in order to separate them on the vertical axis for easy viewing (0.2, 4, 16, 258, and 4096, respectively). The errors indicated are based on counting statistics only. The solid lines represent the model $I(Q)$ profiles calculated using uniform ellipsoids for the reductase, protein B and B', and the crystal structure coordinates for the hydroxylase. For the sMMO complex the solid line represents the model profile calculated using the model shown in Figure 8.15.



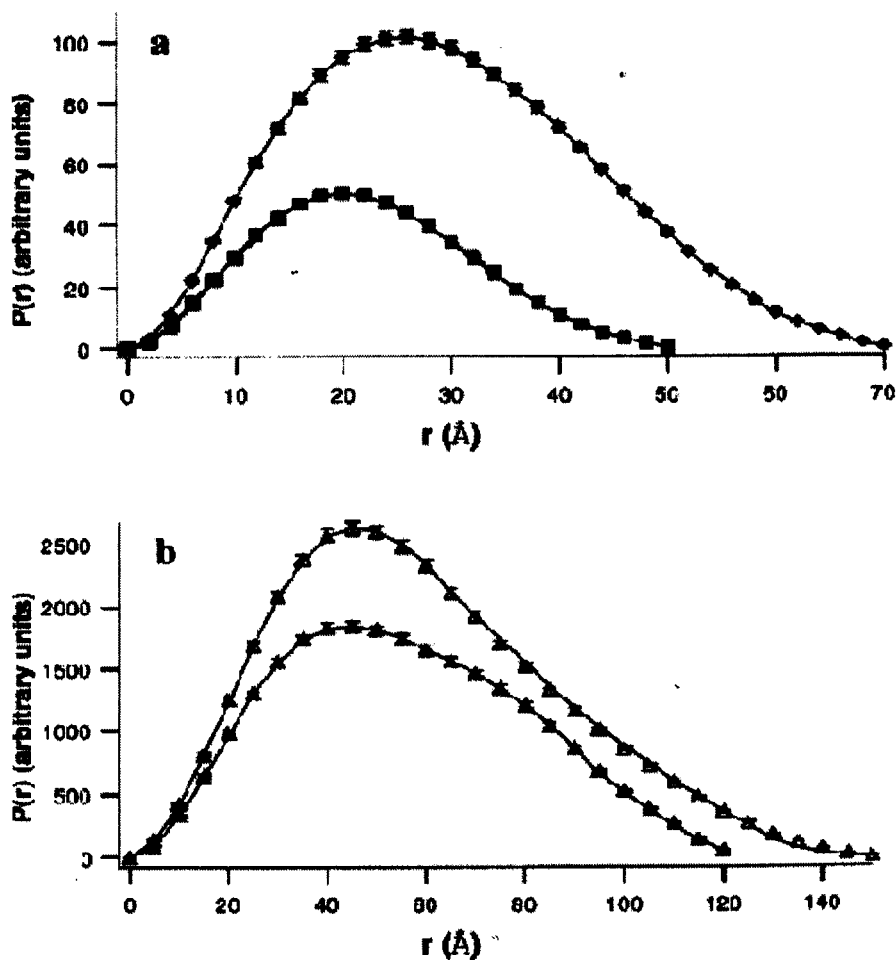
The scattering data were collected for the protein components of sMMO over a range of concentrations from 2 - 15 mg/ml, in 25 mM MOPS pH 7, 13 °C. For each component there was no concentration dependence of scattering data, indicating that

interparticle interference effects were negligible and, hence, no correction was required. As previously detailed in Chapter 4, the technique determined protein B to be monomeric in nature. Scattering data were measured from mixtures of the sMMO components with 1:1:1, 1:2:2, 1:5:5, 1:10:10 and 1:20:20 ratios of the hydroxylase:protein B:redutase. Analysis of the I_0 values indicated for the 1:10:10 mixture was consistent with the formation of the 1:2:2 complex with 8 free equivalents of the reductase and protein B. 1:2:2 complex formation was also observed for the 1:20:20 ratios of hydroxylase:protein B:redutase, with 18 free equivalents of protein B and reductase.

Pair distance, $P(r)$ or vector length distribution function, is a useful function in the interpretation of SAXS data. It is obtained by inverse Fourier transformation of the intensity $I(Q)$ versus Q . $P(r)$ is the frequency of vectors lengths connecting small-volume elements within the scattering particle weighted by their scattering densities and goes to zero at a value corresponding to the maximum dimension of the particle, d_{max} . R_g is calculated as the second moment of $P(r)$. $P(r)$ is sensitive to the symmetry of the scattering particle, and to the relationships between domains or repeating structures (Trehwella *et al.*, 1998). The $P(r)$ functions calculated for the scattering profiles are shown in Figure 8.10. The best fit ellipsoid models for the reductase and protein B have approximate dimensions of 72, 44, 32 Å and 50, 34, 30 Å respectively. These models give reduced χ^2 values of 1.03 and 1.01 respectively indicating a near perfect fit which would have $\chi^2 = 1.0$. The model $P(r)$ function was calculated using the crystal structure coordinates (Rosenzweig *et al.*, 1995) which gives a fit of $\chi^2 = 0.99$.

Figure 8.10: $P(r)$ functions for sMMO and its individual components.

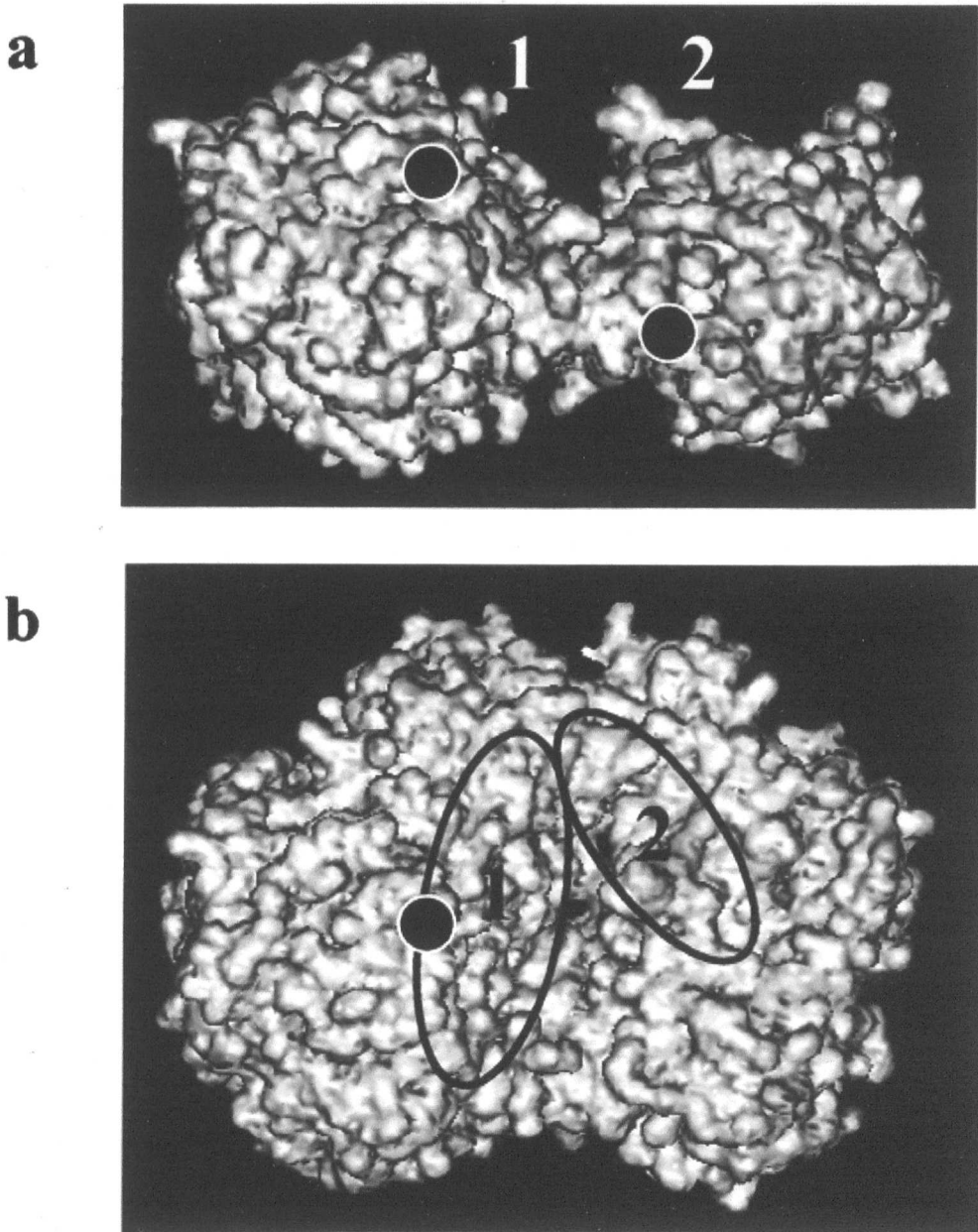
The experimentally derived functions for (a) protein B (■), reductase (◆), and (b) hydroxylase (▲), sMMO (1:10:10 mixture = 1:2:2 complex) (△). The solid lines are the $P(r)$ functions calculated for the models indicated in Figure 8.9. The $P(r)$ profiles are scaled such that their areas are proportional to the molecular weight of the component or complex for convenient comparison of shape changes.



The reductase and protein B components give unimodal $P(r)$ profiles indicative of compact globular proteins (Figure 8.10 (a)) whereas for the hydroxylase the $P(r)$ profile is bimodal with a shoulder at 70 \AA (Figure 8.10 (b)). The shoulder indicates the bi-lobal nature of the hydroxylase which results from the way in which the two $\alpha\beta\gamma$ trimers associate to form the dimer (Figure 8.11).

Figure 8.11: Hydroxylase crystal structure.

(a) Surface representation showing the bilobal nature of the dimerised trimers (George *et al.*, 1996). The active sites are indicated (●). The structure has been rotated to show the two canyon-like features (1 and 2), which previously had been proposed as possible binding sites of protein B and the reductase (Rosenzweig *et al.*, 1993). (b) Top view of the structure in panel (a) showing the positions of the two canyons.



The measured volumes for each of the isolated components, calculated using Equations 2.2 and 2.3 (Chapter 2, Section 2.25), are in good agreement with the expected values based on monodispersed proteins of mass 250, 38.6 and 15.8 kDa

for the hydroxylase, reductase and protein B, respectively and assuming a specific volume of $0.74 \text{ cm}^3/\text{g}$ (Harpaz *et al.*, 1994) (Table 8.1).

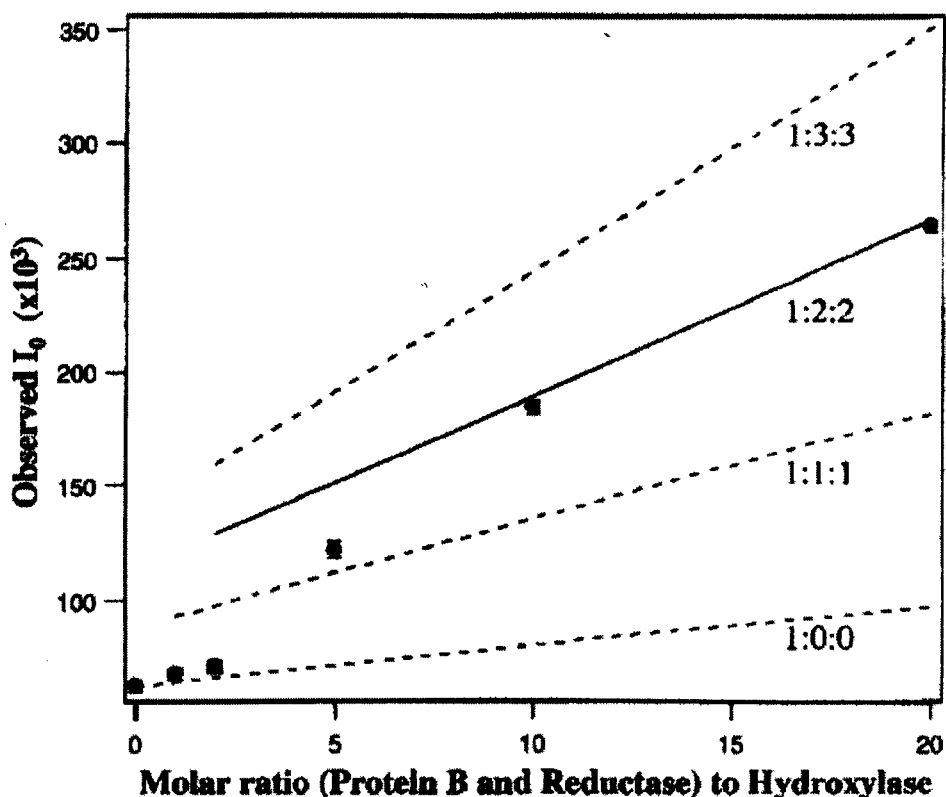
Table 8.1: Molecular Volumes for each sMMO component

Component	Measured volume (\AA^3)	Expected volume (\AA^3)
Protein B	19200 ± 3100	19400
Reductase	43200 ± 2000	47300
Hydroxylase	275000 ± 1800	305800

Figure 8.12 illustrates the formation of the 1:2:2 complex. It shows a plot of the observed I_0 values for the mixtures of sMMO components added to form the complex against the molar ratio of reductase and protein B to hydroxylase in the solution. Also shown are the expected I_0 dependencies assuming different stoichiometries of hydroxylase:reductase:protein B.

Figure 8.12: Titration of hydroxylase with protein B and reductase.

The I_0 values measured for the mixtures of hydroxylase:reductase:protein B plotted as a function of the protein B and reductase to hydroxylase mole ratio. The solid line indicates the expected I_0 values assuming two equivalents of protein B and reductase bind to one hydroxylase. The dashed lines correspond to alternative stoichiometries for binding as indicated.

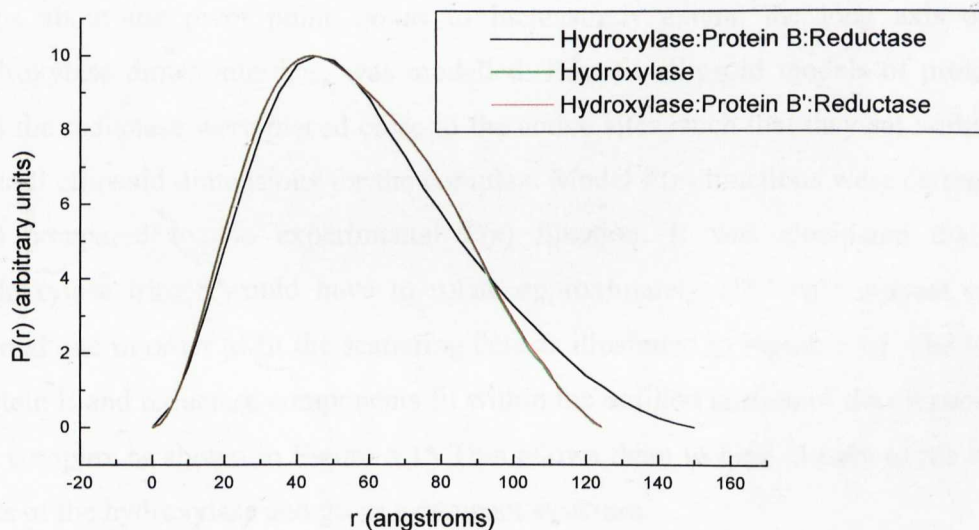


The comparisons showed that the observed data fit the 1:2:2 complex being formed with 10 equivalents of protein B and reductase compared to hydroxylase and that at molar ratios of 1:5:5 and less, only the 1:1:1 complex or hydroxylase alone were observed.

The $P(r)$ profile (Figure 8.10 (b)) illustrates that upon formation of the 1:2:2 complex an increase in d_{\max} was observed from 125 to 150 Å, and the shoulder at 70 Å is lost. This illustrates that the overall structure is more elongated and has lost the bilobal character of the hydroxylase alone. The R_g value for the scattering particle increases from 42 to 46 Å and the molecular volume increases by 26 %, as is expected for the formation of the 1:2:2 complex. Interestingly, these changes are not observed for a mixture of hydroxylase: reductase: protein B' added at a 1:10:10 ratio, as the $P(r)$ profiles are identical (Figure 8.13) and thus illustrate that complex formation has not occurred, and protein B' does not bind to the hydroxylase. Similarly, parallel scattering experiments in which the hydroxylase was titrated with the reductase or protein B, up to 10 equivalents of each, showed no evidence for their binding to the hydroxylase either. Also, addition of hydrogen peroxide up to concentrations of 100 mM, which activates the hydroxylase to function via the peroxide shunt mechanism, did not give rise to any conformational change.

Figure 8.13: $P(r)$ functions for the hydroxylase, sMMO complex and sMMO complex formed with protein B' instead of protein B (1:10:10 mixture of hydroxylase:protein B':reductase).

For ease of viewing, $P(r)$ profiles are not scaled as in Figure 8.10.



The single ellipsoid fit to the scattering data for the 1:2:2 complex of hydroxylase:reductase:protein B gives dimensions of 150, 71, 66 Å with a χ^2 value of 1.04 whereas the best fit ellipsoid for the isolated hydroxylase calculated from the crystal structure data has dimensions of 125, 95, 65 Å compared to the best-fit ellipsoid calculated from the scattering data 127, 98, and 65 Å ($\chi^2 = 1.01$). Upon complex formation there is an accompanying increase in d_{\max} and a narrowing in a second dimension by 24 Å or 25 %, so illustrating that the hydroxylase cannot be accommodated within the molecular envelope of the complex without a conformational change. Since both protein B and reductase are necessary for this observation, it appears that both proteins are required for binding to induce the conformational change.

Modelling studies were subsequently undertaken in order to identify the nature of the conformational change. It was proposed that the required conformational change could occur by means of the rearrangement of the two trimers that associate to form the hydroxylase dimer. The two trimers contact each other with relatively small areas of interaction at each end of their long axes between the two β subunits. At one end of this interaction there is a planar interface of approximately 200 Å², which could provide a potential pivot point in the structure, about which the hydroxylase can rotate to give a structure with an increased d_{\max} , while maintaining a significant area of contact between the trimers. This, similarly, brings about the narrowing of the structure in the second dimension. Rotation of the hydroxylase systematically in 10° steps about the pivot point, so as to increasingly extend the long axis of the hydroxylase dimer interface, was modelled. Best fit ellipsoid models of protein B and the reductase were placed close to the active sites, such that they sat within the overall ellipsoid dimensions for the complex. Model $P(r)$ functions were determined and compared to the experimental $P(r)$ function. It was elucidated that one hydroxylase trimer would have to rotate approximately 180° with respect to the second one in order to fit the scattering data as illustrated in Figure 8.14. The bound protein B and reductase components fit within the unfilled portion of the ellipsoid for the complex as shown in Figure 8.15 This allows them to bind closely to the active sites of the hydroxylase and gives a compact structure.

Figure 8.14: Proposed model for the extended hydroxylase structure.

Ellipsoid models for the isolated hydroxylase dimer (left) and the sMMO complex (right) are shown as yellow dots that fill the ellipsoid volumes. A ribbon representation of the hydroxylase crystal structure is superimposed on the ellipsoids, with the individual trimers that associate to form the dimer coloured blue and red. For the complex (right), the hydroxylase dimer is shown in the extended conformation.

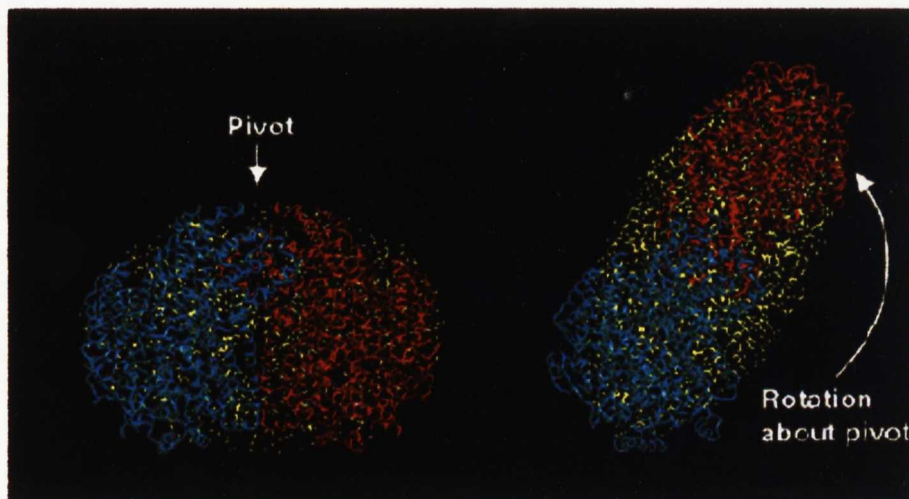
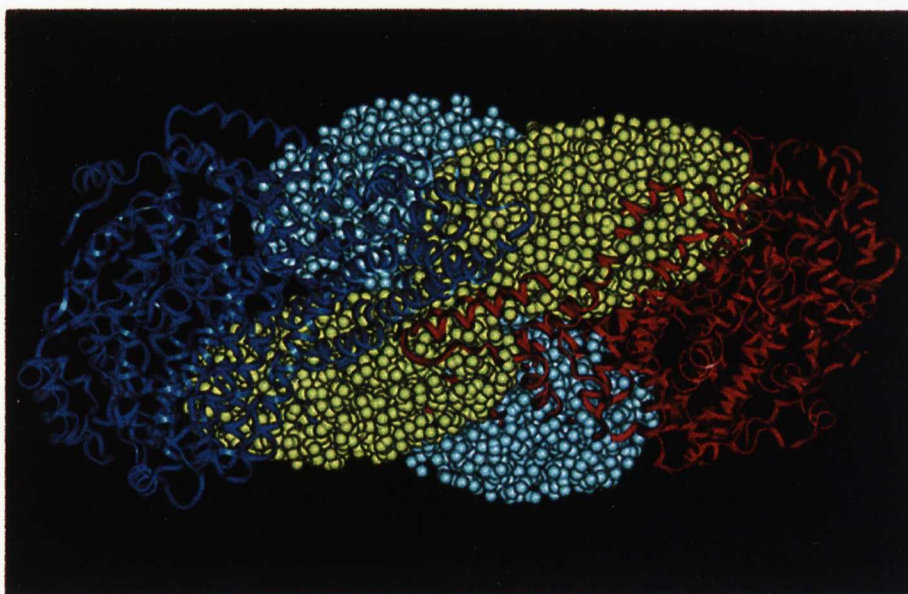


Figure 8.15: Model of the interaction between the three components of sMMO.

The hydroxylase structure is shown in ribbon form (dark blue and red), protein B (light blue) and the reductase (yellow) are represented by ellipsoids filled with small spheres.



The rotation preserves the 2-fold symmetry expected for the dimer. The quality of the model fit to the data is $\chi^2 = 1.13$, indicating excellent agreement. Likewise the

structural parameters for the model and experimental data both have a d_{\max} of 150 Å, the R_g values are both 46 Å and the volumes agree within 10 %.

Models, in which protein B and the reductase were positioned so that they filled the canyon positions indicated in Figure 8.11, could not account for the increases in R_g and d_{\max} obtained upon complex formation. The best χ^2 obtained for such models compared to the scattering data was 16, indicating a very poor fit. Alternative models positioning protein B and the reductase on the surface of the hydroxylase in highly extended conformations could give an increase in d_{\max} , but did not give the correct R_g values or shape functions and at best only gave a fit of $\chi^2 = 6$, similarly indicating poor fits. This evidence further supports the idea that the conformational change observed must occur via the rotation of the hydroxylase trimers.

These results support the previous studies which have suggested that the stoichiometry of the sMMO complex is 1:2:2 hydroxylase:reductase:protein B (Froland *et al.*, 1992; Rosenzweig *et al.*, 1993; Lloyd *et al.*, 1997). However, under the conditions here, 10 equivalents of each of the reductase and protein B are required to see full complex formation. The results of the activity assays containing hydroxylase:reductase:protein B in a 1:10:10 ratio were not significantly different to those obtained for the proteins added at ratios of 1:1:1 or 1:2:2 (Figure 8.6). However, previous studies have observed maximal sMMO activity for mixtures containing 2 equivalents of protein B and reductase to hydroxylase (Froland *et al.*, 1992). Therefore, it appears that the addition of NADH and/or substrate may increase the affinity of the reductase and protein B to the hydroxylase, thus driving the equilibrium towards complex formation.

8.5 Conclusion

The work presented in the Chapter used various techniques to yield new structural information on the component interactions of the multicomponent sMMO enzyme. The SAXS data have been modelled to show that upon formation of the enzyme complex, the hydroxylase undergoes a dramatic conformational change, such that

one dimension is narrowed by 24 Å, whilst the longest dimension increases from 120 Å to 150 Å. Both the reductase and protein B were used to induce the conformational change. However, sMMO retains its 2-fold symmetry expected for a dimer and identifies the complex as consisting of the hydroxylase:reductase:protein B at a ratio of 1:2:2.

The 1:2:2 stoichiometry of the components within the sMMO complex has been implied from various studies. For example, the dimeric form of the hydroxylase, identified from its crystal structure, suggested that 2 equivalents of the reductase and protein B would be required to bind to a single hydroxylase dimer (Rosenzweig *et al.*, 1993). The identification of the possible binding sites of protein B and the reductase to the hydroxylase from analysis of cross-linking data (Fox *et al.*, 1991), crystal structure data for the hydroxylase in the presence of a short peptide of the reductase component (Rosenzweig *et al.*, 1997), and NMR data on the interactions of protein B with the hydroxylase (Walters *et al.*, 1999), have further supported this suggestion. Also the titration of the hydroxylase with reductase and protein B gave an optimum activity ratio of 1:2:2 hydroxylase:reductase:protein B (Froland *et al.*, 1992). Perturbation of the partially and fully reduced EPR signal of the hydroxylase upon addition of 2 mol protein B / mol hydroxylase and the results of isothermal titration calorimetry and stopped flow fluorescence spectroscopy also indicated that the reductase and protein B bind to the hydroxylase with a 2:1 stoichiometry (Fox *et al.*, 1991; Gassner and Lippard, 1999). However, the SAXS studies indicated that under the conditions of the experiments 10 equivalents each of the reductase and protein B were required to see full complex formation. This suggests that the addition of NADH and/or substrate may increase the affinity of the reductase and protein B to the hydroxylase, driving the equilibrium towards complex formation.

The addition of hydrogen peroxide, which activates the hydroxylase to function via the peroxide shunt mechanism, failed to induce any conformational change. For this reason it was thought that protein B primarily facilitated the conformational change in the hydroxylase in order to allow close interaction between the reductase and the hydroxylase. Previous works have also proposed that the formation of a hydroxylase-protein B complex was responsible for inducing either a global or local shape change in the hydroxylase (Rosenzweig and Lippard, 1994; George *et al.*,

1996; Kazlauskaitė *et al.*, 1996; Davydov *et al.*, 1997; Coates-Pulver *et al.*, 1997; Rosenzweig *et al.*, 1997). In the absence of protein B and reductase, the hydroxylase exists in a conformation which hinders access to the active site, as the X-ray crystal structure shows there to be no direct passage for substrate to the active site (Rosenzweig *et al.*, 1993). This further highlights the need for a conformational change in the hydroxylase to occur for substrates to reach the active site for catalysis. Similarly, the conformational change modelled from the SAXS data would most certainly affect the environment of the di-iron centre, thus explaining the alteration in its EPR spectrum and redox potentials upon binding of protein B (Fox *et al.*, 1991; Paulsen *et al.*, 1994; Rosenzweig and Lippard 1994; Kazlauskaitė *et al.*, 1996). CD and MCD have been used previously to observe an induced conformational change, only in the presence of protein B, affecting the active site pocket and di-iron cluster (Davydov *et al.*, 1997; Coates-Pulver *et al.*, 1997) and EXAFS has shown protein B to induce a conformational change near the substrate binding site and di-iron centre (Rosenzweig and Lippard, 1994).

The interactions between the components in the model are also in agreement with previous findings. The primary interactions suggested are between the reductase and the α and β subunits of the hydroxylase, in agreement with the crystal structure of the hydroxylase in the presence of a short peptide of the reductase and cross-linking data, and between protein B and the α subunit of the hydroxylase, in agreement with the cross-linking data (Fox *et al.*, 1991; Rosenzweig *et al.*, 1997). The model also suggests a role for the γ subunit in contributing to the overall stability of the complex by providing additional interactions with protein B.

The SAXS data is in good agreement with the previous studies mentioned. However, the AFM and SPA results did not give the same findings. The use of the technique of AFM proved problematic in obtaining good quality images as the proteins had a tendency to aggregate under the conditions of the experiment. Therefore, it was not possible to collect sufficient accurate data for analysis work.

The technique of SPA clearly visualised the hydroxylase alone as a bi-lobed dimer comparable in size to the dimensions obtained for the crystal structure of the protein

(Rosenzweig *et al.*, 1993). The complex formed upon addition of the hydroxylase:reductase:protein B at a ratio of 1:2:2 was identified as having lost its dimer symmetry, being more 'pear' shaped in character with an increase in the longest dimension from 130 Å to 155 Å, in good agreement with the SAXS data. However, unlike the SAXS data no narrowing was observed. Instead, an increase in the overall size of one hydroxylase trimer was observed, while the second trimer remained the same in dimension as that observed for one trimer of the hydroxylase in the hydroxylase only sample. It was presumed that the increase in size corresponded to the binding of 1 protein B and 1 reductase molecule to the hydroxylase trimer. However, it could not be ruled out that the size increase could be the result of some other combination of these sMMO components binding to the hydroxylase trimer.

Interestingly, the SAXS data observed the 1:1:1 complex of the hydroxylase:reductase:protein B when the components were added in a 1:5:5 ratio. Unfortunately, the SPA data for the complex formed at a 1:5:5 ratio of hydroxylase:reductase:protein B proved difficult to analyse because of the large proportion of unbound smaller proteins (protein B and reductase) interfering with the identification of the complexed particles. Nevertheless, the SPA data agrees with the SAXS results here, as they imply that the formation of the complex by addition of the components at lower ratios does not result in the formation of the 1:2:2 complex. The slight discrepancies in the actual results could be due to the differences in the techniques.

It has also been observed from previous studies that up to 60 % of the binding sites on the hydroxylase are either damaged or temporarily unavailable, so preventing full complex formation from occurring (Gassner and Lippard, 1999). Also iron depleted hydroxylase is routinely purified which contains ~ 2 – 3 mol of iron per mole of hydroxylase instead of the theoretical value of 4. Therefore, it is possible that binding of the other components to only one trimer of the hydroxylase reflected the iron-depleted nature of the second trimer to which the reductase and protein B may not have been able to bind (Liu *et al.*, 1995).

As protein B binds tightly to the hydroxylase in the oxidised state (H_{ox}), and with the hydroxylase having 4 - 5 orders of magnitude higher affinity for protein B in this

form compared to that for hydroxylase in the reduced state (H_{red}) (Liu *et al.*, 1997), it would be expected to observe binding under the conditions of these experiments. This would result in the formation of the activated complex (Liu *et al.*, 1995).

Since the reductase can transfer electrons to the hydroxylase in the absence of protein B, it must be capable of binding to the hydroxylase for the reason of transferring electrons to the active site to reduce the active site iron from Fe(III) to Fe(II) in the absence of protein B (Lund *et al.*, 1985). However, recent studies have revealed that 0.1 reductase to 1 hydroxylase ratio afforded the same shift in redox potentials as the 1:1 reductase:hydroxylase ratio (Waller and Lipscomb, 1996). It was also noted that the ratio of reductase:hydroxylase in cells of *Ms. trichosporium* OB3b was 1:10, suggesting that this observation was of physiological relevance (Waller and Lipscomb, 1996). This phenomenon was also observed for *Mc. capsulatus* (Bath) cells and it was thought that during normal *in vivo* catalysis the reductase was present at 10% of the hydroxylase concentration (Liu *et al.*, 1997). Findings by Gassner and Lippard, (1999) have indicated that the reductase can transfer electrons to several hydroxylase molecules in the time it takes for the hydroxylase to complete a single turnover. This could be the reason for the low levels of reductase present, as one molecule can activate many hydroxylase molecules. This was further supported by their findings that the sMMO system operates most efficiently when the concentration of reductase is one fifth that of the hydroxylase with the concentration of protein B being greater than or equal to that of the hydroxylase. Under these conditions methane hydroxylation and NADH consumption occur with an $\sim 1:1$ stoichiometry. However, further modification of the protein ratios can increase the rate of substrate hydroxylation. Therefore, the reductase can bind and dissociate rapidly from a large population of H_{ox} , as present in this experiment. It is therefore possible that this is partly the reason why the SPA data only visualises protein binding, on average, to 1 trimer of the hydroxylase dimer.

Under normal assay conditions, upon reduction of a hydroxylase-protein B complex by the reductase, a tightly assembled complex containing H_{red} :protein B:redutase would be formed, which enables reaction with molecular oxygen during catalysis (Gassner and Lippard, 1999). However, in the absence of NADH the tight complex

would be prevented from forming. Prior to formation of the reduced hydroxylase, protein B and reductase complex, it is proposed that either protein B or reductase associates with the hydroxylase to form a rapidly equilibrating pre-complex, which slowly isomerises by means of a structural change to give a thermodynamically stabilised equilibrium complex (Gassner and Lippard, 1999). It is also entirely possible that it is one of these 'pre-complexes' that has been visualised by SPA, created under the conditions of adding 1:2:2 ratios of hydroxylase:reductase:protein B and so supports the idea of pre-complex formation occurring during the sMMO reaction. The SAXS data, on the other hand, have identified full complex formation. It is possible that the excess quantities of reductase and protein B present, compared to the hydroxylase, pushed the equilibrium towards complex formation in the absence of the other reaction chemicals.

The collection of the SPA and SAXS data were also conducted at different temperatures, SPA at 4 °C and SAXS at 13 °C. Studies have also identified temperature dependent conformational changes to occur between the hydroxylase and protein B and that the sites of interactions of the proteins differ, which could be linked to the greatly increased rate of catalysis by the hydroxylase at the optimum temperature of 45 °C compared to that at the lower temperatures, at which the SPA and SAXS experiments were conducted (Gassner and Lippard, 1999; Walters *et al.*, 1999). The lack of any significant differences in the activities of the complex when compared at ratios of hydroxylase:reductase:protein B of 1:1:1, 1:2:2 and 1:10:10 could indeed reflect this idea. Therefore, the complexes formed under assay conditions are not equivalent to those identified by the techniques of SPA and SAXS, particularly as the activity assays are conducted in the presence of substrates and NADH, which are absent under the conditions used to visualise the complexes. Similarly the difference between the 'complexes' observed by SPA and SAXS could reflect their formation occurring at different temperatures.

The techniques used in this Chapter have identified methods and conditions suitable for the study of the sMMO complex. Further studies of the complex by SPA would need to involve antibody labelling to clearly identify the proteins involved in forming the complex. Also, it would be important to try to 'capture' the complex in

its active form in the presence of NADH and substrate. One possibility would be to use acetylene, the suicide substrate inhibitor of sMMO in an attempt to immobilise the complex in its active state for visualisation by either/both SPA and/or SAXS. Anaerobic conditions would also prevent turnover of the enzyme and could be used in 'capturing' the nature of the reactive complex. Nevertheless, the results detailed here have provided vital insights into the conformation of the sMMO system and yet the need to obtain crystals of the complex remains apparent as the only means of validating the observations made so far.

Chapter 9

General Discussion

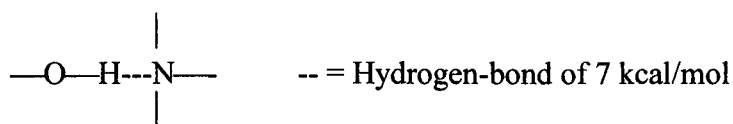
Throughout this work a range of molecular biology, biochemical and structural approaches has been taken to study the regulatory protein, protein B, and component interactions of sMMO. One of the major developments, that facilitated the studies described in this work, was the improvement of the purification protocols for wild-type and recombinant protein B from *Mc. capsulatus* (Bath) and *Ms. trichosporium* OB3b and the single mutant of *Mc. capsulatus* (Bath) protein B, G13Q, and the hydroxylase and reductase components of sMMO from *Mc. capsulatus* (Bath). Many of the characterisational studies of both protein B and the sMMO complex involved the use of techniques requiring significant quantities of highly pure protein. Also, the construction, expression and purification of the M12A:G13Q double mutant and the truncates of *Mc. capsulatus* (Bath) protein B were vital in furthering the understanding of the protein B cleavage reaction.

Since the first observation of the truncation of protein B by Pilkington *et al.* (1990), the mechanism and reason(s) for the occurrence have remained elusive. Work by Bhambra (1996) and Lloyd *et al.* (1997) established that the loss of only the first 12 N-terminal amino acids resulted in the formation of the inactive truncate of protein B known as protein B'. The results from the study of the recombinant N-terminal truncates of *Mc. capsulatus* (Bath) protein B identified that only the first 7 amino acids were actually essential for activity, and that a decrease in specific activity was observed as each amino acid from 1 to 7 was lost. The stability of the truncates with respect to the cleavage reaction also changed significantly between the truncate containing the 7th amino acid, tyrosine, which was observed to be stable, and the truncate lacking the 7th amino acid, which was identified as being unstable. Therefore, a dramatic change occurred whereby both activity and stability were lost upon removal of the Y⁷ amino acid of protein B.

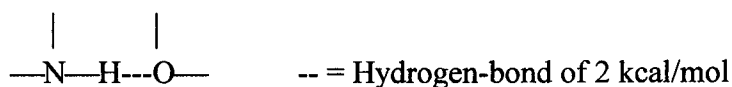
Tyrosine is an amino acid with hydrogen-bonding capabilities. It contains a -OH group, which at pH 7 can serve as a hydrogen-donor. Hydrogen-bonds are present

between main-chain -NH and -CO groups forming α helices and β sheets, but side chains of certain amino acids, such as tyrosine, can also participate in hydrogen-bonding, which is an especially strong type of dipole-dipole interaction. All but two of the first 7 amino acids of protein B have hydrogen-bonding capabilities with S¹, N³, S⁴, and N⁵ serving as both hydrogen-bond donors and acceptors. Residue D⁸ can serve as a hydrogen-acceptor, whereas the remaining amino acids of the N-terminus up to the Met¹²-Gly¹³ cleavage site do not have hydrogen-bonding potential. Inter- and intra-molecular interactions, such as hydrogen-bonding between side chains, can contribute to the higher structure of a protein, with the protein naturally assuming its most stable higher structure.

The loss of activity of the truncates and a decrease in their stability with respect to the cleavage reaction, as they become N-terminally truncated, must indicate a loss of some stabilising effect. Stabilising interactions, which include electrostatic and van der Waals forces, hydrogen-bonds and salt bridges between amino acid side chain groups and disulphide bonds (S-S), may therefore be present. These may possibly maintain the structure of the N-terminal region, either in a specific structure or orientation relative to the protein core, and are conceivably essential for activity. Since the amino acids necessary for the S-S cross-links and salt bridges are not present within the first 12 N-terminal amino acids of protein B, this suggests electrostatic and van der Waals forces and hydrogen-bonding to be important. The loss of hydrogen bonding capabilities of the N-terminal amino acids of protein B, roughly correlates with the loss of activity and stability of the protein. However, both Y⁷ and D⁸ amino acids have hydrogen-bonding potentials, and yet truncate Y7 is observed as being stable and active, whereas this is not the case for truncate D8. Hydrogen-bonds are not all of the same strength, which implies that Y⁷ may form a stronger bond, such as



whereas D⁸ may form a weak bond, such as



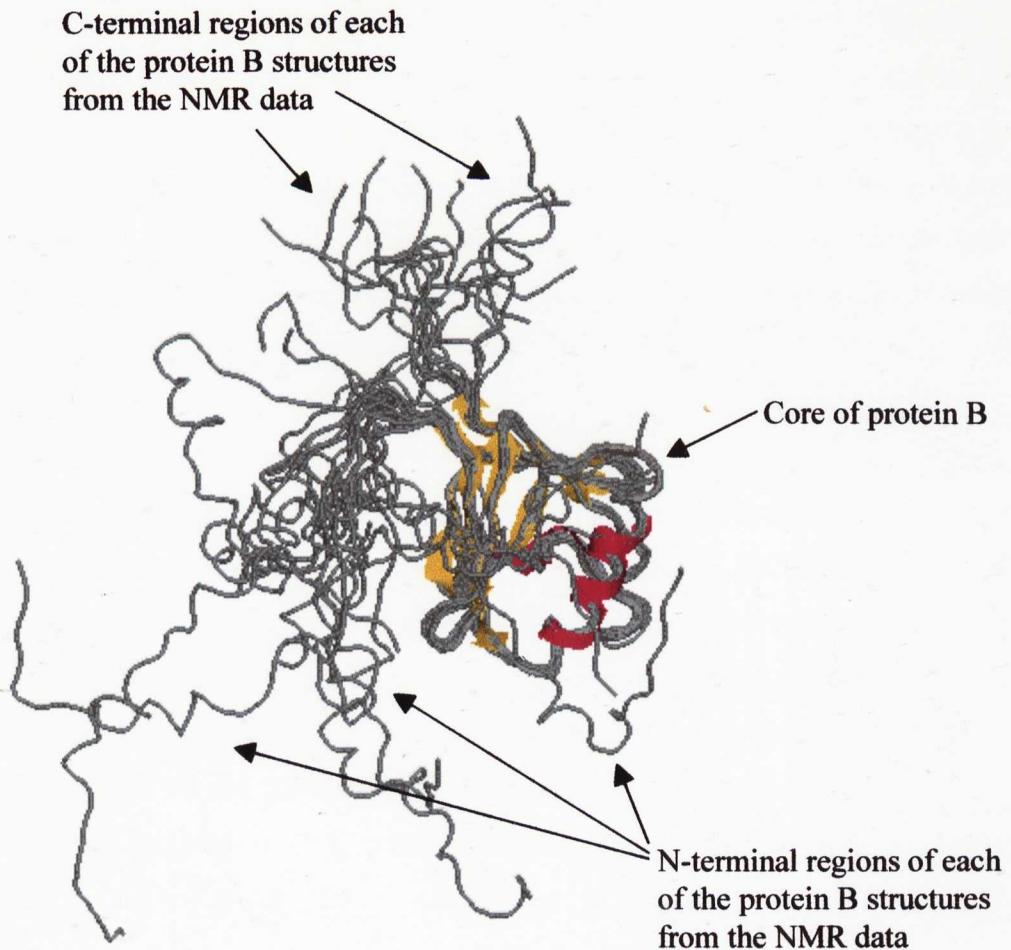
which can be broken more easily. Hence, it could be interpreted that maintenance of the structure and orientation of the N-terminal region of protein B may be aided in truncate Y7 by the presence of hydrogen-bonds between the Y⁷ and D⁸ amino acids and the core of the protein, whereas in the case of the D8 truncate, this effect may be lost. However, since the secondary structure and overall molecular size of truncates Y7 and D8 are virtually the same, it could further imply that the activity of protein B may be more related to the orientation of the N-terminal region relative to the core of the protein than the structure of the N-terminal region alone. This is a proposal which is also supported by the increased hydrogen-bonding potential in the Y7 truncate compared to that of the D8 truncate. With increasing truncation of protein B, such essential interactions required to orientate and stabilise the N-terminal region, relative to the protein core, could be lost, resulting in its increased flexibility, which would mean that the protein could become destabilised and susceptible to cleavage and inactivation.

The recent NMR structure of *Mc. capsulatus* (Bath) protein B (Walters *et al.*, 1999) failed to define the orientation of the N-terminus (residues 1-34) relative to the core, as shown in Figure 9.1, and provided evidence that at 25 °C the N-terminal residues D²²-A²⁶ interacted with the hydroxylase, although it was also found that this may not be the case at 45 °C. The remaining interactions were concentrated within the core region of the protein. These results are in agreement with the observation that the inactive truncate protein B', which lacks only the first 12 N-terminal amino acids and thus retains residues D²²-A²⁶, can inhibit the hydroxylase functioning via the peroxide shunt mechanism. Therefore, it must be capable of interaction with the hydroxylase in the same manner as observed for intact protein B itself. However, inhibition was identified as being less than that for protein B, suggesting interactions to be weaker and thus 'affected' by the loss of the 12 N-terminal amino acids. This is also in agreement with studies by Kazlauskaite *et al.* (1996) and Lloyd *et al.* (1997), in which the binding of protein B' to the hydroxylase was determined, by surface plasmon resonance (SPR), to be weaker than that identified for protein B. It could be possible that maintenance of the structure and/or the orientation of the N-terminal residues D²²-A²⁶ are mediated by the first 12 amino acids of protein B. Therefore, in their absence, the position of residues D²²-A²⁶ relative to the core of the protein is

lost, weakening the protein's interaction with the hydroxylase. Due to time limitations, it was not possible to test the levels of inhibition of the truncates of protein B within the peroxide shunt system in order to identify their strength of binding to the hydroxylase. It would, therefore, be of importance to determine this or alternatively use SPR studies to identify specific binding constants for the interactions of the truncates with the hydroxylase.

Figure 9.1: Orientation of the N- and C-terminal regions of *Mc. capsulatus* (Bath) protein B as determined by NMR analysis (Walters *et al.*, 1999).

Shown are all 14 structures identified for the protein from the NMR data, displayed using Rasmol 2.7.1 (RasWin Molecular Graphs, H. Bernstein).



Proteins B and B' have been shown to have the same secondary structure, although the molecular shapes have been observed as being slightly different. SAXS identified protein B' as being longer and thinner than protein B. This result supports the proposal that the first 12 amino acids could be maintaining a 'shape' aspect of

protein B, which is lost upon their removal. For example, upon loss of interactions within the first few N-terminal amino acids, the remains of the N-terminal region could become exposed and more flexible. The modelled ellipsoids for the scattering data could, therefore, represent this change. Protein B has also been identified as being capable of self-association under certain conditions, whereas protein B' exists as a monomer. This could also be explained as being due to a molecular shape change occurring upon the loss of the first 12 amino acids from the N-terminus. Protein B maintains a structure which allows interactions to be possible, but is reduced upon cleavage to form protein B'. Ultimately, confirmation of these possibilities awaits the elucidation of crystal structures of proteins B and B', which would give details of the orientation of the termini relative to the core and allow a detailed comparison of the two proteins to be possible. However, difficulties were encountered when attempting to obtain crystals of protein B/B', possibly due to the 'flexible' nature of the N-terminal region of the protein. Thus perhaps a better approach may be to crystallise protein B/B' when in complex with the hydroxylase. This would not only serve in attempting to improve the stability of protein B/B' for crystallisation to be possible but would give vital information on aspects of protein B and B' binding to the hydroxylase.

The availability of a system for the optimised expression and purification of the protein B truncates, however, provides a means to identify further how the truncation of protein B prevents sMMO activity, and may enhance the understanding of the sMMO reaction mechanism. For example, future work could involve elucidating the effects of the protein B truncates on the redox potentials of the hydroxylase, their effects on the conformation of the active site of the hydroxylase and their effects on the formation of the reaction intermediates, compounds P and Q. Such findings would help establish fully the means by which protein B carries out its critical role within the sMMO system.

It was established by Bhambra (1996) and Lloyd *et al.* (1997) that cleavage of protein B was not protease mediated. Mutation of the Gly¹³ residue at the cleavage site to a glutamine improved the stability of the protein to the cleavage reaction, although further mutations of Gly¹⁰, Gly¹³ and Gly¹⁶ resulted in a decrease in activity of the protein within the sMMO system (Lloyd *et al.*, 1997; Brandstetter *et al.*,

1999). Further verification that cleavage occurred in the absence of proteases was obtained using chromatofocusing chromatography. The results demonstrated that a highly purified sample of protein B from chromatofocusing chromatography degraded to protein B', which could then be repeatedly resolved and repurified. Since each sample of repurified protein B underwent cleavage to protein B', it is most likely that the truncates are generated autocatalytically. Further studies identified protein B to contain a specifically nucleophilic residue, which provides a means of inducing the cleavage reaction observed. Wild-type and recombinant *Mc. capsulatus* (Bath) protein B, and G13Q have been identified as being similar in terms of secondary structure and cleaved at the same position within the N-terminal region. Combined, these data could be interpreted to suggest that the specifically nucleophilic group is probably a side chain moiety of one of the outer core amino acids which can contact the N-terminal region mediating cleavage, as dictated by the structure of the protein. It is possible that purified protein B experiences destabilising conditions *in vitro* and thus the proposed interactions responsible for maintaining the orientation of the N-terminus are lost. The resultant increased flexibility of the N-terminus, as is observed from the NMR structure of protein B (Walters *et al.*, 1999), could allow the nucleophilic group to access certain N-terminal sites leading to cleavages at these specific positions. This proposal is also supported by the observation that for G13Q at higher concentrations, which helps maintain the delicate balance of non-covalent forces, the protein is stabilised against the cleavage reaction. The concentration effect was also present for WTB although it was less pronounced, possibly reflecting very slight differences in their N-terminal structures due to the difference in the amino acid at position 13 with respect to the wild-type protein B sequence.

Attempts to identify conditions which stabilise protein B identified magnesium as reducing the rate of inactivation due to cleavage. Magnesium is a large ion with a positive charge and would therefore be attracted to any nucleophilic, electron donating groups, such as the proposed side chain moiety of the outer core amino acid which is suggested to be responsible for the cleavage reaction. Thus, it is possible that the binding of Mg^{2+} to the nucleophilic group would prevent its attack on the N-terminal amino acids, and so stabilise protein B against cleavage. This finding also

supports the suggestion that nucleophilic attack is responsible for the cleavage reactions of protein B.

Mutational analysis of wild-type *Mc. capsulatus* (Bath) protein B involving the changing of the Met¹²-Gly¹³ cleavage site to Ala¹²-Gln¹³, forming the double mutant M12A:G13Q, did not affect the structure or activity of protein B. However, the single mutant, G13Q, was identified as possessing slightly more α -helical character in the N-terminal region. In terms of stability and binding to the hydroxylase, M12A:G13Q was observed to differ slightly from WTB and G13Q. It was more stable than G13Q at lower protein concentrations, possibly because the slight α -helical character present for G13Q was lost upon dilution due to solvent exposure effects, whereas M12A:G13Q was less affected due to being less structured. In support of these proposals were the observations of the cleavage sites of M12A:G13Q and G13Q. For M12A:G13Q the cleavage patterns are similar for samples incubated at high and low protein concentrations, whereas for G13Q cleavage patterns are different. The site equivalent to the Met¹²-Gly¹³ cleavage site of *Mc. capsulatus* (Bath) protein B is identified as the main cleavage product for G13Q incubated at high protein concentrations. In comparison, when G13Q is incubated at low protein concentrations, various N- and C-terminal cleavages are identified. This reflects the possibility that for G13Q at high protein concentrations the secondary structure and orientation of the N-terminus are stabilised for longer, whereas at lower protein concentrations they are lost, giving the different cleavages in response to the difference in nature of accessible sites. For M12A:G13Q the results support the observation of the protein being less structured than G13Q because the effect of dilution just enhances the number of cleavage sites, possibly due to an increase in flexibility, as any stabilising interactions of the N-terminus become weakened or lost. Nevertheless, the slight increase in α -helical character of the N-terminal region of G13Q appeared only to stabilise the region against cleavage and not to affect sMMO activity. Interestingly, G13Q did not inhibit the hydroxylase, when functioning via the peroxide shunt mechanism, as much as M12A:G13Q or WTB. This further identifies a slight structural difference between the N-terminal regions of the proteins, where the mutations lie, which affects binding to the hydroxylase but not activity. Since protein B in conjunction with the reductase

has been identified as causing the hydroxylase to undergo a conformational change enabling activity, it is possible that the three proteins mediate this to the same degree but binding to the hydroxylase in the absence of the reductase differs.

Proteins B and B' have been identified as binding copper, which results in dimer formation. The side chain of histidine is an excellent metal ligand and two histidine residues are present, one within each of the unstructured and exposed N- and C-terminal regions of protein B, as identified from its NMR structure (Walters *et al.*, 1999). Therefore, it is possible that copper binds to the His³² and His¹³⁹ residues of the N- and C-termini respectively. Their orientations relative to the core of protein B are undefined and so both histidine residues may be able to complex with copper in solution. This could be aided by the solution environment in which the flexibility of the termini may be enhanced. Also, in order to form dimers, it is possible that copper bound to protein B binds to a second protein B molecule via the two equivalent histidine residues of the second protein, thus giving the usual tetrahedral coordination observed for metal-bound proteins. A combination of the observations that proteins B and B' are affected by copper in the same way, and yet differ with regard to their first 12 N-terminal amino acids, and that analysis of the NMR structure of *Mc. capsulatus* (Bath) protein B indicated no other metal-complex forming residues to be exposed, supports the idea that the N- and C-terminal histidines are involved in complexing with copper, leading to dimer formation in the manner suggested. The ultimate reason for a copper-induced dimerisation effect on proteins B and B' remains unknown. Since copper is important in inducing pMMO expression in *Mc. capsulatus* (Bath) cells, it would be important to determine whether this observation had any functional significance either within the sMMO system or the cell itself.

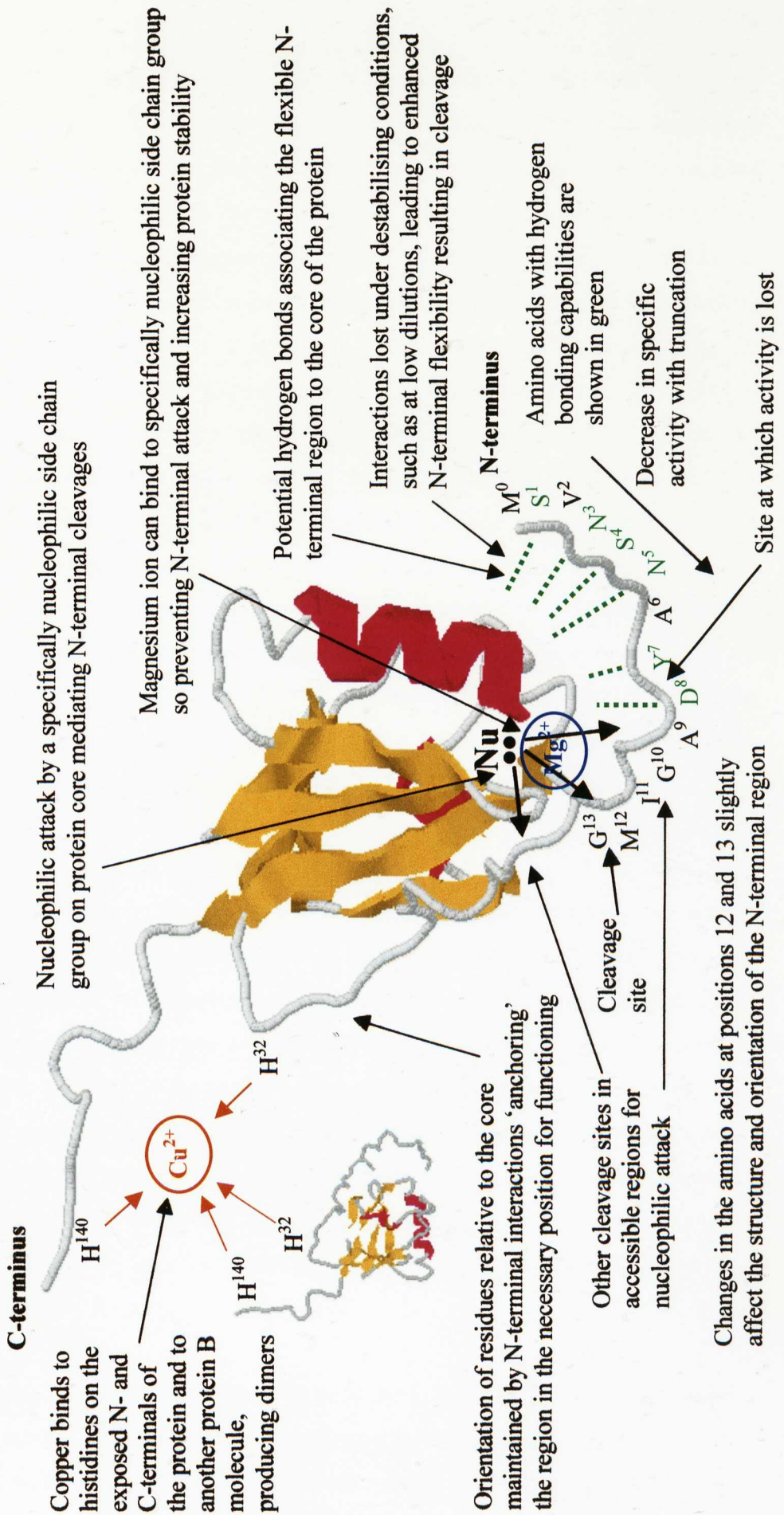
Wild-type and recombinant *Ms. trichosporium* OB3b protein B have been identified as undergoing an inactivatory cleavage reaction like that observed for protein B of *Mc. capsulatus* (Bath). However, the main cleavage sites differ between the wild-type (Thr¹⁵-Gly¹⁶) and recombinant protein (Lys¹⁴-Thr¹⁵) by one amino acid. This difference suggests that in this case the extra amino acids present at the N-terminus of the recombinant protein, as a result of the cloning method used, have affected the protein slightly. Studies also identified *Ms. trichosporium* OB3b protein B to be

more stable than *Mc. capsulatus* (Bath) protein B and the mutants G13Q and M12A:G13Q. They also identified *Ms. trichosporium* OB3b protein B to be only marginally less active than these proteins when assayed within the *Mc. capsulatus* (Bath) sMMO system. Within the N-terminal region *Ms. trichosporium* OB3b protein B differs from *Mc. capsulatus* (Bath) protein B by a few amino acids. The core structure of the protein itself, as recently determined by NMR (Chang *et al.*, 1999), identifies the protein to be structurally different to *Mc. capsulatus* (Bath) protein B, an observation already made by secondary structural analysis. These differences must enhance the stability of the protein to the cleavage reaction. Based on these observations, mutational studies can be devised to try to develop a more stable *Mc. capsulatus* (Bath) protein B for sMMO activation studies. Future work could involve construction and expression of various mixtures of the N- and C-terminal and core regions of the two homologous proteins. This would also further the understanding of the reasons for the instability of *Mc. capsulatus* (Bath) protein B and the stability of the homologous *Ms. trichosporium* OB3b protein B.

Protein B' has been identified in sMMO-expressing *Mc. capsulatus* (Bath) cells but not those of *Ms. trichosporium* OB3b. This further supports the observation that *Ms. trichosporium* OB3b protein B is more stable with respect to cleavage than *Mc. capsulatus* (Bath) protein B and, therefore, any protein B cleavages that did occur may have been present only at very low levels, insufficient for detection. Nevertheless, the identification of protein B' within the *Mc. capsulatus* (Bath) cells would imply that it possesses a function within the cell, although it has been demonstrated that this is not one of switching the substrate specificity of sMMO. It is entirely possible that its formation *in vivo* and *in vitro* is purely a reflection of a destabilising solvent environment. Nevertheless, its presence and identification have provided the basis of much of the work in this thesis, which has furthered the understanding of various aspects of the structure and function of protein B. Reasons for the occurrence of the cleavage reaction and the inactivity of protein B' have been proposed, as have methods to minimise cleavage, and identification of the amino acids necessary for protein B activity have been determined. A schematic representation of the main features of protein B elucidated from the results obtained in this study is shown in Figure 9.2.

Figure 9.2: Schematic representation of the main features of protein B elucidated from the results obtained in this study.

Structure annotated is that of one of the NMR structures of *Mc. capsulatus* (Bath) protein B (Walters *et al.*, 1999). Structure is displayed using RasMol 2.7.1 (RasWin Molecular Graphs, H. Bernstein).



A further understanding of the functioning of *Mc. capsulatus* (Bath) protein B within the sMMO system has also been gained from this study. SAXS data have been modelled to show that protein B and the reductase induce a dramatic conformational change in the hydroxylase such that one trimer of the hydroxylase dimer is rotated by 180° relative to the other, thus preserving the 2-fold symmetry expected for a dimer. The results identified the complex as consisting of the hydroxylase:reductase:protein B in a ratio of 1:2:2, which is in agreement with previous studies investigating the stoichiometry of the complex (Rosenzweig *et al.*, 1993; Froland *et al.*, 1992; Fox *et al.*, 1991; Gassner and Lippard, 1999). Hydrogen peroxide, which can activate the hydroxylase to function via the peroxide shunt mechanism, failed to induce any conformational change in the protein. Consistent with these results was the proposal that protein B primarily facilitated the conformational change in the hydroxylase in order to allow close interaction between the reductase and the hydroxylase for electron transfer to occur efficiently. However, component interaction studies of the sMMO system using the technique of SPA by EM yielded contrasting results, as the complex was identified as having lost its dimer symmetry with binding of the other sMMO components occurring on only 1 trimer of the hydroxylase dimer.

The differences between the 'complexes' observed by the two techniques could reflect the difference in nature of the two processes. Nevertheless, the studies identified methods and conditions suitable for the study of the sMMO system and provided a means of investigating the component interactions of the complex in the absence of crystal structure data. Due to the limitations of time, it was not possible to obtain further insights into the conformation of the sMMO system whilst in its active state in the presence of, for example, NADH and/or substrates. Use of the suicide substrate inhibitor, acetylene, to immobilise the complex in its active state, or anaerobic conditions to prevent enzyme turnover and thus capture the reactive complex, may provide a means of visualising activated sMMO using the techniques of SAXS and/or SPA.

Ultimately the major challenge that will be faced is that of crystallising the sMMO complex, ideally with and without substrate bound. Only then will the true component interactions of the sMMO system in its active form be elucidated. It

would also assist in enabling the understanding of exactly how a small cofactor-less protein, such as protein B, can have such a dramatic effect on the regulation of the activity of the sMMO complex.

References

- Andersson, K. K., Froland, W. A., Lee, S-K. and Lipscomb, J. D.** (1991) Dioxygen independent oxygenation of hydrocarbons by methane monooxygenase hydroxylase component. *New J. Chem.* **15**, 411-415
- Atta, M., Fontecave, M., Wilkins, P. C. and Dalton, H.** (1993) Abduction of iron (III) from the soluble methane monooxygenase hydroxylase and reconstitution of the binuclear site with iron and manganese. *Eur.J. Biochem.* **217**, 217-223
- Balls A. K. and Wood H. N.** (1956) Acetyl chymotrypsin and its reaction with ethanol. *J. Biol. Chem.* **219**, 245-256
- Barber, M., Bordoli, R. S., Sedwick, R. D. and Tyler, A. N.** (1981) Fast atom bombardment of solids as an ion-source in mass-spectrometry. *Nature.* **293**, 270-275
- Bhambra, A.** (1996) The regulatory protein of soluble methane monooxygenase. PhD Thesis, University of Warwick, UK.
- Binnig, G., Quate, C. F. and Gerber, C.** (1986) Atomic force microscope. *Phys. Rev. Lett.* **56**, 930-933
- Bowman, J. P., Sly, L.I., Nichols, P. D. and Hayward, A. C.** (1993) Revised taxonomy of the methanotrophs; description of *Methylobacter* gen. nov., emendation of *Methylococcus*, validation of *Methylosinus* and *Methylocystis* species, and a proposal that the family *Methylococcaceae* includes only the group I methanotrophs. *Int. J. Syst. Bacteriol.* **43**, 735-753
- Bowman, J. P., Sly, L. I. and Stackebrandt, E.** (1995) The phylogenic position of the family *Methylococcaceae*. *Int. J. Syst. Bacteriol.* **45**, 182-185
- Brandstetter, H., Whittington, D. A., Lippard, S. J. and Frederick, C. A.** (1999) Mutational and structural analyses of the regulatory protein B of soluble methane monooxygenase from *Methylococcus capsulatus* (Bath). *Chem. and Biol.* **6**, 441-449
- Bradford, M. M.** (1976) A rapid and sensitive method for the quantitation of microgram quantities of protein utilising the principle of protein-dye binding. *Anal. Biochem.* **72**, 248-254
- Brusseau, G. A., Tsien, H. C., Hanson, R. S. and Wackett, L. P.** (1990) Optimisation of trichloroethylene oxidation by methanotrophs and the use of a colorimetric assay to detect soluble methane monooxygenase activity. *Biodegradation* **1**, 19-29
- Burrows, K. J., Cornish, A., Scott, D. and Higgins, I. J.** (1984) Substrate specificities of soluble and particulate methane monooxygenase of *Methylosinus trichosporium* OB3b. *J. Gen. Microbiol.* **130**, 3327-3333
- Cadieux, E. and Powlowski, J.** (1999) Characterisation of active and inactive forms of phenol hydroxylase stimulatory protein DmpM. *Biochem.* **38**, 10714-10722

Cardy, D. L. N., Laidler, V., Salmond, G. P. C. and Murrell, J. C. (1991a) Molecular analysis of the methane monooxygenase (MMO) gene cluster of *Methylosinus trichosporium* OB3b. *Mol. Microbiol.* **5**, 335-342

Cardy, D. L. N., Laidler, V., Salmond, G. P. C. and Murrell, J. C. (1991b) The methane monooxygenase (MMO) gene cluster of *Methylosinus trichosporium* OB3b: cloning and sequencing of the *mmoC* gene. *Arch. Microbiol.* **156**, 477-483

Chait, B. T. and Kent, S. B. H. (1992) Weighing naked proteins – practical, high accuracy mass measurement of peptides and proteins. *Science.* **257**, 1885-1894

Chang, S. L., Wallar, B. J., Lipscomb, J. D. and Mayo, K. H. (1999) Solution structure of component B from methane monooxygenase derived through heteronuclear NMR and molecular modelling. *Biochem.* **38**, 5799-5812

Coates-Pulver, S., Froland, W. A., Lipscomb, J. D. and Solomon, E. I. (1997) Ligand field circular dichroism and magnetic circular dichroism studies of component B and substrate binding to the hydroxylase component of methane monooxygenase. *J. Am. Chem. Soc.* **119**, 387-395

Colby, J. and Dalton, H. (1976) Some properties of a soluble methane monooxygenase from *Methylococcus capsulatus* Strain Bath. *Biochem. J.* **157**, 495-497

Colby, J. and Dalton, H. (1978) Resolution of the methane monooxygenase of *Methylococcus capsulatus* (Bath) into three components. *Biochem. J.* **171**, 461-468

Colby, J. and Dalton, H. (1979) Characterisation of the second prosthetic group of the flavoenzyme NADH-acceptor reductase (component C) of the methane monooxygenase from *Methylococcus capsulatus* (Bath). *Biochem. J.* **177**, 903-908

Colby, J., Dalton, H. and Whittenbury, R. (1975) An improved assay for bacterial methane monooxygenase: some properties of the enzyme from *Methylomonas methanica*. *Biochem. J.* **151**, 459-462

Colby, J., Dalton, H. and Whittenbury, R. (1979) Biological and biochemical aspects of microbial growth on C₁ compounds. *Annu. Rev. Microbiol.* **33**, 481-517

Colby, J., Stirling, D. I. and Dalton, H. (1977) The soluble methane monooxygenase of *Methylococcus capsulatus* (Bath): its ability to oxygenate *n*-alkanes, *n*-alkenes, ethers and acyclic, aromatic and heterocyclic compounds. *Biochem. J.* **165**, 395-402

Colby, J. and Zatman, L. J. (1973) Triethylamine metabolism in obligate and facultative methylotrophs. *Biochem. J.* **132**, 101-121

Costello, A. N., Peeples, T. L. and Lidstrom, M. E. (1995) Duplicate methane monooxygenase genes in methanotrophs. Poster presentation at the 8th International Symposium on Microbial Growth on C₁ Compounds. 27th August – 1st September 1995, San Diego, USA.

Cover, A. E. and Peterson, J. L. (1988) Remote gas to liquid fuels processing alternatives. American Institute of Chemical Engineers 1988 Spring National Meeting Session 71B, Fuels and Chemicals from Natural Gas, March 6th – 10th New Orleans, USA.

Covey, T. R., Bruins, A. P. and Henion, J. D. (1988) Comparison of thermospray and ion spray mass-spectrometry in an atmospheric-pressure ion-source. *Org. Mass Spec.* **23**, 178-186

Creighton, T. E. (1989) Protein structure: a practical approach. Oxford: IRL Press.

Crutzen, P. F. (1991) Methane's sinks and sources. *Nature* **350**, 380-381

Cuff, J. A. and Barton, G. J. (1999) Evaluation and improvement of multiple sequence methods for protein secondary structure prediction. *Proteins: Structure, Function and Genetics.* **34**, 508-519

Dalton, H. (1991) Structure and mechanism of action of the enzyme(s) involved in methane oxidation. In *Applications of Enzyme Biotechnology*, pp 55-68. Edited by J.W. Kelly and T.O. Baldwin. Plenum Press, New York.

Dalton, H. (1992) Methane oxidation by methanotrophs; physiological and mechanistic implications. In *Methane and Methanol Utilisers*, pp 85-114. Edited by J.C. Murrell and H. Dalton. Plenum Press, New York.

Dalton, H., Prior, S. D., Leak, D. J. and Stanley, S. H. (1984) In *Microbial Growth On C₁ Compounds* (4th International Symposium), pp 75-82. Edited by R. L. Grawford, and R. S. Hanson, American Society for Microbiology, Washington, D.C., USA.

Davydov, A., Davydov, R., Gräslund, A., Lipscomb, J. D. and Andersson, K. K. (1997) Radiolytic reduction of methane monooxygenase dinuclear iron cluster at 77K. *J. Biol. Chem.* **272**, 7022-7026

Davydov, R., Valentine, A. M., Konar-Panicucci, S., Hoffman, B. M. and Lippard, S. J. (1999) An EPR study of the dinuclear iron site in the soluble methane monooxygenase from *Methylococcus capsulatus* (Bath) reduced by one electron at 77K: the effects of component interactions and the binding of small molecules to the di-iron(III) centre. *Biochem.* **38**, 4188-4197

DeRose, V. J., Liu, K. E., Kurtz, D. M., Hoffman, B. M. and Lippard, S. J. (1993) Proton ENDOR identification of bridging hydroxide ligands in mixed-valent di-iron centres of proteins: methane monooxygenase and semimet azidohemerythrin. *J. Am. Chem. Soc.* **115**, 6440-6441

DeWitt, J. G., Bentsen, J. G., Rosenzweig, A. C., Hedman, B., Green, J., Pilkington, S., Papaefthymiou, G. C., Dalton, H., Hodgson, K. O. and Lippard, S. J. (1991) X-ray absorption, Mössbauer, and EPR studies of the dinuclear iron centre in the hydroxylase component of methane monooxygenase. *J. Am. Chem. Soc.* **113**, 9219-9235

DeWitt, J. G., Rosenzweig, A. C., Salifoglou, A., Hedman, B., Lippard, S. J. and Hodgson, K. O. (1995) X-ray absorption spectroscopic studies of the di-iron centre in methane monooxygenase in the presence of substrate and the coupling protein of the enzyme system. *Inorg. Chem.* **34**, 2505-2515

Doi, K., Antanaitis, B. C. and Aisen, P. (1988) The binuclear iron centres of uteroferrin and the purple acid phosphatases. *Struct. Bonding* **70**, 1-26

Duggleby, H. J., Tolley, S. P., Hill, C. P., Dodson, E. J., Dodson, G. and Moody, P. C. (1995) Penicillin acylase has a single-amino-acid catalytic centre. *Nature* **373**, 264-268

Elango, N., Radhakrishnan, R., Froland, W. A., Wallar, B. J., Earhart, C. A., Lipscomb, J. D. and Ohlendorf, D. H. (1997) Crystal structure of the hydroxylase component of methane monooxygenase from *Methylosinus trichosporium* OB3b. *Prot. Sci.* **6**, 556-568

Ericson, A., Hedman, B., Hodgson, K. O., Green, J., Dalton, H., Bentsen, J. G., Beer, R. H. and Lippard, S. J. (1988) Structural characterisation by EXAFS spectroscopy of the binuclear iron centre in component A of methane monooxygenase from *Methylococcus capsulatus* (Bath). *J. Am. Chem. Soc.* **110**, 2330-2332

Ferenci, T. (1974) Carbon monoxide-stimulated respiration in methane-utilising bacteria. *FEBS Lett.* **41**, 94-98

Ferenci, T., Strom, I. and Quayle, R. (1975) Oxidation of carbon monoxide and methane by *Pseudomonas methanica*. *J. Gen. Microbiol.* **91**, 79-91

Fox, B. G., Froland, W. A., Dege, J. E. and Lipscomb, J. D. (1989) Methane monooxygenase from *Methylosinus trichosporium* OB3b. Purification and properties of a three component system with high specific activity from a type II methanotroph. *J. Biol. Chem.* **264**, 10023-10033

Fox, B. G., Liu, Y., Dege, J. E. and Lipscomb, J. D. (1991) Complex formation between the protein components of methane monooxygenase from *Methylosinus trichosporium* OB3b. *J. Biol. Chem.* **266**, 540-550

Fox, B. G., Surerus, K. K., Munck, E. and Lipscomb, J. D. (1988) Evidence of a μ -oxo-bridged binuclear iron cluster in the hydroxylase component of methane monooxygenase. *J. Biol. Chem.* **263**, 10553-10556

- Frank, J., Radermacher, M., Penczek, P., Zhu, J., Li, Y., Ladjadj, M. and Leith, A.** (1996) SPIDER and WEB: Processing and visualisation of images in 3D electron microscopy and related fields. *J. Struct. Biol.* **116**, 190-199
- Frey, P. A.** (1997) Radicals in enzymatic reactions. *Curr. Opin. Chem. Biol.* **1**, 347-356
- Froland, W. A., Andersson, K. K., Lee, S-K., Liu, Y. and Lipscomb, J. D.** (1992) Methane monooxygenase component B and reductase alter the regioselectivity of the hydroxylase component-catalysed reactions. *J. Biol. Chem.* **267**, 17588-17597
- Gekko, K. and Timasheff, S. N.** (1981) Mechanism of protein stabilisation by glycerol: preferential hydration in glycerol-water mixtures. *Biochem.* **20**, 4667-4676
- Gassner, G. T. and Lippard, S. J.** (1999) Component interactions in the soluble methane monooxygenase system from *Methylococcus capsulatus* (Bath). *Biochem.* **38**, 12768-12785
- George, A. R., Wilkins, P.C. and Dalton, H.** (1996) A computational investigation of the possible substrate binding sites in the hydroxylase of soluble methane monooxygenase. *J. Mol. Catal.* **2**, 103-113
- Gesser, H. D., Hunter, N. R. and Drakash, C. B.** (1985) The direct conversion of methane to methanol by controlled oxidation. *Chem. Rev.* **85**, 235-244
- Glocker, M. O., Bauer, S. H. J., Kast, J., Volz, J. and Przybylski, M.** (1996) Characterisation of specific noncovalent protein complexes by UV matrix-assisted laser desorption ionisation mass spectrometry. *J. Mass Spec.* **31**, 1221-1227
- Green, J. and Dalton, H.** (1985) Protein B of soluble methane monooxygenase from *Methylococcus capsulatus* (Bath). *J. Biol. Chem.* **260**, 15795-15801
- Green, J. and Dalton, H.** (1986) Steady-state kinetic analysis of soluble methane monooxygenase from *Methylococcus capsulatus* (Bath). *Biochem. J.* **236**, 155-162
- Green, J. and Dalton, H.** (1988) The biosynthesis and assembly of protein A of soluble methane monooxygenase of *Methylococcus capsulatus* (Bath). *J. Biol. Chem.* **263**, 17561-17565
- Green, J. and Dalton, H.** (1989) A stopped-flow kinetic study of soluble methane monooxygenase from *Methylococcus capsulatus* (Bath). *Biochem. J.* **259**, 167-172
- Green, J., Prior, S. D. and Dalton, H.** (1985) Copper ions as inhibitors of protein C of soluble methane monooxygenase of *Methylococcus capsulatus* (Bath). *Eur. J. Biochem.* **153**, 3688-3701
- Green, P. N.** (1992) Taxonomy of methylotrophic bacteria. In *Microbial Growth On C₁ Compounds*, pp23-84. Edited by J.C. Murrell and D.P. Kelly. Andover: Intercept Press.

Green, W. N. and Ramanathan, R. V. (1988) Conversion of natural gas to transport fuels. American Institute of Chemical Engineers 1988 Spring National Meeting Session 70B, Fuels and Chemicals from Natural Gas, March 6th – 10th New Orleans, USA.

Gu, H. H., Xu, J., Gallagher, M. and Dean, J. E. (1993) Peptide splicing in the vacuolar ATPase subunit A from *Candida tropicalis*. *J. Biol. Chem.* **268**, 7372-7381

Guan, C. D., Cui, T., Rao, V., Liao, W., Benner, J., Line, C. L. and Comb, D. (1996) Activation of glycosylasparaginase – formation of active N-terminal threonine by intramolecular autoprolysis. *J. Biol. Chem.* **271**, 1732-1737

Hanahan, G. (1983) Studies of transformation of *Escherichia coli* with plasmids. *J. Mol. Biol.* **166**, 577-580

Hanson, R. S. and Hanson, T. E. (1996) Methanotrophic Bacteria. *Microbial Reviews* **60**, 439-471

Harpaz, Y., Gertstein, M. and Chothia, C. (1994) Volume changes by protein folding. *Structure* **2**, 641-649

Heidorn, D. B. and Trewhella, J. (1988) Comparison of the crystal and solution structures of calmodulin and troponin-C. *Biochem.* **27**, 909-915

Henderson, S. J., Newsholme, P., Heidorn, D. B., Mitchell, R., Seeger, P. A., Walsh, D. A. and Trewhella, J. (1992) Solution structure of phosphorylase-kinase studied using small-angle X-ray and neutron-scattering. *Biochem.* **31**, 437-442

Hirata, R., Nakano, A., Kawasaki, H., Suzuki, K. and Anraku, Y. (1990) Molecular structure of a gene VMA1, encoding the catalytic subunit of (H⁺) – translocating adenosine triphosphatase from vacuolar membranes of *Saccharomyces cerevisiae*. *J. Biol. Chem.* **265**, 6726-6733

Hodges, R. A., Perler, F. B., Noren, C. J. and Jack, W. E. (1992) Protein splicing removes intervening sequences in an archaea DNA polymerase. *Nucleic Acids Res.* **20**, 6153-6157

Hogan, K. B., Hoffman, J. S. and Thompson, A. M. (1991) Methane on the greenhouse agenda. *Nature* **354**, 181-182

Holm, L. and Sander, C. (1993) Protein-structure comparison by alignment of distance matrices. *J. Mol. Biol.* **1**, 123-138

Jiang, Y. (1993) Studies of the hydroxylase component of soluble methane monooxygenase from *Methylococcus capsulatus* (Bath). PhD Thesis, University of Warwick, UK.

Jiang, Y., Wilkins, P. C. and Dalton, H. (1993) Activation of the hydroxylase of sMMO from *Methylococcus capsulatus* (Bath) by hydrogen peroxide. *Biochim. Biophys. Acta.* **1163**, 105-112

- Jin, Y. and Lipscomb, J. D.** (1999) Probing the mechanism of C-H activation: Oxidation of methylcubane by soluble methane monooxygenase from *Methylosinus trichosporium* OB3b. *Biochem.* **38**, 6178-6186
- Kane, P. M., Yamashiro, C. T., Wolczyk, D. F., Neff, N., Goebel, M. and Stevens, T. H.** (1990) Protein splicing converts the yeast TFP1 gene product to the 66kDa subunit of the vacuolar H(+)-adenosine triphosphatase. *Science* **250**, 651-657
- Karas, M., Bahr, U., Ingendoh, A. and Hillenkamp, F.** (1989) Laser desorption ionisation mass-spectrometry of proteins of mass 100,000 to 250,000 dalton. *Angewandte Chemie-International Edition in English.* **28**, 760-761
- Karas, M., Bahr, U., Ingendoh, A., Nordhoff, E., Stahl, B., Strupat, K. and Hillenkamp, F.** (1990) Principles and applications of matrix-assisted UV laser desorption ionisation mass spectrometry. *Analyt. Chim. Acta.* **241**, 175-185
- Kazlauskaitė, H., Hill, A. O., Wilkins, P. C. and Dalton, H.** (1996) Direct electrochemistry of the hydroxylase of soluble methane monooxygenase from *Methylococcus capsulatus* (Bath). *Eur. J. Biochem.* **241**, 552-556
- Krueger, J. K., Bishop, N. A., Blumenthal, D. K., Zhi, G., Beckingham, K., Stull, J. T. and Trewella, J.** (1998) Calmodulin binding to myosin light chain kinase begins at substoichiometric Ca^{2+} concentrations: a small-angle scattering study of binding and conformational transitions. *Biochem.* **37**, 17810-17817
- Laemmli, U. K.** (1970) Cleavage of structural proteins during the assembly of the head of the bacteriophage T4. *Nature* **227**, 680-685
- Lawrence, A. J. and Quayle J. R.** (1970) Alternative carbon assimilation pathways in methane utilising bacteria. *J. Gen. Microbiol.* **63**, 371-374
- Leadbetter, E. R. and Foster, J. W.** (1959) Incorporation of molecular oxygen in bacterial cells utilising hydrocarbons for growth. *Nature* **184**, 1428-1429
- Lee, S. Y. and Lipscomb, J. D.** (1999) Oxygen activation catalysed by methane monooxygenase hydroxylase component proton delivery during the O-O bond cleavage steps. *Biochem.* **38**, 4423-4432
- Lelieveld, J., Crutzen, P. J. and Bruhl, C.** (1993) Climatic effects of atmospheric methane. *Chemosphere* **26**, 739-768
- Lidstrom, M. E. and Semrau, J. D.** (1995) Metals and microbiology: the influence of copper on methane oxidation. In *Advances in chemistry: aquatic chemistry*. Edited by C. P. Huang. American Chemical Society, Washington, D. C.
- Lipscomb, J. D.** (1994) Biochemistry of the soluble methane monooxygenase. *Annu. Rev. Microbiol.* **48**, 371-399

- Liu, A. M., Li, S. B., Miaw, D. X., Yu, W. L., Zhang, F. and Su, P.** (1991) Isolation and purification of methane monooxygenase from *Methylomonas* sp. GYJ3. *Chinese Chem. Lett.* **2**, 419-422
- Liu, K. E., Johnson, C. C., Newcomb, M. and Lippard, S. J.** (1993) Radical clock substrate probes and kinetic isotope effect studies of the hydroxylation of hydrocarbons by methane monooxygenase. *J. Am. Chem. Soc.* **115**, 939-947
- Liu, K. E. and Lippard, S. J.** (1991) Redox properties of the hydroxylase component of methane monooxygenase from *Methylococcus capsulatus* (Bath): effects of protein B, reductase and substrate. *J. Biol. Chem.* **266**, 12836-12839
- Liu, K. E., Valentine, A. M., Wang, D. L., Huynh, B. H., Edmondson, D. E., Salifoglou, A. and Lippard, S. J.** (1995) Kinetic and spectroscopic characterisation of intermediates and component interactions in reaction of methane monooxygenase from *Methylococcus capsulatus* (Bath). *J. Am. Chem. Soc.* **117**, 10174-10185
- Liu, Y., Nesheim, J. C., Paulsen, K. E., Stankovich, M. T. and Lipscomb, J. D.** (1997) Roles of the methane monooxygenase reductase component in the regulation of catalysis. *Biochem.* **36**, 5223-5233
- Lloyd, J. S.** (1997) Heterologous expression and site directed mutagenesis of soluble methane monooxygenase. PhD Thesis, University of Warwick, UK.
- Lloyd, J. S., Bhambra, A., Murrell, J. C. and Dalton, H.** (1997) Inactivation of the regulatory protein B of soluble methane monooxygenase from *Methylococcus capsulatus* (Bath) by proteolysis can be overcome by Gly to Gln modification. *Eur. J. Biochem.* **248**, 72-79
- Lowe, J., Stock, D., Jap, B., Zwickl, P., Baumeister, W. and Huber, R.** (1995) Crystal-structure of the 20S proteasome from the archaeon *T-acidophilum* at 3.4 angstrom resolution. *Science.* **268**, 533-539
- Lund, J. and Dalton, H.** (1985) Further characterisation of the FAD and Fe₂S₂ redox centres of component C, the NADH : acceptor reductase of the soluble methane monooxygenase of *Methylococcus capsulatus* (Bath). *Eur. J. Biochem.* **147**, 291-296
- Lund, J. Woodland, M. P. and Dalton, H.** (1985) Electron transfer reactions in the soluble methane monooxygenase of *Methylococcus capsulatus* (Bath). *Eur. J. Biochem.* **147**, 297-305
- Maniatis, T., Fritsch, E. F. and Sambrook, J.** (1982) Molecular cloning. A laboratory manual. Cold Spring Harbour, New York: Cold Spring Harbour Laboratory Press.
- Martin, H.** (1994) Molecular genetics of methane oxidation in *Methylosinus trichosporium* OB3b. PhD Thesis, University of Warwick, UK.

- McDonald, I. R., Uchiyama, H., Kambe, S., Yagi, O. and Murrell, J. C. (1997)** The soluble methane monooxygenase gene cluster of the trichloroethylene-degrading methanotroph *Methylocystis* sp. Strain M. *Appl. Environ. Microbiol.* **63**, 1898-1904
- Meng, C. K., Mann, M. and Fenn, J. B. (1988)** Of protons or proteins. *Zeitschrift fur Physik D – Atoms, Molecules and Clusters.* **10**, 361-368
- Minton, A. P. (1997)** Influence of excluded volume upon macromolecular structure and associations in 'crowded' media. *Curr. Opin. Biotech.* **8**, 65-69
- Minton, A. P., Colclasure, G. A. and Parker, J. C. (1992)** Model for the role of macromolecular crowding in regulation of cellular volume. *Proc. Natl. Sci. USA.* **89**, 10504-10506
- Moore, P. B. (1980)** Small-angle scattering. Information content and error analysis. *J. Appl. Crystallogr.* **13**, 168-175
- Murrell, J. C. (1992)** Genetics and molecular biology of methanotrophs. *FEMS Microbiol. Rev.* **88**, 233-248
- Murrell, J. C. (1994)** Molecular genetics of methane oxidation. *Biodegradation* **5**, 145-159
- Nakajima, T., Uchiyama, H., Yagi, O. and Nakahara, Y. (1992)** Purification and properties of soluble methane monooxygenase from *Methylocystis* sp. M. *Biosci. Biotechnol. Biochem.* **56**, 736-740
- Nakano, H., Yamazaki, T., Ikeda, M., Masai, H., Miyatake, S. and Saito, T. (1994)** Purification of glutathione-s-transferase fusion proteins as a non-degraded form using protease negative *E. coli* strain, AD202. *Nuc. Acid. Res.* **22**, 543-544
- Nesheim, J. C. and Lipscomb, J. D. (1996)** Large kinetic isotope effects in methane oxidation catalysed by methane monooxygenase: evidence for C-H bond cleavage in a reaction cycle intermediate. *Biochem.* **35**, 10240-10247
- Nguyen, H. T., Elliot, S. J., Yip, J. H. and Chan, S. I. (1998)** The particulate methane monooxygenase from *Methylococcus capsulatus* (Bath) is a novel copper-containing three-subunit enzyme. *J. Biol. Chem.* **273**, 7957-7966
- Nielsen, A. K., Gerdes, K., Degn, H. and Murrell, J. C. (1996)** Regulation of bacterial methane oxidation: transcription of the soluble methane monooxygenase operon of *Methylococcus capsulatus* (Bath) is repressed by copper ions. *Microbiol. UK* **142**, 1289-1296
- Nielsen, A. K., Gerdes, K., Degn, H. and Murrell, J. C. (1997)** Copper-dependent reciprocal transcriptional regulation of methane monooxygenase genes in *Methylococcus capsulatus* and *Methylosinus trichosporium*. *Mol. Microbiol.* **25**, 399-409

- Nordlund, P., Sjöberg, B. M. and Eklund, H.** (1990) Three dimensional structure of the free-radical protein of ribonucleotide reductase. *Nature* **345**, 593-598
- Patel, R. N., Hou, C. T., Laskin, A. I., Felix, A. and Derelanko, P.** (1979) Microbial oxidation of gaseous hydrocarbons. II. Hydroxylation of alkanes and epoxidation of alkenes by cell-free particulate fractions of methane-utilising bacteria. *J. Bacteriol.* **139**, 675-679
- Patel, R. N. and Savas, J. C.** (1987) Purification and properties of the hydroxylase component of methane monooxygenase. *J. Bacteriol.* **169**, 2313-2317
- Paulsen, K. E., Liu, Y., Fox, B. G., Lipscomb, J. D., Munck, E. and Stankovich, M. T.** (1994) Oxidation-reduction potentials of the methane monooxygenase hydroxylase component from *Methylosinus trichosporium* OB3b. *Biochem.* **33**, 713-722
- Peitsch, M. C.** (1995) Protein modelling by email. *Biotech.* **13**, 658-660
- Penczek, P., Radermacher, M. and Frank, J.** (1992) 3-dimensional reconstruction of single particles embedded in ice. *Ultramicroscopy* **40**, 33-53
- Periana, R. A., Taube, D. J., Evitt, E. R., Loffler, D. G., Wentreck, P. R., Voss, G. and Masuda, T.** (1993) A mercury catalysed, high yield system for the oxidation of methane to methanol. *Science* **259**, 340-343
- Perler, F. B.** (1998) Breaking up is easy with esters. *Nature Structural Biology.* **5**, 249-252
- Perler, F. B., Xu, M. Q. and Paulus, H.** (1997) Protein splicing and autoproteolysis mechanisms. *Curr. Opin. Chem. Biol.* **1**, 292-299
- Pilkington, S. J. and Dalton, H.** (1990) Soluble methane monooxygenase from *Methylococcus capsulatus* (Bath). *Methods in Enzymology.* **188**, 181-190
- Pilkington, S. J. and Dalton, H.** (1991) Purification and characterisation of the soluble methane monooxygenase from *Methylosinus sporium-5* demonstrates the highly conserved nature of this enzyme in methanotrophs. *FEMS Microbiol. Lett.* **78**, 103-108
- Pilkington, S. J., Salmond, G. P. C., Murrell, J. C. and Dalton, H.** (1990) Identification of the gene encoding the regulatory protein B of soluble methane monooxygenase. *FEMS Microbiol. Lett.* **72**, 345-348
- Porod, G.** (1982) General theory. In *Small angle X-ray scattering*. Edited by O. Glatter and O. Kratky. Academic Press. London. Pp 17-51
- Prior, S. D. and Dalton, H.** (1985) Acetylene as a suicide substrate and active site probe for methane monooxygenase from *Methylococcus capsulatus* (Bath). *FEMS Microbiol. Lett.* **29**, 105-109

- Quayle, J. R.** (1972) The metabolism of one-carbon compounds by microorganisms. *Ann. Rev. Micro. Physiol.* **7**, 119-203
- Quayle, J. R.** (1987) An eightieth anniversary of the study of C₁ metabolism. In *Microbial Growth on C₁ Compounds*. Edited by H. W. Van Verseveld, and J. A., Duine, Martinus Nijhoff, Dordrecht, 1-5
- Que, L. and True, A. E.** (1990) Dinuclear iron-oxo and manganese-oxo sites in biology. *Prog. Inorg. Chem.* **38**, 97-200
- Ralston, G. B.** (1990) Effects of 'crowding' in protein solutions. *J. Chem. Educ.* **67**, 857-860
- Ramjee, M. K., Genschel, U., Abell, C. and Smith, A. G.** (1997) *Escherichia coli* L-aspartate-alpha-decarboxylase: preprotein processing and observation of reaction intermediates by electrospray mass spectrometry. *Biochem. J.* **323**, 661-669
- Ribbons, D. W. and Michalover, J. L.** (1970) Methane oxidation by cell-free extracts of *Methylococcus capsulatus*. *FEBS Lett.* **11**, 41-44
- Rosenzweig, A. C., Brandstetter, H., Whittington, D. A., Nordlund, P., Lippard, S. J. and Frederick, C. A.** (1997) Crystal structures of the methane monooxygenase hydroxylase from *Methylococcus capsulatus* (Bath): Implications for substrate gating and component interactions. *Proteins: Structure, Function and Genetics.* **29**, 141-152
- Rosenzweig, A. C., Frederick, C. A., Lippard, S. J. and Nordlund, P.** (1993) Crystal structure of a bacterial non-haem iron hydroxylase that catalyses the biological oxidation of methane. *Nature* **366**, 537-543
- Rosenzweig, A. C. and Lippard, S. J.** (1994) Determining the structure of a hydroxylase enzyme that catalyses the conversion of methane to methanol in methanotrophic bacteria. *Acc. Chem. Res.* **27**, 229-236
- Rosenzweig, A. C., Nordlund, P., Takahara, P. M., Frederick, C. A. and Lippard, S. J.** (1995) Geometry of the soluble methane monooxygenase catalytic di-iron centre in the two oxidation states. *Chem. and Biol.* **2**, 409-418
- Sambrook, J., Fritsch, E. F. and Maniatis, T.** (1989) Molecular cloning: a laboratory manual. 2nd Edition. Cold Spring Harbour, New York: Cold Spring Harbour Laboratory Press.
- Schachman, H. K. and Lauffer, M. A.** (1949) Hydration, size and shape of tobacco mosaic virus. *J. Am. Chem. Soc.* **71**, 536-541
- Schaper, A. and Jovin, T. M.** (1996) Striving for atomic resolution in biomolecular topography: the scanning force microscope (SFM). *BioEssays.* **18**, 925-935
- Scopes, R. K.** (1974) Measurement of protein by spectrophotometry at 205nm. *Anal. Biochem.* **59**, 277-282

Semrau, J. D., Chistoserdov, A., Lebron, J., Costello, A., Davagnino, J., Kenna, E., Holmes, A. J., Finch, R., Murrell, J. C., and Lidstrom, M. E. (1995) Particulate methane monooxygenase genes in methanotrophs. *J. Bacteriol.* **177**, 3071-3079

Shao, Y. and Kent, S. B. H. (1997) Protein splicing: occurrence, mechanisms and related phenomena. *Chemistry and Biology.* **4**, 187-194

Shiemke, A. K., Cook, S. A., Miley, T. and Singleton, P. (1995) Detergent solubilisation of membrane bound methane monooxygenase requires plastoquinol analogues as electron donors. *Arch. Biochem. Biophys.* **2**, 421-428

Shinohara, Y., Uchiyama, H., Yagi, O. and Kusakabe, I. (1998) Purification and characterisation of component B of a soluble methane monooxygenase from a *Methylocystis* sp. M. *J. Ferment. Bioeng.* **85**, 37-42

Shu, L., Nesheim, J. C., Kauffmann, K., Münck, E., Lipscomb, J. D. and Que, L. (1997) An Fe₂(IV)O₂ diamond core structure for the key intermediate Q of methane monooxygenase. *Science.* **275**, 515-518

Smith, D. D. S. and Dalton, H. (1989) Solubilisation of methane monooxygenase from *Methylococcus capsulatus* (Bath). *Eur. J. Biochem.* **182**, 667-671

Smith, D. D. S. and Dalton, H. (1992) Evidence for two histidine ligands at the di-iron site of methane monooxygenase. *Eur. J. Biochem.* **210**, 629-633

Smith, R. D., Loo, J. A., Edmonds, G. C., Baringa, C. J. and Udseth, H. R. (1990) New developments in biochemical mass spectrometry: electrospray ionisation. *Anal. Chem.* **62**, 882-899

Sohnngen, N. L. (1906) Ueber bakterien, welche methan als kohlenstoffnahrung und energiequelle gebrauchen. *Zentralbl. Bakteriol. Parasitenk. Infektionskrankh. Hygiene.* (Abteilung II) **15**, 513-517

Solomon, E. I., Brunold, T. C., Davis, M. I., Kemsley, J. N., Lee, S. K., Lehnert, N., Neese, F., Skulan, A. J., Yang, Y. S. and Zhou, J. (2000) Geometric and electronic structure/function correlations in non-heme iron enzymes. *Chem. Rev.* **100**, 235-349

Stainthorpe, A. C., Lees, V., Salmond, G. P. C., Dalton, H. and Murrell, J. C. (1990) The methane monooxygenase gene cluster of *Methylococcus capsulatus* (Bath). *Gene* **91**, 27-34

Stainthorpe, A. C., Murrell, J. C., Salmond, G. P. C., Dalton, H. and Lees, V. (1989) Molecular analysis of methane monooxygenase from *Methylococcus capsulatus* (Bath). *Arch. Microbiol.* **152**, 154-159

Stanley, S. H., Prior, S. D., Leak, D. J. and Dalton, H. (1983) Copper stress underlies the fundamental change in intracellular location of methane monooxygenase in methane-oxidising organisms: studies in batch and continuous cultures. *Biotechnol. Letts.* **5**, 487-492

Stoddard, B. L. and Pietrokovski, S. (1998) Breaking up is hard to do. *Nature Struct. Biol.* **5**, 3-5

Stryer, L. (1988) Biochemistry, 3rd Edition. W. H. Freeman and Company, New York. USA.

Stubbe, J. (1990) Ribonucleotide reductases: amazing and confusing. *J. Biol. Chem.* **265**, 5329-5332

Thomann, H., Bernardo, M., McCormick, J. M. Pulver, S., Andersson, K. K., Lipscomb, J. D. and Solomon, E. I. (1993) Pulsed EPR studies of mixed-valent [Fe(II)Fe(III)] forms of hemerythrin and methane monooxygenase – evidence for a hydroxide bridge. *J. Am. Chem. Soc.* **115**, 8881-8882

Tonge, G. M., Harrison, D. E. F. and Higgins, I. J. (1977) Purification and properties of the methane monooxygenase enzyme system from *Methylosinus trichosporium* OB3b. *Biochem. J.* **161**, 333-344

Tonge, G. M., Harrison, D. E. F., Knowles, C. J. and Higgins, I. J. (1975) Properties and partial purification of the methane-oxidising enzyme system from *Methylosinus trichosporium* OB3b. *FEBS Lett.* **58**, 293-299

Trehwella, J., Gallagher, S. C., Krueger, J. and Zhao, J. (1998) Neutron and X-ray solution scattering provide insights into biomolecular structure and function. *Sci. Prog.* **81**, 101-122

Valentine, A. M., LeTadic-Biadatti, M. H., Toy, P. H., Newcomb, M. and Lippard, S. J. (1999) Oxidation of ultrafast radical clock substrate probes by the soluble methane monooxygenase from *Methylococcus capsulatus* (Bath). *J. Biol. Chem.* **274**, 10771-10776

Valentine, A. M., Wilkinson, B., Liu, K. E., Komar-Panicucci, S., Priestley, N. D., Williams, P. G., Morimoto, H., Floss, H. G. and Lippard, S. J. (1997) Tritiated chiral alkanes as substrates for soluble methane monooxygenase from *Methylococcus capsulatus* (Bath): probes for the mechanism of hydroxylation. *J. Am. Chem. Soc.* **119**, 1818-1827

Wallar, B. J. and Lipscomb, J. D. (1996) Dioxygen activation by enzymes containing binuclear non-heme iron clusters. *Chem. Rev.* **96**, 2625-2657

Walters, K. J., Gassner, G. T., Lippard, S. J. and Wagner, G. (1999) Structure of the soluble methane monooxygenase regulatory protein B. *Proc. Natl. Acad. Sci. USA.* **96**, 7877-7882

West, C. A., Salmond, G. P. C., Dalton, H. and Murrell, J. C. (1992) Functional expression in *Escherichia coli* of proteins B and C from soluble methane monooxygenase of *Methylococcus capsulatus* (Bath). *J. Gen. Microbiol.* **138**, 1031-1307

Whittenbury, R. and Dalton, H. (1981) The methylotrophic bacteria. In *The prokaryotes*. Edited by M. P. Starr, H. Stolph, H. G. Truper, A. Balowes, and H. G. Schlegel. Springer-Verlag, Berlin pp 894-902

Whittenbury, R., Phillips, K. C. and Wilkinson, J. F. (1970) Enrichment, isolation and some properties of methane-utilising bacteria. *J. Gen. Microbiol.* **61**, 205-218

Whittaker, J. R. and Granum, P. E. (1980) An absolute method for protein determination based on difference in absorbance at 235 and 280nm. *Anal. Biochem.* **109**, 156-159

Wilkins, P. C., Dalton, H., Podmore, I. D., Deighton, N. and Symons, M. C. R. (1992) Biological methane activation involves the intermediacy of carbon-centred radicals. *Eur. J. Biochem.* **210**, 67-72

Wilkins, P. C., Dalton, H., Samuel, C. J. and Green, J. (1994) Further evidence for multiple pathways in soluble methane-monooxygenase-catalysed oxidations from the measurement of deuterium kinetic isotope effects. *Eur. J. Biochem.* **226**, 555-560

Wilkins, P. C. and Wilkins, R.G. (1987) The coordination chemistry of the binuclear iron site in hemerythrin. *Coord. Chem. Rev.* **79**, 195-214

Wilkins, R. G. (1992) Binuclear iron centres in proteins. *Chem. Soc. Rev.* **21**, 171-178

Woodland, M. P. and Dalton, H. (1984) Purification and characterisation of component A of the methane monooxygenase from *Methylococcus capsulatus* (Bath). *J. Biol. Chem.* **259**, 53-59

Woodland, M. P., Patil, D. S., Cammack, R. and Dalton, H. (1986) ESR studies of protein A of the soluble methane monooxygenase from *Methylococcus capsulatus* (Bath). *Biochim. Biophys. Acta.* **873**, 237-242

Yoshizawa, K., Shiota, Y. and Yamabe, T. (1998) Methane-methanol conversion by MnO^+ , FeO^+ , and CoO^+ : a theoretical study of catalytic selectivity. *J. Am. Chem. Soc.* **120**, 564-572

Zahn, J. A. and DiSpirito, A. A. (1996) Membrane-associated methane monooxygenase from *Methylococcus capsulatus* (Bath). *J. Bacteriol.* **178**, 1018-1029

Zhao, J., Hoye, E., Boylan, S., Walsh, D. A. and Trewhella, J. (1998) Quaternary structures of a catalytic subunit-regulatory subunit dimeric complex and the holoenzyme of the cAMP-dependent protein kinase by neutron contrast variation. *J. Biol. Chem.* **273**, 30448-30459

Appendix

Global Conformational Changes Control the Reactivity of Methane Monooxygenase[†]

Stephen C. Gallagher,[‡] Anastasia J. Callaghan,[§] Jinkui Zhao,^{||} Howard Dalton,[§] and Jill Trehwella*[†]

Chemical Science and Technology Division, Mail Stop G758, Los Alamos National Laboratory, Los Alamos New Mexico 87544, and Biological Sciences, University of Warwick, Coventry, CV47AL, U.K.

Received December 21, 1998; Revised Manuscript Received March 15, 1999

ABSTRACT: We present here X-ray scattering data that yield new structural information on the multicomponent enzyme methane monooxygenase and its components: a hydroxylase dimer, and two copies each of a reductase and regulatory protein B. Upon formation of the enzyme complex, the hydroxylase undergoes a dramatic conformational change that is observed in the scattering data as a fundamental change in shape of the scattering particle such that one dimension is narrowed (by 25% or 24 Å) while the longest dimension increases (by 20% or 25 Å). These changes also are reflected in a 13% increase in radius of gyration upon complex formation. Both the reductase and protein B are required for inducing the conformational change. We have modeled the scattering data for the complex by systematically modifying the crystal structure of the hydroxylase and using ellipsoids to represent the reductase and protein B components. Our model indicates that protein B plays a role in optimizing the interaction between the active centers of the reductase and hydroxylase components, thus, facilitating electron transfer between them. In addition, the model suggests reasons why the hydroxylase exists as a dimer and that a possible role for the outlying γ -subunit may be to stabilize the complex through its interaction with the other components. We further show that proteolysis of protein B to form the inactive B' results in a conformational change and B' does not bind to the hydroxylase. The truncation thus could represent a regulatory mechanism for controlling the enzyme activity.

Soluble methane monooxygenase (sMMO) from methanotrophs, such as *Methylococcus capsulatus* (Bath) or *Methylosinus trichosporium* OB3b, catalyzes the biologically and environmentally important conversion of methane to methanol (1, 2). Methane has been implicated as contributing to the greenhouse effect, interacting with atmospheric oxygen to yield CO₂ and water vapor (3). sMMO can reduce the amount of methane released to the atmosphere through microbial oxidation. Further, an understanding of the sMMO mechanism of action may help in the design of robust catalysts that can effect the direct oxidation of methane to methanol at ambient temperature and pressure—a reaction that has so far eluded the chemical industry.

The sMMO enzyme has three functional components: the hydroxylase, which is a non-heme diiron-containing protein that exists as a dimer of $\alpha\beta\gamma$ -subunits [$(\alpha\beta\gamma)_2$, 250 kDa] and contains the site of oxidation where dioxygen and methane bind; the reductase (38.6 kDa), which contains a 2[Fe–S] cluster and an FAD center and transfers electrons from NAD(P)H to the hydroxylase; and the small (15.8 kDa) regulatory protein B, which has a variety of roles including

enhancing electron transfer between the other components, altering the redox potential of the diiron site, changing substrate specificity of the hydroxylase, among others (2, 4–6). The regulatory protein B can exist in two forms, one active and an inactive variant (B') that has lost between 12 and 30 residues from the N-terminus (5, 7, 8). The evidence for the stoichiometry of the three components in the active sMMO complex (1 hydroxylase dimer:2 reductase:2 protein B) will be discussed below in the context of published data as well as our scattering experiments.

In recent years, there have been great strides toward an understanding of the mode of action of sMMO. In particular, crystallization of the hydroxylase component (9, 10) has allowed a detailed examination of the residues involved in the binding of substrates (11) and activation of oxygen required in the oxidation processes (10). The field has also benefited from extensive investigation of the mechanism of methane oxidation using kinetic approaches (12, 13). Other techniques, such as EPR, electrochemistry, CD, MCD, EXAFS, and fluorescence spectroscopy (5, 14–20), have provided insights into local conformational changes and perturbations which occur upon reduction of the diiron center or binding of the regulatory protein B. To date, however, our knowledge of the physical interactions of the individual components of sMMO has come from interpreting binding studies which give no direct information on global conformational changes that may occur. Small-angle scattering is a powerful technique for probing global conformational changes in proteins arising from the addition of substrates, inhibitors, regulators, and other cofactors (21, 22). In

[†]This work was performed under the auspices of the Department of Energy under contract to the University of California and was supported by DOE project KP1101010 (J.T.) and the Biotechnology and Biological Sciences Research Council via a studentship (A.J.C.).

* To whom correspondence should be addressed. Phone: 505-667-2031. Fax: 505-667-0100. E-mail: jtrehwella@lanl.gov.

[‡] Los Alamos National Laboratory.

[§] University of Warwick.

^{||} Present address: Solid State Division, Oak Ridge National Laboratory, Oak Ridge TN 37831.

addition, information on the relative disposition of components within a complex can be obtained. We have therefore used small-angle X-ray scattering to determine the solution conformations of each of the isolated sMMO components and to investigate the effects of binding of the reductase and protein B components on the conformation of the hydroxylase dimer in a single oxidation state. This new structural information helps to explain previous observations about sMMO and also provides new insights into the component interactions, regulatory mechanisms, methane oxidation, and the role of the various protein components in this process.

MATERIALS AND METHODS

Protein Preparation. The hydroxylase and reductase, as well as the B' form of protein B, were purified from *M. capsulatus* as previously described (7). The protein B used in our experiments was a mutant form with a Gln residue substituted for Gly13 in the wild-type sequence, thus making the protein more resistant to inactivation by truncation at this position. This recombinant protein B was expressed in *Escherichia coli* and purified as described previously (7). The purified proteins were stored at $-70\text{ }^{\circ}\text{C}$ and thawed immediately prior to the scattering experiments. Protein concentrations were initially determined colorimetrically by the method of Bradford (23) using bovine serum albumin as a standard and commercially available reagents (Bio-Rad). More accurate protein concentrations were obtained by analysis of the I_0 values from the small-angle scattering data (see below). The sMMO complex was prepared by simple mixing of the components, and its activity was followed by the production of propene oxide in the liquid phase by gas chromatography (24) with 25 mM MOPS, pH 7.0, and a preincubation time of 30 s.

X-ray Scattering Data Acquisition and Analysis. X-ray data were collected using either the small-angle X-ray scattering station at Los Alamos described previously (25) or our newer instrument which has a two-dimensional detector and a rotating anode source with double focusing mirrors to give a point-source geometry. The data from each instrument gave identical structural parameters for the same protein samples, although the brighter source and two-dimensional detector of the newer instrument give dramatically improved counting statistics. Samples were maintained at $16\text{ }^{\circ}\text{C}$ during data acquisition. Typical data collection times were 10 min to 2 h, depending on protein concentration and molecular mass. All scattering experiments were repeated at least two times using samples from independent preparations.

Scattering data were reduced and analyzed as previously described (25). Parameters used in the interpretation of the scattering data included radius of gyration, R_g , forward (or zero-angle) scattering intensity, I_0 , and the pairwise length distribution function, $P(r)$. $P(r)$ is the probable frequency of vector lengths connecting small-volume elements within the scattering particle. $P(r)$, therefore, goes to zero at the maximum linear dimension of the particle, d_{max} . For a dilute solution of monodisperse, identical particles the scattering intensity, $I(Q)$, and $P(r)$ are related by a Fourier transformation:

$$P(r) = r^2/2\pi^2 \int I(Q)Q^2(\sin(Qr)/Qr) dQ \quad (1)$$

where $Q = (4\pi \sin\theta)/\lambda$ is the amplitude of the scattering

vector, θ is half the scattering angle, and λ the wavelength of the scattered radiation (1.54 \AA). $P(r)$ is calculated from the experimental scattering profile using an indirect Fourier transform method (26). R_g and I_0 are calculated as the second and zeroth moments of $P(r)$, respectively.

I_0 , when normalized to molar concentration, is proportional to the square of the molecular weight for particles with the same mean scattering densities. By using a standard protein of known molecular weight (lysozyme in this study), one can determine the molecular weight of another monodisperse protein sample by taking ratios of the I_0 values. An I_0 analysis can thus be used to check the monodispersity in samples of known protein concentration or to determine accurate protein concentrations for solutions known to be monodisperse (27). In addition, I_0 is highly sensitive to complex formation (27). For a three component system with component molecular weights M_a , M_b , and M_c , I_0 is proportional to $(M_a + M_b + M_c)^2$ for the 1:1:1 complex but to the much smaller $M_a^2 + M_b^2 + M_c^2$ if the components do not form a complex. For a mixture of partially complexed components, I_0 is proportional to the concentration-weighted average of the I_0 values for the complexed and uncomplexed components.

Molecular volumes were calculated from the scattering data using the equation:

$$V = 2\pi^2 I_0 / Q_i \quad (2)$$

where Q_i is the scattering invariant (28):

$$Q_i = \int Q^2 dQ I(Q) \quad (3)$$

Because the scattering data are measured only over a finite Q -range, the scattering invariant, and hence molecular volume, calculations are subject to systematic error. These errors vary for different experiments and in our case are of the order of 10% based on comparison of the expected volumes with those calculated from the scattering data.

Modeling the Scattering Data. In the absence of high-resolution crystal structure data, the scattering from globular proteins can be effectively modeled using uniform-density ellipsoid shapes (29, 30). Protein B and the reductase were each modeled as uniform density ellipsoids, and model scattering profiles were calculated using a Monte Carlo simulation program [SASMODEL (30)]. SASMODEL generates models using one or more ellipsoid shapes with dimensions constrained within a range given by the user. Large numbers of models are generated by an algorithm that assigns random values (within the defined constraints) to the lengths of each semi-axis. For each model generated, a $P(r)$ function is calculated using a rapid Monte Carlo integration method (25) in which the ellipsoids are filled with random points and all possible vector lengths between the points are summed to give $P(r)$. Model $P(r)$ functions based on the hydroxylase crystal structure [Protein Data Bank (PDB) accession no. P22869], as well as for the sMMO complex, were calculated using a program (PRPDB) that utilizes a rapid Monte Carlo integration method similar to that used by SASMODEL. The atomic coordinates from the crystal structure are placed in a box with a three-dimensional grid. An option to include a hydration layer, in which the solvent layer at the surface of the protein is assigned a different mean scattering density to the bulk solvent, is included. The

thickness and contrast of the hydration layer are parameters that can be chosen by the user. The volume elements of the grid are assigned scattering density values based on the number of electrons that fall within the volume element (from either the protein or hydration layer components). Alternatively, a uniform density can be assigned to grid elements occupied by the structure. The model $P(r)$ is calculated by filling each volume element occupied by the molecular shape with 4000 random points and summing all vector-lengths between pairwise combinations of the saved points. PRPDB can also use the output from SASMODEL and calculate $P(r)$ profiles from uniform density ellipsoid shapes as well as composite models made up from uniform density ellipsoids combined with crystal structure coordinates. Typically, 4000 points were used in our model $P(r)$ calculations which gave smooth well-determined profiles. Both SASMODEL and PRPDB calculate model scattering profiles for comparison with experiment by Fourier transformation of $P(r)$. Model fits are evaluated using least-squares methods and saved in PDB format for ease of viewing.

RESULTS AND DISCUSSION

Analysis of the sMMO Component Structures. To evaluate the sMMO component structures, as well as to aid in interpretation of the scattering profile of the sMMO complex, we first measured the solution-scattering profiles of each of the isolated components (Figure 1). Scattering data were measured for a series of five protein concentrations in the range 2–15 mg/mL, in 25 mM MOPS, pH 7.0, $T = 13^\circ\text{C}$. For each component, there was no concentration dependence of the scattering data, indicating that interparticle interference effects (31) were negligible and hence required no correction. The vector length distribution functions for each component, calculated as the inverse Fourier transform of the scattering profiles (26), are shown in Figure 2. The best-fit ellipsoid models for the reductase and protein B have approximate dimensions 72, 44, 32 Å and 50, 34, 30 Å, respectively. These models give reduced χ^2 values of 1.03 and 1.01, respectively, indicating a near perfect fit (which would have $\chi^2 = 1.0$) to the scattering data. For the isolated hydroxylase, a model $P(r)$ function was calculated using the crystal structure coordinates (10). This fit gives $\chi^2 = 0.99$ without inclusion of a hydration layer. Thus, under the conditions of our experiments, hydration layer effects are not detected and the crystal and solution structures for the hydroxylase are the same. Figures 1 and 2 show the excellent fits of the model $I(Q)$ and $P(r)$ functions to those derived from experiment for each component.

The reductase and protein B components give unimodal $P(r)$ profiles typical for compact globular proteins (Figure 2a). In contrast, the $P(r)$ function for the hydroxylase is bimodal with a shoulder at 70 Å (Figure 2b). This shoulder is due to the bilobal shape of the hydroxylase that arises from the way in which the two $\alpha\beta\gamma$ trimers associate to form the dimer (Figure 3). The values obtained for d_{\max} , R_g , and molecular volume for each of the isolated components are in good agreement with the expected values based on monodisperse proteins of mass 250, 38.6, and 15.8 kDa, for the hydroxylase, reductase, and protein B, respectively, and assuming a specific volume of 0.74 cm³/g (Table 1). The

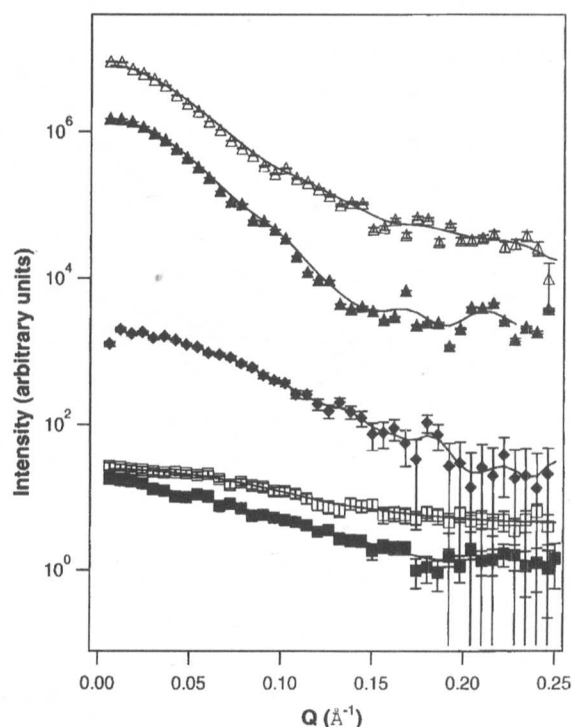


FIGURE 1: $I(Q)$ versus Q data for sMMO and its individual components. Experimental data are depicted by the symbols: protein B (■), B' (□), reductase (◆), hydroxylase (▲), sMMO (1:10:10 mixture = 1:2:2 complex) (Δ). The scattering profiles are offset by multiplication factors in order to separate them on the vertical axis for easy viewing (0.2, 4, 16, 258, and 4096, respectively). The errors indicated are based on counting statistics only. The solid lines represent the model $I(Q)$ profiles calculated using uniform ellipsoids for the reductase, protein B and B', and the crystal structure coordinates for the hydroxylase. For the sMMO complex, the solid line represents the model profile calculated using the model shown in Figure 6.

molecular volumes were calculated from the scattering data using eqs 2 and 3 (Materials and Methods).

Structural Differences between Protein B and B'. Figure 2a shows a comparison of the $P(r)$ functions for protein B and B'. A significant increase in d_{\max} is observed for B' compared with B. The best-fit ellipsoid which approximated the scattering from B' has dimensions 66, 28, and 27 Å ($\chi^2 = 1.02$) compared to 50, 34, and 30 Å for protein B, i.e., B' is longer and thinner than B. (As a measure of the discrimination between these fits to the data one can compare the scattering data for B to the best-fit ellipsoid determined for B' which gives a χ^2 of 12.5. Vice versa, the experimental data for B' compared to the best-fit model for B gives a χ^2 of 13.0). The measured I_0 values and molecular volumes show that both protein B and B' are monodisperse in solution, indicating that the observed changes in structural parameters cannot be attributed to aggregation (Table 1). The observed extension of the structure upon removal of the N-terminal segment of protein B therefore must be due to a partial unfolding or to some sort of opening of the structure triggered by the loss of interactions with the N-terminal residues. In subsequent scattering experiments on mixtures of the hydroxylase with the reductase plus protein B or B' under conditions whereby binding of B is observed (see below),

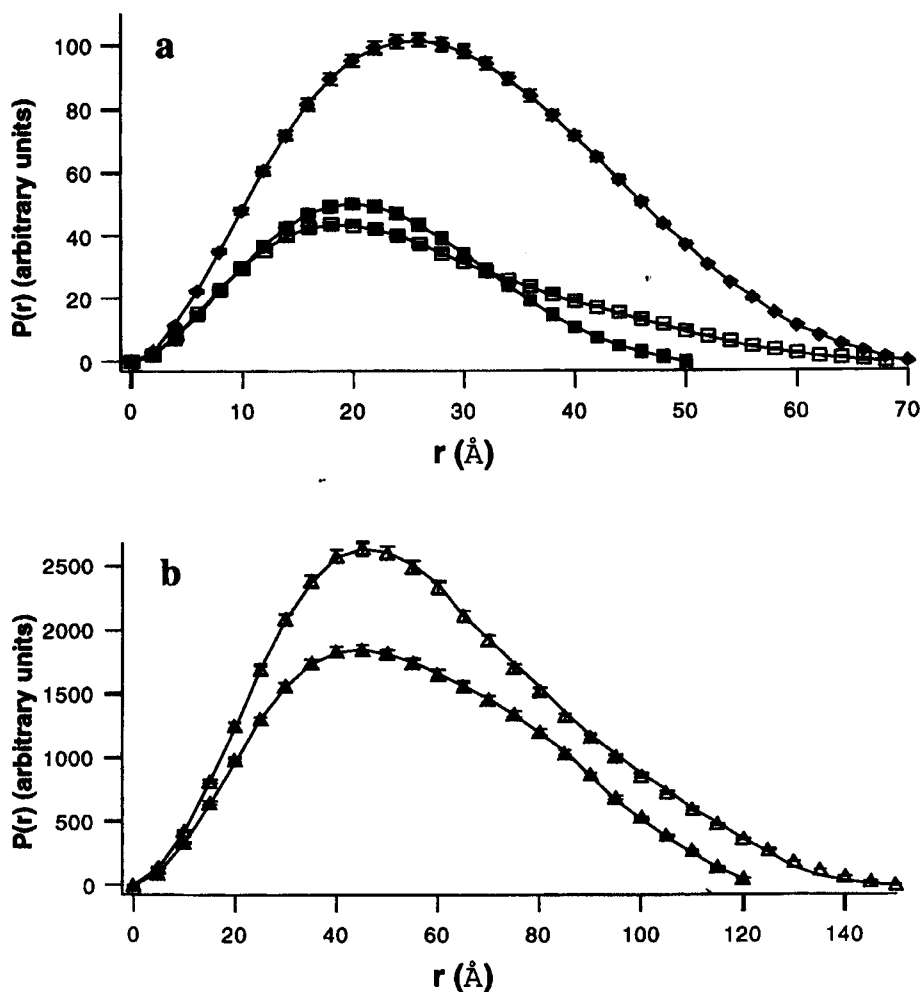


FIGURE 2: $P(r)$ functions for sMMO and its individual components. The experimentally derived $P(r)$ functions for (a) protein B (■), B' (□), reductase (◆), and (b) hydroxylase (▲), sMMO (1:10:10 mixture = 1:2:2 complex) (△). The solid lines are the $P(r)$ functions calculated for the models indicated in Figure 1. The $P(r)$ profiles are scaled such that their areas are proportional to the molecular weight of the component or complex for convenient comparison of shape changes.

there is no evidence for binding of B', including in the I_0 data that are most sensitive to complex formation.

Several authors have suggested that the *in vivo* proteolytic cleavage of the 12 N-terminal residues of protein B to yield an inactive form of the protein, designated as B', may represent a means for controlling activity of the enzyme complex (5, 7, 8). In the absence of methane, the uncoupling of sMMO activity from NADH oxidation by inactivation of protein B would prevent consumption of limited cellular NADH resources. Kazlauskaitė and coauthors (5), for example, found that although protein B alters the potentials at which the hydroxylase component is reduced, B' does not. It has been unclear, however, how the loss of the 12 N-terminal residues of protein B (to give B') results in inactivation. The scattering data show that a conformational change occurs in B upon cleavage of the N-terminal segment and binding is inhibited.

Titration of Hydroxylase with Reductase Plus Protein B to Determine Stoichiometry within the sMMO Complex. Scattering data were measured from mixtures of the sMMO components with 1:1:1, 1:2:2, 1:5:5, 1:10:10, and 1:20:20 ratios of hydroxylase:reductase:protein B. The measured I_0

value is proportional to the square of the molecular weight of the scattering particle and, for protein solutions of known concentration, is extremely sensitive to molecular associations (see Materials and Methods). Analysis of the I_0 values indicate that 0, ≤ 10 , and $\leq 25\%$ of the total protein B and reductase were bound to the hydroxylase for the 1:1:1, 1:2:2, and 1:5:5 mixtures, respectively (Table 1). This minimal binding is consistent with the minimal changes observed in R_g and $P(r)$ compared to the isolated hydroxylase. The I_0 values for the 1:10:10 and 1:20:20 mixtures are consistent with formation of the 1:2:2 complex with 8 and 18 free equiv of the reductase and protein B, respectively. Figure 4 shows a plot of the observed I_0 values for the mixtures plotted against the molar ratio of (reductase and protein B) to hydroxylase in the solution. Also shown are the expected I_0 dependencies assuming different stoichiometries of hydroxylase:reductase:protein B. The comparisons show clearly that the observed data fit the 1:2:2 complex being formed with ≥ 10 equiv of protein B and reductase compared to the hydroxylase. The discrimination between the different stoichiometries is excellent and well beyond the errors in the data.

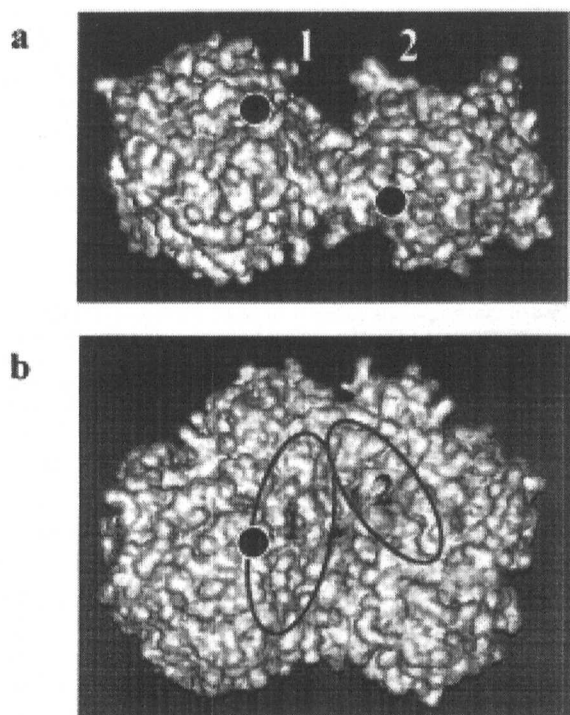


FIGURE 3: Hydroxylase crystal structure. (a) Surface representation showing the bilobal nature of the dimerized trimers (11). The active sites are indicated (●). The structure has been rotated to show the two canyon-like features (1 and 2) which previously had been proposed as possible binding sites of protein B and the reductase (9). (b) Top view of the structure in panel a showing the positions of the two canyons.

The scattering results are consistent with prior evidence for the physical interactions within the sMMO complex, including titrations of the hydroxylase with reductase and protein B, which give an optimum ratio for activity at 1:2:2 (hydroxylase: reductase: protein B) (15); cross-linking studies which provided a tentative assignment of the binding sites of protein B and reductase to the hydroxylase (20); the crystal structure of the hydroxylase in the presence of a short peptide of the reductase component (32); and perturbation of the partially and fully reduced EPR signal of the hydroxylase by addition of protein B (20). Combined, these data suggest possible sites of interaction between the three components and that the stoichiometry of components within the complex is 1:2:2. The stoichiometry of components within the sMMO complex has also been implied from the dimeric form of the hydroxylase, which suggests that two equivalents of the reductase and protein B will be required to bind to a single hydroxylase dimer (9).

Because interpretation of small-angle scattering data in structural terms requires a homogeneous solution of monodisperse, identical particles, our titration experiments were done in the absence of NAD(P)H and substrates in order to prevent turnover which would result in a mixture of different states. Under these conditions, 10 equiv each of the reductase and protein B are required to see full complex formation, whereas maximal activity of sMMO from *Methylosporium trichosporium* OB3b is observed for mixtures containing 2 equiv of both the reductase and protein B per hydroxylase (15). It therefore appears that the addition of NAD(P)H and/

or substrate may increase the affinity of the reductase and protein B to the hydroxylase, thus driving the equilibrium toward complex formation.

Structural Changes Observed Upon Binding of Reductase and Protein B to the Hydroxylase. To determine the structural parameters of the sMMO complex, we used the scattering data from the 1:10:10 mixture of hydroxylase:reductase:protein B. The 8 free equiv of reductase and protein B in this mixture make relatively small contributions to the scattering (4% and 10% total intensity for protein B and reductase, respectively) due to their small size compared to the complex. This contribution is most evident in the overall intensity and I_0 values, and will be less evident in the shape of the scattering profile from which the particle shape parameters are calculated. Since we know the amount of free protein B and reductase, as well as their scattering profiles, we can subtract their contributions proportionately according to their known concentrations. These corrected curves gave $P(r)$ profiles, R_g and d_{max} values that are indistinguishable, within the limits of the experimental errors, from those calculated from the uncorrected data. Nevertheless, all of the interpretation and modeling for the sMMO complex were done using these corrected data.

Accompanying formation of the 1:2:2 sMMO complex, we observe in the $P(r)$ profiles an increase in d_{max} , from 125 to 150 Å and the shoulder at 70 Å is lost, indicating that its overall structure is more elongated and has lost the bilobal character of the hydroxylase alone (Figure 2b). In addition, the R_g value for the scattering particle increases from 42 to 46 Å and the molecular volume increases by 26%. This latter increase is, within the statistical error, what is expected for the formation of a 1:2:2 complex (Table 1).

The single ellipsoid fit to the scattering data for the complex gives dimensions 150, 71, and 66 Å with a χ^2 value of 1.04. In comparison, the best-fit ellipsoid for the isolated hydroxylase calculated from the crystal structure coordinates has dimensions of 125, 95, and 65 Å, which agree well with those of the best-fit ellipsoid calculated from the scattering data 127, 98, and 65 Å ($\chi^2 = 1.01$). These ellipsoid fits indicate that the molecular envelopes of both the hydroxylase and the complex can be reasonably approximated with uniform density ellipsoid models. Importantly, upon complex formation and the accompanying increase in d_{max} , there is a narrowing in a second dimension (by 24 Å, or 25%), indicating that the hydroxylase cannot be accommodated within the molecular envelope of the complex without a conformational change. The point is illustrated in Figure 5 which shows the best fit ellipsoids for the hydroxylase and the sMMO complex superimposed with the crystal structure for the hydroxylase and the hydroxylase in the sMMO complex derived from the scattering data (see below).

Parallel scattering experiments in which the hydroxylase was titrated either with the reductase or protein B alone, up to 10 equiv of each, showed no evidence for their binding to the hydroxylase, either in terms of the expected increases in I_0 values or conformational changes. These results show that both the reductase and protein B are required for binding and inducing the conformational change

Modeling the sMMO Complex. The crystal structure of the hydroxylase shows two extended canyon-like features

Table 1: R_g , d_{max} , and Molecular Volumes for Each Component of sMMO and Component Mixtures^a

component/mixture	R_g (Å)	d_{max} (Å)	measured I_0 (arbitrary units)	measured volume (Å ³)	expected volume (Å ³)
protein B	17.5 ± 0.9	50	3950 ± 150	19 200 ± 3100	19 400
protein B ^b	19.8 ± 0.9	70	3650 ± 160	20 300 ± 1700	17 900
reductase	23.1 ± 0.4	70	9650 ± 470	43 200 ± 2000	47 300
hydroxylase	41.1 ± 0.04	125	62 500 ± 2100	275 000 ± 1800	305 800
1:1:1	42.1 ± 0.7	125	67 350 ± 2200	298 100 ± 13 100	
1:2:2	43.3 ± 1.6	125	71 020 ± 2350	280 700 ± 29 200	
1:5:5	44.1 ± 0.6	130	121 520 ± 3520	294 600 ± 19 200	
1:10:10	46.4 ± 0.4	150	185 000 ± 2680	346 300 ± 11 800	
1:20:20	46.5 ± 0.5	150	264 200 ± 2450	348 200 ± 10 040	

^a Errors indicated are based on counting statistics alone. Expected volumes are calculated using eqs 2 and 3 in Materials and Methods and a partial specific volume of 0.74 cm³/mg (37). The expected volume for a 1:2:2 complex of the hydroxylase:reductase:protein B is 373 900 Å³. In absolute terms, the volumes determined from the scattering for the hydroxylase and the complex are ~90% of the values expected based on calculation from their specific volumes and molecular mass, with ~4% statistical error. This agreement is excellent given the finite Q-range of the experimental data (see Materials and Methods).

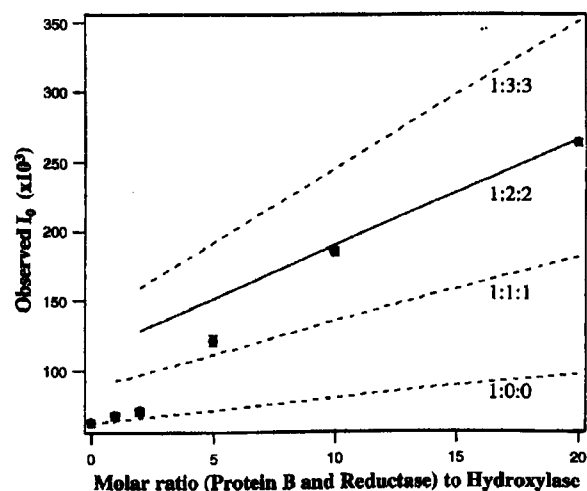


FIGURE 4: Titration of the hydroxylase with protein B and reductase. The I_0 values measured for the mixtures of hydroxylase:reductase:protein B plotted as a function of the protein B and reductase to hydroxylase mole ratio. The solid line indicates the expected I_0 values assuming two equivalents of protein B and reductase bind to one hydroxylase. The dashed lines correspond to alternative stoichiometries for binding as indicated.

(Figure 3) which have been proposed as potential binding sites for the reductase and protein B (9). Models for the complex in which protein B and the reductase were positioned so that they filled these canyon-like features, however, cannot account for the increases in R_g and d_{max} observed upon complex formation. The best χ^2 obtained for such models compared with the scattering data was 16.0, a result that is not surprising since we know that the overall dimensions of the hydroxylase cannot fit within the molecular envelope calculated for the complex. It is possible to obtain the observed increase in the d_{max} for the complex by positioning protein B or the reductase on the surface of the hydroxylase in highly extended arrangements. These types of models, however, do not give the correct R_g values or shape functions. In general, they do not have the correct ratios of d_{max} to cross-sectional area for the elongated shape of the complex, and models of this type all gave χ^2 values ≥ 6 , indicating poor fits.

Inspection of the hydroxylase structure suggests that the required conformational change can be achieved via a rearrangement of the two trimers that associate to form the hydroxylase dimer. Within each trimer, the individual

subunits have convoluted surfaces of interaction, whereas the two trimers contact each other with relatively small areas of interaction at each end of their long axes between the two β -subunits. At one end of this interaction, there is a planar interface of approximately 200 Å². This planar interface provides a potential pivot point in the structure about which the hydroxylase can rotate to give a structure with an increased d_{max} , while maintaining a significant area of contact between the trimers. Rotating about this pivot point takes advantage of the long axes of the trimers to obtain the increase in d_{max} of 25 Å while at the same time narrowing the structure in a second dimension (Figure 5). To test this hypothesis against the scattering data, the hydroxylase was rotated systematically in 10° steps, about the pivot point so as to increasingly extend the long axis of the hydroxylase dimer interface. At the same time, best-fit ellipsoid models of the reductase and protein B (two of each) were placed as close to the hydroxylase active site such that they sat within the overall ellipsoid dimensions for the complex. Model $P(r)$ functions were determined and compared to the experimental $P(r)$ function. If the extension of the hydroxylase structure in this manner accounts predominantly for the increase in d_{max} , one hydroxylase trimer would have to rotate approximately 180° with respect to the second to fit the scattering data (Figures 5 and 6). This rotation preserves the 2-fold symmetry expected for the dimer. It also increases the distance between the active sites from 45 to 75 Å. A plot of $\log I(Q)$ vs Q for the experimental data from the complex and that determined from the model (Figure 1) shows the quality of this model fit to the data ($\chi^2 = 1.13$). Further, the model $P(r)$ agrees well with that determined from the experimental data (Figure 2b). There is likewise excellent agreement for the structural parameters determined for the model and the experimental data. Both have a d_{max} of 150 Å, the R_g values are both 46 Å and the volumes agree within 10% (346 300 Å³ for the experimental and 379 100 Å³ for the model).

Interpretation of the sMMO Model and Relationship to Previous Work. The precise binding site of the reductase and protein B components on the extended form of the hydroxylase cannot be determined from the X-ray scattering data alone. Further, we cannot rule out the possibility of there being some small rearrangements of the subunits within the hydroxylase trimers as the dimer opens. However, Figure 6 shows our model for the interaction between the extended hydroxylase and the other components that gives the best

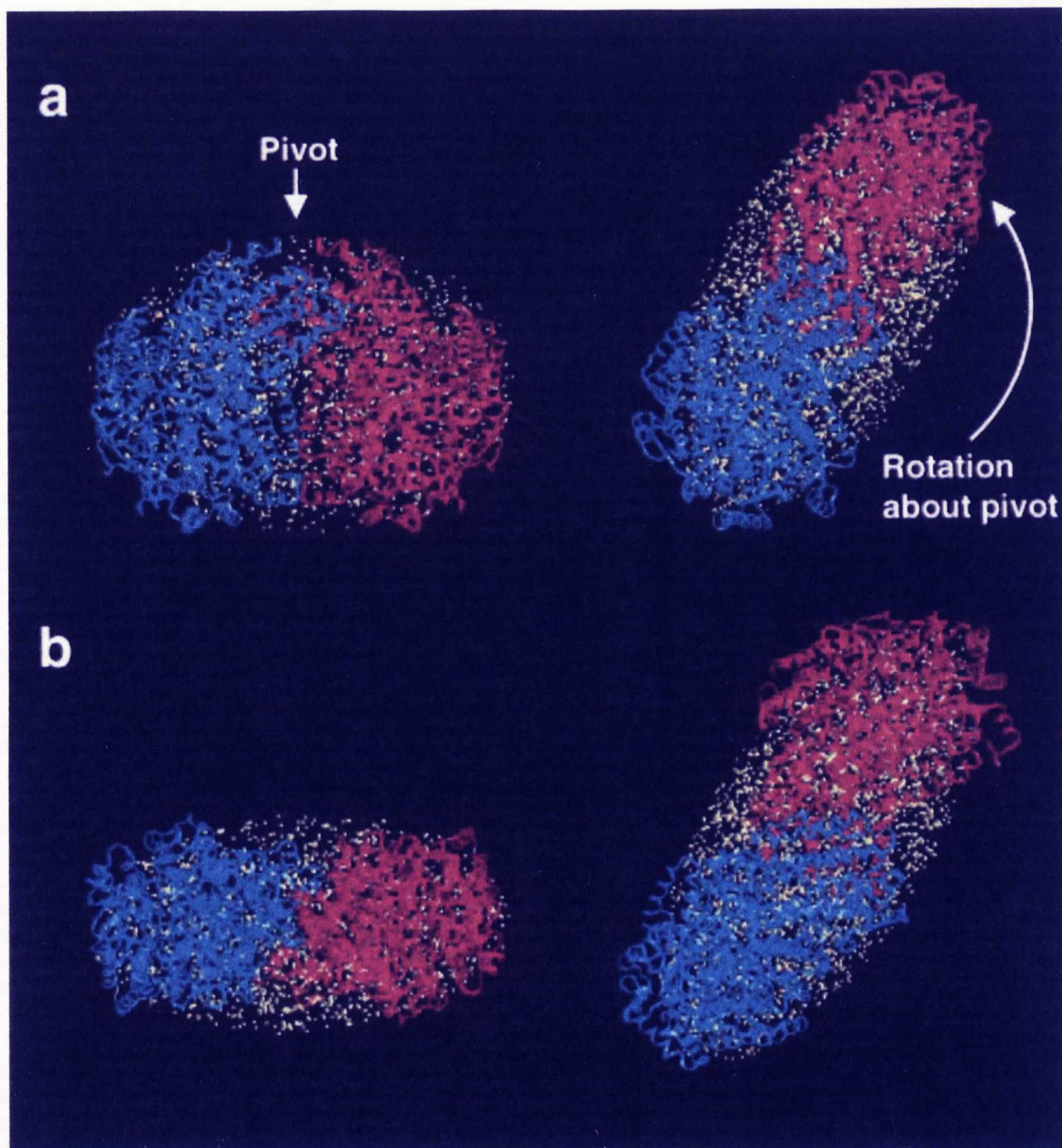


FIGURE 5: Proposed model for the extended hydroxylase structure. Ellipsoid models for the isolated hydroxylase dimer (left) and the SMMO complex (right) are shown as yellow dots that fill the ellipsoid volumes. The upper and lower representations (a and b) are obtained by rotating the respective structures 90° about their long axes. A ribbon representation of the hydroxylase structure is superimposed on the ellipsoids, with the individual trimers that associate to form the dimer colored blue and red. The two orientations of the isolated hydroxylase are shown (left) with the ribbon representations based on the unmodified crystal structure. For the complex (right), the hydroxylase dimer is shown in an extended configuration obtained by a rotation of the long axes of each trimer about a pivot plane between the trimers, opening them by approximately 180° . Note, the orientation of the blue trimer is held constant in the views shown in panel a to aid in the comparison. The reorientation of the hydroxylase dimer upon forming the complex accounts for the observed increase in d_{\max} as well as the narrowing of the structure in a second dimension. The bound protein B and reductase (shown in Figure 6) fit within the unfilled portion of the ellipsoid for the complex.

fit to our scattering data consistent with everything we currently know about sMMO. In this model, protein B binds close to the pivot point in the hydroxylase, and we propose that it plays a role in maintaining the extended form of the hydroxylase dimer. This arrangement would allow the reductase component to bind close to the hydroxylase active site and could, therefore, represent the manner in which protein B enhances electron transfer, binding of molecular oxygen, and substrate oxidation (5). No evidence for complex formation, or conformational changes, was

observed upon addition of either the reductase or protein B alone to the hydroxylase, indicating that both are required to bring about the conformational change under the equilibrium conditions of the scattering experiments. It appears then that protein B may facilitate the conformational change of the hydroxylase, but that the reductase is also required and may play a role in locking the hydroxylase in the extended configuration. Hydrogen peroxide can provide electrons and oxygen to the hydroxylase for the methane oxidation reaction in the absence of the reductase and protein

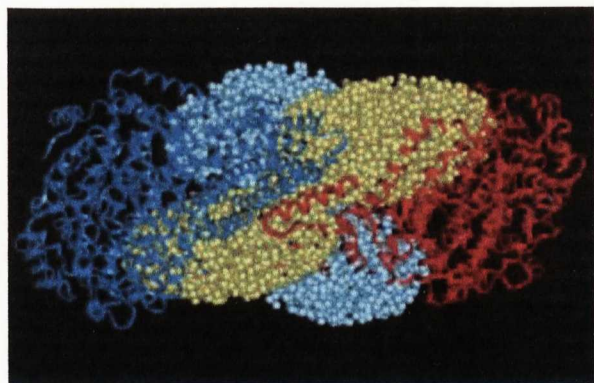


FIGURE 6: Model of the interaction between the three components of sMMO. The hydroxylase structure is shown in ribbon form (dark blue and red), protein B (light blue), and the reductase (yellow) are represented by ellipsoids filled with small spheres. The rotation of the hydroxylase trimers about the pivot region shown in Figure 5 allows B and C to bind closely the hydroxylase giving a compact structure with protein B and the reductase interacting with the active sites. The ellipsoids of the reductase and protein B are effectively rotational averages of their structures. As a result, their volumes are somewhat larger than the actual protein structure is (51 600 and 26 700 \AA^3 for the ellipsoid models compared to 43 300 and 19 200 \AA^3 for the reductase and protein B, respectively), and they therefore were allowed to overlap some with the hydroxylase such that they fit within the overall molecular boundary for the complex.

B (33). Addition of hydrogen peroxide up to concentrations of 100 mM did not give rise to any conformational change in the hydroxylase as evidenced by the scattering data. This result supports our proposal that the role of protein B is primarily to facilitate the conformational change in the hydroxylase in order to allow close interaction between the reductase and hydroxylase. Our model for the complex also suggests why the hydroxylase exists as a dimer since contacts between protein B and both of the hydroxylase trimers occur. These contacts could enhance the interactions between the reductase and protein B with the hydroxylase.

We have compared the interactions between the components in our model with other data collected under equilibrium conditions such as chemical cross-linking studies (20) and the crystal structure of the hydroxylase in association with a short peptide from the reductase (32). The primary interactions suggested from these data are between the reductase and the α - and β -subunits (crystal and cross-linking data) and between protein B and the α -subunit (cross-linking studies only). Our model supports these assignments, but also suggests that there are further interactions. Indeed there appear to be interactions between the reductase and protein B with all three subunits of the hydroxylase. The active site is centered in the α -subunits, and the surface of interaction between the two hydroxylase trimers is provided by the β -subunit. The γ -subunit, however, is situated toward the outside of the hydroxylase dimer, and its precise role has been to date unclear. The scattering data presented here suggest that the γ -subunit contributes to the overall stability of the complex by providing additional interactions with protein B.

Our scattering data on the fully oxidized hydroxylase are also consistent with previous electrochemical and EPR experiments carried out under nonequilibrium conditions during reduction of the hydroxylase. The electrochemical measurements suggest that while protein B can alter the

reduction potentials of the hydroxylase in the absence of reductase, B' cannot (5). In addition, Fox and co-workers (20) showed that the EPR spectrum of the hydroxylase is altered by addition of protein B. If the binding of protein B were to affect the hydroxylase in the manner proposed here, it would most certainly affect the environment of the diiron center thus explaining the alteration in its EPR spectrum and redox potentials (5, 20). In addition to the effects on the environment of the diiron center of the hydroxylase, the proposed close association between protein B and the hydroxylase suggests how protein B could alter the hydroxylase substrate specificity (15). Protein B is positioned such that it can be involved in recognition of substrates entering the hydroxylase active site. A similar proposal was suggested for phenol hydroxylase, a closely related enzyme (34).

CONCLUSIONS

In summary, we have shown that formation of the sMMO complex results in a conformational change in the hydroxylase that involves an extension in one dimension and a narrowing in a second. We have proposed a model that fits the scattering data for the complex in which the pair of trimers that associate to form the hydroxylase dimer are rotated with respect to each other about a pivot plane such that the 2-fold symmetry expected for a dimer is preserved. The best-fit model of the complex is a compact structure containing one hydroxylase dimer and two molecules each of the reductase and protein B, and requires close interaction between all of the protein components. In the model, the conformational change in the hydroxylase allows the reductase to bind close to the hydroxylase active site. Both protein B and the reductase are required for the conformational change. The reductase thus not only provides reducing power for the methane oxidation process but also appears to act in concert with protein B to induce the extended conformation of the hydroxylase dimer. Inactivation of protein B to B' by cleavage of 12 N-terminal residues is accompanied by a conformational change that renders the protein unable to bind and alter the global structure of the hydroxylase. This inhibition of binding provides a means to regulate the activity of the enzyme *in vivo*.

There are other examples of regulation of enzyme activity via conformational changes induced by proteins binding and modulating access to, or the configuration, of the active site. An example is the binding of calmodulin to the autoinhibitory region of myosin light chain kinase that results in its removal from the surface of the catalytic core and a subsequent closure of the catalytic cleft upon substrate binding (35, 36). The sMMO example presented here involves a much more dramatic movement of molecular mass, however, than the more typical calmodulin/kinase/substrate interaction and associated conformational transitions.

ACKNOWLEDGMENT

We thank Dominico Vigil for technical assistance with the X-ray data collection and Brian MacDonald for technical assistance with the X-ray instrumentation. We thank Susan Slade for her help in the preparation of proteins.

REFERENCES

1. Liu, K. E., and Lippard, S. J. (1995) *Adv. Inorg. Chem.* 42, 263.

2. Colby, J., and Dalton, H. (1978) *Biochem. J.* 171, 461.
3. Badr, O., Probert, S. D., and Ocallaghan, P. W. (1992) *Appl. Energy* 41, 95.
4. Fox, G. G., Froland, W. A., Dege, J. E., and Lipscomb, J. D. (1989) *J. Biol. Chem.* 264, 10023.
5. Kazlauskaitė, H., Hill, A., Wilkins, P. C., and Dalton, H. (1996) *Eur. J. Biochem.* 241, 552.
6. Liu, Y., Nesheim, J. C., Lee, S.-K., and Lipscomb, J. D. (1995) *J. Biol. Chem.* 270, 24662.
7. Lloyd, J. S., Bhambra, A., Murrell, J. C., and Dalton, H. (1997) *Eur. J. Biochem.* 248, 72.
8. Shinohara, Y., Uchiyama, H., Yagi, O., and Kusakabe, I. (1998) *J. Ferment. Bioeng.* 85, 37.
9. Rosenzweig, A. C., Frederick, C. A., Lippard, S. J., and Nordlund, P. (1993) *Nature* 366, 537.
10. Rosenzweig, A. C., Nordlund, P., Takahara, P. M., Frederick, C. A., and Lippard, S. J. (1995) *Chem. Biol.* 2, 409.
11. George, A. R., Wilkins, P. C., and Dalton, H. (1996) *J. Mol. Catal.* 2, 103.
12. Liu, K. E., Valentine, A. M., Wang, D., Huynh, B. H., Edmunson, D. E., Salifgou, A., and Lippard, S. J. (1995) *J. Am. Chem. Soc.* 117, 10174.
13. Nesheim, J. C., and Lipscomb, J. D. (1996) *Biochemistry* 35, 10240.
14. Woodland, M. P., Patil, D. S., Cammack, R., and Dalton, H. (1986) *Biochim. Biophys. Acta* 873, 237.
15. Froland, W., Andersson, K. K., Lee, S. K., Liu, Y., and Lipscomb, J. D. (1992) *J. Biol. Chem.* 267, 17588.
16. Rosenzweig, A. C., and Lippard, S. J. (1994) *Acc. Chem. Res.* 27, 229.
17. Paulsen, K. E., Liu, Y., Fox, B. G., Lipscomb, J. D., Munck, E., and Stankovich, M. T. (1994) *Biochemistry* 33, 713.
18. Davydov, A., Davydov, R., Graslund, A., Lipscomb, J. D., and Andersson, K. K. (1997) *J. Biol. Chem.* 272, 7022.
19. C-Pulver, S., Froland, W. A., Lipscomb, J. D., and Solomon, E. I. (1997) *J. Am. Chem. Soc.* 119, 387.
20. Fox, B. G., Liu, Y., Dege, J. E., and Lipscomb, J. D. (1991) *J. Biol. Chem.* 266, 540.
21. Trehwella, J. (1997) *Curr. Opin. Struct. Biol.* 7, 702.
22. Trehwella, J., Gallagher, S. C., Krueger, J., and Zhao, J. (1998) *Sci. Prog.* 81, 101.
23. Bradford, M. (1976) *Anal. Biochem.* 72, 248.
24. Pilkington, S., Salmund, G., Murrell, J. C., and Dalton, H. (1990) *FEMS Microbiol. Lett.* 72, 345.
25. Heidorn, D. B., and Trehwella, J. (1988) *Biochemistry* 27, 909.
26. Moore, P. B. (1980) *J. Appl. Crystallogr.* 13, 168.
27. Krueger, J. K., Bishop, N. A., Blumenthal, D. K., Zhi, G., Beckingham, K., Stull, J. T., and Trehwella, J. (1998) *Biochemistry* 37, 17810.
28. Porod, G. (1982) in *Small-Angle X-ray Scattering* (Glatter, O., and Kratky, O., Eds.) Academic Press, London.
29. Henderson, S. J., Newsholme, P., Heidorn, D. B., Mitchell, R., Seeger, P. A., Walsh, D. A., and Trehwella, J. (1992) *Biochemistry* 31, 437.
30. Zhao, J., Hoye, E., Boylan, S., Walsh, D. A., and Trehwella, J. (1998) *J. Biol. Chem.* 273, 30448.
31. Wu, C.-F., and Chen, S.-H., (1988) *Biopolymers* 27, 1065.
32. Rosenzweig, A. C., Brandstetter, H., Whittington, D. A., Nordlund, P., Lippard, S. J., and Frederick, C. A. (1997) *Proteins: Struct., Funct., Genet.* 29, 141.
33. Jiang, Y., Wilkins, P. C., and Dalton, H. (1993) *Biochim. Biophys. Acta* 1163, 105.
34. Qian, H., Edlund, U., Powlowski, J., Shingler, V., and Sethson, I. (1997) *Biochemistry* 36, 495.
35. Krueger, J. K., Olah, G. A., Rokop, S. E., Zhi, G., Stull, J. T., and Trehwella, J. (1997) *Biochemistry* 36, 6017.
36. Krueger, J. K., Zhi, G., Stull, J. T., and Trehwella, J. (1998) *Biochemistry* 37, 13997.
37. Harpaz, Y., Gerstein, M., and Chothia, C. (1994) *Structure* 2, 641.

BI982991N